COST Action FP1004

Experimental Research with Timber

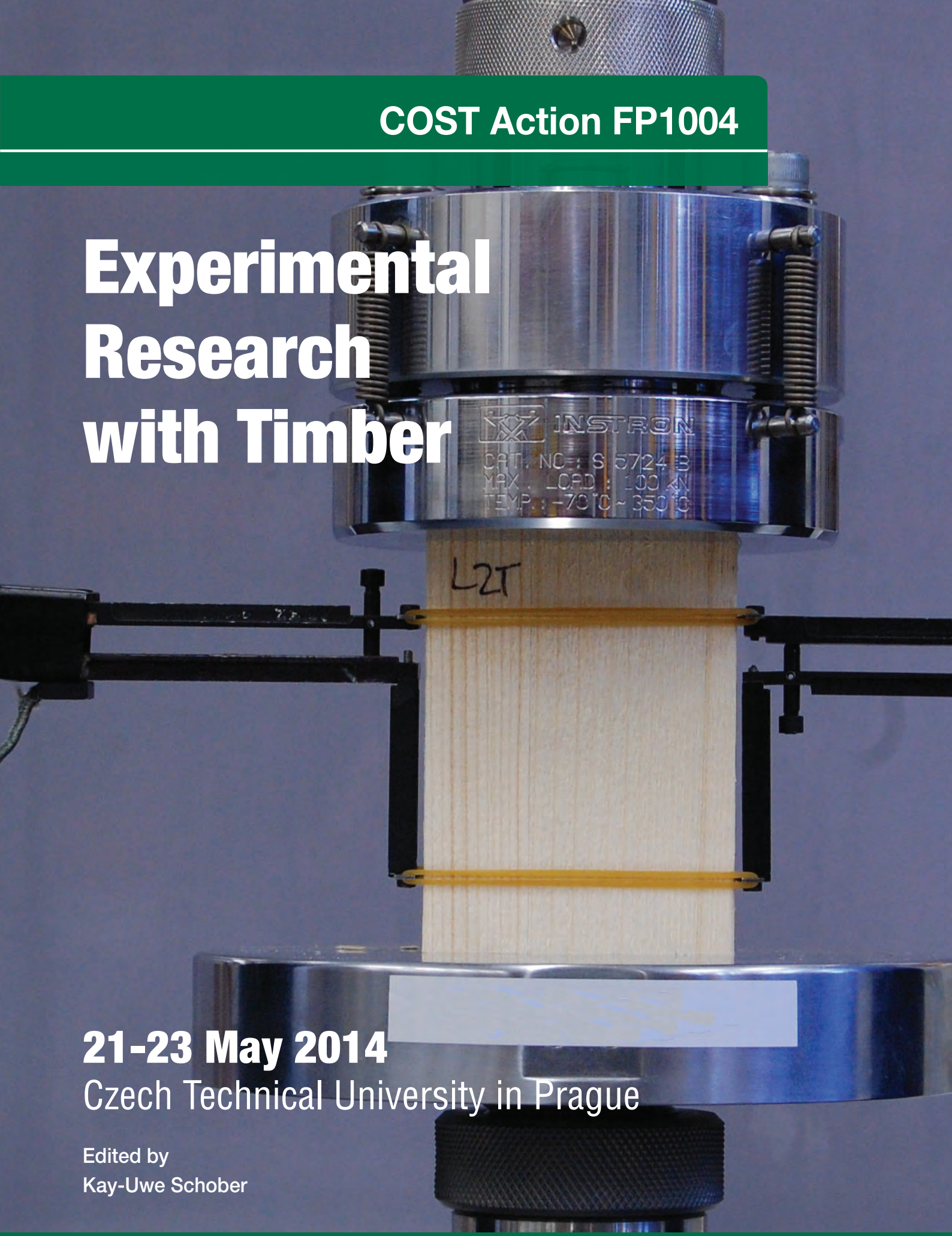

21-23 May 2014

Czech Technical University in Prague

Edited by
Kay-Uwe Schober

UNIVERSITY OF BATH

COST Action FP1004

Enhance mechanical properties of timber,
engineered wood products and timber structures

Experimental Research with Timber

May 21-23, 2014, Prague, Czech Republic

Edited by

Kay-Uwe Schober

May 2014

ECOST-MEETING-FP1004-210514-040049

ISBN 1 85790 183 5

Published by: University of Bath

Preface

The COST program exists to strengthen Europe and other countries in scientific and technological research, for peaceful purposes, through the support of cooperation and interaction between European researchers. Timber and wood-based engineered products are important as structural materials, especially in the drive towards sustainable technologies and construction. It is very important to improve the properties of these products, making them more competitive and reliable.

Research ensures that wood and wood products are at the forefront of the move to more sustainable construction. The Czech Technical University has built a reputation as a leader in experimental research and it is very appropriate that the Department of Steel and Timber Structures should host this conference.

COST Action FP1004, "Enhance mechanical properties of timber, engineered wood products and timber structures" provides a network for learning and development in a range of connected topics. This conference is convened as a forum for Early Stage Researchers to present their work. It brings young and experienced researchers together, to learn from one another and to build networks for future research and development. It actively promotes the COST principles of cooperation and interaction and the organizers hope that this will be instilled in the new generation of researchers.

The theme that binds the topics is experimental work. The conferences sessions are: Test Methods; Structural Performance; Composites and Reinforcement; Connections. These are at the heart of COST Action FP1004. Proceedings are a key output for the COST Action in defining current work in Europe. Combined with the network built between delegates, they provide a point of reference from which future collaboration will build.

Richard Harris — Chairman of COST FP1004

Petr Kuklík — Host and Member of COST DC FPS

About COST Action FP1004

Timber and wood-based engineered products are becoming very important as structural materials, especially in the drive towards sustainable technologies and construction. For structural wooden products, it is very important to improve their properties to be more competitive and reliable as a sustainable low-carbon material and a major contributor to affordable buildings. This applies particularly to larger, more complicated structures where timber is becoming a realistic alternative.

This Action aims to boost the performance of structural timber products and construction, thereby improving use of timber in construction in existing and new applications. This includes the enhanced predictability and reliability of timber structures. Improving the mechanical performance of connections and reinforcing timber in weak zones are large-scale research domains in Europe, which will require coordination and scientific/engineering approaches. This COST Action will deliver increased knowledge of improving strengthening, stiffening and toughening techniques, modeling enhanced performance and experience in real projects to create new opportunities for timber construction. Exchanging information will highlight gaps in knowledge and inform future work and potential collaboration between research groups, supporting timber construction and its wider uptake in the European construction industry. This Action may also create opportunities for patenting possible new technologies and products for reinforcing timber mechanical properties.

The scientific program is divided into three main scientific areas expressed as Work Groups (WG) with the same aims but different perspectives:

WG 1: Enhance performance of connections and structural timber in weak zones

WG 2: Enhance the mechanical properties of heavy timber structures with particular emphasis to timber bridges

WG 3: Modeling the mechanical performance of enhanced wood-based systems

COST FP1004 Core Group

Richard Harris	Chairman	R.Harris@bath.ac.uk
Robert Kliger	Vice-Chairman	Robert.Kliger@chalmers.se
Jan Willem Van De Kuilen	WG 1	Vandekuilen@wzw.tum.de
Roberto Crocetti	WG 2	Roberto.Crocetti@kstr.lth.se
Daniel Ridley-Ellis	WG 3	D.Ridley-Ellis@napier.ac.uk
Kay-Uwe Schober	STSM	Kay-Uwe.Schober@fh-mainz.de

COST FP1004 Management Committee

http://w3.cost.eu/index.php?id=183&action_number=FP1004

COST FP1004 Website

http://costfp1004.holz.wzw.tum.de

Conference Host

Petr Kuklík, CTU Prague, Thákurova 7, 166 29 Prague 6, Czech Republic

Table of Content

Session 1: Connections

Session 2: Structural Performance 1

Session 3: Test Methods 1

Session 4: Composites and Reinforcement

Session 5: Structural Performance 2

Session 6: Test Methods 2

Session 7: Structural Performance 3

Monotonic and cyclic behavior of joints with self-tapping screws in CLT structures

Katarina Bratulic[1], Georg Flatscher[2], Reinhard Brandner[3]

Summary

One segment of an intensive research regarding the seismic behavior of cross laminated timber (CLT) structures currently investigated at the Institute of Timber Engineering and Wood Technology and holz.bau forschungs gmbh, deals with screwed joints and their contribution to the overall structure behavior. The aim was to investigate the influence of varying types of self-tapping screws (partially- and fully threaded), as well as their varying screw-load angle (crossed under 45° and parallel under 90°) on the monotonic and cyclic behavior of joints in CLT structures. This paper presents the testing program and the analysis methods, as well as an overview of the results gained within the scope of this sub-project. Furthermore, obtained data were compared with different models for calculating the load carrying capacity given in the literature. Since lack of research was found on the topic of modeling the head pull-through capacity of screws in CLT, its estimation was carried out with an emphasis on the compressive strength of CLT.

1. Introduction

An important aspect, when designing structures in seismic regions, is to ensure their adequate ductility and sufficient energy dissipation. When it comes to brittle failing timber structures, these demands can be achieved with proper joint design. Ratios for evaluating their seismic resistance, such as the impairment of strength and the damping ratio can be obtained empirically by carrying out the monotonic and cyclic

[1] Research Assistant, holz.bau forschungs gmbh, Graz, Austria

[2] Research & Teaching Associate, Institute of Timber Engineering and Wood Technology, TUGraz Austria

[3] Assistant Professor, Institute of Timber Engineering and Wood Technology, TU Graz, holz.bau forschungs gmbh Austria

tests as guided in [1]. Presented research is focused particularly on the screwed joints in CLT structures. Tests were conducted and obtained data processed in accordance to current standards [1]-[3]. Due to possible divergence of the results that may emerge from several available suggestions for data analysis, it is wise to specify which models were used prior to the interpretation of the results.

2. Test configurations

Within this project, several configurations were developed according to the examined joint types and the load direction they were exposed too. Present paper focuses on the wall/wall joint, designed with an overlap of 50 mm, that was loaded in longitudinal shear and the floor/wall joint loaded in longitudinal shear or tension. Implying that the outer elements were clamped in the load direction (in withdrawal test the bottom element was clamped), screws were stressed as shown in Fig. 1. Monotonic and cyclic tests were carried out according to [1] using either fully- or partially threaded screws (FT and PT, respectively) drilled under $\alpha = 90°$ between the screw axis and the load direction. Additionally, same configurations were tested with the crossed position of the screws inserted under $\alpha = 45°$. Two additional configurations with FT screws, which results are not covered within this paper, were tested as well. First, one is comparable to Fig. 1b) but loaded in shear out of plane, while the second one included in-plane shear according to configuration in Fig. 1a) but stressed horizontally.

Common screw diameters, edge distances and spacing were used. Furthermore, the penetration depths are maintained nearly constant in both joined elements. Teflon was used in configuration T2 (Fig. 1b) in order to reduce the influence of friction. Altogether 74 tests were carried out, 27 monotonic and 47 cyclic.

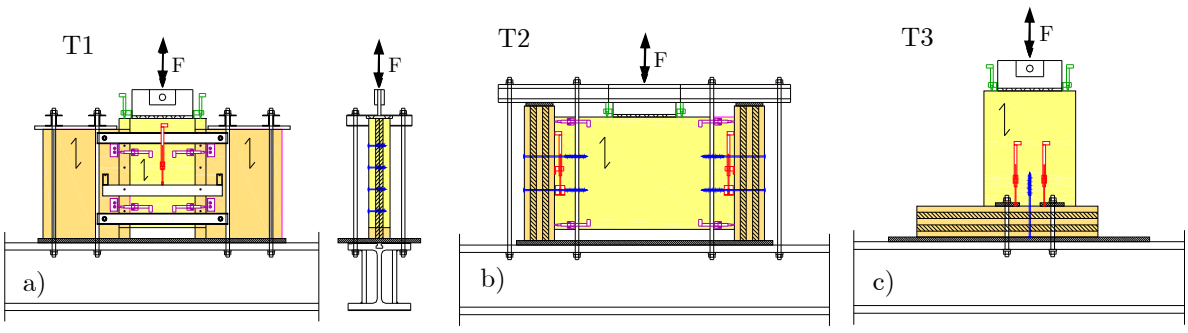

Fig. 1 Tested configurations:
a) wall/wall joint-shear, b) floor/wall joint-shear, c) floor/wall joint-tension

3. Test results

3.1 Failure modes

Typical failure mechanisms of joints with parallel orientation of screws are singled out and presented in Fig. 2. However, failure of the joints was often caused by a combination of presented failure modes.

In cyclic T1 tests, all PT screws failed at the beginning of the thread, as shown in Fig. 2a). Furthermore, 4 of 6 cyclic T3 tests with FT screws failed in withdrawal of screws ($\alpha = 90°$) in the bottom floor element as presented in Fig. 2b), while other specimens failed in withdrawal ($\alpha = 90°$) in upper wall elements. Head-pull through failure, as presented in Fig. 2c), was for example observed in the monotonic T2 test with PT screws. As exemplary shown in the monotonic T2 test with FT screws shows in Fig. 2d), shear tests are also associated with the yielding of the screws and crushing of the timber.

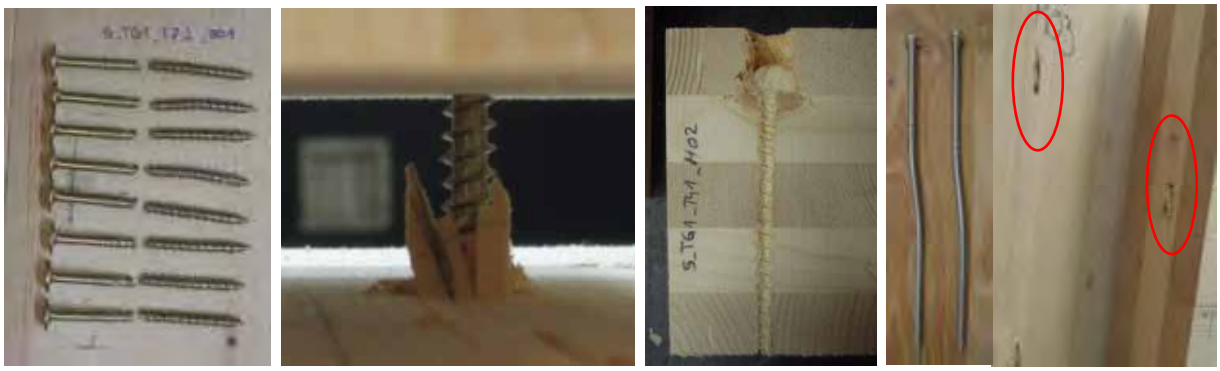

a) b) c) d)

Fig. 2 Failure modes of joints with parallel screws:
a) screw failure at cyclic T1 tests with PT screws,
b) withdrawal of FT screws from floor element at T3 cyclic tests,
c) head-pull through of PT screws in monotonic T2 tests and
d) yielding of the screws and crushing of the timber in monotonic T2 tests with FT screws

Furthermore, Fig. 3 gives comparison between the floor/wall joints with parallel FT and PT screws. As it can be seen, joints with PT screws show considerable plastic behavior in comparison to the joints with FT screws. This is associated with the failure mode of the compared joints – head-pull through in joints with PT and withdrawal in joints with FT screws. Numerical values are given in section 3.2.

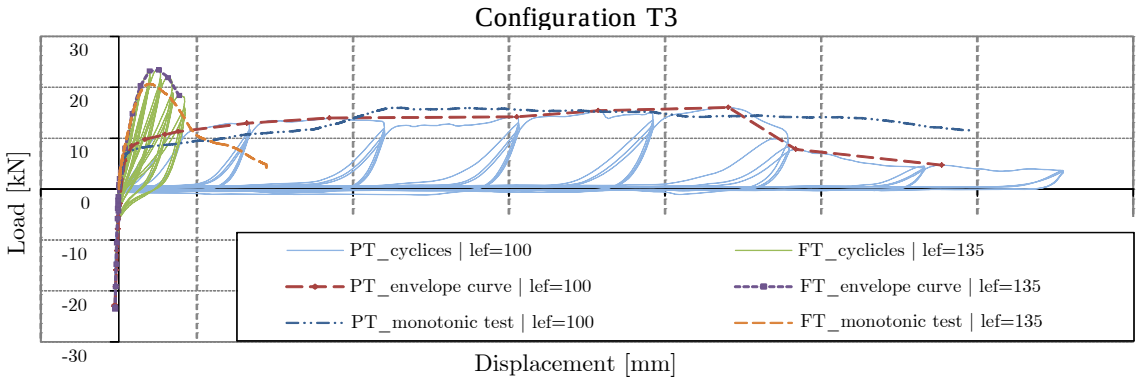

Fig. 3 Monotonic and cyclic tests of the T3 config. with parallel fully- and partially threaded screws

Finally, even if results of the monotonic floor/wall tests with parallel FT screws loaded out of plane are not given in detail within this paper, it is important to emphasize that these were prone to brittle timber failure in tension perpendicular to the grain (see Fig. 2b) before fasteners yielded, and therefore the re-design of the test configuration was required.

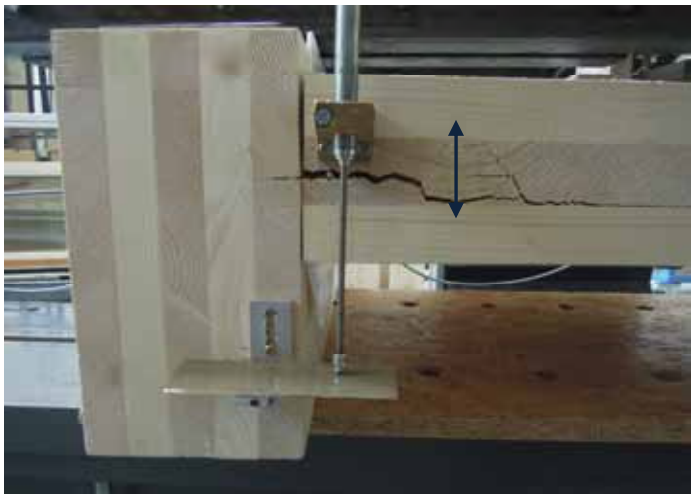

Fig. 4 Timber failure of configuration T2 loaded out of plane

3.2 Data processing

Test results presented in Tab. 1 are based on [1, 3]. For the cyclic tests, this means that the maximum load (F_{max}), initial stiffness (K_{ser}) and ductility (μ) were extracted from the first envelope curve, which was defined by the points of maximum load per cycle [1]. Furthermore, impairment of strength (ΔF) and damping ratio (v_{eq}) were derived from envelope curves based on the points of maximum displacement per cycle [3] as an average of the cycles prior to joint failure. Furthermore, it is important to mention that the ultimate displacement necessary for determination of ductility is taken partly consistent with [3] as either $v_{0.8Fmax}$, v_{Fmax} or v_{end} (displacement at 80% of the maximum load, displacement at maximum load and displacement at the end of

the measurement, respectively) whichever occurs first. Energy dissipation is taken as $v_{eq} = E_d/(E_p \cdot 4\pi)$ [4], where E_d stands for the energy dissipation of the full cycles and E_p for the available potential energy.

Tab. 1 gives the test results for configuration T2 where K_{ser} and F_{max} are given in relation to one screw. As it can be seen, values of K_{ser} and F_{max} are comparable for monotonic and cyclic tests. Differences between the ultimate displacements are also influenced by the configuration setup. This means that deformations for cyclic tests were limited due to reverse loading, while monotonic tests were allowed to deform to a large extent. Comparison of the results between the configurations is given in chapter 4.

Tab. 1: Mean test results for monotonic (M) and cyclic loading (C) of configuration T2

	α		n	$K_{ser,mean}$ [kN/mm]	$F_{max,mean}$ [kN]	$v_{u,mean}$ [mm]	μ_{mean} [-]	ΔF_{mean} [%]	$v_{eq,mean}$ [%]
FT	90°	M	2	0.5	10.3	43.8	2.3	-	-
		C	6	0.6	12.4	36.3	2.0	22.1	7.5
	45°	M	2	19.9	30.0	6.1	4.6	-	-
		C	4	21.7	32.6	3.5	2.7	4.1	6.8
PT	90°	M	3	0.5	9.5	73.6	7.6	-	-
		C	4	0.7	7.3	44.6	8.6	15.5	11.2
	45°	M	2	7.3	15.6	69.1	89.0	-	-
		C	4	5.7	15.5	35.4	31.0	6.4	9.0

3.3 Comparison of the results with the models [6]-[9]

Load carrying capacity of the joints with parallel fasteners (result R1) was calculated according to Johansen's yield theory extended with the "rope effect" ΔR_k as suggested in [5]. Capacity of joints with the inclined screws was estimated in accordance with suggestions given by Blaß and Bejtka [6] and Bejtka and Blaß [7], where simplified calculation (result R2) considers only capacities of withdrawal in tension and compression [6] and detailed calculation (result R3) considers shear component as well. This is done by extending Johansen's equations extended with the withdrawal capacity, the friction between the elements and the angle between the screw axis and force direction [7].

Axial load carrying capacity is taken as minimum between withdrawal-, head-pull through- and screw tensile capacity, whereby is the load carrying capacity of the firstly drilled element defined as maximum between head-pull through- and withdrawal capacity. Models given in [8] and [9] were used for prediction of the mean withdrawal strength of FT screws in the narrow and side faces as well as for mean embedment strength of timber. However, the axial load carrying capacity of PT screws in floor/wall joints was determined by the head-pull through capacity. Hereby, in wall/wall tests with PT screws the withdrawal capacity was decisive due to low l_{ef}. Head-pull through capacity was therefore predicted based on the suggestion given in the approval [10]. Therein given characteristic head-pull through parameter $f_{2,\mathrm{k}}$ is transformed to $f_{2,\mathrm{mean}}$ assuming a normal distribution and a coefficient of variation [COV] of 10%, see Eq. (1).

$$f_{2,mean} = \frac{f_{2,k}}{(1 - 1{,}645 \cdot COV\left[f_2\right])}. \tag{1}$$

The assumption of COV [f_2] = 10% is based on observation of Ciampitti [10] who tested CLT in compression perpendicular to grain. Tab. 2 gives an overview of the models used for prediction of decisive mean capacities (Eq. 2-4,6) and characteristic capacity (Eq. 5):

Tab. 2: Models used for prediction of axial load carrying capacity of screws and embedment of timber

	$R_{ax,mean}$ [kN]	$f_{h,mean}$ [N/mm²]
FT, side f.	$R_{withdr.} = \frac{0{,}6 \cdot \sqrt{d} \cdot l_{ef}^{0,9} \cdot \rho_{mean}^{0,8}}{1{,}2 \cdot \cos^2\alpha + \sin^2\alpha}$ [8] (2)	$f_h = 0{,}022 \cdot d^{-0,3} \cdot \rho_{mean}^{1,24}$ [8] (3)
FT, narrow f.		$f_h = 0{,}862 \cdot d^{-0,5} \cdot \rho_{mean}^{0,56}$ [9] (4)
PT, side f.	$R_{head} = f_{2,k} \cdot d_{head}^{\ 2} \cdot \left(\frac{\rho_k}{350}\right)^{0,8}$ [4] (5)	$f_{h,dowel} = \frac{0{,}035 \cdot \left(1 - 0{,}015 \cdot d\right) \cdot \rho_{mean}^{1,16}}{1{,}1 \cdot \sin^2\alpha + \cos^2\alpha}$ [8] (6)

Tab. 3 shows comparison of the models with the test results and its review is given in next section:

[4] In Eq. (5) for comparison density correction is done by using $(\rho_{obs.}/\ 420)^{0,8}$, whereby $\rho_{observed}$ is taken as the density of the test, and 420 [kg/m³] as mean density of strength class C24

Tab. 3: Comparison between monotonic test results and models given in literature

		α	$R1$ [kN]	R_2 [kN]	R_3 [kN]	F_{max} [kN]
T1	FT	90°	20.4			24,2
		45°		37.3	46.3	35,2
	PT	90°	22.7			23,5
T2	FT	90°	15.3			41,2
		45°		56.6	62.6	60,0
	PT	90°	16.1			37,9
		45°		10.96		31,2
T3	FT	90°	16.4			20,8
		45°		27.6		33,6
	PT	90°	6.8			17,3
		45°		10.3		21,7

4. Conclusion and future work

Monotonic and cyclic tests were carried out on wall/wall and floor/wall screwed joints, whereby the screw types and angle between screw axis and load direction were varied. As expected, considerably high stiffness and load carrying capacity of axially loaded self-tapping screws, in comparison to screws loaded transversely, come into foreground in configurations with inclined screws where the withdrawal component dominates the joint behavior (Tab. 1). Lower impairment of strength and damping ratio were recorded in tests with primarily axially loaded screws. If joints fail due to screw head-pull through, as it was the case in configurations T2 and T3 with PT screws, ductility increases considerably in comparison to the joints with withdrawal or screw failure. Furthermore, it was noticed that certain gap between the elements might occur when the joints are assembled with fully threaded screws. This gap can be reduced if the partially threaded screws are applied instead. Influence of such gaps on joint stiffness and ductility remains to be analyzed.

Regarding the compared models (Tab. 3), calculation of the joints with the screws loaded in shear underestimated the test results in each configuration. Furthermore, simplified calculation (R2) for the ultimate load of joints with crossed, fully threaded screws (considering only capacity of withdrawal in tension and compression [6]) allows good predictability. Detailed calculations (R3) based on extended Johansen's equations (shear component considered as well [7]) slightly overestimates the actual results. However, calculations of ultimate load for joints failing in head pull through,

regardless to the inclination of the partially threaded screws, considerably underestimated the test results. Thus, further research on this topic is proposed.

5. Acknowledgement

Tests were carried out in the frame of the ongoing COMET K-Project “focus_sts” at the Institute of Timber Engineering and Wood Technology (Graz University of Technology) and the holz.bau forschungs gmbh. The support of the industrial and scientific partners is gratefully acknowledged.

References

[1] ISO 16670:2003: Timber structures – Joints made with mechanical fasteners – Quasi static reversed-cyclic test method

[2] ÖNORM EN 12512:2005-12-01: Timber Structures – Test methods – Cyclic testing of joints made with mechanical fasteners (consolidated version)

[3] EN 26891:1991: Timber structures – Joints made with mechanical fasteners – General principles for the determination of strength and deformation characteristics (ident with ISO 6891:1983)

[4] Flatscher G., Bratulic K., Brandner R., Schickhofer G. Zusammenfassende und weiterführende Arbeiten zum Verhalten von BSP-Tragwerken bei der Beanspruchungssituation Erdbeben, COMET K-Projekt „focus_sts“ SGSC 3.1.1_1, holz.bau forschungs gmbh, 2013 (in German)

[5] Schickhofer G., Bogensberger T., Moosbrugger T., Jöbstl A. et al. BSPhandbuch, Institute of Timber Engineering and Wood Technology, holz.bau forschungs gmbh, 2009 (in German)

[6] Blaß H. J., Bejtka I. Verbindungen mit geneigt angeordneten Schrauben, Bauen mit Holz, 105(10):68–85, 2003 (in German)

[7] Bejtka I., Blaß H. J. Joints with inclined screws, CIB-W18, paper 35-7-4, Kyoto, Japan, 2002

[8] Blaß H. J., Bejtka I., Uibel T. Tragfähigkeit von Verbindungen mit selbstbohrenden Holzschrauben mit Vollgewinde, Universität Karlsruhe, 2006 (in German)

[9] Blaß H. J., Uibel T. Tragfähigkeit von stiftförmigen Verbindungsmittel in Brettsperrholz, Karlsruher Berichte zum Ingenieurholzbau, Band 8, Lehrstuhl für Ingenieurholzbau und Baukonstruktionen, Universität Karlsruhe, 2007 (in German)

[10] Z-9.1-514 Allgemeine bauaufsichtliche Zulassung, Würth ASSY II-Holzschrauben und Würth ECOFAST-ASSY II-Holzschrauben als Holzverbindungsmittel, Adolf Würth gmbh & Co. KG, 2006

[11] Ciampitti, A. Untersuchung ausgewählter Einflussparameter auf die Querdruckkenngrößen von Brettsperrholz, Master thesis, Institute of Timber Engineering and Wood Technology, Graz University of Technology, 2013 (in German)

Design of three-dimensional nailing plates

Petr Sejkot[1], Petr Kuklík[2]

Summary

There is a significant possibility to improve calculated load bearing capacities of spatial connections with thin walled metal nailing plates making them more consistent with the results from tests. The reason is that the design of these connecting elements has inadequate support in the existing Standards. Therefore, it is the intention of the research to improve on this state of knowledge. This paper describes the whole process of the research, which consists of the full-scale experiments, 3D FEM models in Abaqus CAE, and the developing of an existing analytic solution.

1. Introduction

Timber connection using thin-walled metal elements gradually supplant traditional carpentry joints. Their main advantage is that they do not weaken connected timber elements. Other advantages include the possibility of in-situ implementing or possibility of direct connection of timber elements to steel and concrete structures. The most common thin-walled metal connector is steel angle with annular ring nails (see Fig. 1).

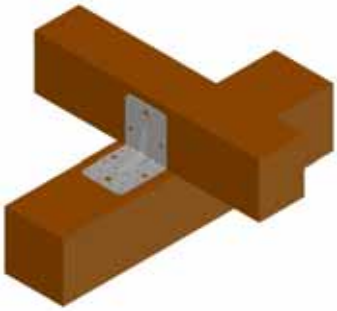

Fig. 1: Spatial joint by steel angle

2. Behavior of spatial connections by thin-walled metal elements

Connections by thin walled metal elements are very ductile. This is very favorable, because the over-loaded structure can be easily identified by eye. Load bearing capacity of these connections can be generally determined by three possible forms of collapse: failure of steel, splitting of timber caused by tension and failure of nails.

[1] Scientific assistant, CTU Prague, Czech Republic

[2] CTU Prague, Czech Republic

Nevertheless, it has been proved by experiment that the failure of nails is predominant. The splitting of timber element is eliminated by the check according to EC5 [1], which must be part of every static design. In addition, steel plates are punched to avoid inappropriate stresses.

3. Current support in Standards and the specialized literature

Eurocode 3 [2] contains the calculation procedure for steel membrane that can be used to determine the stresses in steel plate. There is also a table of minimum spacing and edge and end distances for nails.

The Structural Timber Education Program (STEP) [3] contains general knowledge about static schema of spatial joints by thin-walled metal elements and the example of calculation of end of the beam connection to main beam by U-lug.

The Technical Report 17 (TR17) [4] published by the European Organization for Technical Approvals (EOTA) contains the example of calculation of a spatial joint of timber elements by steel angle loaded in a direction that is opening to the angle. The load bearing capacity is determined according to the model, where the resisting features are two plastic hinges and a group of nails in tension, which is expressed by equation:

$$F_{\max} = \left[M_{purlin,k} + M_{beam,k} + k_{ax} F_{ax,k} \left(n \cdot x_y - \sum x \right) \right] / x_y \qquad (1)$$

$F_{\max}$	maximum force per angle bracket
$M_{purlin,k}$	moment capacity of the plastic hinge in the corner of the angle bracket
$M_{beam,k}$	moment capacity of the plastic hinge in the shoulder of the angle bracket
k_{ax}	efficiency factor for axially loaded nails
$F_{ax,k}$	withdrawal capacity of the used annular ring nail
n	number of efficient nails
x_x	position of plastic hinge in the shoulder of the angle bracket
$\sum x$	sum of coordinates of nails

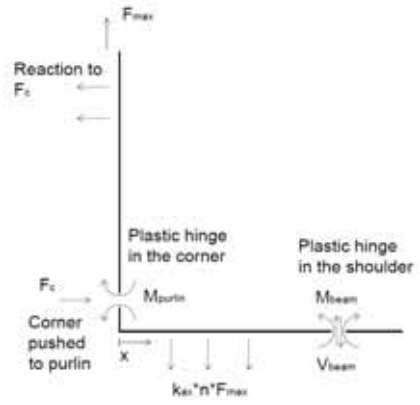

Fig. 2 Static schema of approach used in EOTA TR TR17

This approach is not only very simplified but also difficult to use. The first simplification is that the hinges are not linear. It is proved by experiment that their real shape is determined according to the rules of the path of least resistance. The

second simplification is that the secondary reinforcement of the nails due to prying of the nails is neglected. In addition, the third and the most important simplification is that there is neglected the dangerous influence of the pushing end of the angle bracket. This simplification is dangerous because the pushing end acts at the dangerous side of the calculation.

The main reason why this calculation is difficult to use is incalculable input data. The moment capacities and places of plastic hinges are determined experimentally. Withdrawal capacity of the used nail is not according to the Eurocode 5 [1] but according to the Danish timber code. Moreover, the number of efficient nails is determined without any explanation.

Given these reasons, one part of the author's research was to develop this calculation. This part is used as a model example to describe the whole research project.

4. Research at The Czech Technical University in Prague

The research is in cooperation with two companies: BOVA Březnice (Czech producer of thin-walled three-dimensional metal plates) and FINE (Czech software company, SW for civil engineers). The fundamental steps of the research are described as follows.

Optimization on 3D FEM models

To determine positions of the nails and shapes of the thin-walled steel elements, FEM models were made in Abaqus CAE. The model of the material of the steel element was elasto-plastic. Timber was simplified to elastic boundary conditions. In addition, nails were fixed by springs in tension; the reduced model was accurate enough.

Experiments

Full-scale experiments according to EOTA TR 16 [5] were made to determine experimental load bearing capacities of chosen angle brackets. Partial load bearing capacities were determined by two limits – collapse and maximal displacement of 15 mm. Each set of the experiments had 10 samples. Final characteristic load bearing capacities were firstly calculated according to EC0 [6] and then reduced according to EOTA TR 16 [5].

5. Methods and Prospects

Analysis of the experiments shows that the approach from EOTA TR17 [4] can be easily simplified. Plastic hinges can be placed to the corner of the rib and to the end of the rib. In addition, load distribution to the nails between the hinges can be conservatively set as being linear. Nevertheless, it is important to do more experiments so as for example to verify the check on the possibility of the rib to resist to the bending moment between the plastic hinges.

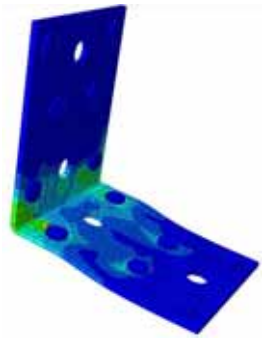

Fig. 3: Steel angle numerical model

Fig. 4: Spatial joint by steel angle loaded during experiment

6. Acknowledgement

This work has been supported by the European Union, OP RDI project No. CZ.1.05/2.1.00/03.0091 – University Centre for Energy Efficient Buildings. Experimental research was supported by a grant SGS13/171/OHK1/3T/11.

References

[1] EN 1995-1-1 Eurocode 5: *Design of Timber structures – Part 1-1: General – Common rules and rules for buildings.*

[2] EN 1993-1-1 Eurocode 3: *Design of steel structures – Part 1-1: General rules and rules for buildings.*

[3] Koželouh, B, *Dřevěné konstrukce podleEurokódu 5 – STEP1.* Zlín: KODR, 1998. ISBN 80-238-2620-4

[4] EOTA TR17: *Worked example calculation of characteristic load-carrying capacities of 90°angle bracket with a rib.* TECHNICAL REPORT 17, EUROPEAN ORGANISATION FOR TECHNICAL APPROVALS, Edition February 2002, Amended October 2012.

[5] EOTA TR16: *Method of testing Three-Dimensional Nailing Plates with examples.* TECHNICAL REPORT 16, EUROPEAN ORGANISATION FOR TECHNICAL APPROVALS, 2012.

[6] EN 1990 Eurocode 0: *Basis of structural design.* Ed. 2

Visco-elastic creep of dowel type timber connections

Daniel Brandon[1], Pete Walker[2], Richard Harris[2], Martin Ansell[2], Julie Bregulla[3]

Summary

This paper presents an experimental study of visco-elastic creep of dowel-type timber connections. It is widely known that timber can creep when loaded. In timber structures, connections often creep most, since stresses are locally higher than in other parts of the structure. In this study, the long-term behavior of dowels embedded in timber is introduced as a key property, required to determine the creep behavior of full connections. This embedment creep is determined experimentally for timber loaded in parallel and perpendicular to grain directions. The creep behavior of full connections is also experimentally determined with parallel and perpendicular to grain loaded connection tests. Regarding the full connection creep behavior, a comparative study is presented of non-metallic connections - comprised of FRP dowels and a hot-pressed plywood flitch plate - and conventional metallic flitch plate connections.

1. Introduction

It is well known that timber deforms (creeps) in time and a lot of research has been done on creep of beams. Significantly, less research has been done to creep of timber connections, while creep deformations in connections can be much larger, than those in beams. A better understanding of creep in timber connections is of main importance for new developments of timber frame structures. Creep tests take much space and time and are therefore expensive and rare. Only a limited number of full-scale connection creep tests are found in the literature. Results of these tests are dependent on a large number of factors including; the dimensions of the timber members, number of dowels, the type of dowels and the load to grain angle. In the

[1] PhD Candidate, University of Bath, United Kingdom

[2] BRE CICM, University of Bath, United Kingdom

[3] BRE, Watford, United Kingdom

present research, the embedment creep is introduced as the key property that can be used to predict the creep behavior of dowel type connections with different dimensions, number of dowels, type of dowels and load to grain angle.

2. Dowel embedment

Dowel embedment properties can be used to predict the capacity of a doweled connection using for example the European Yield Model EC5[1]. In addition, models to predict the stiffness of timber connections can be made using these properties [2,3]. Similarly, time dependent deformation (creep) can be determined using time dependent embedment responses. In this research, the time dependent behavior of dowel embedment is studied using a setup similar to a standard embedment test.

2.1 Standard embedment tests

Dowel embedment stiffness and embedment strength are commonly used to predict the behavior of dowel-type timber connections. Test methods to determine the embedment properties are given in the EN383 [4] and ASTM D5764 [5] standards. Santos et al. [6] showed with a large number of tests that the results for both standards are very similar. The differences in tests are mainly practical. Both configurations are shown in Fig.1. The test described in the ASTM D5764 standard requires a smaller sample and allows the measurement of displacement directly on top of the dowel without a correction for the dowel deformation.

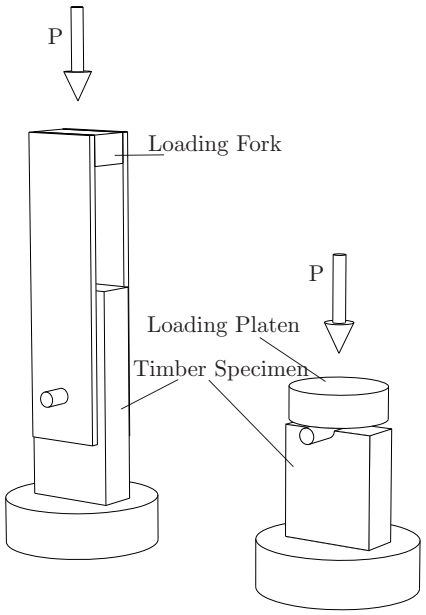

Fig. 1: Embedment test according to EN383 (left) & ASTM D5764 (right)

2.2 Creep embedment tests

For this research, long duration embedment tests were performed to obtain the embedment creep of dowels loaded parallel and perpendicular to the grain. The specimens were loaded at 20% and 40% of the embedment strength. Four samples were tested at each load level and load to grain angle.

Kerto-S laminated veneer lumber (LVL) was used, which shows less scatter in results than sawn timber. The creep test was performed at constant relative humidity of 60% ±3% and a constant temperature of 20°C ±2°C.

The test setup of the embedment creep test is shown in Fig.2 and is similar to the test described in ASTM D5764. Chains of embedment specimens are loaded in tension with a lever arm. The resulting tensile force compresses the 12.5mm dowels in the LVL samples. The embedment of the dowels in the LVL is measured directly on the dowel with dial gauges. The applied force is measured with a load cell at the top of the chain. This accounts for the loss due to friction in the hinge of the lever arm.

Fig. 2: Creep embedment tests

3. Full connection tests

In order to show the value of creep embedment properties, full connection tests were performed (Fig.3). Flitch plate connections were loaded parallel and perpendicular to the grain direction using a lever arm. The connection slip is measured with dial gauges and will be compared to a creep prediction model in future work. A comparison is made between a connection with a steel flitch plate and a 10mm steel dowel and a non-metallic connection with a hot-pressed plywood flitch plate and a 10mm glass fibre reinforced polymer (GFRP) dowel. The parallel to grain loaded connections carry a load of 2 kN, which is equal to 20% of the strength of the non-metallic connection. Similarly, the perpendicular to grain connections bears a load of 1.4 kN.

Fig. 3: Full connection creep tests

4. Future work

The experimental work is part of an ongoing study of the creep behavior of dowel-type timber connections. The tests started in December 2013 and will be continued for seven months. A temporary malfunction of the conditioning room, resulting in a change in relative humidity and hence the moisture content of the LVL, showed the significance of mechano-sorptive (moisture dependent) creep. A creep test under controlled humidity cycles will be performed to study the influence of the mechano-sorptive creep. In addition, a comparative study between visco-elastic and mechano-sorptive creep will be performed.

5. Acknowledgement

The support of the Building Research Establishment (BRE) TRUST is gratefully acknowledged.

References

[1] European Committee for Standardization CEN, EN 1995-1-1: Eurocode 5: Design of timber structures - Part 1-1: General - Common rules and rules for buildings, 2004, CEN, Bruxelles, Belgium.

[2] Cachim, P.B., Franssen, J.M., Numerical modeling of timber connections under fire loading using a component model. *Fire Safety Journal* 44, 840-853, 2009.

[3] Brandon, D., Ansell, M., Harris, R., Walker, P., Bregulla, J., Modelling of non-metallic timber connections at elevated temperatures. *Materials and Joints in Timber Structures*. 2013, Springer, Dordrech, The Netherlands.

[4] European Commision (1993) EN383, Timber structures. Tests methods. Determination of embedding strength and foundation values for dowel type fasteners. European standard, Bruxelles, Belgium.

[5] American Society of Mechanical Engineers (2002) ASTM D5764, Standard test method for evaluating dowel bearing strength of wood and wood-based products. Annual book of ATSM standards, Vol. 04.10., West Conshohocken, PA, United States of America.

[6] Forest Santos, C.L., De Jesus, A.M.P., Morais, J.J.L. & Lousada, J.L.P.C., A comparison between the EN 383 and ASTM D5764 test methods for dowel-bearing strength assessment of wood: Experimental and numerical investigations. *Strain,* 2010, 46, 159-174.

Glued-in rods in timber joints: Characterization of failure modes dependent on the test set-up

Michael Drass[1], Kay-Uwe Schober[2], Michael Kuechler[3]

Summary

This paper presents recent experimental investigations on the structural behavior of glued-in rods (GIR) using concrete-type adhesives. The aim of the research was the characterization of failure modes dependent on the test set-up. Two different types of timber specimen were tested under different support conditions.

1. Introduction

In the past years of GIR investigations, three different testing methods have been established to analyze the load-bearing behavior, which exhibit various advantages and disadvantages [1]. In this paper, two of these test setups will be analyzed more precisely to obtain advantages and disadvantages concerning the load-bearing behavior related to the chosen test setup. Furthermore, conventional casting compounds has been substituted using concrete-type adhesives (CTA), embedded in very large drill holes. The application of CTA within the bond lines is affiliated to the objective of optimizing the load carrying capacity of GIR under neglecting the in situ observable disadvantages concerning the preparation of GIR [2-4].

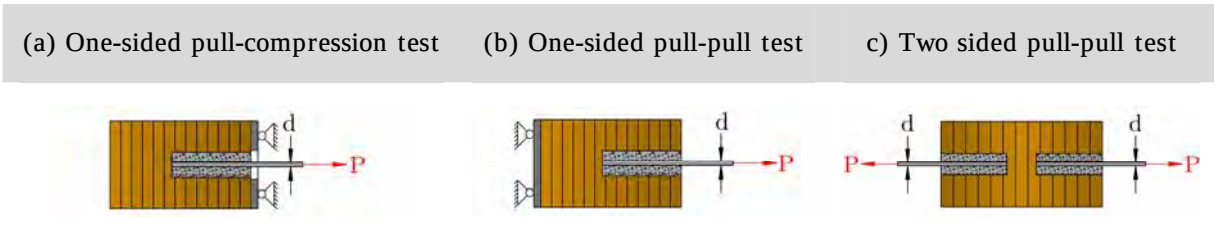

Fig. 1: Three types of testing methods for conventional Glued-in Rods (GIR)

[1] Research Associate, Mainz University of Applied Sciences, iS-mainz - Institute of Innovative Structures, Holzstr. 36, 55116 Mainz, Germany

[2] Professor of Timber Engineering and Structural Design, iS-mainz, Mainz, Germany

[3] Professor of Reconstruction in Civil Engineering, iS-mainz, Mainz, Germany

2. Experimental Investigations

In this chapter, the experimental investigations concerning GIR bonded with concrete-type adhesives will precisely constituted. Here, two different testing methods were performed to analyze correlation and deviations between both test set-ups. Furthermore, the chosen set-ups will be examined for bonding behavior and failure modes. The experimental investigations were performed with glued-laminated timber GL24h.

One-sided pull-compression test setup [2]	One-sided pull-pull test setup

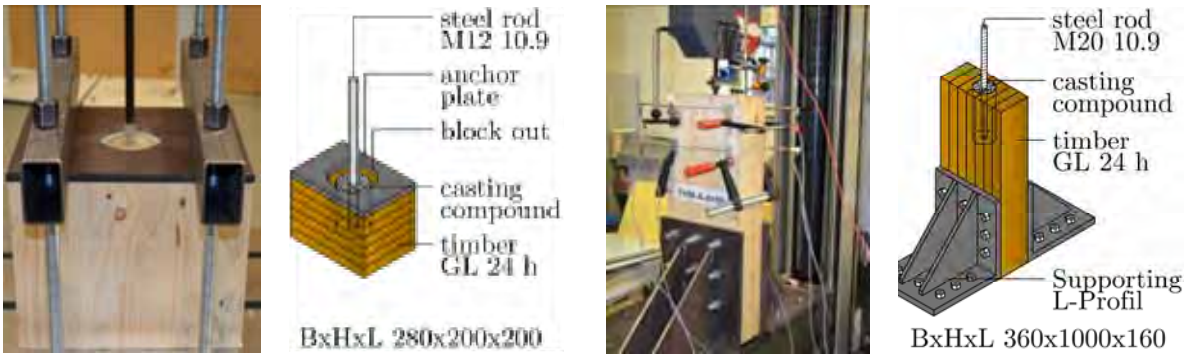

Fig. 2: Appliance of the test specimens

2.1 One-sided pull-compression testing method

For these tests a drill hole depth of $l_{bo} = 150$ mm and a steel rod diameter of $d = 12$ mm was chosen. The glued-in length was constrained to $l_{Bl} = 120$ mm. The load direction varied between parallel and perpendicular to the grain loading. In Fig. 2, the top-sided support and particularly the blocked-out steel plate are depicted, which provoke failure in the bond line. The experimental tests have been achieved by clamping the specimens after an equal setting time for all series in a special appliance to induce the fracture only in the adhesive bond line. The drill hole diameter amount to $d = 50$ mm and $d = 75$ mm, whereas the steel rod diameter was constraint to an amount of $d = 12$ mm (Fig. 2).

2.2 One-sided pull-pull testing method

Here, the drill hole length amount to $l_{Bl} = 250$ mm, while the drill hole diameter were varied from $d = 50$ mm till $d = 100$ mm. The steel rod was in accordance to a quality grade of 10.9 with a diameter of $d = 20$ mm. The bonding between the components was achieved using CTA. To ensure a stiff support of the test specimen, nine dowels

were connected with thick steel L-profiles, which were grouted, anchored to the ground. The specimen were stress-controlled prestressed to avoid slippage first, then strain-controlled loaded parallel to grain until the bearing load was reached.

2.3 Comparison of experimental investigations

In this chapter, a comparison concerning the failure modes and bonding behavior of the two analyzed test set-ups are discussed. Explicit differences of both test set-ups can be elaborated regarding the fracture pattern and especially the chronological load sequence.

With regard to the one-sided pull-compression test set-up, neither a ductile load bearing behavior nor fracture pattern within the CTA was observable, whereby a letter of indication of the collapse of the joint is obviated. The structural response was very consistent and stable, except small rigidity losses, which are caused by crack initiation and in CTA. With regard to the experimental results, it is conspicuous that in all specimens a brittle cohesive failure occurred when reaching the ultimate stresses along the bond line (loss of rigidity I). Unfortunately, the experiments with a drill hole diameter of $d = 75$ mm were cancelled at a load point of 100 kN, because the maximum tensile load of the testing machine was reached.

This failure mode is characterized by a glued joint cohesive failure, which is enforced by the supporting plate above the specimen. Hence, the crack path was systematically regulated through the chosen test set-up. The load-displacement behavior is linear-elastic till global failure occurs. To outline the negative aspects of the chosen test set-up, the support of the specimen has to be analyzed more precisely. Through the fact of supporting the test specimen in the area of the load application, constraint forces were generated. Out of this, compressive stresses arise along the bond line and especially along the GIR, which can erroneously increase the pull-out strength. Furthermore, frictional forces occur between the supporting steel plate and timber, which improve the load-carrying capacity of the test specimen. Especially the loaded area is statically enhanced due to the minimization of peel stresses within the bond line caused by compression forces occurring along the bond line.

In contrast to the above-discussed set-up, the one-sided pull-pull setup is characterized by three failure modes, which are conterminous with three steps of losing rigidity. The first loss of rigidity I is independent of the drill hole diameter and

appears at a specimen loading of 70-88 kN. Thereby, the crack propagation occurs in the instantaneous adjacency to the convolutions of the steel rod. When reaching the shear stiffness and shear strength of the CTA, small concrete brackets along the convolution are bending loaded, whereby a shear fracture process starts [5, 6]. After that, load redistributions occur, whereby the loading of the composite structure continues with loss of rigidity.

The second **loss of rigidity II** is characterized through a bidirectional disruption within the CTA cylinder. This fracture pattern starts with the occurrence of micro-cracks near the steel rod, which regroup to near-surface macro-cracks under a constant rate of loading. At this particular time the actual failure of the composite structure begin, which is conterminous with the third **loss of rigidity III**. Within this test set-up, constraint forces can be neglected, so that lateral strains can unconstraint occur, whereby the processes along the bond line can be better analyzed.

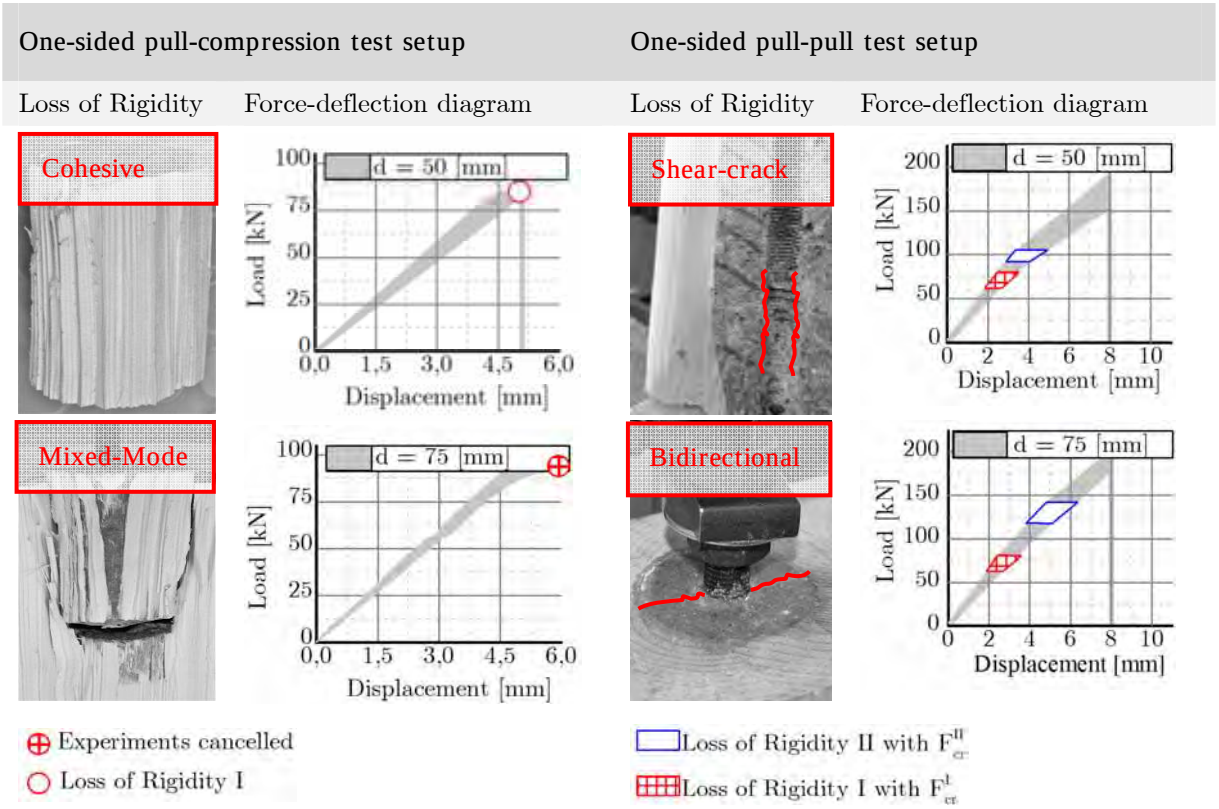

Fig. 3: Characteristic failure modes and force-displacement diagrams of both test setups

Fig. 3 shows the characteristic failure modes as well as the force-displacement behavior of both experimental test set-ups. For the one-sided pull-compression tests, the **loss of rigidity I** is conterminous with global failure of the test specimen, whereas the one-sided pull-pull test is characterized through **two characteristic rigidity-losses**, which result into a global failure after further loading of the specimens.

3. Results

The significant differences within the failure modes, which have a constitutive influence on the load bearing behavior as well as the bearing load, are occasioned through the fact of a constraint / unconstraint loading near the area of the load application. With regard to the one-sided pull-pull test, which is conspicuous through an unconstraint loading, the load-bearing behavior is totally different characterized in comparison to the one-sided pull-compression tests. Therefore, it is of importance to make preliminary consideration concerning the test set-up, expected failure modes and bearing loads, before testing GIR. Particularly, in this case under modifying the geometrical boundary conditions of conventional GIR, the conventional test setups should be reflective adapted. Hence, the experimental design and analysis should be carefully estimated accounting a realistic load bearing behavior.

References

[1] Tlustochowicz, G., Serrano, E. & Steiger, R. (2010). State-of-the-art review on timber connections with glued-in steel rods.

[2] Schober, K.U., Becker, W. & Drass, M. (2012). Advanced interface interaction in timber engineering joints with dowel-type fasteners embedded in high-performance ceramic fillers. *Proceedings of the 12th World Conference on Timber Engineering (WCTE 2012)*, Auckland, New Zealand, 2012.

[3] Schober, K.U., Drass, M. & Becker, W. (2013). Adhesive strength of timber joints with unconventional glued-in rods. *Proceedings of Wood Adhesives 2013*, Toronto, ON, Canada.

[4] Schober, K.U. & Drass, M. (2013). Concrete-based adhesives used in connections. Enhance mechanical properties of timber, engineered wood products and timber structures - COST FP1004 ESR conference Nicosia, Cyprus, Schober, K.U. (ed.), Bath, United Kingdom, 8-11. ISBN 1-85790-178-9, 2013.

[5] Lettow, S. (2006). Ein Verbundelement für nichtlineare Finite Element Analysen - Anwendung auf Übergreifungsstöße. Stuttgart.

[6] Wildermuth, A. (2012). Untersuchungen zum Verbund-verhalten von Bewehrungsstäben mittels vereinfachter Versuchskörper. Institut für Werkstoffe im Bauwesen, Stuttgart.

Strength of glued-in rods under combined axial and lateral loading

James Walker[1], Robert Xiao[2]

Summary

Glued-in rod connections are normally designed to resist axial loads only. When subjected to axial and lateral loading, experimental tests show a rapid reduction in the strength of glued-in rod connections as the proportion of lateral load is increased. A modified Hankinson's equation, including the dowel action of the rod, is used to model the load at failure of the connection under combined axial and lateral loading.

1. Introduction

Glued-in rods have been used as a method of connecting timber elements since the 1970s, yet design guidelines are generally only available for single rods loaded axially. With a view to designing moment resisting portal frame connections, the failure load of glued-in rods under combined axial and lateral loading is required.

2. Experimental Studies

2.1 Axial Load Tests

Rod pull out tests were carried out using M12 threaded steel rods (grade 8.8) bonded into Laminated Veneer Lumber (LVL) using three different anchorage lengths. Fig. 1 shows the load at failure of the glued-in rod connection compared to predicted strength values calculated using different design equations [1][2][3][4].

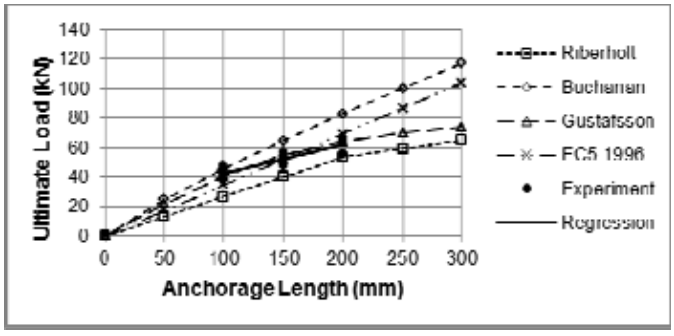

Fig. 1: Ultimate pull out load of axially loaded glued-in rods with increasing anchorage length.

Although there is generally a good agreement between the experimental and theoretical results, there is a large spread in the predicted strength values between the different design equations.

2.2 Combined Axial and Lateral Load Tests

To introduce lateral loading into the glued-in rod connection, steel rods were bent to angles (θ) ranging from 5° to 45° using an anchorage length of 100 mm in all cases. The embedded end of the bent rod was aligned with the grain, and a larger diameter reaction rod was axially aligned with the protruding length of the bent rod. Fig. 2 shows the arrangement of the experimental test specimens.

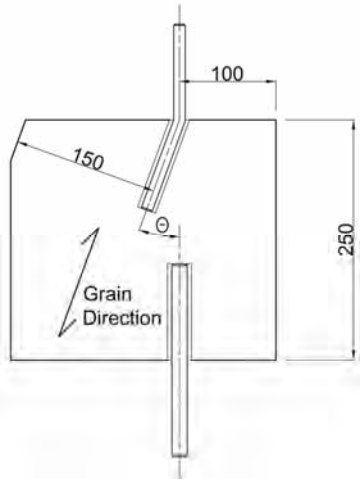

Fig. 2: Layout of angled pull out test specimen

Large reductions in the strength of the connection were observed with a relatively low proportion of lateral load. The introduction of lateral loading into the glued-in rod connection produces tension perpendicular to the grain and the failure mode of the connection changes from brittle in-plane shear fracture (Mode II) of the timber to a more progressive failure, commencing with a tensile fracture of the timber (Mode I) followed by an out of plane shear fracture (Mode III). Fig. 3 shows the progressive failure of the glued-in rod connection when the angle of the applied load (θ) to the embedded rod axis was 20°.

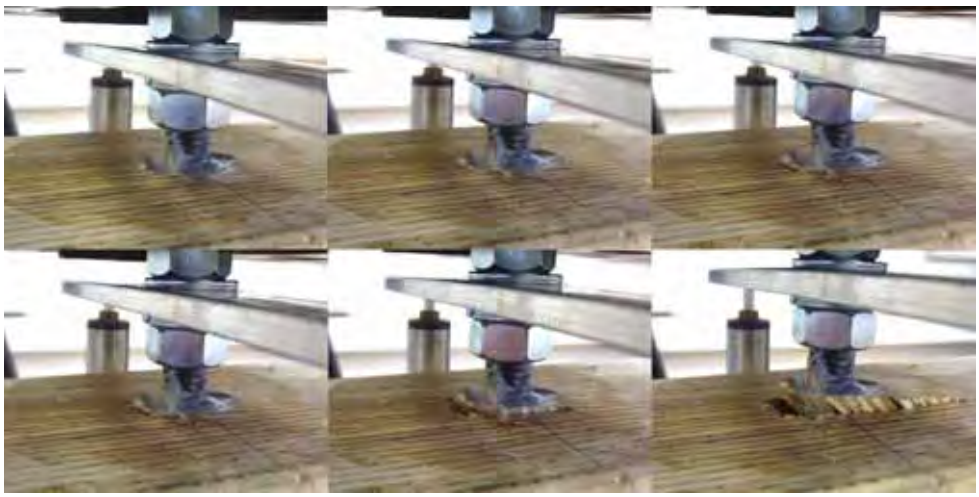

Fig. 3: Angled rod failure mechanism at 20°

3. Theoretical Model

The reduction in the ultimate load of the connection with varying angle of load resembles the relationship proposed by Hankinson [5], to predict the compressive strength of timber at various angles to the grain. Fig. 4 shows the results of the experimental testing along with a theoretical model (Eqn. 1.1) to predict the failure of glued-in rod connections by combining a Hankinson type trigonometric equation (Eqn. 1.2) for the axial load contribution and Johansen's equation [6] for the lateral load contribution of the equivalent dowel (Eqn. 1.3).

$$F_{\theta} = F_{ax,\theta} + F_{v,\theta} \qquad (1.1)$$

$$F_{ax,\theta} = \frac{F_{ax,0}}{k_{\theta} \sin^2 \theta + \cos^2 \theta} \qquad (1.2)$$

$$F_{v,\theta} = F_{v,90} \sin \theta \qquad (1.3)$$

θ = Angle of load to grain direction

F_{θ} = Load capacity at load angle θ

$F_{ax,\theta}$ = Axial load component

$F_{v,\theta}$ = lateral load component

$F_{ax,0}$ = Axial load capacity of connection

$F_{v,90}$ = Lateral load capacity of connection

k_{θ} = Axial strength reduction factor

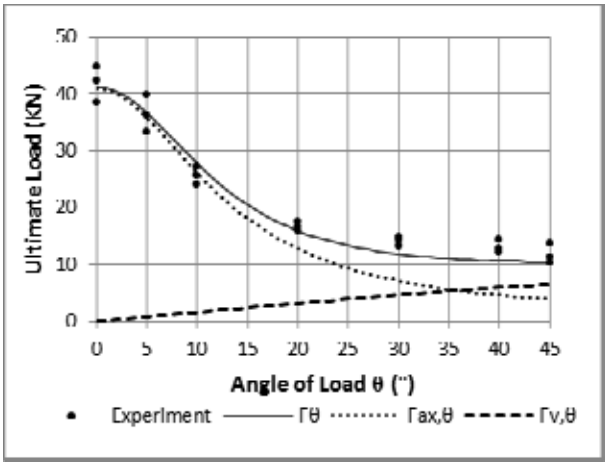

Fig. 4: Ultimate load as angle of load is varied

The experimental arrangement allowed testing at angles of load up to 45°, so it was not possible to test the strength of the connection under pure lateral loading ($F_{v,90}$). The embedment strength is required to predict the lateral load capacity of a dowel type connection for which there exist many equations when the dowel is aligned perpendicular to the grain, but there is limited guidance when the dowel is aligned with the grain. An equation [7] based on the equivalent doweled connection is given to calculate the lateral load carrying capacity of a glued-in rod inserted into end grain. Other studies [8] show that the embedment strength of a dowel aligned with the grain has approximately 40% of the embedment strength of the same dowel perpendicular to the grain. Some design codes [9] provide a modification factor to decrease the lateral load capacity of a dowel type fastener aligned with the grain to 0.67 times the value of the fastener aligned perpendicular to grain. These different methods predict the lateral load capacity of an M12 threaded rod glued into the end grain of LVL to be 6.7 - 9.3kN.

The rate at which the axial contribution to the connection strength decreases with angle of load is controlled by the parameter k_θ, which is influenced by the ratio of tensile and compressive strength parallel and perpendicular to the grain, due to the changing failure mechanism. For Kerto-S LVL, the ratio of compressive strengths is 10 and the ratio of tensile strengths is 44. For softwoods (C16 - C50) the ratio of compressive strengths is between 8 and 9, while the ratio of tensile strengths varies between 10 and 75. For the purposes of this study, k_θ is taken to be 20. However, further work must be undertaken to define this parameter more generally.

EC5 defines a failure envelope for dowel type connections under combined axial and lateral load by the following elliptic equation:

$$\left(\frac{F_{ax,Ed}}{F_{ax,Rd}}\right)^2 + \left(\frac{F_{v,Ed}}{F_{v,Rd}}\right)^2 \leq 1 \qquad (2)$$

The failure envelope of a glued in rod connection under combined axial and lateral loading can be described using equation 1.

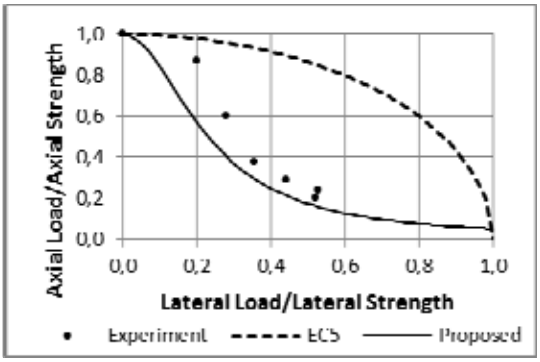

Fig. 5: Combined loading failure envelope

4. Conclusion

Experimental testing shows that the strength of glued-in rod connections subjected to combined axial and lateral load is significantly reduced as the proportion of lateral loading increases. A design equation has been presented to predict the ultimate load capacity of a glued in rod connection subjected to combined loading.

References

[1] Riberholt H, Glued bolts in Glulam, *Technical University of Denmark Series R No. 210*, 1986.

[2] Gustafsson et al, A strength design equation for glued-in-rods, *Proceedings of the International RILEM Symposium on Joints in Timber Structures,* 2000, Stuttgart, Germany.

[3] Buchanan AH, Deng XJ, Strength of epoxied steel rods in glulam timber. *Proceedings of International Wood Engineering Conference, IWEC,* 1996, New Orleans.

[4] European Committee for Standardization CEN, EN 1995-1-1: Eurocode 5: Design of timber structures - Part 2: Bridges, 1996, *CEN*, Bruxelles, Belgium

[5] Hankinson RL, Investigation of crushing strength of spruce at varying angles of grain, *Air Force Information Circular No. 259,* 1921, U. S. Air Service

[6] Johansen KW, Theory of Timber Connections, *International Association for Bridge and Structural Engineering, No. 48,* 1949.

[7] IStuctE, Manual for the design of timber building structures to Eurocode 5, *TRADA*, 2007.

[8] Blaß HJ, Advances in self-tapping screws and hidden fastener connections, *Proceedings of the International RILEM Symposium on Materials and Joints in Timber Structures,* 2013, Stuttgart, Germany.

[9] National Design Specification for Wood Construction, *American Wood Council*, 2012.

Traditional timber carpentry joints: monotonic tests and modeling

Artur O. Feio[1], José S. Machado[2]

Summary

The structural safety and behavior of traditional timber structures depends significantly on the performance of their connections. The behavior of a traditional mortise and tenon timber joint is addressed using physical testing of full-scale specimens. New chestnut wood and old chestnut wood obtained from structural elements belonging to ancient buildings is used. In addition, nonlinear finite element analysis is used to better understand the behavior observed in the full-scale experiments, in terms of failure mode and ultimate load.

The results show that the failure mechanism and load-displacement diagrams observed in the experiments are well captured by the proposed non-linear finite element analysis, and the parameters that affect mostly the ultimate load of the timber joint are the compressive strength of wood perpendicular to the grain and the normal stiffness of the interface elements representing the contact between rafter and brace.

1. Introduction

In the past, timber structural design was dominated by carpenter know-how, resulting from tradition and empirical knowledge. With respect to traditional wood-wood joints, rules-of-thumb dominated the technology and the present knowledge is still rather limited. In the present work, a mortise and tenon joint, see Fig. 1, was selected because it is one of the most commonly

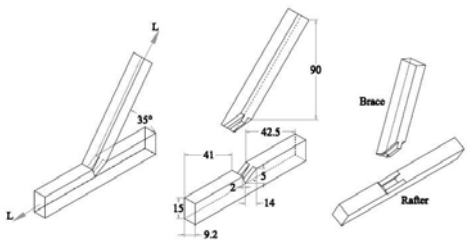

Fig. 1: Details of a typical tenon and mortise joint, geometry adopted in testing program (in mm)

[1] Auxiliary Professor, Faculty of Architecture, University Lusíada, Portugal

[2] Research Officer, National Laboratory for Civil Engineering, Timber Structures Division, Portugal

used in ancient timber structures and a typical example of an interlocking joint, forming usually an “L” or “T” type configuration. The key problem found in these joints is the possible premature failure induced in the structure caused by large displacements in the joint.

The bearing capacity of mortise and tenon joints is a function of the angle of the connection, and length of the toe and mortise depth. The lack of knowledge about this particular joint is determinant in the assessment of the load carrying capacity of existing wooden structures. Here, the objectives are to quantify the strength capacity of the joint by physical testing of full-scale specimens and to validate the adequacy of an anisotropic failure criterion to represent the behavior of the joint by the comparison between experimental and numerical results.

The finite element method is adopted to simulate the structural behavior and obtain a better understanding of the failure process observed in experimental tests. Calculations are performed using a plane stress continuum model and the failure criterion is based on multi-surface plasticity. Using the finite element model, the influence of compression perpendicular to the grain and elastic stiffness on the response is addressed in detail.

2. Experimental Program

2.1 Description of test specimens

Chestnut wood (*Castanea sativa* Mill.) is usually present in historical Portuguese buildings and all the wood used in the test specimens came from the North of Portugal. In order to assess the influence of service time in the response, two groups were considered: New Chestnut Wood (NCW), obtained from recently sawn timber, and Old Chestnut Wood (OCW), obtained from structural elements belonging to ancient buildings (date and precise origin unknown) with unknown load history. The old logs were obtained from rehabilitation works and were provided by a specialist contractor claiming that the wood has been in service for over 100 years.

2.2 Ultimate force and failure patterns

Table 1 shows the results of the tests in terms of ultimate force (ranging between 121.6 kN up and 161.5 kN). Even if the number of specimens is rather low, the average force in terms of groups NCW and OCW exhibits only a marginal difference.

The compressive damage in the brace occurred either localized at the toe or distributed along the full contact length. Often, out-of-plane bulging of the rafter under the contact length was observed. In some cases, compressive damage was accompanied with shear failure in the rafter in front of the toe. Fig. 2 illustrates the typical damages observed at ultimate load. The specimens were produced avoiding the presence of large defects although accepting small defects.

(a)  (b)  (c) 

Fig. 2: Experimental failure patterns observed:
(a) joint collapsed in compression, with uniform distribution of damage,
(b) joint collapsed in compression, with out-of-plane bulging, and
(c) combined failure in compression and shear parallel to the grain at the toe

2.3 Load-displacement diagrams

The envelope of all tests in terms of load-displacement diagrams is given in Fig. 3. In a first phase, the diagrams exhibit a nonlinear response, which is due to the adjustment of the tenon and the mortise. It is noted that unloading-reloading cycles within working stress levels provide a constant stiffness, which is higher than the loading stiffness.

The justification of this behavior is attributed to the nonlinear behavior of the interface between rafter and brace, which exhibits a closure phenomenon. Finally, after the ultimate force the displacement increases rapidly with a much lower stiffness, due essentially to the compressive failure of the wood in the rafter around the joint.

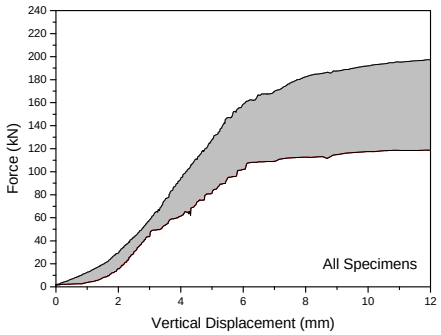

Fig. 3: Envelope of load-absolute displacement of the brace diagrams

3. Numerical Simulation

In order to further discuss the experimental results, a finite element simulation of the tests has been carried out and continuum quadratic elements (8-noded) were used to represent the wood and to represent the line interface between rafter and brace quadratic elements (6-noded) were used.

The integration schemes used are 2x2 Gauss integration points for the continuum elements and 3 Lobatto integration points for the interface elements. The simulations have been carried out using a globally convergent solution process, combining a Newton-Raphson method with arc-length and line search. The adopted failure criterion for wood consists of an extension of conventional formulations for isotropic quasi-brittle materials to describe orthotropic behavior. It is based on multi-surface plasticity, including a Hill yield criterion for compression and a Rankine yield criterion for tension, and having different strengths in the directions parallel and perpendicular to the grain, see Lourenço *et al.* (1997) for details.

In the present case, the tensile part of the yield criterion was ignored due to the irrelevant contribution of the tensile strength in the global behavior of the joint. This means that the yield surface reduces to the standard Hill criterion in compression. The adopted elastic and inelastic materials properties are detailed in Table 2 and have been obtained from a testing program aiming at characterizing chestnut, see Lourenço *et al.* (2007) and Feio (2006).

Tab. 1: Test results: ultimate force properties

	Ult. Force (kN)	Average	Std. Dev.	Group
J_1	121.6	145.4		NCW
J_2	161.5			
J_3	159.7			
J_4	138.9			
J_5	126.4	145.5	16.7	OCW
J_6	157.1			
J_8	153.0			

Tab. 2: Adopted elastic and inelastic material

E_x	E_y	G_{xy}	υ_{xy}
800 MPa	8500 MPa	1500 MPa	0.3
$f_{c,x}$	$f_{c,y}$	β	γ
7 MPa	45 MPa	-1.0	3.0

3.1 Numerical vs. experimental results

A structured mesh is used for the rafter and the brace, whereas an irregular transition mesh is used in the vicinity of the connection between rafter and brace. Interface elements are also used between the rafter and the brace. The thickness ranges 62-93 mm, shown in Fig.4. This aims at representing the thickness of the mortise.

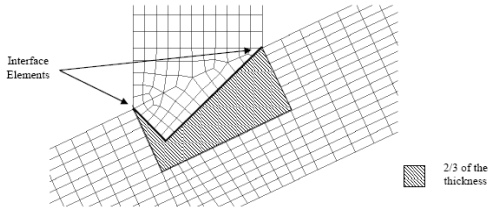

Fig. 4: Localization of the interface elements

The comparison between numerical and experimental load-displacement diagrams is given in Fig. 5.

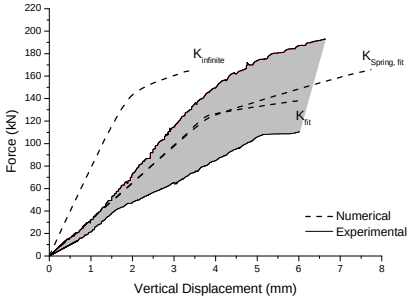

Fig. 5: Comparison between numerical and experimental load-displacement diagrams

A first conclusion is that the stiffness of the interface elements has considerable influence on the yield strength of timber joints. In Fig. 5, three distinct situations are presented:

- a numerical simulation with infinite stiffness of the interface elements in the normal direction, *kn*, and shear direction, *ks* ($k_{\text{infinite}} = k_n = k_s = 10^9\,\text{N/mm}^3$);
- a numerical simulation with an adjusted stiffness of the interface elements obtained by inverse fitting of the experimental results (*kfit*), assuming that the shear and normal stiffness are related via the Poisson's coefficient ν by $k_s = k_n / 2 / (1+v)$; $k_n = 6000\,\text{N/mm}^3$ and $k_s = 2308\,\text{N/mm}^3$;
- a numerical simulation with a spring ($k_{spring} = 10^6$ N/m) located in the brace to simulate the reaction cell used in the experimental sets. The stiffness of the spring was again obtained by inverse fitting of the experimental results, keeping the adjusted stiffness of the interface elements.

The numerical results, in terms of force-displacement diagrams, with the adjusted stiffness for the interface elements, provide very good agreement with the experimental results both in the linear and nonlinear parts.

A more relevant conclusion is that the usage of infinite stiffness for the interface (rigid joint) results in an increase of the slope of the first part of the response, from

30 kN/mm to 80 kN/mm (+ 266.7%). The ultimate force of the joint, given by an offset of the linear stretch by 2% in terms of strain values, also changes from 130 kN to 152 kN (+ 17%), once the joint becomes fully rigid.

Fig. 6 shows the contour of minimum principal stresses at ultimate load. It is possible to observe a concentration of stresses in a narrower band with peak stresses at the joint (zone where the interface elements were placed), upon increasing loading. As observed in the experiments, failure is governed by wood crushing, being the compressive strength of the wood, in the direction perpendicular to the joint, exhausted at failure.

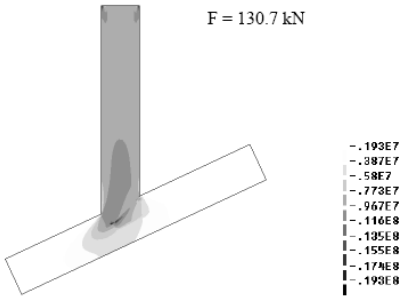

Fig. 6: Minimum principal stresses (values in N/m²) at ultimate load

4. Sensitivity study

A strong benefit of using numerical simulations is that parametric studies can be easily carried out and the sensitivity of the response to the material parameters can be easily evaluated. This allows a better understanding of the structural response.

The influence of the key parameters of the model in the response will be analyzed separately. The values k_n (normal stiffness of the interface), k_s (tangent stiffness of the interface), E_x and E_y (Young's moduli in the directions parallel and perpendicular to the grain, respectively) are assumed to be less well known and variations of 50% and 100% are made. f_x and f_y (compressive strengths in the directions parallel and perpendicular to the grain, respectively) are assumed to be well known and variations of +25% and -25% are made, corresponding to 0.75 and 1.25 times the initial value.

4.1 Normal and tangential stiffness of the interface

Fig. 7a shows a comparison between the results of the variation of the normal joint stiffness: with a reduction of 50% in k_n, the ultimate force of the joint, given by an offset of the linear stretch by 2%, decreases from 127.2 kN to 120 kN (-6%).

Multiplying k_n by a factor of 2 the ultimate force of the joint, given by an offset of the linear stretch by 2%, increases from 127.2 kN to 135.0 kN (+7%).

The reduction/increase of the normal stiffness of the interface also affects the global stiffness of the joint; the global stiffness of the joint decreases as the normal stiffness of the interface decreases, being more sensitive to this variation when compared with the ultimate force. The reduction of 50% of the k_n parameter, results in a decrease of the slope of the first part of the response, from 32 kN/mm to 26 kN/mm (-23%). On the other hand, the multiplication by a factor of 2 of this parameter results in an increase of the slope of the first part of the response, from 32 kN/mm to 41 kN/mm (+ 28%).

Fig. 7b shows a comparison between the results of the variation of the k_s parameter. The ultimate force is insensitive to a k_s variation, whereas the reduction/increase of the k_s parameter affects the global stiffness of the joint: the global stiffness of the joint decreases as the k_s parameter decreases.

The reduction of 50% of the k_s parameter, results in a decrease of the slope of the first part of the response, from 32 kN/mm to 28 kN/mm (-14%). On the other hand, the multiplication by a factor of 2 of this parameter results in an increase of the slope of the first part of the response, from 32 kN/mm to 37 kN/mm (+16%).

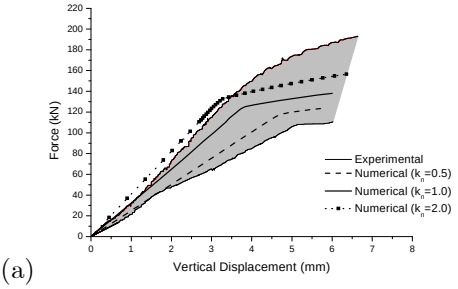

(a)

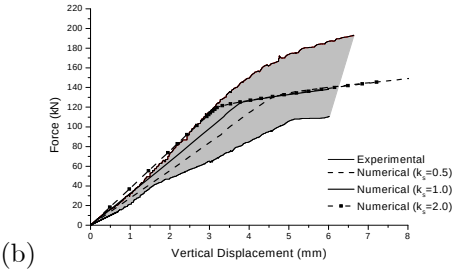

(b)

Fig. 7: Effect of the variation of parameter: (a) k_n, and (b) k_s on the model response

4.2 Elastic modulus

The effect of the variation of the modulus of elasticity parallel and perpendicular to the grain was considered individually. The ultimate force is almost insensitive to the variation of the elastic modulus for wood (± 4%), in both considered directions. The inclusion of the effects of the elastic modulus does change significantly the elastic stiffness of the joint.

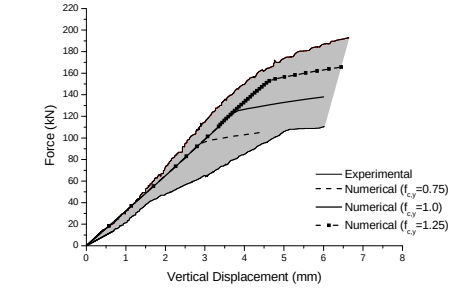

Fig. 8: Effect of the variation of parameter k_s on the model response

4.3 Compressive strength

The ultimate force and the global stiffness of the joint are insensitive to the variation of the compressive strength of wood in the direction parallel to the grain. Fig. 8 indicates the sensitivity of the ultimate force of the joint to the variation of the compressive strength of wood in direction perpendicular to the grain, as expected: with a reduction of 0,75, the ultimate force of the joint, given by an offset of the linear stretch by 2‰, decreases from 130 kN to 100 kN (-30%); multiplying by a factor of 1.25 the ultimate force of the joint, given by an offset of the linear stretch by 2‰, increases from 130 kN to 160 kN (+23%). However, the global stiffness of the joint is insensitive to the variation of the compressive strength perp. to the grain.

5. Conclusions

Despite the wide use of mortise and tenon joints in existing timber structures scarce information is available for design and in situ assessment. The objective of the present study was to quantify the strength capacity of a wood-wood mortise and tenon joint by physical testing of full-scale specimens. In addition, the adequacy of an anisotropic failure criterion to represents the behavior of a traditional mortise and tenon joint was assessed from the comparison between experimental and numerical results.

Two different wood groups have been used, one from new logs and another one from old logs (date, precise origin and load history unknown). Reducing the defects to a minimum, no influence could be attributed to service time. Thus, safety assessment of new timber structures, made from old or new wood elements, can be made using similar mechanical data.

The failure mechanism and load-displacement diagrams observed in the experiments are well captured by the used non-linear finite element analysis. Nevertheless, the normal stiffness of the interface has considerable influence in the yield strength and deformation of timber joints. The parameters that affect mostly the ultimate load of the timber joint are the compressive strength of wood perpendicular to the grain and the normal stiffness of the interface elements representing the contact between rafter and brace. The tangential stiffness of the interface and the Young's moduli of wood have only very limited influence in the response. The compressive strength of wood parallel to the grain has no influence in the response.

References

[1] CEN, *EN 26891 – Timber structures. Joints made with mechanical fasteners general principles for the determination of strength and deformation characteristics*. European Committee for Standardization, Brussels, Belgium, 1991.

[2] CEN, *EN 408 – Timber structures. Structural timber and glued laminated timber. Determination of some physical and mechanical properties*. European Committee for Standardization, Brussels, Belgium, 2003.

[3] Eckelman, C., Haviarova, E., Rectangular mortise and tenon semirigid joint connection factors. *Forest Products Journal*, 58(12), pp. 49-55, 2008.

[4] Feio, A., Inspection and diagnosis of historical timber structures: NDT correlations and structural behaviour, *PhD Thesis, University of Minho, Portugal*. from www.civil.uminho.pt/masonry, 2006.

[5] Lourenço, P., De Borst, R., Rots, J., A plane stress softening plasticity model for orthotropic materials, *Int. J. Numerical Methods in Engineering*, 40, p. 4033-4057, 1997.

[6] Palma, P., Cruz, H. (2007), Mechanical behaviour of traditional timber carpentry joints in service conditions - results of monotonic tests. In From material to Structure – Mechanical behaviour and failures of the timber structures XVI International Symposium, Venice, Italy. ICOMOS IWC.

Development of a structural insulated panel (SIP) with wood-based material

Laurent Léoskool[1], Thierry Descamps[2]

Summary

Structural insulated panel (SIP) is mainly used in North America. It is composed of rigid foam plastic insulation glued between two structural skins of wood-based material. These panels are able to bear loads for residential buildings and are used for walls, floors and roofs. The development of a new SIP is studied. The skins are composed of cross-laminated timber (CLT) and the insulation is non-rigid. The mechanical behavior is preserved thanks to inclined screws that join the wood panels. This new product presents advantages: it could be used for bigger buildings; it could improve the CLT construction by a higher level of prefabrication and a reduction of the wood consumption. In order to understand the mechanical behavior of this new product, experimental and numerical studies are carried out. The embedment strength of the CLT is measured. These experimentations allow showing the importance of the crossed and glued laminated boards. Different types of panel assemblies are made, their load bearing capacity and their failure mode are presented. As predicted, the screwing angle turns out to be important. The load bearing capacity can be changed by a factor of three and the failure can be ductile or brittle depending on the case.

1. Introduction

Experimental and numerical campaigns are in progress in order to determine the mechanical behavior locally. CLT panels of a thickness of 57 millimeters and WR-T 13 screws are used. The distance between the panels is determined to respond to the passive standards in Belgium (thermal transmittance lower than 0,15W/m²K). In order to compare the results with the Johansen's equations, other models are also

[1] PhD Student, Civil Engineering and Structural Mechanics Dpt., University of Mons, Belgium

[2] Civil Engineering and Structural Mechanics Dpt., University of Mons, Belgium

made without gap and with a thin gap of 18mm (suppression of the effects due to friction). This paper will present a brief part of these experimentations and present the context of this research.

2. Structural insulated panels

Structural insulated panel (SIP) is mainly used in North America. It is composed of rigid foam plastic insulation glued between two structural skins (see Fig.1). In most cases, the insulation consists of polystyrene, polyurethane or polyisocyanurate and the boards consist of oriented strand board (OSB) or plywood. These kinds of panels are able to bear loads for residential buildings and are used for walls, floors and roofs. Except some difficulties to minimize thermal bridging, it presents a lot of pros like the rapidity of erection (due to a high level of prefabrication) and the low weight and the few materials used.

Fig. 1: Structural insulated panel, Normanton Laminating Serv. LTD

3. Cross-laminated timber

CLT appeared in the industry in the 2000 s. It is a panel composed of 3, 5 or 7 layers (sometimes more) of sawn timber. Every layer is crossed and consists of small planks that are generally glued together (similar to glulam). Some elements are mechanically joined by aluminum nails instead of glue. The so created panel can have dimensions reaching 24 m length and 3,5 m wide, the thickness varying generally between 6 to 30 cm. Elements are completely custom-made by CNC machines (doors, windows, sometimes electricity…) and assembled to each other on site. The assemblies are generally made by screws and metal brackets. Plywood strips (Kerto) are sometimes used to connect panels in the same plane.

The principal advantages of CLT are the good resistance to fire, the good acoustic and vibratory properties and the creation of a panel less anisotropic and less fragile than wood (reducing the effect of knots, etc.).

4. Development of a new SIP based on CLT

The development of a new SIP is studied at the University of Mons, Belgium. The skins are composed of cross-laminated timber (CLT) and the insulation is non-rigid. By the way, it is possible to use eco-friendly insulation like wood wool. The mechanical behavior is preserved thanks to inclined screws that join the wood panels (see Fig.2). If the amount of connections is sufficient, the new SIP can be mechanically compared to an I-beam where the CLT panels have the function of the flanges and the screws have the function of the web. This new product presents two main advantages. Firstly, it offers a SIP that could be used for bigger buildings and could respond to higher loads. Secondly, it could improve the CLT construction by a higher level of prefabrication (insulation is no longer installed on-site) and a reduction of the wood consumption. In order to understand the mechanical behavior of this new product, experimental and numerical studies are done. The embedment strength of the CLT is measured and compared to the formula given for solid timber. These experimentations allow showing the importance of the crossed and glued laminated boards.

Fig. 2: Structural insulated panel composed of cross-laminated timber

Different types of panel assemblies are made: without a gap between the panels and with gaps of 18 mm (experimental research in progress with gaps of 23 cm). Rapidly, the first category has been dismissed. These assemblies present a higher rigidity due to the friction between the panels and due to the compression, which could appear between them, parameters that will not be present subsequently. For the moment, the screws are placed with angles of -30°, 0° and 30° with regard to the perpendicular of the panels. The negative (positive) sign signifies that the screws are solicited by a combination of shear stress and compressive (tension) stress.

5. Experimental results

CLT panels used for these experimentations are made by KLH. They are composed of 3 plies of Norway Spruce and they have a thickness of 57 mm. Each ply has a C24 strength class. The embedment strength of the panel has been measured thanks to the European Standard EN 383:2007 [2] considering an imbedding in parallel with the external plies. The mean value of the embedment strength is worth 26 N/mm². First

results on panels with gaps of 18mm have shown different kinds of failure mode. When the screws are solicited by compressive and shear stress (Fig. 3, left), the ruin is due to the appearance of plastic hinges in the external panels (Fig. 3, centre). The load bearing capacity per screw approximately equals to 5.5 kN at the ultimate limit state, as it can be seen in graph 1.

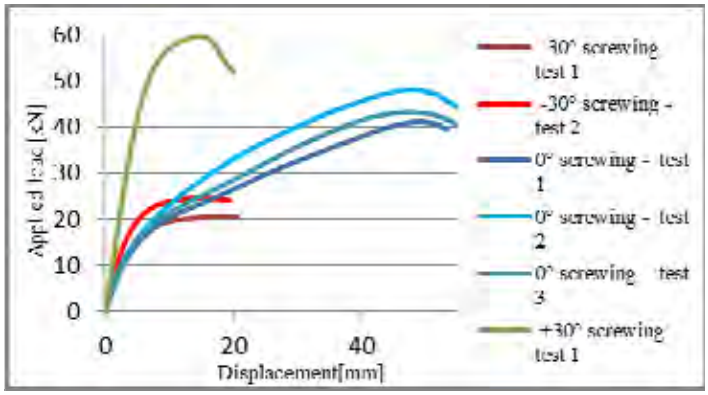

Graph. 1: Experimental results for panel assemblies with a gap of 18 mm, values given for 4 screws in simple shear

Perpendicularly screwed assemblies show two successive mechanical behaviors. Firstly, plastic hinges appear as for compressive elements and for a similar load. Then the assemblies continue to resist thanks to the appearance of a rope effect in the screws. The ruin is due to the withdrawal capacity of the middle panel and appears for a load of approximately 10.5 kN per screw. Considering the measured value of the embedment strength, Johansen's equations also give us a load bearing capacity of 10.5 kN and a failure mode with embedment of the wood [1]. This shows us that these equations remain valid for the cross-laminated timber.

Fig. 3 Experiments for panels with 18mm gaps:
panels screwed with an angle of -30° (left)
and presence of a plastic hinge on the right after test (centre),
panelsscrewed with an angle of +30°(right)

For the screws solicited by tension and shear stress (Fig. 3, right), the load bearing capacity per screw is equal to 15 kN. At this value, the withdrawal capacity of the wood is reached in the middle panel and a brittle failure occurs.

6. Numerical studies

Finite element models have been established in order to approach the experimental results as close as possible. The software used is Abaqus. Timber is modeled as an anisotropic material and the orientation (longitudinal and radial/tangential) respects the layout of the crossed layers of the CLT panels. Hill model is used for this purpose [4, 5]. The model used for the screws is elastic-perfectly plastic. The screws have been modeled precisely and the interface properties between steel and timber are "contact and friction" type (see Fig. 4).

Nevertheless these kind of models are time-consuming, so simplified models have been developed with unthreaded shanks and different properties for the material interfaces (contact and friction, cohesive surfaces, tied surfaces) to be able to model more complex simulations like entire walls or floors. The totality of these numerical models and their pros and cons will be presented in the Civil-Comp Press Conference (CST2014) in Naples in September 2014.

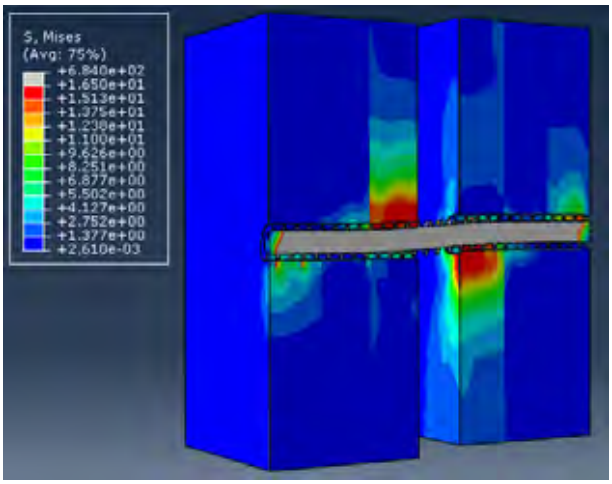

Fig. 4 Numerical model with Hill criteria and a gap of 18 mm

7. Conclusion

The use of cross-laminated timber presents many advantages. Nevertheless, this type of construction requires a large wood consumption. In order to reduce this principal disadvantage, a new product is studied at the University of Mons using CLT with an analogy to the structural insulated panels. First experimentations have been done on assemblies using WR-T screws. These screws will be used to stiffen the whole without the use of a rigid insulation. Results show the importance of the screwing angle, a screwing angle of 30 degrees being able to increase or decrease the load bearing capacity of the connection by 50% in the presented case. In parallel, the embedment

strength of the CLT has been measured and the panel assemblies have been calculated theoretically thanks to the Johansen's theory. These results show a good correlation and tend to say that the equations are valid as for massive wood if the embedment strength of the CLT is known. Numerical developments are in progress, they give a good estimation of the assemblies' rigidity and of the beginning of the deformations. These results will be presented soon.

8. Acknowledgement

I would like to thank MM. Albino Angeli and M. François Varacca, Rothoblaas and SFS for their support and the screws given for these experimentations. I also thank M. José Pérard, iTech-Wood and KLH Massivholz for their support and the CLT panels given for these experimentations.

References

[1] European Committee for Standardization CEN, EN 1995-1-1: Eurocode 5: Design of timber structures - Part 1-1: General - Common rules and rules for buildings, 2004, CEN, Bruxelles, Belgium.

[2] European Committee for Standardization CEN, EN383: timber structures - test methods - determination of embedment strength and foundation values for dowel type fasteners, 2007, CEN, Bruxelles, Belgium.

[3] European Organisation for Technical Approvals EOTA, ETA-12/0062 SFS self-tapping screws WR, 2012, EOTA, Vienna, Austria.

[4] Descamps T., VanParys L., Datoussaïd S., Development of a Specific Finite Element for Timber Joint Modeling, International Journal for Computational Methods in Engineering Science and Mechanic, 12, 1, (page 1-13), 2011

[5] Hill R., A Theory of the Yielding and Plastic Flow of Anisotropic Metals. Proceedings of theRoyal Society of London. Series A, Mathematical and Physical Sciences, Vol. 193, N°1033, May 27, 1948

Buckling behavior of *Blockhaus* timber walls under in-plane vertical loads

Chiara Bedon[1], Massimo Fragiacomo[2], Claudio Amadio[3], Annalisa Battisti[4]

Summary

Blockhaus structural systems represent a construction technology of ancient origins, which is widely used in practice also for the construction of modern buildings. Their basic features consist in the optimization of multiple interactions between timber logs offered by notches, simple carpentry joints and contact surfaces. Despite these basic assembling techniques, however, their structural behavior is rather complex to describe, due to several mechanical and geometrical aspects. At the same time, current available standards for the design of timber structures do not provide analytical models for the appropriate verification of these structural systems. As a result, the capabilities of timber log-walls under specific loading and boundary conditions cannot be properly estimated. In this paper, preliminary results of ongoing research activity are presented and discussed for the buckling behavior of *Blockhaus* timber walls under in-plane vertical loads. The final aim of this current research project is the development and proposal of analytical formulations of practical use for the buckling verification of vertically loaded log-walls having different mechanical and geometrical properties (e.g. log cross-section, size and location of openings, load eccentricities), as well as restraints (e.g. orthogonal walls, pillars, in-plane rigid diaphragms, etc.).

[1] University of Sassari, Department of Architecture, Design and Urban Planning, Alghero (SS), Italy

[2] University of Sassari, Department of Architecture, Design and Urban Planning, Alghero (SS), Italy

[3] University of Trieste, Department of Engineering and Architecture, Trieste, Italy

[4] Rubner Haus Spa, www.haus.rubner.com, Chienes (BZ), Italy

1. Introduction

Blockhaus systems represent a traditional construction technology where metal fasteners are minimized and the structural resistance is obtained by direct contact between multiple timber surfaces obtained via carvings, notches and ancient-types of joint. Although this technology is frequently used in practice for the construction of buildings (Fig. 1), due to the complexity of various phenomena (loading perpendicular to the grain, effect of friction, influence of gaps in the joints, creep, etc.), their structural behavior is not completely known, especially in the case of complex geometries. The interaction between multiple logs, as well as the restraint effectiveness of carpentry timber joints, possible load eccentricities or openings (e.g. doors and windows), and the anisotropy of timber can strongly affect the load-carrying capacity of these structural systems.

Fig. 1: Examples of Blockhaus structural systems (Rubner Haus Spa)

In this context, experimental and numerical studies have been recently undertaken to investigate the structural behavior of *Blockhaus* systems [1, 2, 3], highlighting the high flexibility and damping capability of this construction technology under seismic loads. Preliminary studies have been also carried out, over the last decades, to analyze the buckling strength of log-walls under mid-span in-plane vertical loads [4, 5]. In that case, experiments were performed on small prototypes of log-walls having various geometries (e.g. (i) no openings, (ii) single opening (door), (iii) double opening (door and window)). However, tests were limited to few configurations and further studies are consequently recommended.

In current practice, the traditional log-wall is generally obtained by assembling together a series of C24 spruce logs (Fig. 2a). These logs have typical slender $b \times h$ cross-sections characterized by small notches and protrusions which provide interlocking between the adjacent logs (Fig. 2b). In *Blockhaus* buildings, the structural interaction between the main walls is provided by appropriate carpentry joints (Fig. 2c). Permanent gravity loads are then transferred onto each main wall by the inter-storey floors, which typically realize an in-plane rigid diaphragm (e.g. using

OSB panels, glulam panels arranged on their edges, etc.) able to restrain the out-of plane deflections of the wall top logs.

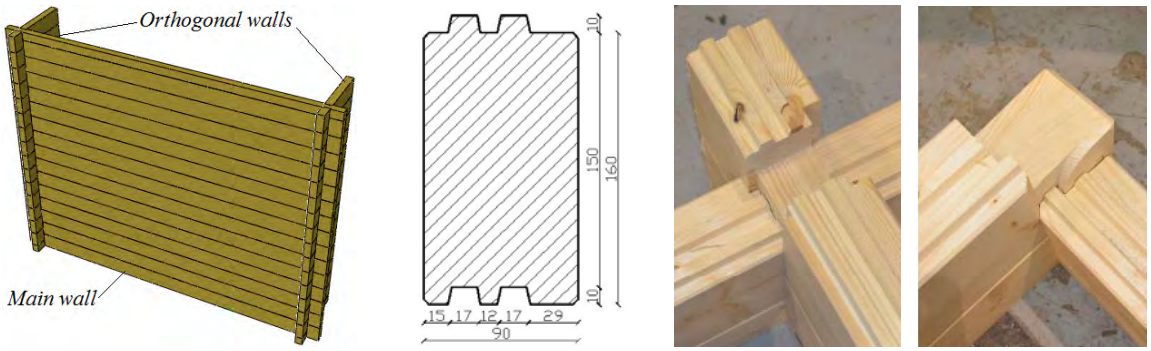

(a) *(b)* *(c)*

Fig. 2: Example of a Blockhaus wall.
a) Overview; b) cross section (dimensions in mm); c) different types of carpentry joints.

In this work, sophisticated finite-element (FE) numerical models, able to appropriately take into account the effective interaction between multiple timber logs, are developed using the ABAQUS/Standard software package [6] to investigate the effects of several parameters on the buckling capacity of these walls. Preliminary linear elastic modal analyses (*lm*) and nonlinear incremental buckling simulations (*ib*) are performed using these numerical models. Numerical predictions are also compared with critical loads obtained from analytical approaches proposed in literature, to assess their accuracy and applicability to *Blockhaus* timber walls. The final aim of this current research project is the development of practical formulations for the design and verification of timber log-walls vertically loaded in their plane.

2. Existing analytical formulations

Few literature references are available for the estimation of the buckling strength of log-walls under in-plane vertical loads. Heimeshoff and Kneidl [4, 5], based on preliminary experiments of log timber walls under concentrated mid-span vertical loads (Fig. 3), proposed an analytical formulation which has been implemented in the DIN1052 standards for timber structures [7]. Based on their theoretical model, the typical wall is schematized as a series of horizontal bars (e.g. timber logs) supported by translational and torsional springs. The flexural and torsional stiffness's of a single timber log are then taken into account for the estimation of the spring elastic constants. In accordance with [4, 5], for a wall without openings and composed of main logs having b-wide and h-thick cross-section, the critical buckling load $N_{cr,0}^{(E)}$ can be estimated as (Fig. 3).

$$N_{cr,0}^{(E)} = E_{\parallel} \frac{b^3 h^2}{L^3} + 0.8 \; G \; \frac{b^3}{L}, \tag{1}$$

where $E_{\parallel}$ and G represent the Young's modulus in the direction parallel to grain and the shear modulus of timber. As highlighted in [4, 5], Eq. (1) can only provide a rough estimate the Euler's critical load of a log-wall under in plane vertical load.

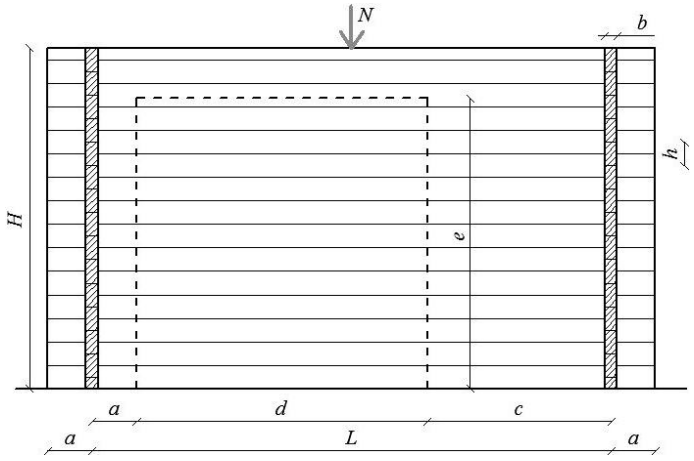

Fig. 3: Elevation of specimens tested in [4, 5]

In any case, with proper modifications, the same analytical model can be applied also to log-walls with openings (Fig. 3). The corresponding critical load can be estimated as [4, 5]:

$$N_{cr,0}^{(E)} = 0.8 \; G \; \frac{b^3}{L} \left[\frac{e}{H} + \frac{\left(H - e\right)}{H} \frac{L - d}{L} \right]. \tag{2}$$

Alternatively, analytical formulations could be taken from classical theory of thin plates simply supported along the four edges and subjected to in-plane vertical loads. This approach would allow the implementation of the top restraint offered by in-plane rigid floors, but would not allow a proper estimation of the interlocking effect between multiple logs. Specifically, each timber log-wall would be regarded as a 'monolithic' wall having thickness b, height H, width L, hence resulting in a critical buckling load:

$$N_{cr,0}^{(E)} = k_{\sigma} \pi^2 E_{\perp} \frac{b^3}{L} \frac{1}{12\left(1 - \nu^2\right)}, \tag{3}$$

with $$k_{\sigma} = \left(\frac{mL}{H} + \frac{H}{Lm} \right)^2, \tag{4}$$

$m = 1$, $E_{\perp}$ the minimum Young's modulus of timber (e.g. perp. to grains) and $\nu = 0.2$ the Poisson's ratio.

3. Finite-Element numerical modeling

The numerical studies discussed in this work have been performed with the software package ABAQUS/Standard [6]. The typical Finite-Element (FE) model consisted of 8-node, linear brick solid elements with reduced integration (C3D8R), available in the ABAQUS element library. In each simulation, a single main wall only (Fig. 2a) has been taken into account, with appropriate boundary conditions. Careful consideration has been given to the geometrical description of the studied structural systems and its main logs. At the same time, suitable surface contact algorithms have been used, to properly describe the mechanical behavior of the studied timber walls. Specifically, *master-slave* surface interactions have been considered at the interface between overlapping logs. In this manner, possible tangential slidings have been allowed between logs (*tangential behavior*), with $\mu = 0.4$ being the static friction coefficient [3]. At the same time, possible detachment of overlapping logs in the direction perpendicular to the contact surfaces has also been taken into account (*normal behavior*). Concerning the mechanical characterization of timber, C24 spruce has been described in the form of indefinitely linear elastic, isotropic material having density ρ= 420kg/m^3, Young's modulus $E \equiv E_{\perp} =$ 370 MPa and Poisson' ratio $\nu = 0.2$ [3]. Boundaries have been finally introduced at the base of the wall (u_x= 0, u_y= 0, u_z= 0) and at the lateral ends of each log. In this latter case, based on earlier studies, the orthogonal walls have been schematized as vertical rollers able to prevent possible out-of-plane and in-plane displacements for the main walls, hence resulting in linear lateral supports (u_x= 0, u_z= 0). Linear modal buckling analyses (*lm*) and incremental buckling simulations (*ib*) have then been performed on the same FE-models, in order to compare the results. Although modal analyses can be used to estimate the critical load of the examined systems, this quantity alone does not exhaustively describe the structural behavior of the studied walls up to failure. Consequently, incremental buckling simulations should be generally performed, in order to appropriately take into account the possible effects of multiple mechanical and geometrical variables.

3.1 Preliminary simulations and assessment of FE-models

Preliminary validation of the numerical modeling assumptions has been performed against the experimental tests performed by Heimeshoff and Kneidl on three different small log-wall prototypes [4, 5]. An overview of their main nominal dimensions and configurations is provided in Fig. 3. The typical timber component consisted of $b = 2.5$ cm $\times$ $h = 4$ cm $\times$ L, C24 spruce log, with L the distance between the lateral

end supports ($a = 0.14$ m) and $H = 0.625$ m the total height. In the case of specimens S01 and S02, the wall prototypes was obtained by assembling 15 logs having span $L = 1.125$ m (S01) and $L = 0.75$ m (S02). For specimen S03 ($L = 1.125$ m), a door opening was also considered ($d = e = 0.525$ m, $a = 0.14$ m). Each main wall had the log at the base restrained with small angle brackets against out-of-plane displacement, and was laterally restrained by means of two $L = 2a \times H = 0.625$ m orthogonal walls representative of continuous supports.

Lm analyses have been firstly performed on the corresponding ABAQUS FE-models. Examples of the corresponding buckled modal shapes are displayed in Figs. 4a and 5a for specimens S01 and S03 respectively. In addition, also the effects of possible in-plane rigid inter-storey floors connected to the top log of each wall have been taken into account (Figs. 4b and 5b). Generally, as highlighted by comparisons shown in Figs. 4-5, the presence of openings resulted in strong reduction of the buckling strength. At the same time, the introduction of the rigid inter-storey floor resulted in significantly different global behaviors (thus critical loads) for the same specimens.

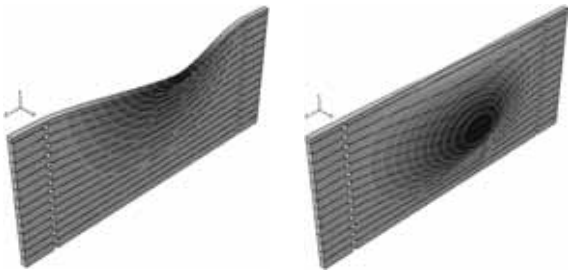

(a) flexible floor (b) rigid floor

Fig. 4: Buckled modal shapes for specimen S01

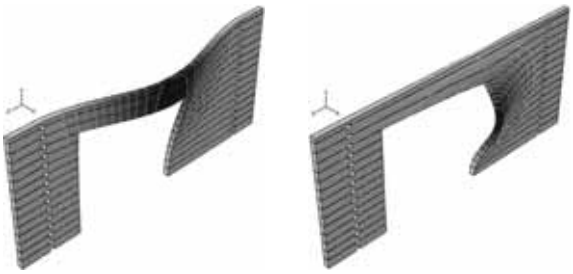

(a) flexible floor (b) rigid floor

Fig. 5: Buckled modal shapes for specimen S03

Tab. 1: Comparison between experimental, numerical and analytical critical loads

		Flexible floor		Rigid floor	
Specimen	Experimental [4, 5]	Analytical [kN]	Numerical (ABAQUS) [kN]	Analytical [kN]	Numerical (ABAQUS) [kN]
S01	11.6	5.73 (Eq.(1))	5.45	24.23 (Eq.(3))	24.35
S02	15.5	8.93 (Eq.(1))	8.16	27.30 (Eq.(3))	33.49
S03	9.93	3.38 (Eq.(2))	3.23	-	11.05

In any case, it is interesting to notice that rather good correspondence was generally found between analytically predicted critical loads based on Eqs.1-3 and corresponding *lm* numerical results (Table 1). Further *ib* simulations performed on the same numerical models confirmed that the presence of possible openings (single

door, door and window together) significantly decreases the buckling strength of the studied structural systems. In any case, the presence of rigid inter-storey floors can provide considerable increase in total strength, as shown for example in Fig. 6 for specimen S01.

In Fig. 6, numerical results obtained from *ib* simulations are compared with the curves vertical load N vs. u over H ratio, u signifying the maximum out-of-plane deflection of the wall (x-direction) estimated at each load increment as the envelope of the occurring transversal displacement, and H denoting the total height of specimen S01. As also highlighted from previous *lm* analyses, the *ib* simulations confirmed that the in-plane rigid inter-storey floor avoids the occurring of local collapse mechanisms in the top logs of the wall, hence resulting in higher initial stiffness and more stable overall buckling behavior of the wall up to failure (Fig. 6, curve (*ib*) ABAQUS-Rigid floor). However, unlike the predictions obtained from the corresponding *lm* analyses, *ib* simulations are able to take into account more accurately the effects of possible detachments between the overlapping logs (Fig. 6, point A). Consequently, the effective global buckling strength numerically predicted for the specimen S01 (Fig. 6, point B) is lower than the corresponding critical load (Eq. (3) or (*lm*) curve of Fig. 6).

Since several mechanical and geometrical aspects could further decrease the effective buckling strength of the examined walls (e.g. the maximum amplitude u_0 of possible initial imperfections, as for example shown in Fig. 6), careful consideration should be paid for a proper estimation of the structural effects of the main influencing parameters.

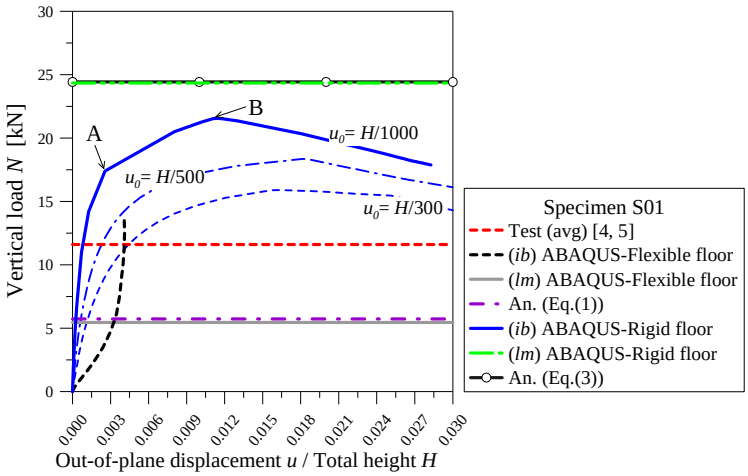

Fig. 6: Comparison between analytical, numerical and experimental results for specimen S01

4. Conclusions

Preliminary numerical studies have been presented for the assessment of the buckling behavior of *Blockhaus* walls under in-plane vertical loads. Simulations highlighted that the presence of openings strongly affects their global buckling strength, markedly reducing their collapse load. Conversely, the presence of inter-storey rigid floors generally resulted in large increase of the buckling strength, hence leading to nearly global rather than local failure mechanisms. Consequently, particular attention should be paid to a correct estimation of the corresponding critical load. The final aim of this ongoing research project is the development of analytical design formulations for the prediction of the buckling resistance of vertically loaded log-walls.

5. Acknowledgements

Rubner Haus Spa is gratefully acknowledged for the financial and technical support.

References

[1] Branco, J., Araújo, J.P., *Lateral Resistance of Log Timber Walls subjected to Horizontal Loads*, 2010, Proceedings of WCTE 2010, World Conference on Timber Engineering.

[2] Branco, J., Araújo, J.P., *Structural behaviour of log timber walls under lateral in-plane loads*, 2012, Engineering Structures, 40: 371-382.

[3] Bedon, C., Fragiacomo, M., Amadio, C., Sadoch, C., *Experimental study and numerical investigation of Blockhaus shear walls subjected to in-plane seismic loads*, 2014, Journal of Structural Engineering, published online, DOI: 10.1061/(ASCE)ST.1943-541X.0001065.

[4] Heimeshoff, B., Kneidl, R., *Zur Abtragung vertikaler Lasten in Blockwänden – Experimentelle Untersuchungen*, 1992, Holz als Roh- und Werkstoff 50: 173-180, Springer-Verlag.

[5] Heimeshoff, B., Kneidl, R., *Bemessungsverfahren zur Abtragung vertikaler Lasten in Blockwänden*, 1992, Holz als Roh- und Werkstoff 50: 441-448, Springer-Verlag.

[6] Simulia, 2012. ABAQUS v.6.12 [Computer Software], Dassault Systems, Providence, RI, USA.

[7] DIN1052 Teil 1: Holzbauwerke; Berechnung and Ausführung, 1988.

Pre-stressing of wood with full thread screws

Michael Steilner[1]

Summary

Reinforcement of modern timber and glulam structural members with full thread woodscrews is state of the art. The high axial strength of the screws and the excellent composite action between the timber and the screws are perfect to reinforce the 'weak' direction perpendicular to the grain of the timber.

In reinforced timber members, the reduction of the moisture content and the subsequent shrinking deformation results in tensile stresses perpendicular to the grain near the screw because of the high axial stiffness of the screw.

In a research project, screws with a variable pitch of the thread were developed. Due to the variable thread, the screw pre-stresses the timber resulting in a compressive stress in the timber along the axis of the screw. Consequently, the strength of the reinforced timber increases and the influence of the shrinking in the area of the screw decreases.

To optimize the variation of the pitch, a numerical model was developed. In a parameter study two different thread geometries were determined that yielded the best results in terms of pretension of the timber.

FSR-sensors suited to measure a compressive force were used to determine the preload force of the screws in test series. The test series confirm the results of the numerical model. Therefore, it is possible to calculate the effect of the pretension with the model and the thread geometry can be optimized.

[1] Scientific assistant, KIT Holzbau und Baukonstruktionen, Germany

1. Introduction

Reinforcement of timber perpendicular to the grain with self-tapping screws is effective. The screws, e.g. in members with notches, transfer the splitting force and avoid an uncontrolled crack growth in the timber beam. The screws act like the reinforcement in concrete members: The load carrying action is not activated until a little crack occurs in the timber. Furthermore, the deformation perpendicular to the grain in high glulam beams resulting from changing moisture content, e.g. in heated factory buildings, is significant. Especially the shrinking deformation near reinforcing screws results in tensile stresses perpendicular to the grain because of the high axial stiffness of the screw. A compressive pre-stress hence increases the strength of the reinforced timber and decreases the influence of climatic loads.

2. Pre-stressing with screws

2.1 Screws with a variable pitch of the thread

Because of the low compressive strength of timber, perpendicular to the grain the potential compressive force that can be put on the surface of timber for pre-stressing the cross section of the timber is low too. In addition, the stress spreads under the load application resulting in a lower stress level in the middle of the cross section. For that reason, screws with variable pitch of the thread were developed. The variable pitch of the thread generates a systematic compressive stress perpendicular to the grain in the cross section of a timber element.

Fig. 1 shows the geometry of the thread of a self-tapping screw with variable pitch of the thread. In areas I and III the pitch p_0 is constant. In area II the pitch $p(x)$ changes functionally. In area II the pitch of the thread is always less than in area I and III.

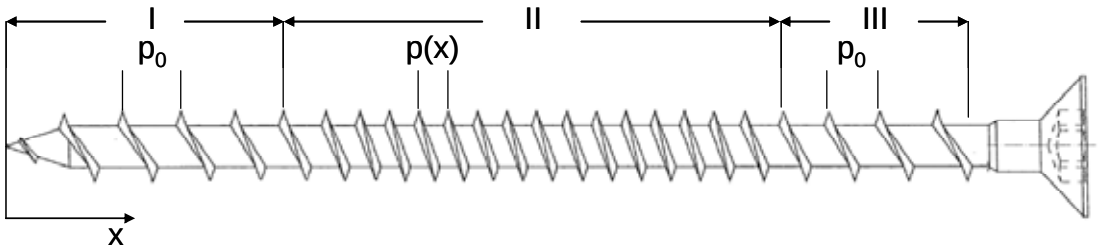

Fig. 1: Self-tapping screw with a variable pitch of the thread. In areas I and III, the pitch p_0 is constant and in area II the pitch p(x) is variable.

The pitch of the thread is equal to the distance a screw covers in one turn during screwing in. A screw with a constant pitch of the thread covers the same distance along the axis by one turn. A screw with a variable pitch of the thread covers "different" distances along the axis by one turn. Because of that, restraints are generated along the axis of the screw. Those result in a compressive stress in the timber cross section. The compressive stress depends for the main part of the variation of the pitch of the thread. Fig. 2 schematically shows the "deformation" of a timber cross section during the screwing of a screw with a variable pitch of the thread.

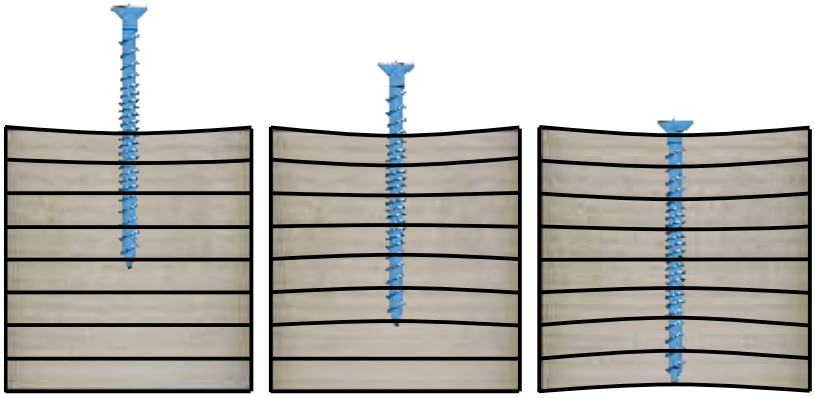

Fig. 2: "Deformation" of the timber during the screwing of a screw with a variable pitch of the thread in timber

The restraints must not pass a critical limit. Otherwise the wood matrix will be destroyed and the load transmission between the timber and the screw is no longer possible ([1],[2],[3]).

2.2 Compressive pre-stress

To optimize the variation of the pitch of the thread, a numerical model was developed. In a parameter study two different thread geometries were determined that yielded the best results in terms of pretension of the timber. Fig. 3 shows the compressive stress distribution within a 200 mm high test block for a screw with variable pitch of the thread.

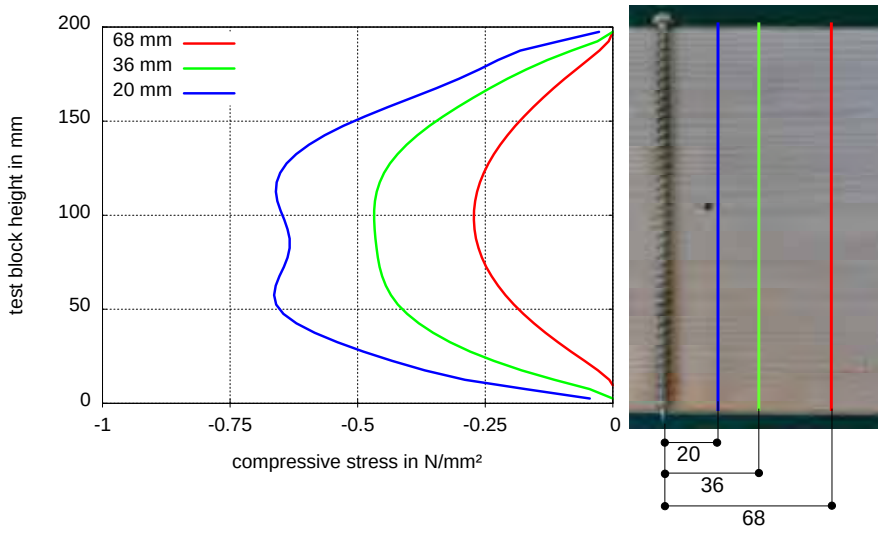

Fig. 3: Calculated compressive stress over the test block height depending of the distance from the screw axis in the direction of the grain.

3. Tests

3.1 Compressive force measurement with Force-Sensing Resistor (FSR)

To measure the influence of the screw with variable pitch of the thread on the load distribution of the timber, a thin measuring element is necessary that can be inserted between two pieces of a timber test block. The Force-Sensing Resistor (FSR) is a thin measurement element that changes its electrical resistance depending on a force reaction. The FSR consists of two laminated plastic films. One film is semi-conductively covered and the other one contains two conducting finger-shaped paths gearing into each other but electrically separated. If the films are compressed, the electrical resistance decreases depending on the compression force.

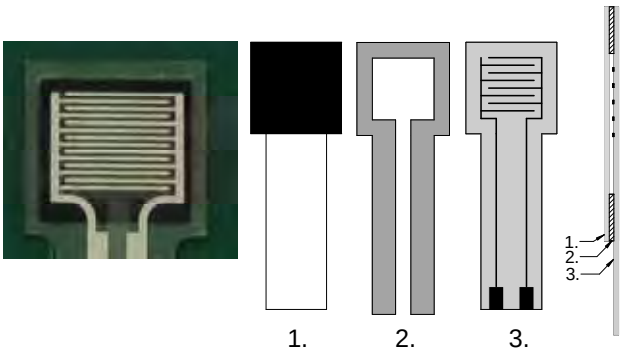

Fig. 4: Picture of a FSR and the setting of a FSR:
1. film semi-conductive covered,
2. adhesive layer,
3. Film with finger-shaped electrode.

3.2 Test blocks and test configuration

To confirm the calculated compressive pre-stress, tests with glulam blocks and screws with variable pitch of the thread were performed. The test blocks had a height of 200 mm that corresponded with the length of the test screws and a base area of 160 x 160 mm². For each test block, the dynamic modulus of elasticity and the density was determined. To measure the compressive force the test blocks were cut in three different heights. Fig. 5 shows three test blocks with measurement heights of 50 mm, 100 mm and 150 mm. The FSRs were fixed on a plastic film and the FSR configuration was put between the two parts of test blocks as shown in Fig. 6. The test block was placed into the hinge moment analysis system, the screw was screwed in and the compressive force was measured continuously with the FSRs.

Fig. 5: Glulam test blocks for compressive force measuring in the height of 50 mm, 100 mm and 150 mm.

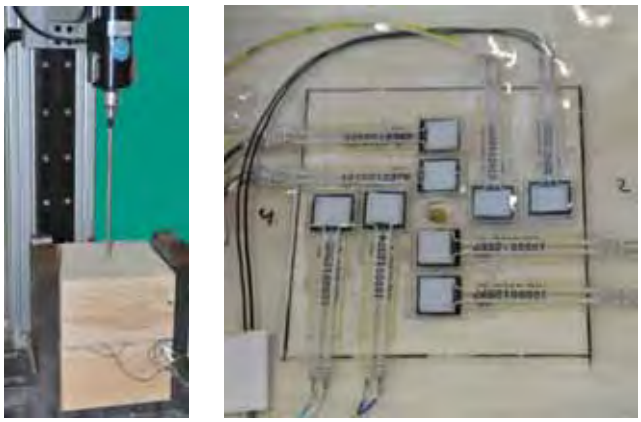

Fig. 6: Test configuration.

3.3 Test results

Fig. 7 shows the results of two test series with different thread geometries. Except for the values in 50 mm depth from variation 1, the measured values agree with the calculated values from the numeric model. The test series show that a preload with screws with a variable pitch of the thread is possible and the numeric model is able to calculate the effect of the pretension. Therefore, the thread geometry can be optimized for different applications of the screw.

A compressive pre-stress of -0.5 N/mm² was reached with the chosen thread geometry. Referring to the low tensile strength perpendicular to the grain, the reached pre-stress is remarkable.

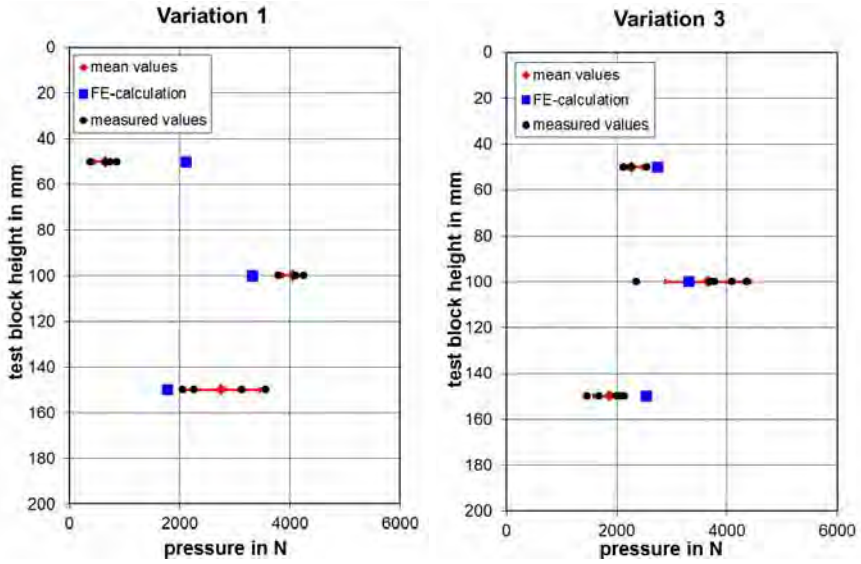

Fig. 7: Test results from two different thread geometries.

4. Summary and Outlook

The test results show that screws with a variable pitch of the thread are suitable to apply a remarkable compressive pre-stress to timber elements. The numerical model can calculate the pre-stress depending on the thread geometry so that the thread geometry can be optimized.

To study the long-term behavior of timber-members pre-stressed by means of screws further research with regard to relaxation, shrinking and swelling is needed. For this purpose, long-term tests are in progress.

5. References

[1] Bejtka, I., Verstärkungen von Bauteilen aus Holz mit Vollgewindeschrauben, *Karlsruher Berichte zum Ingenieurholzbau*, Bd. 2, Universitätsverlag Karlsruhe, 2005

[2] Steilner, M., Blaß, H.J., Selbstbohrende Holzschrauben mit veränderlicher Gewindesteigung, *Doktorandenkolloquium, Holzbau Forschung und Praxis*, Institut für Konstruktion und Entwurf (Hrsg.), Universität Stuttgart, 2010, P 107-112

[3] Steilner, M.: Querdruckvorspannung von Holz, *Dorktorandenkolloquium, Holzbau Forschung und Praxis*, Institut für Konstruktion und Entwurf (Hrsg.), Universität Stuttgart, 2012, P 53-60

[4] Neuhaus, H.: Über das elastische Verhalten von Fichtenholz in Abhängigkeit von der Holzfeuchtigkeit, *Holz als Roh- und Werkstoff*, Band 42, 1983, P 21-25

In-plane cyclic tests on historic timber frame walls: Outcomes comparison[1]

Nicola Ruggieri[2]

1. Introduction

Timber framed wall constructive system was spread in many countries of the world and over the centuries. This popularity is due to an easy availability and a simple workable of the timber, which represented one of the most suitable materials to execute load bearing structures. Among those types, some examples show an aware use as anti-seismic device in the building, in Minoic culture for example (Knossos and Phestos) or in other earthquake prone area, such as Portugal and Italy, as well as in the Middle-East (Pakistan and India). In particular in such European countries, planners and executors discovered the advantages of the timber frames under dynamic actions with an empirical attitude: the existing edifices realized with a wooden skeleton had showed a proper response during the past earthquakes. Hence the *Gaiola,* realized after the Lisbon earthquake in 1755, based its structural arrangement on former examples; the *Pombaline* type is characterized by an internal cage constituted by masonry infill timber frames fastened to the external masonry wall [1]. In South Italy, Ferdinando IVth the Borbone, by means of a government dictate, which represents the first anti-seismic code of Europe, obliged technicians to use masonry reinforced with timber frame in the Calabria reconstruction after the 1783 destructive seism, founding on an ancient timber structure knowledge present in the region [2]. Relative to the types widespread in Kashmir (*Dhajji-Dewari)*, even if originated to answer to soft soil settlements, proved a certain effectiveness to reduce building damages during recent seism's [3]. Such a constructive system is characterized by timber frames with random rubble masonry infill.

The 3D structural systems above described can be divided, based on their mechanical

[1] The numerical test results presented in the herein document derive from different loading protocols and consequently can entail inaccuracy in the outcomes comparison.

[2] PhD candidate, University of Calabria, Italy

behavior, in "timber frame walls" *(Gaiola* and *Dejja Dewari)*, in which wooden elements bear the vertical loads and the infill stones/bricks has the aim to stiffen the wall under horizontal forces and "masonry reinforced with timber frames" *(Casa baraccata)*. The latter is characterized by timber members that don't participate, at the most in a limited way, to the load bearing system in static field; under dynamic actions the answer is different, when the wooden skeleton acts, enhancing the masonry panel by means of an additional tension resource.

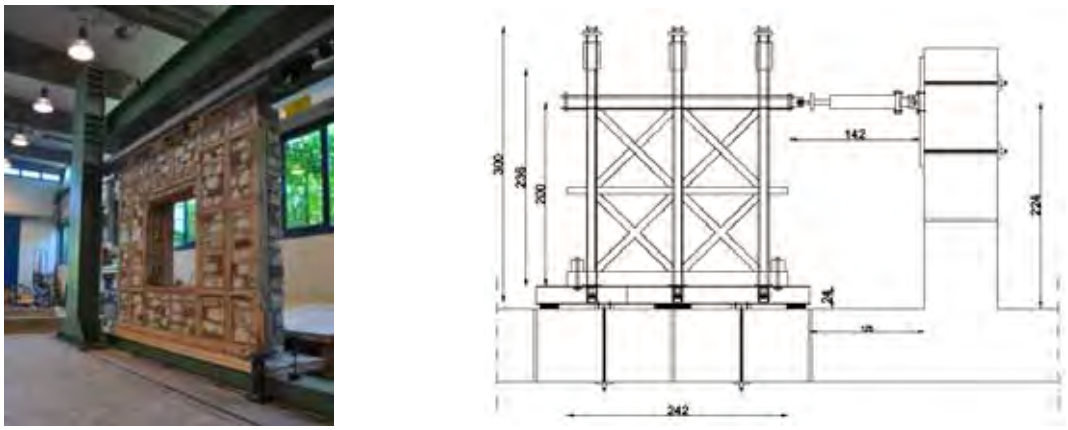

Fig. 1: Cyclic test performed on Casa Baraccata specimen in full scale (left). Cyclic test performed on Gaiola sample (from Poletti et al., 2012).

2. Cyclic tests

In recent years experimental campaign was performed on full scale *Gaiola* specimen, in Minho[3] at the ISISE [4] and in Lisbon (LNEC) [5] respectively followed the ISO DIS 21581 (F_{max} 55 kN, D_{max} 27 mm, D_u 89 mm) and the CUREE loading procedure (strength of 70 kN for a ultimate displacement of 120 mm). Three Dhajji panels [6] were constructed in the EEC laboratory in Peshawar to decode by means of cyclic tests its seismic behavior. Whereas a *Baraccato* wall was reproduced in September 2013 at the CNR/Ivalsa [7] laboratory in Trento with the aim of subjecting it to cycling actions based on UNI 12512 loading protocol, until a displacement of 80 mm (F_{max} of about 100 kN, D_{max} 60 mm).

[3] The Portuguese experimental campaign, carried out by the research team from Minho (Lourenco, Poletti, Vasconcelos), included several specimen tested, reinforced and un–reinforced, timber frame with masonry infill and empty. In the manuscript, we have preferred to include only the "UIW 25" sample results, that presented brick infill and similar vertical load value imposed to the Borbone one.

2.1 Damage patterns

All the tested walls presented a proper answer to cyclic loading confirming the anti-seismic response of the timber frames showed in some past earthquakes [8] (Calabria, 1908; Kashmir, 2005). A similar behavior characterized the "timber frame wall" constructive technique, with a significant rocking mechanism (uplift reached 50 mm, relative to *Gaiola* specimen with lower vertical load, and 70 mm concerning the *Dhejja* walls) and a consequent predominant flexural response. Relative to such a structural system the infill damage was slight if compared to the timber members and joints. The tension diagonals experienced a detachment, with the load direction variation; the compressed bracings were characterized by a rupture at the intermediate connections, preceded by the buckling of the member. Hence the cumulative damage and the plastic deformations were concentrated mainly in the joints. Under cyclic loading, the Borbone constructive system, "masonry reinforced with timber frame", showed different behavior in which had a fundamental role the masonry infill. The frame, confined by masonry, underwent, at least for the early cycles, only limited displacement, allowing timber members to perform their action in the elastic field. Simultaneously the wooden frame had the capacity to bring back the wall in its initial position or close to it. The timber joints and elements did not point out, for the entire test, damage, if we exclude the shear rupture at the bottom post due to the, even if non significant, wall uplift (less 3 cm). The masonry infill experienced bedjoints cracking and few expulsions of stones.

Fig. 2: Rocking mechanism on Baraccato sample and joint collapse in the Gaiola wall.

2.2 Evaluation of seismic parameters: hysteretic curve, ductility, energy dissipation and equivalent viscous damping ratio

The envelope curves, relative to different wall types analyzed, exhibited a similar qualitative behavior characterized by a certain diagram symmetry between the two load directions and a terminal softening branch even if the strength impairment was not much remarkable (strength loss of 6% concerning the Gaiola sample; an average value of 11% for Baraccato one). The average initial stiffness pointed out by Gaiola specimen was of 3.03 kN/mm, lower than what was observed in the Borbone wall (6.3 kN/mm), thanks to the presence of a larger thickness of the masonry. Comparing the ductility value obtained from the Gaiola wall with the Baraccato constructive system, the first showed a ductility of 4.5; lower than the Italian type (7.6) in which the high friction generated led an increasing of the ultimate displacement value.

The equivalent viscous damping ratio (EVDR) is correlated to energy dissipation, the latter always associated to the increase of damage. The Dhajji sample reached values of EVDR of 20%, higher than what encountered in the Pombalino system (a constant value of 0.1). It is easily understandable if we consider that Kashmir connections were better notched, characterized by tenon and mortise with the presence of a mild steel nail, namely more friction and deformations, consequently they dissipated a large amount of energy. The Baraccato type exhibited values variable between 6% and 8.9%.

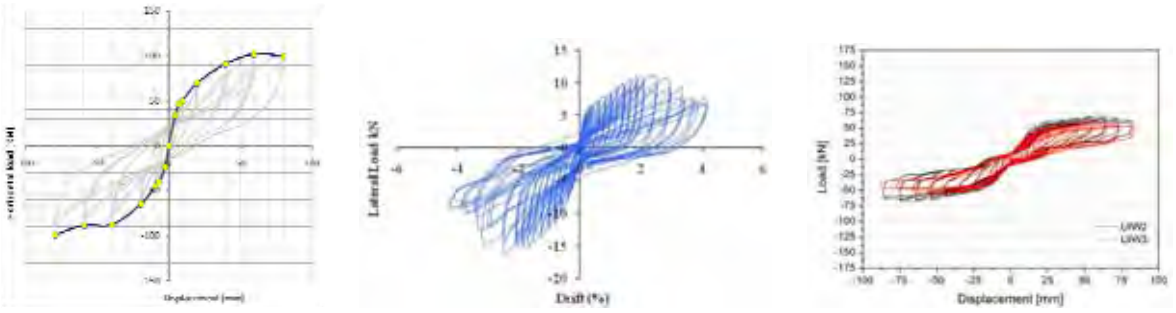

Fig. 3: Load-displacement diagram on Baraccato (Ruggieri et al., 2013), Dhejja wall (Ali et al., 2013) and Gaiola wall (Poletti et al. 2012).

3. Conclusion

The entire tested specimen, even if with different loading protocols, showed a proper behavior under cyclic loading; withstand severe deformation with, in the Borbone case, slight damage. The paper point out the different mechanical behavior that characterizes the "masonry braced with timber frames" from "timber frame walls". In fact, relative to the latter, the inelastic behavior was governed almost uniquely by the joints, the infill masonry does not increase the lateral load even if is able to dissipate seismic energy. Instead, concerning the Baraccato system it is worth to note that the masonry infill represents a dominant influence in the lateral resistance and in all the other cyclic tests outcomes. Furthermore during the test large amount of energy dissipation could occur by means of frictions generated among the infill stones and at the frame and masonry interface. The joints could dissipate seismic energy even if in a reduced way.

4. Acknowledgement

The author would like to acknowledge the Regione Calabria for its financial support to the experimental research on the Borbone structural system. Furthermore my gratitude goes to Professor Zinno that has permitted to perform the tests and Professor Ceccotti for his precious advices.

References

[1] França, J., A, *Una città dell'Illuminismo. La Lisbona del marchese di Pombal*, Officina Edizioni, 1972, Roma.

[2] Ruggieri, N. *Il sistema antisismico borbonico, muratura con intelaiatura lignea, genesi e sviluppo in Calabria alla fine del '700"* in Bollettino degli Ingegneri, ISSN 2035-2433, n.10, 2013, Firenze.

[3] Langhenbach, R., *Don't Tear It Down. Preserving the Earthquake Resistant Vernacular Architecture of Kashmir* United Nations Educational, Scientific and Cultural Organization (UNESCO), India, 2009.

[4] Vasconcelos, G.; Poletti, E.; *Seismic Behaviour of Traditional Half Timbered Walls: Cyclic tests and Strengthening Solutions,* Structural Analysis of Historical Constructions, Jerzy Jasienko (ed), 2012, Wroclaw, Poland.

[5] Meireles H., Bento R., Cattari S., Lagomarsino S. , *A hysteretic model for "frontal"walls in Pombalino buildings.* Bulletin of Earthquake Engineering (2012), 10(5): 1481-1502.

[6] Ali Q, Schacher T, Ashraf M, Alam B, Naeem A, AhmadN,UmarM, *In-plane behavior of Dhajji-Dewari structural system (wooden braced frame with masonry infill).* Earthq. Spectra, 2012

[7] Ruggieri, N.; Zinno*, R. Behaviour of the Borbone Constructive System under Cyclic Loading. Preliminary Report*, in proceedings of 1st International Conference on Historic Earthquake-Resistant Timber Frames in the Mediterranean Area, 2013, ed. Ruggieri N.; Tampone G.; Zinno R.- in press.

[8] Ruggieri, N.; Tampone, G.; Zinno*, R.; Typical failures and Safety Seismic Behavior of the Bourbon system with Timber Framing*, *in* Advanced Materials Research Vol. 778 (2013), Trans Tech Publications, Switzerland, pp 58-65.

Knot-related stiffness inhomogeneity within wood board

Antanas Baltrušaitis[1], Vytenis Kalėda[2]

Summary

The main aim of the research was to investigate the influence of number and size of scattered knots and knot clusters on wooden board modulus of elasticity (MOE). More than 100 structural size Lithuanian-grown Scots pine wood pieces having various lengthwise knot configurations has been tested. In the first part of the research global MOE of the wood pieces was specified using "Timber Grader MTG" and related to the location and sizes of knots. Effects of total board surface knot area ratios as well as dominant knot cluster influence on board global stiffness was evaluated and compared to specify verifiable and simplified stiffness prediction method. Afterwards local MOE profiles in specific parts of the wood (especially with knots) lengthwise wood pieces were established using acoustic time-of-flight method and Strength Meter developed at KTU. Other physical wood properties like density, annual rings, and moisture content has been incorporated into data processing and modeling.

The focus of investigating was knots-related effects. Every knot in all the samples (diameter higher than 10 mm) has been counted, and their surface areas ratios calculated. Also certain areas, having the biggest knots concentrations were specified as dominant and interrelated with MOE values.

Comparative analysis of the main features of all the samples allowed evaluating the knots effects (location of knots, size and areas of knots and clusters) and other properties on wood MOE with the graphical 3D models for visualization the results.

[1] Associate professor, Kaunas University of Technology, Lithuania

[2] Master student, Kaunas University of Technology, Lithuania

1. Introduction

Timber is one of the most popular structural materials in building. However, wood is a biological compound and estimating its strength can by a challenge. So numerous researches, tests were done to predict the strength of lumber. It is well known the presence of knots in structural lumber is one of the most important strength-reducing factors. Knots are the remains of branches in the tree trunk. Knots materially affect cracking and warping, ease in working, and cleavability of timber. They are defects, which weaken timber and lower its value. The longitudinal tensile strength is the most affected property, followed by the flexural strength, the compressive strength parallel to the grain and the modulus of elasticity (MOE). It has been shown for some softwood like Pinus sylvestris, that under tensile stress, the strength contribution of knots is very low that sometimes it is better to consider them as holes. Therefore, they reduce the mechanical properties of structural lumber. Usually knots can be specified in several groups: unsound encased, inter-grown, loose, fixed, pith, sound, tight, firm, decaying knots. Knots do not necessarily influence the stiffness of structural timber; this will depend on the size and location. One of the most common ways to identify these defects is estimation visually.

Strength of structural lumber can by predicted by calculating the modulus of elasticity (MOE). It measures wood's stiffness, and is a good overall indicator of its strength. MOE is one of the most important mechanical properties and it is largely influenced by density and microfibril angle [1]. One non-destructive technique of identifying wood's MOE is by measuring ultrasonic wave velocity using acoustic tools. A non-destructive materials evaluation is to identify the physical and mechanical properties of a piece of material without altering it.

Acoustic tools are a non-destructive method of predicting the physical and mechanical properties of timber and wood-based materials. These tools measure the speed at which an indicated sound or stress wave travels through wood material. The velocity of stress wave is related to the stiffness (MOE) of the material and its density. The velocity can be measured by resonance or time-of-flight-method. This approach is based on the principle that stress wave introduced into a wood sample will cause the sample to vibrate at its natural frequency. The velocity can be calculated from the frequency of the vibration and the length of the wood sample.

2. Materials and methods

More than 80 structural size Lithuanian-grown Scots pine (Pinus sylvestris) wood pieces having various lengthwise knot configurations has been tested. All of the samples were 3015mm long, 185mm width and 50mm thick (3015x185x50) and before tests has been kept in a conditioning chamber. All specimens were weighed and overall density was calculated. All knots (d>10mm) were counted and their surface area measured using simple match formulas ("NORDIC TIMBER grading rules"). In addition, areas having most knot concentration were found and evaluated as dominant knot cluster.

Fig. 1: Hardboard strength meter and Timber Grader MTG

Moisture content was measured using a moisture meter. Knowing the length, MC and weight, modulus of elasticity was measured using a non-destructive acoustic tool "Timber Grader MTG" (Fig. 1). Samples were assigned to strength classes. Each specimen MOE was measured again using "Hardboard strength meter" working on time-of-flight method (Fig. 1). Local MOE profiles (Fig. 2) and global modulus of elasticity were calculated and compared with "Timber Grader MTG".

3. Results

Tab. 1 and 2 show the results measured by "Timber Grader MTG" and "Hardboard strength meter".

Tab. 1: MOE using "Timber Grader MTG"

Samples	Class
1	Reject
8	C18
21	C24
27	C30
17	C35
5	C40

Tab. 2: MOE using "Hard-board strength meter"

Samples	Class
2	Reject
10	C18
20	C24
26	C30
15	C35
7	C40

Fig. 2: Wood samples classification using "Timber Grader MTG" and "Hardboard Strength meter"

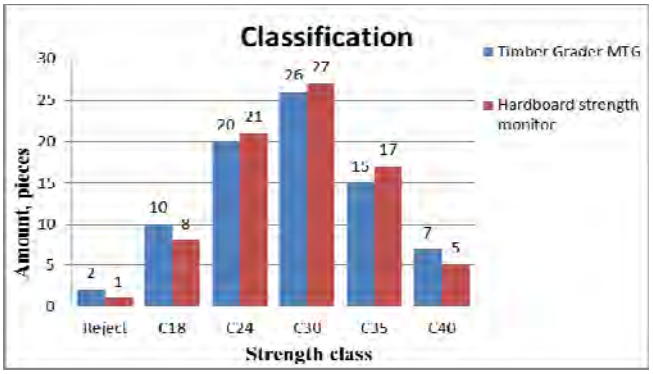

In Fig. 2 we can see that there is only a slight difference in MOE values using these two devices. Fig. 3 shows us how MOE changes in relation to knots in different places throughout the sample using "Hardboard strength meter",

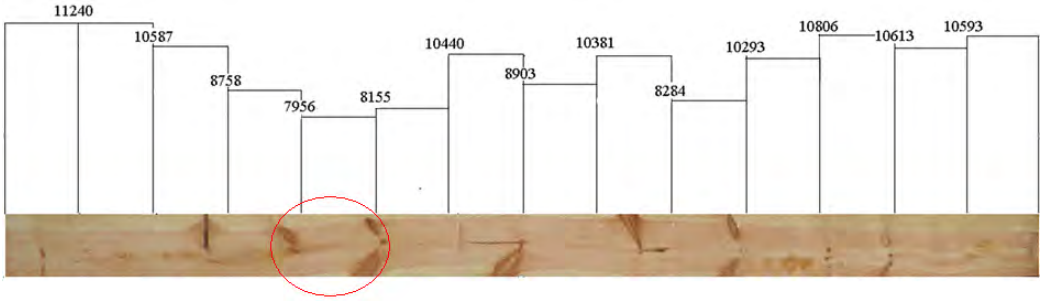

Fig. 3: MOE profiles, MPa, lengthwise 3015 x 185 x 50 specimen

Lowest MOE profile values clearly superpose with the visually specified dominant knot cluster. Effects on total board surface knot area as well as dominant knot cluster influence on board global stiffness were evaluated and compared (Fig. 4, 5).

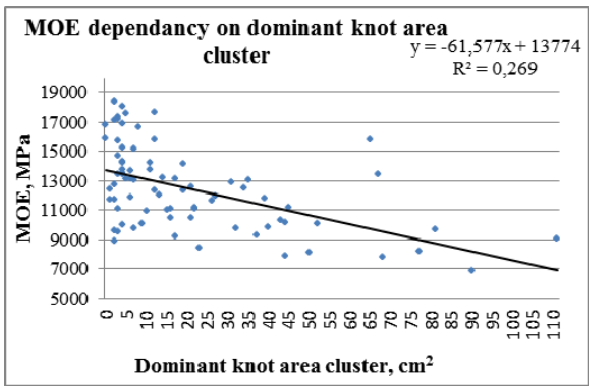

Fig. 4: MOE dependency on total surface knot area.

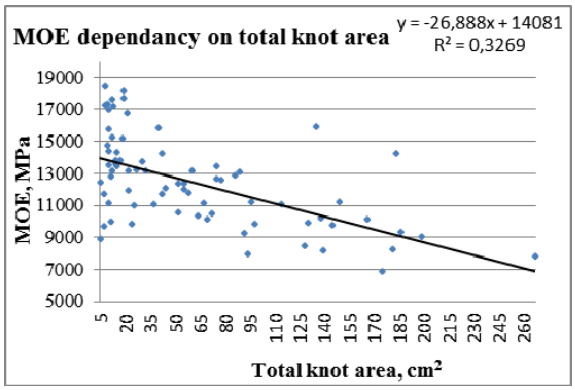

Fig. 5: MOE dependency on dominant knot cluster area.

As we can see results are similar comparing measurements of total knot area and dominant knot area cluster. We can clearly see reliable dependence between knot area ratios and MOE. Board stiffness linearly decreases when knot area gets higher. Both figures show that MOE little differs when area ratio is from 0 to 20. This shows that a small knot area does not or little affects stiffness properties. Nevertheless, linear modeling has to be reconsidered on the basis of further experimental data.

In Fig. 6 effects of density and dominant knot cluster area on moduli of elasticity are shown. Here we see that density has a larger impact in MOE than knot area.

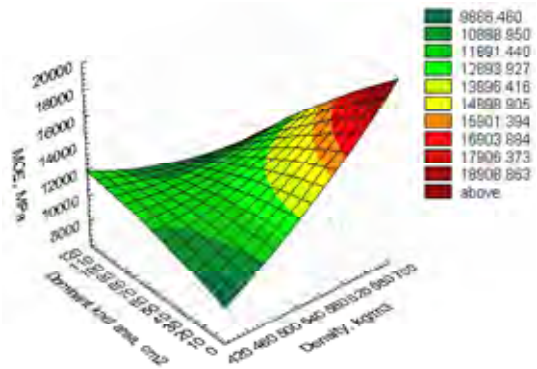

Fig. 6: 3D model of density and dominant knot area cluster influence on MOE

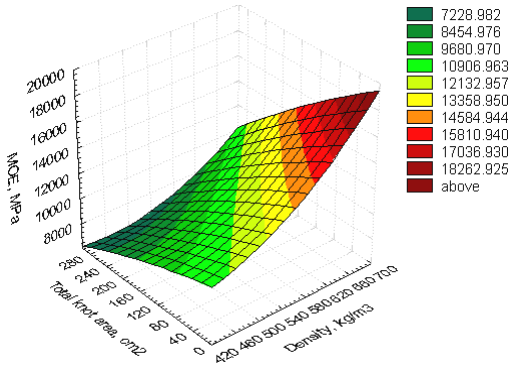

Fig. 7: 3D model of density and total knot area cluster influence on MOE

After data processing MOE dependencies on total knot area, dominant knot area, density and width of annual rings were elucidated in the following equations (1-6):

$$MOE = 1928,51 + 28,065\rho + 21,172A_T \qquad R^2=0,5728 \qquad (1)$$

$$MOE = 2475,254 + 28,533\rho + 45,746A_D \qquad R^2=0,5205 \qquad (2)$$

$$MOE = 21742,413 + 194,322\rho + 89,721w_{ar} + 32,472A_D \qquad R^2=0,3286 \qquad (3)$$

$$MOE = 16723,187 + 734,901\rho + 77,829w_{ar} + 48,265A_T \qquad R^2=0,3624 \qquad (4)$$

$$MOE = 14621,943 + 271,443w_{ar} + 26,619A_T \qquad R^2=0,6031 \qquad (5)$$

$$MOE = 15521,08 + 875,352w_{ar} + 59,64A_D \qquad R^2=0,5875 \qquad (6)$$

with: A_T – Total knot area (cm^2), A_D – Dominant knot area (cm^2), w_{ar} – Annual rings width, ρ – Density kg/m^3.

4. Conclusions

- Modulus of elasticity values measured with "Timber Grader MTG" and "Hardboard strength meter" are similar and comparable. This enables to receive structural timber MOE local profiles and global stiffness values.
- "Hardboard strength meter" allows specifying knots effects on local moduli of elasticity in certain places. Generally, MOE is lower in areas prevailing with larger knots. Small knots (d<20mm) have little influence on MOE.
- Measuring total knot area comprehensively estimates the influence on the stiffness of wood but is time-consuming and not suitable for industrial practice.
- Measuring dominant knot and cluster areas shows the effects it has on MOE at the accuracy comparable with the total knot area results. Bigger concentration of

knots lowers the stiffness of whole wood piece. It also serves for identification the weakest points on the structural wood.

- Simple statistical modeling revealed effective influences of physical wood properties on timber MOE. Density together with knot areas has dominant impact in timber MOE.

References

[1] J.L. Yang, R. Evans. Prediction of MOE of eucalypt wood from microfibril angle and density. Holz als Roh- und Werkstoff 61 (2003) 449–452.

[2] Helene Unterwieser, Gerhard Schickhofer. Influence of moisture content of wood on sound velocity and dynamic MOE of natural frequency and ultrasonic runtime measurement. Eur. J. Wood Prod. (2011) 69: 171–181.

[3] D. Sandberg, H. Holmberg. Knots - *number, type and size in star-sawn triangular profiles of pine (Pinus silvestris L) and spruce (Picea abies Karst).* Royal Institute of Technology, Div of Wood Technology and Processing, 100 44 Stockholm, Sweden

[4] F. Divos & F. Sismandy Kiss. *Strength Grading of Structural Lumber by Portable Lumber Grading - effect of knots.* Cost Action E53

[5] W. Sonderegger, P. Niemz. Influence of moisture content of wood on sound velocity and dynamic MOE of natural frequency- and ultrasonic runtime measurement. Eur. J. Wood Prod. (2011) 69: 171–181.

[6] Sławomir Krzosek, Marek Grzeskiewicz. Polish structural sawn timber grading using Timber Grader MTG. Grant no N309 003 31/0635

[7] EN 338:2012 Structural timber — Strength classes.

[8] W. Sonderegger, P. Niemz „The influence of compression failure on the bending, impact bending and tensile strength of spruce wood and the evaluation of non-destructive methods for early detection“ (2004) 62:335–342.

[9] Jinghui Jiang, Jianxiong Lu, Haiqing Ren, Chao Long „Effect of growth ring width, pith and visual grade on bending properties of Chinese fir plantation dimension lumber“ 2012, 70:119–123.

[10] Jean-Luc, S. and Yann, B. *Timber grading machine using multivariate parameters based on ultrasonic and density measurement.* COST E 53 Conference – Quality Control for Wood and Wood Products, Warsaw, Poland, 2007: pp. 167 – 173

[11] Masashi Nakamura, Takayuki Kondo „*Quantification of visual inducement of knots by eye-tracking*“ (2008) 54:22–27. The Japan Wood Research Society 2007

[12] Ronald Anthony. Non-destructive Evaluation: Wood. United States Department of Agriculture. General Technical Report FPL-GTR-70

[13] Sumire Kawamoto, R. Sam Williams. Acousto-Ultrasonic Techniques for Wood and Wood-Based Composites. Forest Service. General Technical Report FPL-GTR-134

[14] NORDIC TIMBER *"Grading rules for pine and spruce sawn timber".* Foreningen Svenska Sagverksman (FFS), Suomen Sahateollisuusmiesten Yhdistys (STMY).

Utilization of microwave measurement in timber strength grading

Julia K. Denzler[1], Peter Linsenmann[2]

Summary

Machine strength grading evolved from bending machines in the first days to utilizing X-rays, longitudinal frequency, laser and cameras nowadays. These efforts made it possible to constantly improve grading quality as well as the detectable timber characteristics. The possibility to use microwave radiation makes this also true for the detection of grain deviations. The developed microwave prototype is capable of measuring grain deviations in plane as well as perpendicular to the plane. Combining the microwave information with the information obtained by existing grading principles, an improvement in strength prediction of up to 8% can be realized. Another benefit of microwave measurements is the possibility of measuring moisture content and density contact-less in one pass over the whole specimen.

1. Introduction

Within the last ten years machine strength grading evolved from an idea to predict strength and stiffness of sawn timber into a significant branch with notable impact on economy and product safety in wood milling industry. This evolution is also present in the techniques used to grade timber: Starting with bending machines as outcome of engineering ingenuity and utilizing X-rays, longitudinal frequency, laser and cameras nowadays. Due to these efforts, grading quality as well as the detectable timber characteristics were constantly improved, but are still not solved satisfyingly concerning one main characteristic, which is exceptionally difficult to detect: grain deviations. This specific wood characteristic is so far detectable on the surface – or might even be undetectable at all – and can reduce timber strength significantly. Therefore, timber industry undertakes big efforts to find solutions for a reliable detection of grain deviations. The utilization of microwaves has great potential to

[1] Head of unit, Holzforschung Austria, Austria

[2] Scientific assistant, Holzforschung Austria, Austria

solve this challenge and has the additional benefit that contact-less measurement of density and moisture content of each piece of timber in one pass is possible, too.

2. Microwaves in Timber Strength Grading

2.1 Grain Deviations

Grain deviations occur on a global or local scale on the sawn timber: Global grain deviations mainly result from growth properties of the log like sweep or spiral grain and influence the whole piece of sawn timber. Local grain deviations are only present in a limited area of the sawn timber normally coming from knots or top rupture. This specific defect significantly reduces the strength of the sawn timber – grain deviation from top rupture up to 90% – leading to safety issues in timber construction. This impact is well known for decades. The development of knot detection is based on this issue, taking into account grain deviations occurring adjacent to knots but leaving severe slope of grain undetected without the presence of knots or based on top rupture. They are only detectable visually on the surface and often are not discernible at all. This is the reason for the effort undertaken to find a solution for the detection of grain deviation. The innovation aims to detect grain deviations on a local scale. The local resolution is necessary to detect especially severe grain deviations resulting e.g. from top rupture. Additionally, it is necessary to detect these grain deviations in three dimensions. Neither the local nor the stereoscopic resolution is possible until now.

The basic physical principles during the transition of microwaves through timber are damping and phase shift (Fig. 1). The waves are damped, mostly by the water embedded. As the water content changes parallel and perpendicular to grain, damping and phase shift of the waves are changed differently for these too directions ([3] Torgovnikov). Respectively, the phase shift parallel to grain differs from the one orthogonal to grain. Testing the three-dimensional distribution of damping and phase shift in timber is done using microwaves of two orthogonal planes. The mathematical superposing of the resulting waves, leads to an electromagnetic field vector, which is rotating along an elliptic path. The semi-minor axis of this ellipse is in line with the grain direction. Measuring the angular position of the ellipse yields the grain.

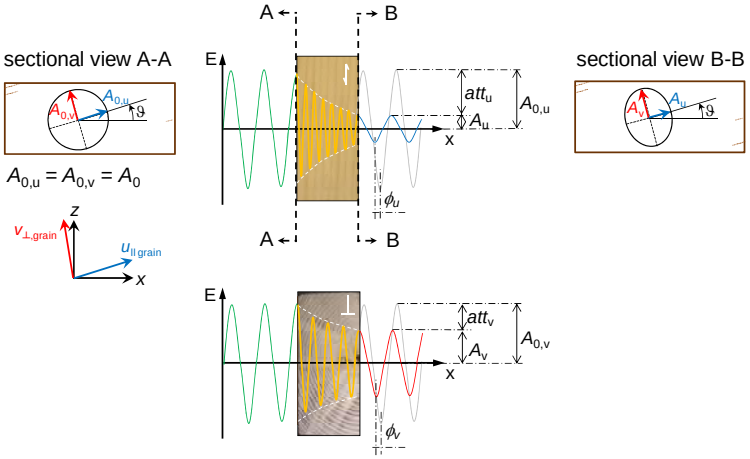

Fig. 1: Principle of transition of microwaves through wood

Holzforschung Austria together with Vienna Technical University – group EMCE developed a prototype microwave system whose layout consisted of 28 transmitting antennas in total, arranged in two rows and 3 receiving antennas arranged in different angles to the timber surface, which uses a frequency of 12 GHz. This setup enables a resolution of 1.25 x 1.25 cm² but also made the development and construction of the prototype very complex.

Very complex and unpredictable physical, mathematical, geometrical, technical and last but not least timber technological challenges have been addressed and solved:

- three dimensional measurement – external reflection on the wood surface as well as internal refraction have to be addressed as soon as the angle between microwave direction and timber surface is different than 90 degrees;
- required combination of antennas is highly complex;
- electromagnetic transmission – due to the transmission of microwaves through air and matter, the necessity of shielding arises to prevent measuring only results from the field around the piece of timber;
- edge diffraction – microwaves are diffracted on edges and the resulting boarder effect distorts the receiving signal.

Various test series show that the prototype is able to identify 84% of the specimens breaking due to top rupture correctly, 16% have not been detected. On the other hand, 28% of the specimens without top rupture have been marked as affected by severe slope of grain ([2] Denzler & Weidenhiller). A comparison between two different available grading machines and a “prototype” machine utilizing the microwave unit was prepared. The results are given below:

grading principle	coefficient of determination
frequency + density	0.61
frequency + density + microwave	0.69
frequency, length, density, knots	0.67
frequency, length, density, knots + microwave	0.70

Grading machines utilizing frequency and density measurements are very common in industry. When combined with the microwave unit the R^2 improves from 0.61 to 0.69, which represents a significant increase in grading accuracy and stands for an improvement in grading.

Grading machines additionally utilizing information on length and knots are much more expensive, hence not that widespread in industry. These machines achieve better grading results on their own – the R^2 value is 0.67 – and improve in combination with the microwave unit to a R^2 of 0.70.

2.2 Density and Moisture Measurement

The detection of density and moisture content is so far still not solved satisfyingly for timber industry. Until now, two separate systems are needed. Systems for density detection utilize X-ray sensors or weight measurements to derive density whereas neither system usually has the means to detect moisture content. Even more, moisture content measurement often requires a direct connection between the moisture meter and the timber, which slows production down. Additionally, moisture content is not evenly distributed in a piece of timber but depends on species and production history.

The use of microwaves enables the detection of density and moisture content contact-less in one and the same pass. In the course of the evaluation of the microwave prototype density and moisture content determination were analyzed. Density was predicted with a COV of approx. 88% (as comparison X-ray devices achieve COV of approx. 97%). Moisture content is predicted with a COV of approx. 90% (as comparison: resistance moisture meters achieve COV of approx. 94%, X-ray devices of 98%) ([1] Denzler & Lux). Not only is the microwave measurement contact-less and therefore fast, is it capable of measuring the whole specimen. As a result, lengthwise moisture and density distribution is available for a more detailed quality assessment of timber.

3. Conclusion

Utilization of microwave measurement in grading will improve existing strength grading techniques. Especially the detection of grain deviation improves the reliability of timber products and eliminates a major obstacle in grading. Additionally, moisture content and density can be detected contact-free in one and the same pass over the whole length of the piece of timber.

4. Acknowledgement

This work was supported by the Austrian Research Promotion Agency - FFG and Wirtschaftsagentur Wien – ZIT within the COMET K-project “HFA-TiMBER A.1.3”, (project nr. 820501). We also thank our project partners DOKA Group Austria, MiCROTEC s.r.l, the institute EMCE of Vienna University of Technology and University of Natural Resources and Life Sciences, Vienna.

References

[1] Denzler J.K., Lux C., Contactless moisture content and density evaluation of sawn timber using microwave transmission, s*ubmitted to European Journal of Wood and Wood Products*, 2013.

[2] Denzler J.K., Weidenhiller A., New perspectives in maschine strength grading - or how to identify a top rupture, Materials and Joints in Timber Structures RILEM Bookseries 9, 2014, p.761-771 DOI 10.1007/978-94-007-7811-5_68, 2013.

[3] Torgovnikov G.I., Dielectric properties of wood and wood-based materials, Springer-Verlag, Heidelberg, 1993.

The comparison of methods for assessment of modulus elasticity and strength of spruce samples

Robert Jára[1], Jan Pošta, Petr Ptáček, Jakub Dolejš, Petr Kuklík

Summary

This paper is focused on comparison of mechanical properties obtained by various procedures. Spruce samples were tested by means of visual assessment, two grading machines, three devices for measuring in-situ and destructive tests. The measuring was carried out on 40 spruce laths with nominal cross section 35/70 mm and length 2.7 m. At first visual assessment was performed. Classification by using grading machines Goldeneye 702 and Metriguard HLT 7200 followed. Three devices were used to measuring the velocity of acoustic wave (Sylvatest, Fakopp and Timber Grader MTG). Destructive tests were performed according to EN 408 to compare results obtained from non-destructive tests. The most important result is the comparison of static and dynamic modulus of elasticity and comparison of strength classes obtained by different methods.

1. Introduction

Structural timber can be sorted into strength classes based on visual assessment or machine grading. Given time efficiency in the woodworking industry (e.g. during production of glued laminated timber, cross-layer timber or massive construction timber) is preferable to use a machine grading of wooden laths or squared timber. Different non-destructive or semi-destructive methods provide information about the physical quantities such as a speed of acoustic signal propagation in the material, energy required for a penetration of a steel tip, X-rays attenuation, and electrical conductivity of the wood and finally a weight of the wood sample. The values of these physical quantities represent input information to determine material properties that determine the strength class of structural timber [2].

[1] Czech Technical University in Prague, University Centre for Energy Efficient Buildings, Faculty of Civil Engineering, Czech Republic

2. Visual assessment

Visual grading is based on the standard [3]. Visual classes can be transferred to the strength classes in accordance to CSN EN 1912 [4] as shown in Tab. 1. The diameter of knot, width of tree annual ring, slope of grains and depth of crack belong among the crucial sorting criteria. For nominal visual classes S7, S10 and S13, criteria for squared timber were used, which are more accurate and can better reflect usage of timber elements loaded mainly in bending. The comparison of results shows a low value of bending strength obtained by destructive tests on the samples, which have been classified to visual class S7. This fact proves a high applicability of the visual grading procedure.

Tab. 1: Transfer of the visual classes on strength classes according to standard [4]

Visual class in the Czech Republic	Strength class in accordance with [2]
S7	C18
S10	C24
S13	C30

3. Machine grading[2]

3.1 Goldeneye 702

The first machine was a Golden Eye 702, which uses X-rays, color and laser scanner. The output quantities are a density (minimum, maximum and average value), dimensions of the element and a modulus of elasticity in a longitudinal direction. The modulus of elasticity is measured over the entire length of the element.

3.2 Metriguard HLT 7200

As the next grading tool, Metriguard HLT 7200 was chosen. This machine uses real deflection of the sample for the calculation of the modulus of elasticity. The average and the minimum values of modulus of elasticity were used for subsequent processing. The achieved outputs are strength class (S0, SI and SII) and the average and the lowest recorded value of the modulus of elasticity.

[2] Machine grading of timber laths was performed on machines of company Stora Enso Wood Products Planá, s.r.o.

4. Non-destructive tests

4.1 Sylvatest

The testing device Sylvatest measures the velocity of ultrasonic wave. This device is able to classify the element into strength class (S0, SI and SII) and to determine modulus of elasticity, based on the species of wood (spruce/pine), shape of the cross section (squared timber, round timber), length and moisture content. Modulus of elasticity was also determined based on the ultrasonic velocity and the material density (Eq. (1)).

$$E = \rho \cdot v^2 \tag{1}$$

where: E is a modulus of elasticity [MPa]
ρ is a density [kg/m^3]
v is a velocity of the ultrasonic wave [m/s]

4.2 Fakopp

Fakopp allows to measure the time of acoustic wave propagation. A way of the calculation of the dynamic modulus of elasticity is the same as in the case of the device Sylvatest. Values of the dynamic modulus of elasticity obtained from the two devices are very similar.

4.3 Timber Grader

Next device for detecting the mechanical properties is the Timber Grader. It determines the strength class according to the standard [2] and the modulus of elasticity based on mechanically generated stress wave and dimensions, moisture content and weight of the sample. The main disadvantage of this device is a necessity of the measurements from the head of the element. It is often unrealistic for the in-situ testing.

5. Destructive tests

The samples were adjusted according to standard [3] for the destructive tests (Fig. 1). Three samples of 700 mm were prepared from laths 2.7 m long. Loading of the sample was controlled by deformation. The maximum force and deformation were recorded for each sample. The aim of destructive tests is to obtain static modulus of elasticity E_{stat} and bending strength f_m.

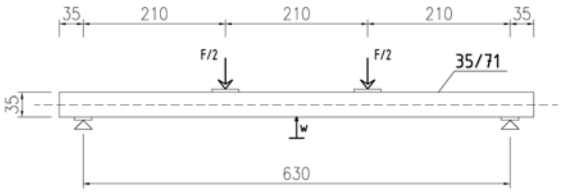

Fig. 1: destructive testing scheme

6. Conclusion

Various procedures for investigation of timber quality are described in this paper. The most interesting result represents the comparison of the modulus of elasticity obtained by means of grading machines and devices for non-destructive testing in-situ with the modulus of elasticity obtained from destructive tests. The highest coefficient of correlation was found for the device Timber grader (Tab. 2). Other acoustic devices Sylvatest and Fakopp also show a high degree of correlation. However, the fact that all three of these procedures require the knowledge of density cannot be overlooked. The coefficient of correlation for grading machine is lower, but this fact had been expected due to the speed of the sorting and zero input data.

Tab. 2: Coefficients of correlation between the modulus of elasticity obtained from destructive tests and other procedures

	Golden Eye 702	Metriguard HLT 7200	Sylvatest	Fakopp	Timber grader
coefficients of correlation R	0,795	0,937	0,936	0,947	0,966

7. Acknowledgement

This work has been supported by the European Union, OP RDI project No. CZ.1.05/2.1.00/03.0091 – University Centre for Energy Efficient Buildings and by the project SGS14/123/OHK1/2T/11.

References

[1] EN 408:2010+A1:2012 Timber structures. Structural timber and glued laminated timber. Determination of some physical and mechanical properties.

[2] EN 338:2009 Structural timber - Strength classes.

[3] CSN 73 2824-1 Strength grading of wood - Part 1: Coniferous sawn timber

[4] EN 1912:2012 Structural Timber - Strength classes - Assignment of visual grades and species.

A new test configuration to determine the slip modulus of connections between crosswise bonded boards

Marcus Flaig[1], Nico Meyer[2]

Summary

A new test method is presented that allows for a more accurate determination of the slip modulus of crossing areas between orthogonally bonded boards compared to the methods used so far. The slip moduli obtained by the new method are compared to the values evaluated from bending tests with CLT beams and from tests with crossing areas subjected to unidirectional shear stresses and the agreement is found to be good.

1. Introduction

In CLT members loaded in plane, the connections between orthogonally bonded boards are subject to shear stresses. While the glued connections themselves can be considered rigid, the wood matrix near the adhesive joint undergoes deformation, which is large enough to affect the global deformation behavior of CLT members significantly. The overall shear deformation of CLT members loaded in plane therefore can be considered as being composed of two parts, i.e. the shear deformation of boards and the shear deformation of crossing areas. While the former part depends on the shear modulus of the boards, the latter part can be described by means of a slip modulus K of crossing areas that indicates the stiffness of connections with crosswise bonded boards. Blaß and Flaig [1] proposed an analytical approach for the calculation of an effective shear modulus of CLT members loaded in plane that takes account of both components of shear deformation. However, while the shear modulus of boards is given in standards, only little information is available on the deformation behavior of connections with orthogonally bonded boards that are subjected to torsional or unidirectional shear

[1] KIT Holzbau und Baukonstruktionen, Karlsruhe, Germany

[2] KIT Holzbau und Baukonstruktionen, Karlsruhe, Germany

stresses. Blaß and Görlacher [1] and Jöbstl et al. [2] performed tests to determine the torsional stiffness of crossing areas but the values obtained from either test series differ considerably. Partly, the disparity can be explained by the different methods that were used in testing: The results presented by Jöbstl et al. include shear distortions within the entire thickness of the two bonded boards whereas deformations due to compressive stresses perpendicular to the grain are contained in the values given by Blaß and Görlacher who applied the torsional moment by means of a clamping. Wallner [3] performed tests with crossing areas subjected to unidirectional shear stresses. Again, the measured displacements comprised deformation not originating from the glued connections and due to CLT untypical loading. Therefore, in all of the earlier studies, the stiffness of crossing areas is underestimated by far and a test method to determine the slip modulus of crossing areas without any influence of test setup and board thickness is needed.

2. Effective in-plane shear modulus of CLT members

In Fig. 1 the two components of shear deformation occurring in CLT members loaded in plane are illustrated. The distortion γ_S in the left picture is due to shear strain in the boards and equals the shear deformation in solid materials (In CLT members with edge-glued lamellae this is the only component of shear deformation). The distortion γ_{CA} shown in the right figure results from mutual displacements and rotations in the crossing areas that occur in CLT members in which the edges of lamellae are unglued. The latter can be calculated in dependence of the slip modulus K of crossing areas and the shear stresses acting in crossing areas. By assuming a linear stress strain relation a fictive shear modulus $G_{\mathrm{eff,CA}}$ can be derived that represents the proportion of shear deformation resulting from the crossing areas. For rectangular cross sections Eq. 1 is obtained where b is the board width, n_{CA} is the number of crossing areas in thickness direction and m is the number of lamellae in direction of the member height [1], [4].

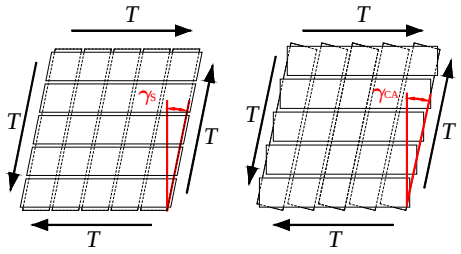

Fig. 1: The two components of shear deformation in CLT members loaded in-plane

$$G_{eff,CA} = \frac{K \cdot b^2}{5} \cdot \frac{n_{CA}}{t_{gross}} \cdot \frac{m^2}{\left(m^2+1\right)} \qquad \text{Eq. 1}$$

The superposition of shear deformation in the lamellae and the crossing areas yields an effective shear modulus $G_{\text{eff,CLT}}$ of CLT members that include both components.

$$G_{eff,CLT} = \left(\frac{1}{G_{lam}} + \frac{1}{G_{eff,CA}} \right)^{-1} \qquad \text{Eq. 2}$$

3. Experimental study

3.1 Single crossing areas - new test configuration

3.1.1 Material

To determine the torsional stiffness of individual crossing areas 24 cross-shaped specimens were cut from two orthogonally arranged layers of CLT slabs. Around the crossing areas to be tested gaps with a width of 25 mm were cut in transversal layers to allow for mutual rotations of the two central boards and for the mounting of measuring devices. Otherwise, transversal layers were not removed to strengthen areas of supports and load application and to reduce the eccentricity in thickness direction. The CLT slabs were bonded with a melamine based adhesive, which is the most common type of adhesive in CLT manufacturing. However, to investigate a possible influence of the adhesive type ten additional specimens with identical dimensions were assembled in the laboratory using one-component poly-urethane adhesive.

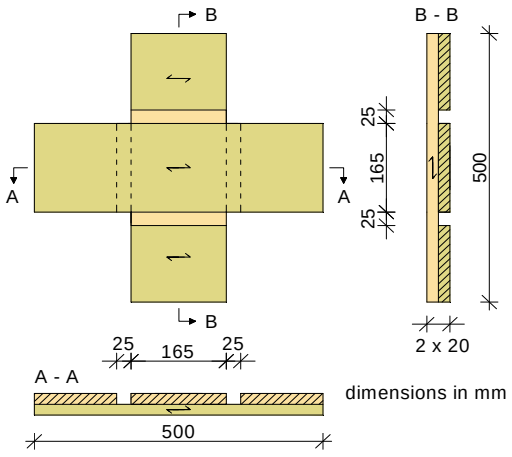

Fig. 2: Dimensions of test specimens

All specimens consisted of Norway spruce (picea albies) with a MC of 10±1%.

3.1.2 Test setup

A steel frame consisting of two crosswise arranged steel bars as illustrated in Fig. 3 was used to apply a torsional moment to the central crossing area of the specimens. The vertical bar of the frame was fixed to the testing machine at its lower end whereas the horizontal arm was connected to the former with only one bolt in the center of the crossing area. The bolted connection allowed free rotation of the horizontal bar but prevented horizontal and vertical displacements relative to the

center of the crossing area. At the ends of both bars, steel plates were welded at right angles to form supports for the vertical board and to apply loads at the ends of the horizontal board.

To enforce a rotation about the centre of the crossing area a single load was applied on one side of the horizontal bar. In the corners of the crossing areas four displacement transducers were arranged in such way that the mutual rotation between the boards could be measured immediately in the plane of the bonded board surfaces. In addition, the rotation of the horizontal board was measured in the centre of the crossing area.

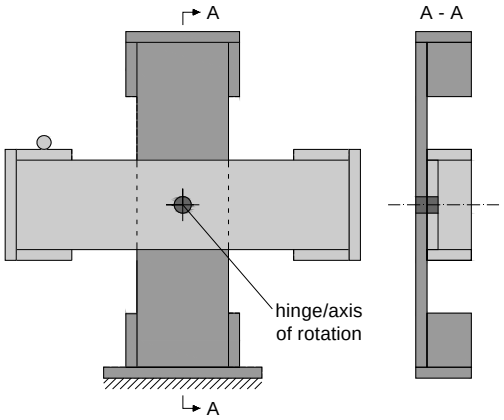

Fig. 3: Hinged steel frame

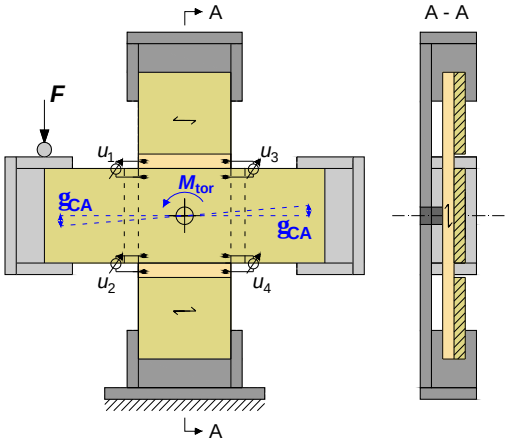

Fig. 4: Test setup

3.1.3 Results

The slip moduli K were calculated from the load rotation curves between 10% and40% of of the ultimate load according Eq. 3 where γ_{CA} is the mutual rotation between the two bonded boards that was calculated from the mean values of the four measured displacements and I_p is the polar moment of inertia of the crossing area.

$$K_{CA} = \frac{\Delta M_{01-04}}{\Delta \gamma_{01-04} \cdot I_p} \qquad \text{Eq. 3}$$

The values obtained for the specimens bonded with the melamine based adhesive range between 6.3 N/mm³ and 10.3 N/mm³ with a mean of 8.3 N/mm³. The test series with polyurethane adhesive resulted in slightly lower slip moduli with a mean of 7.1 N/mm³ and individual values ranging between 5.3 N/mm³ and 8.9 N/mm³. The rotations measured in the centre of the crossing area were rather inaccurate since the measuring devices on the horizontal board had to be fixed to the outer surface averted from the bond line. Consequently, these values were not used to evaluate slip moduli. The torsional shear strength of the crossing areas was calculated according Eq. 4 where M_u is the torsional moment calculated with the ultimate load and b is

the side length of the quadratic crossing area. The results of all tests are given in Tab. 1 and Tab. 2. The compilation also contains the densities of the two boards of each connection.

$$\tau_{tor} = \frac{M_u}{I_p} \cdot \frac{b}{2} \qquad \text{Eq. 4}$$

Tab. 1: Test results - melamine adhesive

No.	ρ_1 kg/m³	ρ_2 kg/m³	τ_{tor} N/mm²	K_{CA} N/mm³
1	581	509	2.71	7.00
2	361	518	2.28	9.40
3	347	395	2.25	7.55
4	535	422	2.49	9.18
5	459	414	3.03	7.77
6	441	447	3.18	8.99
7	369	451	2.93	10.3
8	436	352	2.67	6.42
9	479	482	3.46	8.15
10	419	386	2.79	7.42
11	510	459	3.01	9.16
12	430	412	3.28	8.63
13	451	357	3.50	6.50
14	353	387	2.97	9.77
15	468	418	2.10	9.18
16	382	470	2.04	6.54
17	462	355	3.65	8.04
18	483	409	3.20	7.68
19	383	464	3.19	10.1
20	416	435	2.87	7.52
21	354	380	2.33	7.09
22	386	369	2.69	6.33
23	466	417	2.38	8.95
24	423	473	2.15	9.24
mean	433	424	2.80	8.26

Tab. 2: Test results - polyurethane adhesive

No.	ρ_1 kg/m³	ρ_2 kg/m³	τ_{tor} N/mm²	K_{CA} N/mm³
1	417	420	3.22	8.33
2	387	393	3.44	5.87
3	510	549	4.07	8.91
4	433	436	3.47	8.80
5	415	426	2.88	6.35
6	360	382	3.15	6.29
7	345	344	2.96	5.98
8	557	553	3.87	8.92
9	360	394	3.59	5.28
10	375	398	3.61	5.85
mean	416	430	3.43	7.06

3.2 Comparative tests

3.2.1 Bending tests

In four-point bending tests with CLT beams, the global deflection in the middle of the span and the local deflection between the two single loads were measured [4]. The differences between local and global MOEs evaluated from the respective deflections were used to estimate the effective shear moduli of the CLT beams. From these the slip moduli K_{CA} were calculated using Eq. 1 and Eq. 2 and a shear modulus of the lamellae of 690 N/mm².

Tab. 3: Stiffness properties evaluated from bending tests

series 2-2	$E_{lok,gross}$ [N/mm²]	$E_{glob,gross}$	$G_{eff,CLT}$	K_{CA} [N/mm³]	series 3-2	$E_{lok,gross}$ [N/mm²]	$E_{glob,gross}$	$G_{eff,CLT}$	K_{CA} [N/mm³]
	12160	10880	300	7.35		9255	8685	409	11.1
	13024	11528	291	6.99		9240	8558	336	7.27
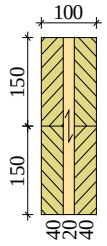	13752	11744	233	4.89	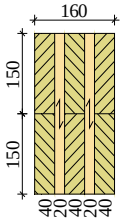	10568	9495	271	4.96
	10400	9376	276	6.39		9165	8573	384	9.64
	10952	9416	195	3.76		9983	9353	430	12.6
	7680	7216	346	9.64		7433	6893	275	5.08
	8120	7424	251	5.47		7613	7163	351	7.95
	7872	7016	187	3.56		6983	6630	381	9.43
	8048	7560	361	10.5		7200	6863	424	12.2
	8184	7448	240	5.11					
mean			268	6.36				362	8.92

3.2.2 Diagonal compressive tests

Compressive tests according to a method proposed by Kreuzinger and Sieder [5] have been performed to determine the in-plane shear strength and stiffness of three-layered CLT slabs. Rectangular specimens were cut at an angle of 45° to the direction of boards and compressive load acting in plane direction was applied at the narrow side of the specimens. The test setup is shown in Fig. 5. From the vertical shortening u_y that was measured on both surfaces of the specimens the MOE at an angle of 45° to the materials principle axes was evaluated. Assuming the MOEs of the lamellae with values of 11000 N/mm² parallel to the grain and 370 N/mm² perpendicular to the grain, respectively, the shear modulus $G_{xy,M}$ of the specimens, which is equal to the effective shear modulus $G_{eff,CLT}$, was calculated by transformation into the material coordinate system (x_M,y_M). The slip moduli of the crossing areas were calculated as described in section 68.2.1.

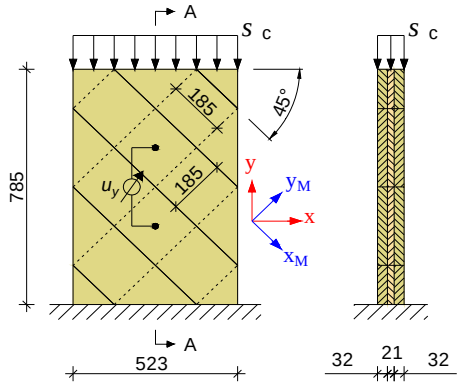

Fig. 5: Setup of diagonal compressive tests

Tab. 4: Results of diagonal compressive tests

No.	E_v in N/mm²	$G_{eff,CLT}$ in N/mm²	K_{CA} in N/mm³
C1	1493	449	10.0
C2	1809	569	25.2
C3	1532	464	11.0
C4	1618	495	13.6
C5	1692	523	16.8
mean	1629	500	15.3

4. Discussion and conclusions

The presented test method allows for the measurement of rotations immediately in the plane of the bonded board surfaces and the experimental determination of the slip modulus of crossing areas without any influence of the test setup and the board thickness. The obtained values are suitable to calculate the proportion of shear deformation of CLT members resulting from stresses in the crossing areas. This allows for the distinction between shear deformation in the crossing areas and shear deformation within the boards, which is useful in the calculation of the overall shear deformation of CLT members by means of an effective shear modulus, which depends on the layup and the board width and therefore is not a constant value.

The torsional stiffness of crossing areas that was determined by means of the new test method are roughly two times as high as found in earlier studies. The slip moduli of the specimens bonded with the polyurethane adhesive were slightly smaller than for the melamine bonded, however, the influence of the adhesive type was found to be rather small. In Tab. 5 the slip moduli obtained from different test series with individual crossing areas are given together with the slip moduli evaluated from beam tests and from diagonal compressive tests. The comparison of the values shows that there is good agreement between the slip moduli determined by the new test method and both, the values evaluated from bending tests and the values presented by Blaß and Flaig (2013) for crossing areas subjected to unidirectional shear stresses. The slip moduli that were evaluated from diagonal compressive tests, in contrast, are even higher than the former. The higher values are mostly due to unintended gluing between the edges of adjacent lamellae that was observed in the tested specimens but may also result from friction to some extent.

Tab. 5: Slip moduli of crossing areas obtained by different test methods

Author	Test method	Slip modulus in N/mm^3
Blaß and Görlacher(2002)	single crossing areas (torsion)	4.87
Jöbstl (2004)	single crossing areas (torsion)	3.45
Wallner (2004)	single crossing areas (unidirectional)	4.26
Flaig and Meyer (MUF)	single crossing areas (torsion)	8.28
Flaig and Meyer (PU)	single crossing areas (torsion)	7.06
Flaig (2013)	four point bending tests with CLT beams	7.57
Blaß and Flaig (2013)	two crossing areas (unidirectional)	7.67
Flaig and Meyer	diagonal compressive tests with CLT slabs	15.3

References

[1] Blaß H. J., Görlacher R.: Zum Trag- und Verformungsverhalten von Brettsperrholzelementen bei Beanspruchung in Plattenebene. Bauen mit Holz, 104 (11/12): H.11, 2002, S.34-41, H.12 S.30-34.

[2] Jöbstl, RA; Bogensperger, T; Schickhofer, G: Mechanical Behaviour of Two Orthogonally Glued Boards. In: Proceedings. 8th World Conference on Timber Engineering, Lahti, Finland, 2004

[3] Wallner, G: Versuchstechnische Ermittlung der Verschiebungskenngrößen von orthogonal verklebten Brettlamellen. Diploma thesis, TU Graz, Institut für Stahlbau, Holzbau und Flächentragwerke, 2004

[4] Flaig, M: Biegeträger aus Brettsperrholz bei Beanspruchung in Plattenebene. Dissertation, Karlsruhe Institute of Technology, Holzbau und Baukonstruktionen, Karlsruher Berichte zum Ingenieurholzbau, Bd. 26, KIT Scientific Publishing, 2013

[5] Kreuzinger H, Sieder M: Einfaches Prüfverfahren zur Bewertung der Schubfestigkeit von Kreuzlagenholz / Brettsperrholz. Bautechnik, 90(5) 2013:314–316

[6] Flaig M., Blaß H. J.: Shear strength and shear stiffness of CLT-beams loaded in plane. In: Proceedings. CIB-W18 Meeting 46, Vancouver, Canada, 2013, Paper 46-12-3

Performance study of displacement transducers for timber material under compression tests using photogrammetric approach

Ahmed Mohamed[1], Rémi Caudoux[2], Hexin Zhang[1]

Summary

Many different test methods have been developed and adopted by different researchers to evaluate the mechanical properties of timber materials. Among these methods is compression test method, which is one of the most common used methods to determining modulus of elasticity and the other elastic and strength properties. The test results are among those essential properties to be used to establish the product specifications or design of buildings. Measuring the deflection of timber specimen accurately during testing is essential to evaluate the value and variation of the modulus of elasticity.

Displacement transducers (LVDTs) are commonly used for assessing the deformation or displacement measurements on timber. Even though these sensors themselves are proven to be accurate and reliable, limited research has been conducted to assess their performance on monitoring the deformation of timber samples especially together with the system that attached them onto the sample surface during compression test. To study the system performance of these LVDTs, the non-contact photogrammetric approach has proved to be an efficient and accurate way of monitoring this performance. The ability of monitoring multi-point/region on a sample surface at the same time will enable us to monitor not only the sensor itself but also the performance of the mounting system.

In this study, a non-contact binocular stereo system developed in this project was used to evaluate the performance of LVDT displacement transducer. This test result has revealed how to find a proper way to mount the sensor on the surface of the timber sample to minimize the error. Several test series were conducted with nine

[1] School of Engineering and Built Environment, Edinburgh Napier University, Edinburgh, UK

[2] Department of Civil Engineering, University of Glasgow, Glasgow, UK

timber samples in compression perpendicular to grain direction. After validating the proposed approach, its measurements were compared with the conventional measuring displacement transducers. The experimental results show that the readings measured by the LVDT sensor were mostly influenced by the setup of this device when mounted on timber. The results also showed that the optical system not only allowed assessing performance and reliability of this sensor but also allowed monitoring the deformation of the samples at various locations by providing more information, which would not be possible to obtain using the traditional techniques. This will provide a better understanding of the deformation of the test sample and may assist in finding a proper way to mount this device on timber when a high measuring accuracy is needed.

1. Introduction

There are many different test methods that have been developed and adopted by different researchers to evaluate the mechanical properties of timber and timber-based composite materials. Among these methods and according to EN 408 (2010) [4], the compression test is used in timber as a method to determine modulus of elasticity (MOE) and some other elastic and strength properties of this material. The test results are of considerable importance as they are among those essential properties to be used to establish the product specifications or design. To understand the material characterizing the behavior of glulam timber, it is essential to obtain accurate measurement of its material properties but this can be challengeable especially for commonly used properties such as modulus of elasticity.

Measuring the deflections of the timber specimen accurately and effectively during the compression test plays an important role in evaluating the value and variations of the MOE. Displacement transducers are commonly used for assessing the deformation or displacement measurements on timber. These sensors have been widely used and proven to perform accurate, reliable and immediate displacement measurements. However, the setup of these devices in timber during the compressive loading test is challengeable and significantly more difficult. It requires applying a mounting system to accommodate LVDTs and this system should be placed in contact with the surface of the specimen to be tested and this might affect their reading values. Moreover, limited research has been conducted to assess the performance of transducers on monitoring the deformation of timber samples especially together with the system

that is used to attach them onto the sample surface during compression test. Therefore, additional measurement technique that improves understanding the behavior of these sensors during testing is the binocular stereo vision approach.

Monitoring tools using photogrammetry and image processing have been used in timber to measure mechanical properties, 3D displacements, or deformations at various points of the same member, as proposed in various experiments [1-3, 5-6, 8-9]. The binocular stereo vision approach is proposed and developed in this study for the deformation measurements. Binocular stereo vision is a non-contact measurement technique that can be used to extract reliable measurements of physical objects from stereo images. The main advantages of this technique compared to the traditional techniques are that it offers the capability to measure three-dimensional (3D) location of any point located on the object surface; in addition to that it can be used to monitor the deformations of the object at various locations without having to touch the object.

The main objective of the work presented has been to use the developed non-contact binocular stereo system for evaluating the performance of LVDT displacement transducer during the compression test. Another objective of this project was to measure the displacements of the sample at various locations to understand its behavior and give basis for further studies. An experimental study was conducted to validate the proposed technique. After being validated, this technique was applied to an experimental study of timber specimens subjective to compressive loading perpendicular to grain in the elastic range. The contact-free technique is found promising as a method of determining deflection of timber specimens under loading. These measurements allowed us to evaluate the performance and reliability of LVDT transducers as well as their mounting system, which should be in contact with the timber specimen during compressive loading. The methodology and measurement process performed in this study are discussed in the following sections and can be summarized in the workflow diagram in Fig. 1.

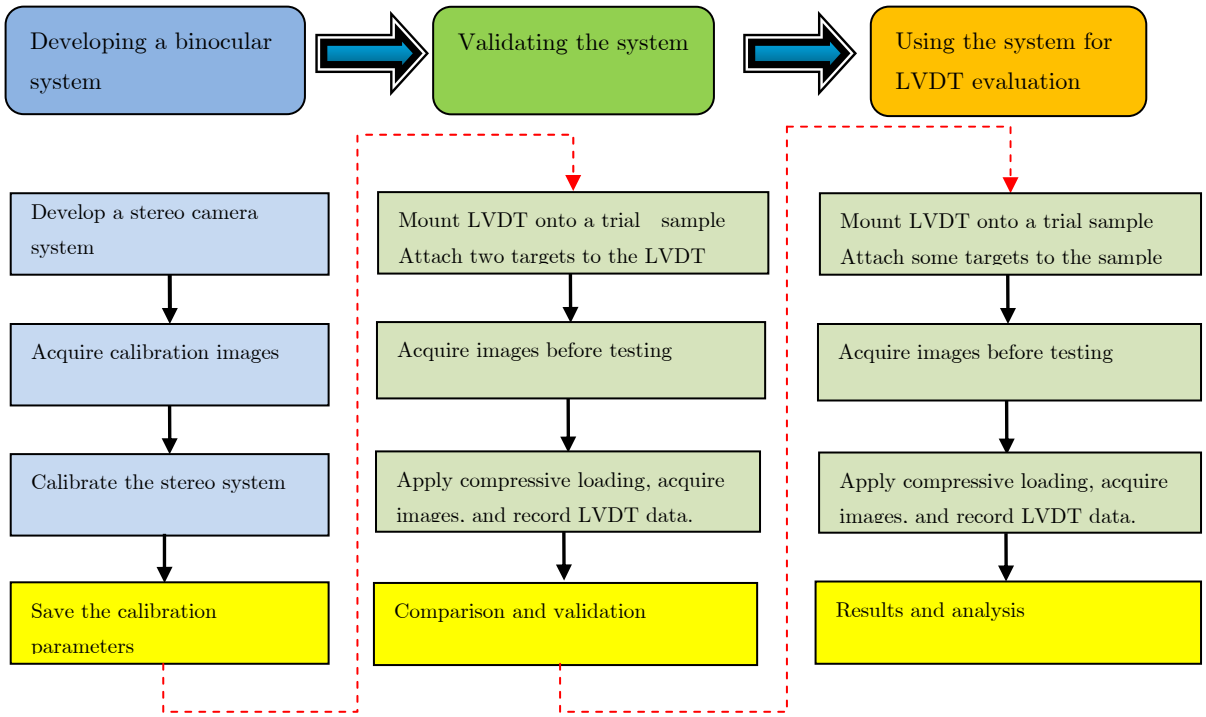

Fig. 1: Workflow diagram of the experimental work

2. The Binocular stereo system

The principle of this technique is based on the comparison between two stereo images of the same object taken from different locations and orientations by two cameras [12]. To obtain 3D reliable measurements and to correct lens distortions, the two-camera system must be calibrated before acquiring the stereo images of the targets. After calibrating the system, the position of the measurement targets on the object can be tracked and evaluated by software algorithms based on the principals of photogrammetry and stereo vision.

In order to identify the 3D locations of the target points on the object, the corresponding points in the two images captured by the binocular stereo system have to be determined. The correspondence problem is the main step in the stereo reconstruction, in which the disparity of each point is determined. Once the stereo vision system has been calibrated and the corresponding points have been identified and matched in two stereo images, the 3D positions of the points can be determined based on triangulation technique and the calibration parameters [12]. These 3D measurement data can then be used to calculate different properties such as the relative displacements between the points or strain.

Generally, the steps for the derivation of 3D information mainly include: acquiring calibration images, calibrating the stereo camera system, rectifying images, using region of interest, 3D reconstruction, transforming the results into world coordinates, and visualizing the results [11]. Detail discussion of each step can be found in [11].

Fig. 2 shows the optical system consisting of a pair of Basler Pilot piA2400-17gm cameras, calibration plate, two motorized pan tilt units with remote controls, a tripod with a frame for adjusting the cameras. These cameras were connected via Gigabit Netgear switch to a desktop computer (PC2) with frame grabber and the image processing software installed. Additionally two LED light sources were employed to assist in providing a homogenous illumination of the calibration plate during the calibration process. The two stereo cameras used for image acquisition have a resolution of 2456 x 2058 pixels (5 megapixels) and were fitted with a Computar (M2518-MPW 2/3" F1.8) Megapixel lenses with a constant focal length of 25mm and pixel size of 3.45 microns. To produce images that cover the area of interest utilizing these lenses, the two-camera system was placed at approximately 74 cm from the sample to be monitored; resulting in a field of view covered an area of about 220 x 220 mm. The Basler cameras were mounted on motorized pan tilt units to enable panning and tilting the cameras by using a remote control connected to them. The pan tilt units were fixed on a frame with a stereo baseline of approximately 30 cm.

Prior to all the tests, the left and right cameras must be calibrated. The calibration of the binocular system is an important step to determine the internal camera parameters (focal length and lens distortion parameters) describing the mapping of the 3D world into pixels and the external camera parameters describing the relative pose of the left camera in relation to the right one (3D position and orientation between the two cameras). A100mm x100 mm standard calibration plate, chosen according to the estimated dimensions of the region of interest to be captured as described in [10], was placed in front of the two cameras as can be seen in Fig. 2-a and it was acquired from the left and right cameras in 54 different positions and orientations relative to the vision system. The image coordinates of the calibration images were extracted and the parameters of the stereo setup are determined via a least square solution with suitable chosen parameters of the cameras that can be determined from the specification of the camera sensor and lens [10]. A software package was developed based on visual C++ 2010 with the use of libraries for the

image processing software HALCON version 11 [10]. This software provides all necessary tools required to easily and accurately perform the calibration of the binocular stereo system. Implemented in the Microsoft Foundation Classes (MFC), the graphical user interface (GUI) for this package provides the functions necessary to calibrate the binocular system and to record the image data during testing. Fig. 2-b, shows an image of the GUI providing two calibration images of the calibration plate acquired from the two cameras in the process of calibrating the stereo camera system. This Figure is also shows the extracted calibration marks and calibration parameters for each camera. These parameters were then saved to be used in the calculation of the 3D positions of the photogrammetric targets from its stereo projections by triangulation. Using these 3D data, the relative displacements were determined.

(a) (b)

Fig. 2: Camera calibration: a) Stereo camera systems during calibration, b) Image of the implemented GUI during stereo camera calibration

3. Materials and methods

3.1 Materials and displacement measurement sensors

Glulam timber beams, as can be seen in Fig. 3-a, were cut into cubic glulam blocks to provide samples to be used in the present study. The dimension of these samples is shown in Fig. 3-b. As described in EN 408(2010) standards, in order to ensure uniform loading, the test blocks were accurately prepared and their loaded surfaces were cut smoothly and accurately to be parallel to each other and perpendicular to the test piece axis. Prior to testing, all wood samples were stored in a conditioned

room with a temperature of approximately 20°C and a relative humidity of approximately 60 % in accordance to the standards.

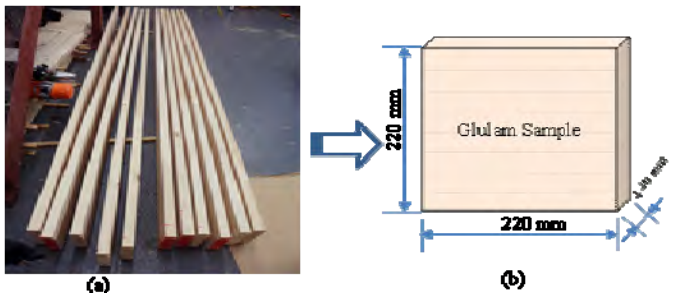

Fig. 3: Material used in the study: a) Image of glulam timber beams, b) Schematic view of a compression test sample with its dimensions

In this study, two different measurement methods, LVDT displacement transducers and a non-contact deformation measurement system were used to monitor the deformation of the samples during testing. The LVDTs (model D5-200A GRA)[7] make an accurate displacement measurements with a range of ±5 mm and a sensitivity of ±0.015 mm. This sensor needs a mounting system, which should be in contact with the compressive load samples. In order to get more reliable and accurate measurements, the contact surfaces between the wood and the mounting system, which is used to accommodate the LVDT sensor, should be minimized. This was achieved by fabricating special clamps, composed of a steel plate and a steel angle, and these clamps were attached to the sample using a single screw. In order to clamp the LVDT body into the mounting system, a plastic fitting was fabricated and glued securely to the steel plate.

3.2 Experimental validation of the approach

After conducting the calibration of the binocular system and before applying this system for evaluation purposes, it is important that the system should be validated. The first experiment setup, shown in Fig. 4, was used for the validation of the method proposed in this study. In this setup, LVDT sensor and the calibrated binocular stereo system were both employed to monitor displacements between two points over the gauge length (8cm) on the sample during the compressive loading. The LVDT sensor was mounted in a trial sample using the fabricated mounting system. Two targets were attached to LVDT transducer at two points representing the gauge length of the sensor and they were intended to be used for comparing the LVDT readings with the optical system.

Four compression evaluation tests were carried out according to the European standard procedures described in the EN 408(2010) [4] at E65 timber laboratory at university of Edinburgh Napier. A Zwick/Roell Z050 (Zwick GmbH & Co, Germany) universal testing machine with maximum load capacity of 50 kN was used to test the specimens. This machine was equipped with a load cell connected, via a data acquisition system, to a desktop computer (PC1) that has its own software to be used for controlling and monitoring the experiments and collecting the data (time, load, deformations). Due to capacity limitation, the testing machine was only used to perform the compression tests perpendicular to the grain direction. These tests were conducted in displacement control, with 0.02 mm/second cross-head displacement rate of the testing machine. Timber sample was placed in the Zwick testing machine in front of the optical system. An initial pair of stereo images was captured by the two cameras before applying loads to the timber sample to allow comparison with the subsequent data. During the load application, the load and relative deformation measured from the LVDT were recorded through the data acquisition system and the implemented software was used to automate recording images of the surface of the sample with a time interval of about 1 second.

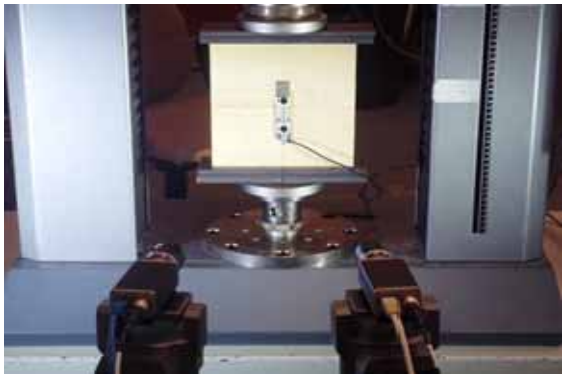

Fig. 4: Stereo camera systems and targets attached to LVDT

3.3 Experimental setup and procedure of the compression test

Nine specimens, which were cut from the same timber beam, were selected to be tested with the compression tests performed in this study and carried out according to the procedure described in the previous section. The same configuration of the binocular stereo system, which was used during the calibration process, was also used during conducting the sample with compressive loading. Before performing these tests, a total of thirty targets were applied to the timber samples for optical deflection measurements. These targets (named as P1 to P30) represent black circular marks on a white background to be easily distinguished during image processing

stage. They were glued to one side of the timber sample as shown in Fig. 5. Some of these targets (P9, P10, P21, and P22) were installed in accordance to LVDT and were intended to be used for comparing the LVDT readings with the optical system. The compression test sample was then centered between two spherically seated loading heads enabling the application of a compressive force free of bending [6]. Two LVDTs (LVDT1 and LVDT2) with gauge length of 8 cm were placed at the mid-height of the timber sample on two opposite sides, providing a local displacement measurement. Fig. 5 shows a schematic plot of the experiment setup and equipment used during testing, including the Zwick testing machine and the binocular vision system. An Image of the experimental setup is shown in Fig. 6.

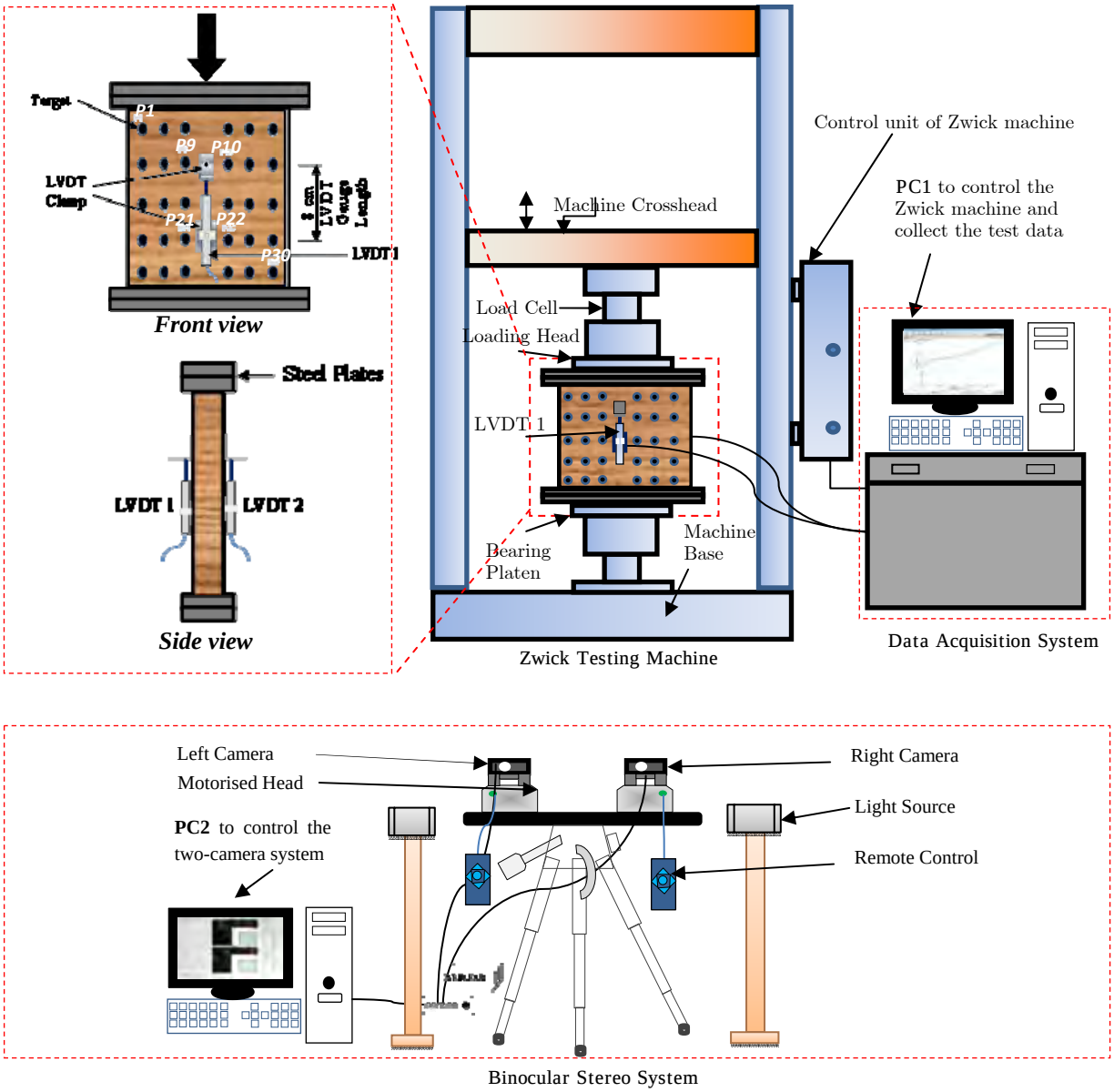

Fig. 5: Schematic plot of the experimental setup of compression test with instrumentation

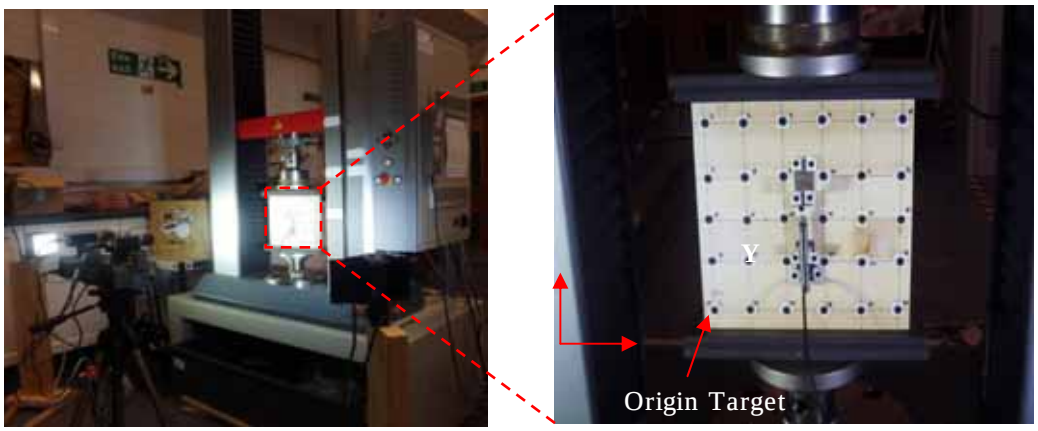

Fig. 6: Image of experimental setup of compression test (left) and a detail of a timber sample (right).

After calibrating the stereo camera system, three tests were conducted on each timber sample in the direction perpendicular to the grain. The two camera system, placed at one side in front of the testing machine, was only used during the second test for each sample. Before starting the actual compression tests, preliminary tests were conducted on a trial sample to determine the rate of loading and to estimate the elastic range of the sample in order to ensure that no permanent deformation occur during the compression test and to avoid any damage that might occur during testing.

The deflection of the sample, rate of loading, and the maximum load to be applied to the system were then determined and a 12 kN was found to be appropriate to load the sample in the elastic range. The timber samples were tested based on these measurement data. Before applying the actual load, pre-loaded with a force of 1kN was first applied to the wood test sample in order to enable it to be seated properly. The sample was then efficiently held to allow the two cameras to capture the initial state of the sample and the LVDTs were initialized to zero displacements through the data acquisition system. Using a displacement control of 0.02 mm/second, the samples were loaded constantly thought the test. The loading and displacements were recorded simultaneously using load cell and LVDT sensors connected to a data acquisition system at 0.1 second interval.

During loading, the implemented application software was used to automate recording images of the sample surface acquired by the two cameras with a time interval of about 1 second. At the end of loading the sample, the machine was set to let the crosshead displacement control to stay in the same position to allow capturing the final state of the sample.

4. Results and discussions

4.1 Validation tests results

The relative displacement in Y direction (the load direction) between the centroid of two targets (P1 & P2) was obtained by processing the images these targets captured by the cameras, and the corresponding relative displacement between two points (gauge length) was measured by the LVDT. These measurements were plotted in the same figure to be compared to each other. Fig. 7 shows some selected examples of these comparisons and indicates remarkable correspondence. In this figure, the displacements obtained from the two-camera system describe very well the measured vertical displacement using the LVDT sensor, which highlights the efficiency of the proposed approach.

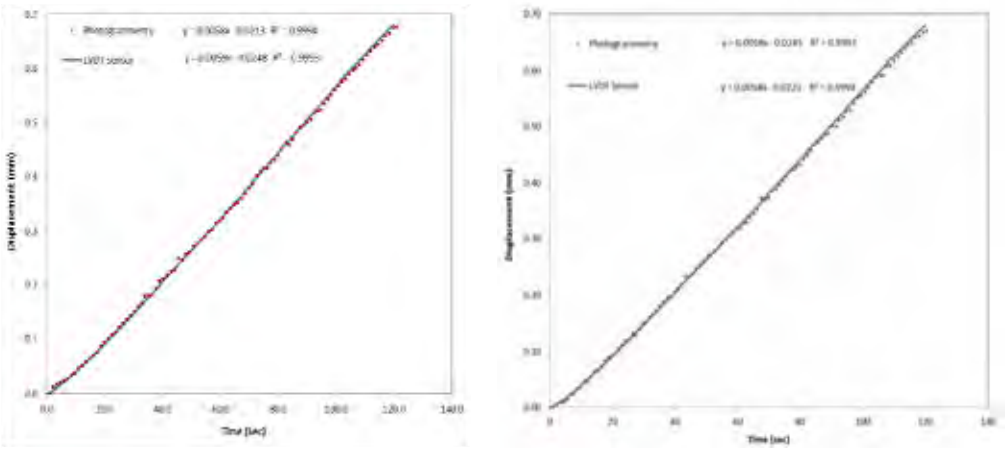

Fig. 7: comparisons between LVDT and optical measurements for sample 1 (left) and sample 2 (right)

4.2 The compression test results

The relative displacements between the targets P9 and P21 as well as those between P11 and P22 were calculated in the vertical direction using the photogrammetric measuring system in order to be compared with those measured by the LVDT sensor. The averages of these measurements in addition to the corresponding relative displacements measured by the LVDT are shown in Fig. 7. Although the trends followed are similar, but there is a considerable difference in deflection values measured by the two methods. This may be attributed to the fact that the setup of LVDT on timber will affect its reading values and the clamps used to attach this sensor might move during loading. This result also highlight that it is important to carefully select different fixture system for the LVDT to reduce the errors.

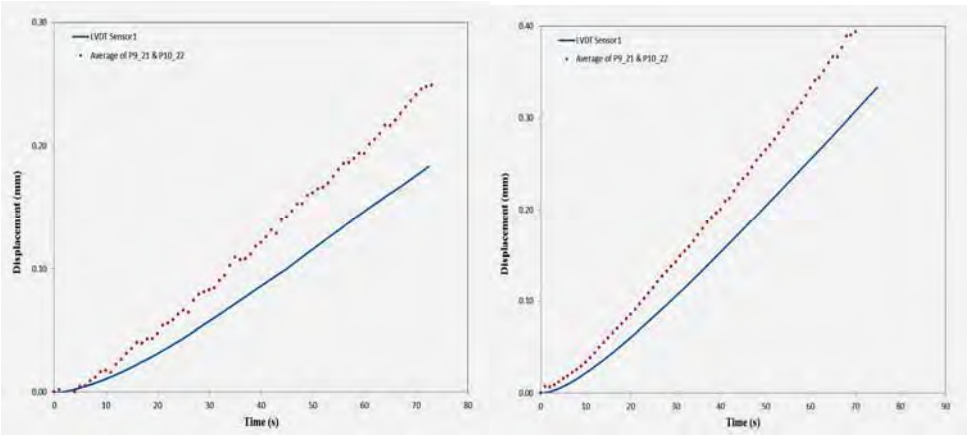

Fig. 8: Comparison of the measurement results for sample 1 (left) and sample 2 (right).

References

[1] Choi, D., J. Thorpe, and R. Hanna, *Image analysis to measure strain in wood and paper.* Wood Science and Technology, 1991. 25(4): p. 251-262.

[2] Dahl, K. B., and K. A. Malo. "Planar strain measurements on wood specimens." *Experimental mechanics* 49.4 (2009): 575-586.

[3] Dahl, Kristian B., and K. A. Malo. "Linear shear properties of spruce softwood." Wood science and technology 43.5-6 (2009): 499-525.

[4] EN 408:2010 Timber structures - Structural timber and glued laminated timber - Determination of some physical and mechanical properties, CEN, Brussels, 2010EN 408:2010.

[5] Franke B., Hujer S., Rautenstrauch K., Strain analysis of solid wood and glued laminated timber constructions by close range photogrammetry. International Symposium of Non-Destructive Testing in Civil Engineering, 16-19 September, Berlin, Germany. , 2003.

[6] Garcia, Dorian, and Jean-José Orteu. "3D deformation measurement using stereo-correlation applied to experimental mechanics." Proceedings of 10th FIG International Symposium on Deformation Measurements, Orange, California, USA. 2001.

[7] I RDP. Electronics Ltd, http://www.rdpe.com/ .

[8] Jaroslav Hrázský, Pavel Král. Analysis of Selected Mechanical Properties of Construction Wood KVH and Parallam 2.0 E.

[9] Maas, H-G., and Uwe Hampel. "Photogrammetric techniques in civil engineering material testing and structure monitoring." *Photogrammetric engineering and remote sensing* 72.1 (2006): 39.

[10] Mvtec. (2006). HALCON/HDevelop Reference Manual, In HALCON Application Note, Germany.

[11] MVTech Software GmbH. HALCON. The software for Machine Vision Applications. http:// www.mvtech.com/halcon/

[12] R. Hartley and A. Zisserman. Multiple View Geometry in Computer Vision. Cambridge University Press, 2003.

Utilization of nanotechnologies for prevention of fungal growth

Monika Terebesyová[1,2], Pavla Ryparová[1], Petr Ptáček[2]

Summary

The early stages of fungal decay are often characterized by dramatic decreases in some mechanical properties that can lead to serious failure of construction. Although the proper maintenance and well-designed durability can minimize damage from the biodeterioration agents, some uses require special chemical treatments to extend economic life of wood products. With regard to toxicological and ecological considerations, many chemicals based on arsenic, chromium, pentachlorphenol or creosotes are being prohibited because of the health risk or leaching to environment. As alternative, combinations of environmentally friendly biocides and nanotechnology have been consequently investigated. As an additional protection, nanofiber textiles enhanced by active substances could be also used. They create a thin layer on the surface of the protected material and prevent attack by deterioration agents. The aim of this project is to study the properties and behavior of nanofiber-wood interactions.

1. Introduction

The ability of a construction to resist degradation depends on its materials and design, on maintenance and on the surrounding environment. The problem of wood building materials, components or systems is their porous structure that causes the propensity to some form of moisture attack. Water damage in wood buildings is caused by moisture exceeding the tolerance of structure and usually starts occurring slowly. It can take several months before the effects are detected and a substantial part of the building or object may be already affected. Rising damp not only have an aesthetic effects on walls but also cause considerable damage to buildings, high moisture content often leads to structural destruction, cracking walls and contribute to the vulnerability of people.

[1] CTU in Prague, Faculty of Civil Engineering, Prague, Czech Republic

[2] UCEEB - University Centre for Energy Efficient Buildings, Buštehrad, Czech Republic

Excess moisture on almost all indoor materials leads to contamination and growth of microbes, such as mould, fungi and bacteria, which initiates chemical or biological degradation of materials, pollutes indoor air and induces a potential health risk. Some wood-decaying fungi are able to reduce the strength of building materials as much as several tens of percent, causing devastating effects in the whole building.

2. Background approaches

2.1 Fungal attack

Wood decay fungi obtain nourishment by digesting wood cell walls, thus causing deterioration of the wood. Fungal hyphae secrete extracellular enzymes and other agents that depolymerize wood cell wall, these depolymerized materials are then absorbed into the fungal hyphae where they are assimilated and further metabolized [1]. On the basis of physical and chemical changes produced in wood and the resulting alterations in color and appearance of decaying wood, decay fungi are classified as brown, rots, white rots, and soft rots. Brown-rot fungi cause the wood to darken, shrink, break into cubicles that are easily crumbled and they preferentially attack softwoods. Since softwood species have predominantly been used for building construction, brown-rot decay fungi have been the most common agents of decay in buildings [2].

In the early stages of decay, wood may undergo discoloration or take on a mottled appearance, but will not undergo obvious changes in appearance. Despite the fact that incipient decay may be difficult to detect visually with certainty, it can cause significant reductions in wood strength [2]. Wilcox [3] indicated that the properties most likely to be of consequence in light frame walls could be reduced by approximately 20% before decay can be reliably identified as being present. He also indicated that bending strength is more sensitive to incipient decay than compression of shear parallel to the grain.

Yang et *al.* [4] specified weight loss and strength loss in slash pine wood after a 12 week exposure period to white-rot and brown-rot decay fungi. The data are shown in Table 1. The results demonstrated that considerable bending strength loss occurs before any appreciable weight loss occurs. The weight loss, WML, MOR, and MOE reductions of all growth rate samples caused by the brown-rot fungi were greater than those exposed to the white-rot fungi, with the exception of the early stages of

decay [4]. One explanation may be brown-rot decay fungi degrade mainly the cellulose and hemicelluloses by depolymerization without extensive loss of lignin, and the effect of hemicelluloses degradation on the mechanical properties of wood during brown-rot decay is significant [5].

Tab. 1: Comparison of mechanical property and weight loss due to fungi type and exposure period. [5] (modulus of rupture (MOR), modulus of elasticity (MOE), and work to maximum load (WML))

Dependent Variable	Fungi	Exposure period (weeks)					
		2	4	6	8	10	12
Weight loss (%)[1]	White-rot[2]	0.63[3]	0.66	0.79	1.03	1.08	1.20
	Brown-rot	0.01	1.12	3.43	6.63	9.72	11.59
WML loss (%)	White-rot	1.33	2.26	1.69	2.51	4.60	3.14
	Brown-rot	6.24	15.96	32.17	32.32	34.18	44.56
MOR loss (%)	White-rot	0.66	1.06	0.83	1.57	2.76	3.99
	Brown-rot	5.14	14.39	29.07	28.51	28.07	40.37
MOE loss (%)	White-rot	0.96	5.35	0.63	1.20	7.53	6.04
	Brown-rot	0.27	8.53	15.50	16.69	23.15	25.42

[1] All loss values were calculated based on to the control test. N=360.

[2] N=30 for white-rot and brown-rot fungi with every exposure period, respectively.

[3] Every value in this table is an average value from 30 specimens, which is according to the control test at fast, medium, and slow growth rate, respectively.

2.2 Nanotechnology

In the present, the service life of wooden products exposed to wet conditions is usually increased by using more durable wood species or by treatment of wood with effective and ecologically convenient fungicides [6]. Nanotechnologies are surely promising for wood preservation, as well. Nanoparticles of metal (silver, zinc, copper, titan, etc.) have been mostly verified in regard to wood protection. Nanometal characteristics may be totally different from the characteristics of the elemental metals and potentially may perform in an unusual manner. If their particle size is smaller than the diameter of pores in the bordered pits or in the wood cells, complete penetration and uniform distribution in wood can be expected [7].

The copper compounds and NPs have enhanced antimicrobial activities toward a broad spectrum of microorganism, including pathogenic bacteria. Several copper-based nanostructures have been investigated for their potential bactericidal photocatalyst and for self-sterilizing biosensor application [8]. Ghasemian et al.[9] is reported the antibacterial effect of copper and silver NPs for strain of *Escherichia coli*

and *Bacillus subtilis*. The elemental silver or silver ions are well known as antimicrobial agents in curative and preventive health care for many centuries [8]. This metal is caused of destroy DNA or enzymes, that it have strong toxicity to broad range of microorganism but simultaneous a remarkable low human toxicity [10]. However, a report on ionic silver showed little effect on inhibition of decay and mold fungi in laboratory tests [11].

Another approach in application of nanotechnologies for wood protection is additional application of nanofiber textile augmented by antimicrobial agents. Because of the specific and extraordinary properties of nanotextiles, such as low weight per unit area or large specific area, it is possible to apply the nanofiber coating directly on the surface of the protected materials. This layer creates a thin film, since the fibers are only 100-500 mm thin; therefore, the host material (e.g. wood) does not lose its color or texture [12].

In our study, we focused on utilization of nanofiber textile doped with commercially available biocides (based on Propiconazole, IPBC and H_3BO_3) for antifungal purpose. The biocide agents are strongly bound to the fibers and that reduces their leaching into the surrounding environment.

2.3 Experimental method

The nanofiber fabrics were prepared by electrospinning on Nanospider TM LB 500 device (Elmarco, Czech Republic) in the Center for Nanotechnology in construction at the faculty of Civil Engineering. "Nanospider" technology works on principle of needleless electrospinning where the cylinder (cathode) is connected to a high voltage source covering itself with a thin film of polymer solution The anode is created by a slab on which are the nanofiber formed (Fig. 1). The electric field pulls out, elongates and thins the fibers that are finally collected on the slab (Fig. 2). The resulting fibers have typical thickness from tents to hundreds of nanometers. The process of electrospinning itself is dependent on many parameters, choice of polymer type and viscosity of its water solution, or different solvent solution [13].

The nanofiber textiles were prepared at common laboratory conditions at the temperature of 23°C and relative humidity of about 40%. The nanofibers themselves were spun on a polymeric support textile substrate. A polypropylene (PP) base substrate with the width 500 mm, weight of 18g/m² and an antistatic treatment was used. The basic solution for electrospinning was prepared from PVA polymer with

addition of commercial fungicides at different concentrations. We prepared 18 types of samples, half of them are single-layer membrane and the other half is double-layer.

Coniophora puteana was chosen as a model wood destroying. The experiment will be made on Petri dishes with malt-agar cultivating soil as a screening test with poisoned filter papers and nanofiber textiles.

This study will show if the prepared nanofiber textiles base on PVA doped by different fungicides represent potential protective layer for building constructions.

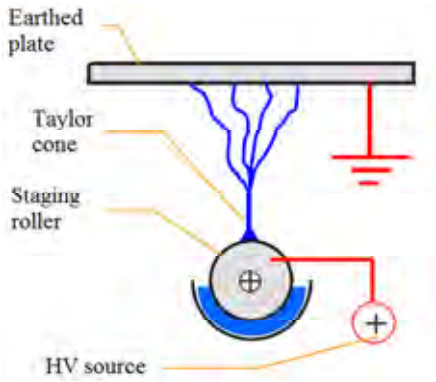

Fig. 1: Schema of technology Nanospider

Fig. 2: Process of electrospinning

3. Acknowledgement

This work has been supported by the European Union, OP RDI project No. CZ.1.05/2.1.00/ 03.0091 – University Centre for Energy Efficient Buildings.

References

[1] Zabel, R. and Morrell, J.: *Wood Microbiology.* Academic Press, San Diego, CA, 1992

[2] Carll, C.G. and T.L. Highley. *Decay of wood and wood-based products above ground in buildings.* J. Test. Eval. 27(2): 150-158, 1999

[3] Wilcox, W.: *Review of Literature on the Effects of Early Stages of Decay on Wood Strength.* Wood and Fiber, Vol. 9, No. 4, pp. 252-257. 1978

[4] Yang, Z.; Jiang, Z.; Hse, Ch. Y.; Shupe, T. F.:*Strength reduction in slash pine (Pinus elliotii) wood caused by decay fungi.* Hse, Chung-Yun; Jiang, Zehui; Kuo, Mon-Lin, eds. Advanced biomass science and technology for bio-based products: Proceedings of the meeting: 2007 May 23-25; Beijing, China. People's Republic of China: Chinese Academy of Forestry: 383-390. 2009

[5] Curling, S. F., J.E. Winandy, and C.A. Clausen. *An experimental method to simulate incipient decay of wood basidiomycete fungi.* Doc. No. IRG/WP 00-20200. International Res. Group on Wood Preservation, Stockholm, Sweden. 2000

[6] Brischke, C. R., Rapp, A. O.: *Dose- response relationships between wood moisture content, wood temperature and fungal decay determined for 23 European field test sites*. Wood Science and Technology, 42:507-518. 2008

[7] Akhtari, M., Arefkhani, M.: *Application of nanotechnology in wood preservation*. The International Research Group on Wood Protection, (Biarritz - France), IRG/WP 10-30542, 7 p. 2010

[8] Rypárová, P. Wasserbauer, R., Tesárek, P., Rácová, Z.: *Preparation of Antimicrobial Treatment Interiors Using NanoTextiles*. Central Europe towards Sustainable Building 2013. Praha: Grada, p.453-456. 2013

[9] Ghasemian, E., Naghoni, A., Tabaraie, B., Tabaraie, T.: *In vitro susceptibility of filamentous fungi to copper nanoparticles assessed by rapid NTT colorimetry and agar dilution method*. Journal de Mycologic Médicale / Journal of Medical Mycology. 22. p. 322-328. 2012

[10] Dallas, P., Sharma, V.K., Zboril, R.: *Silver polymeric nanocomposites as advanced antimicrobial agents: Clasification, synthetic paths, applications and perspectives*. Adv. Colloid Interface Sci. 166, p 119-135, 2011

[11] Dorau, B, Arango, R A, Green III, F: *An investigation into the potential of ionic silver as a wood preservative*. In: Proceedings from the Woodframe Housing Durability and Disaster Issues Conference. Las Vegas, Nevada, pp. 135-145. Forest Products Society. 2004

[12] Rácová, Z., Ryparová, P., Wasserbauer, R., Ne erka, V., Tesárek, P., Demo, P.: *Verification of the Use of PVA Based Nanofiber Textiles as Rehabilitation for the Structures Attack by Wood Decaying Fungi*. In: 5th International Conference NANOCON 2013 Conference Proceedings. Ostrava: TANGER, spol.s.r.o., 2013

[13] Křelinová, V. - Tesárek, P. - Klicmanová, I. - Ryparová, P. - Mukařovský, J.: *Macro-mechanical properties of nanotextiles on PLGA base - tensile strengt*. Engineering Mechanics 2012. Prague: Institute of Theoretical and Applied Mechanics Academy of Sciences of the Czech Republic, p. 194-195. 2012

Behavior of basalt fiber reinforced polymer rods glued-in parallel to the grain in low-grade timber elements by pullout-bending tests

Caoimhe O'Neill[1], Danny McPolin[2], Su Taylor[3], Annette Harte[4]

Summary

Glued-in rod connections in timber possess many desirable attributes in terms of efficiency, manufacture, performance, aesthetics and cost. In recent years research has been conducted on such connections using fiber reinforced polymers (FRPs) as an alternative to steel. This research program investigates the pull-out capacity of Basalt FRP rods bonded-in to low-grade Irish Sitka Spruce. Besides the diameter of rod used, embedded length is thought to be the most influential variable contributing to pull-out capacity of glued-in rods. Previous work has established an optimum embedded length of 15 times the hole diameter. However, this previous work considered solely the effects of axial stress on the bond using a pull-push testing system. This pull-push system may have given an artificially high pull-out capacity as bending effects, which are present in many applications of glued-in rods, were neglected. This paper gives a summary of an experimental program that was undertaken to examine how the glued-in BFRP rods perform in low-grade timber, with the focus on how varying the embedded length of the rods influences pull-out strength.

1. Background

Since the late 1980s there have been many research projects commissioned on the use of glued-in rods in timber construction e.g. GIROD and LICONS. In spite of this, no universal standard exists for their design. There had been an informative annex in the pre-standard PrBS ENV 1995-2:1997 [1] which provided limited coverage of the design of glued-in rods using steel bars, however this document was replaced by BS

[1] PhD Candidate; Queen's University Belfast, Northern Ireland

[2] Lecturer; Queen's University Belfast, Northern Ireland

[3] Senior Lecturer, Queen's University Belfast, Northern Ireland

[4] Senior Lecturer, National University of Ireland, Galway, Ireland

EN 1995-2:2004 in which no guidance on glued-in rods is included. There are three key elements to be considered when designing glued-in rod connections: the timber, the rod and the adhesive. The following sections outline the timber, rod and adhesive materials used in this research program.

Timber

The majority of research into glued-in rods to date has been steel rods glued-in to glued laminated (glulam) elements with lamellae of a high strength class timber. There has however been some degree of research on the behavior of glued-in rods in lower grade timber e.g. glulam beams using laminations of low-grade Sitka Spruce, Spruce of strength class C16 in its sawn form, Pine beams and Beech laminated veneer lumber. This research investigates the use of locally sourced Irish Sitka Spruce. Sitka Spruce grown in Ireland has a fast growth time of approximately 30 to 40 years, as a result of this high growth rate the cell structure of the wood is less dense and therefore the timber generally has relatively poor strength and is of a low classification, typically C16. Although the strength classification of the timber in its sawn form is poor, low transportation costs relative to imported timber means that Irish Sitka Spruce can be a very cost-effective building material if its full potential is utilized. Class C16 Irish Sitka Spruce (Picea Sitchensis) of 75mm x 225 mm sawn section was used. The C16 classification shows that the timber has a minimum bending strength of 16 N/mm^2.

Rod

As well as alternative timber types, rod materials other than steel are being investigated in recent years, namely Fiber Reinforced Polymers (FRPs). FRPs are composite materials made of a polymer matrix reinforced with different fibers. They are more corrosion-resistant than steel and so they will have a longer service life, with less maintenance and monitoring required. Even the weakest FRP is stronger in tension than steel and they are all much lighter, meaning that an equally strong joint can be formed with less material being required. Earlier studies investigated the use of glass fiber reinforced polymer (GFRP) as an alternative to steel while carbon fiber reinforced polymer (CFRP) has been used more recently. Despite its significant cost effectiveness compared to CFRP and its greater tensile strength compared to GFRP, basalt fiber reinforced polymer (BFRP) has only been touched upon in the literature with regards to its use in glued-in technology [2]. BFRP has a Young's modulus

closer to timber than the more commonly used material, steel. It is also a much lower cost material compared to the other FRPs. 12 mm diameter Basalt Fiber Reinforced Polymer (BFRP) rods were used in this experimental program. These rods were found to have a tensile strength of 920 N/mm² under a loading rate of 0.2 kN/s [3]. Unlike steel or some other FRPs, no extensive cleaning of the rods is required prior to bonding as they are sand-coated which provides a good surface for adhesion.

Adhesive

Many investigations have been undertaken to determine which adhesive type is best suited to glued-in rod applications. The adhesive must have good gap-filling properties to ensure a good bond along the entire length of rod, good adhesion to both the rod material and the timber and higher shear strength and stiffness than the timber being used. In a number of studies it was determined that Epoxy adhesives had higher strength than phenol resorcinol and polyurethane alternatives and that epoxies are most suitable for glued-in rod applications [4], [5]. A two-part thixotropic gap filling epoxy was used. This adhesive only flows under shear so is ideal for applications such as overhead beam repair and jointing overhead.

Geometric Variables

In order to create a strong connection, a large surface area of the glue around each rod must be in contact with the timber. Variables that can be altered to increase this surface area include: thickness of the glue-line, length of rod glued (embedded length), number of rods used and rod diameter. Edge distance between the centre of the rod and the edge of the sample must also be considered to ensure the connection does not split prematurely. Embedded length, lb, was the variable examined in this piece of research. Embedded length is thought to be the most influential variable contributing to pull-out capacity after the diameter of rods used [6], [7].

Pull-out Test Methods

There are several test configurations seen in the literature that can be used to assess pull-out capacity of a rod bonded-in to timber. The five most common are pull-pull, pull-push, pull-pile foundation, pull-beam and pull-bending. Each test configuration has its own merits, however pull-pull was identified as the most representative test method, producing relatively higher pull-out strengths [9]. In applications such as a moment resisting timber connection it is highly likely that some bending forces would

be acting on the bar rather than axial-only as in the pull-pull set-up. In order to include these bending effects a hinge system, based on the concrete beam test proposed by RILEM 1982 [10] can be used. This type of pull-out test is known as a pull-bending test. The pull-bending set-up allows the effects of bending forces to be taken in to consideration along with axial forces in what is essentially a modified pull-pull type test. The system allows bending strength of the glued-in rod connection to be evaluated by removing the timber in the section being loaded so that the only resistance is from the BFRP bars glued-in to the timber. This type of pull-out test has been used successfully in investigating the bond behavior between glulam elements and GFRP [11], [12]. It is this system that was used in this research to establish pull-out capacity, with the set-up as shown in Fig. 1 1.

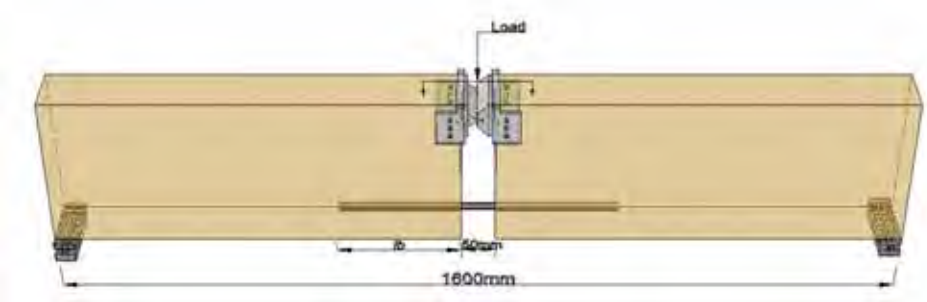

Fig. 1: Pullout-bending test set-up

2. Preliminary Results

Samples were prepared as per Tab. 1 and were loaded in 0.5 kN increments to failure using the accurately calibrated 600 kN capacity hydraulic actuator. Deflection at mid-span and net horizontal movement of the bar as the sample was loaded was recorded with data acquisition connected to transducers. Failure load was recorded when the sample could not take any additional load.

Tab. 2: Sample Specification

Embedded length, l_b (mm)	Rod Diameter, d (mm)	Glueline Thickness, t (mm)	Edge Distance, a (mm)	Direction to gain	Moisture Content	No. Repetitions
80	12	2	30	Parallel	<12%	9
130	12	2	30	Parallel	<12%	9
180	12	2	30	Parallel	<12%	9
230	12	2	30	Parallel	<12%	9
280	12	2	30	Parallel	<12%	9
330	12	2	30	Parallel	<12%	7

The most prevalent failure mode was a failure in shear of the timber with a total of 64% of all samples failing in this manner. This was as expected due to the timber being the weakest element in the bond. When splitting of the timber occurred the length of the split was often equal to the embedded length of rod. Tensile failure of the rod never occurred as the load required for the rupture of the rod was never reached.

As shown in Fig. 2, a clear increase in pull-out strength was observed with an increase in embedded length. An increase in pull-out capacity of 162% was observed between the shortest embedded length of 80mm and the longest length of 330 mm. The overall relationship between embedded length and pull-out capacity was almost linear.

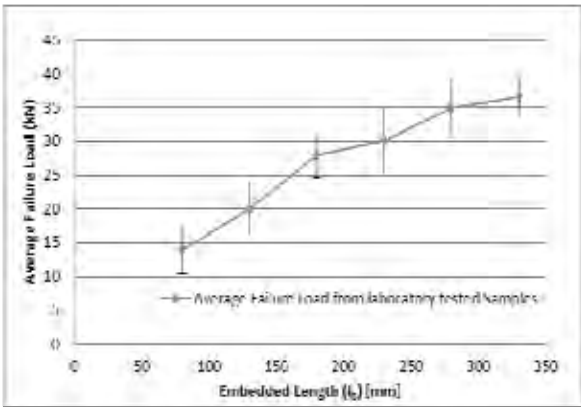

Fig. 2: Failure Loads of Samples

3. Conclusions

A clear increase in pull-out capacity was seen with increasing embedded length of the glued-in BFRP rods. It is planned that additional longer lengths are investigated to determine at which point the additional length becomes inactive. It is suggested also that an investigation where edge distance is increased is undertaken to determine if failure due to splitting of timber can be avoided.

4. Acknowledgements

This work has been carried out as part of the project entitled 'Innovation in Irish timber Usage' (project ref. 11/C/207) funded by the Department of Agriculture, Food and the Marine of the Republic of Ireland under the FIRM/RSF/COFORD scheme.

References

[1] CEN, Design of Timber Structures, Part 2: Bridges. Final Project Team Draft. Stage 34. Brussels, Belgium, 1997.

[2] D. Yeboah, "Rigid Connections in Structural Timber Assemblies," Queen's University Belfast, 2012.

[3] G. Tharmarajah, "Compressive Membrane Action in Fibre Reinforced Polymer (FRP) Reinforced Concrete Slabs," Queen's University Belfast, 2010.

[4] E. Serrano, "Glued-in rods for timber structures — a 3D model and finite element parameter studies," Int. J. Adhes. Adhes., vol. Vol. 21, no. Issue 2, p. p 115–127, 2001.

[5] J. G. Broughton and A. R. Hutchinson, "Adhesive systems for structural connections in timber," Int. J. Adhes. Adhes., vol. 21, no. 3, pp. 177–186, 2001.

[6] R. Steiger, E. Gehri, and R. Widmann, "Pull-out strength of axially loaded steel rods bonded in glulam parallel to the grain," - Mater. Struct., vol. Vol. 40, no. 8, p. p 69–78, Jan. 2006.

[7] K. Harvey and M. P. Ansell, "Improved timber connections using bonded-in GFRP rods," in Proceedings of 6th World Conference on Timber Engineering, Whitsler, British Columbia,, 2000.

[8] D. Yeboah, S. Taylor, D. McPolin, and R. Gilfillan, "Pull-out behaviour of axially loaded basalt fibre reinforced polymer (BFRP) rods bonded parallel to the grain of glulam elements," Struct. Eng., vol. May, pp. p42–51, 2012.

[9] P. Gustafsson, E. Serrano, S. Aicher, and C. Johansson, "A strength design equation for glued-in rods," Proc. Int. vol. 3, no. 1, 2001.

[10] RILEM TC, "RC 5 Bond test for reinforcement steel. 1. Beam test, 1982," in RILEM Recommendations for the Testing and Use of Constructions Materials, RILEM, Ed. E & FN SPON, 1994, pp. 213 – 217.

[11] J. Sena-Cruz, J. Branco, M. Jorge, J. A. O. Barros, C. Silva, and V. M. C. F. Cunha, "Bond behavior between glulam and GFRP's by pullout tests," Compos. Part B Eng., vol. 43, no. 3, pp. 1045–1055, Apr. 2012.

[12] J. Barros, J. Sena-Cruz, and R. Faria, "Assessing the embedded length of epoxy-bonded carbon laminates by pull-out bending tests," 2001.

Enhancing low grade Sitka spruce glulam beams with bonded-in BFRP rods

Conan O'Ceallaigh[1], Annette Harte[2], Karol Sikora[3], Daniel McPolin[4]

Summary

The reinforcement of timber elements using fiber reinforced polymer (FRP) rods or plates is widely accepted as an effective method of increasing the stiffness of members, while at the same time reducing the variability in properties. There are many options to choose from in relation to the FRP material and one of the least documented is basalt fiber reinforced polymer (BFRP). BFRP is the reinforcement chosen in this project due to its superior properties over more commonly used FRPs. Twenty low-grade Irish glued laminated beams are reinforced with two near surface mounted BFRP rods. They are tested in four-point bending in both their unreinforced and reinforced state and the percentage increase in bending stiffness is calculated. The average increase in local bending stiffness is 16.30% with a standard deviation of 1.65%. In addition, the variability in the bending stiffness of the beams is reduced after reinforcement.

1. Introduction

This paper focuses on the short-term stiffness testing of reinforced and unreinforced glued laminated beams constructed from low-grade material. These short-term experiments form the basis of a more substantial project examining the long-term effects of such reinforced timber beams. The most common structural grade produced by Irish grown Sitka spruce is C16 grade. This low-grade Irish timber has been reinforced successfully in previous studies [1, 2] using glass fiber reinforced polymer

[1] PhD Student, Dept. of Civil Engineering, National University of Ireland, Galway, Galway, Ireland

[2] Senior Lecturer, Dept. of Civil Engineering, National University of Ireland, Galway, Galway, Ireland

[3] Post-Doctoral Researcher, Dept. of Civil Engineering, National University of Ireland, Galway, Galway, Ireland

[4] Lecturer, School of Planning, Architecture and Civil Engineering, Queen's University, Belfast

(GFRP). The effect of externally bonded GFRP plate reinforcement and near surface mounted GFRP rod reinforcement has been shown to enhance the flexural properties of low-grade Sitka spruce. Kelly [3] examined the positive effect of BFRP reinforcement on Irish Sitka spruce glued laminated beams. Her results demonstrated the potential of BFRP as a possible substitute for GFRP. These studies on Sitka spruce show promising results, however, the long-term effects on these reinforced beams has received less attention and must be examined. In order to evaluate long-term effects such as duration of load effects and moisture effects, a comprehensive experimental program was created. In total, thirty six glued laminated beams (98 mm x 125 mm x 2300 mm) were manufactured from Irish grown Sitka spruce. Subsequently twenty of these beams were reinforced using two 12 mm diameter BFRP rods centered 30 mm from each edge on the bottom tensile laminate. Prior to creep testing of the beams, non-destructive short-term flexural testing of the beams was carried out to provide baseline data. In this paper, results of these short-term bending tests on the unreinforced beams and reinforced beams are presented and the percentage increase in stiffness properties due to the reinforcement is reported.

2. Glued laminated beam manufacture

2.1 Unreinforced glulam manufacture

The manufacture of each glued laminated beam began by grading each laminate in a mechanical grading machine. Each laminate was strength graded and ranked accordingly. It was desirable to manufacture thirty six beams of equal properties to create matched groups for comparative studies of long-term effects at a later stage. The beam lay-up was designed by arranging each laminate based on the strength graded data. Laminates were bonded together using a waterproof 1:1 phenol resorcinol formaldehyde adhesive chosen due to its suitability for timber structural applications [4]. The final beam consisted of four laminations giving an overall depth of 125 mm. To ensure a solid bond at the timber-timber interface, each laminate was knife planed in order to achieve a surface free from irregularities and torn grain in accordance with EN 14080 [5]. The planing

Fig. 1: Clamping rig

decreased the thickness of each laminate from 34 mm to 31.25 mm on average. The adhesive was applied using a rubber roller to each surface ensuring an even spread of 350 g/m^2. The beams were then clamped into a rig applying a minimum pressure of 0.6 N/mm^2 as seen in Fig. 1. The beams were allowed to cure under pressure for duration of 24 hours. They were subsequently placed in a conditioning chamber for 5 weeks at a temperature of 20 ± 2°C and at a relative humidity of 65 ± 5% prior to short-term testing.

2.2 Reinforced glulam manufacture

Twenty beams from the total were selected for reinforcement with BFRP rods. BFRP is a relatively new FRP material that has been shown to demonstrate superior properties when compared to GFRP [6]. When comparing GFRP and BFRP, Lopresto et al.[6] showed that BFRP has a 35-42% higher elastic modulus as well as better compressive strength and flexural performance. Basalt is one of the most common types of rock on earth, and this makes basalt fibers an excellent and sustainable alternative to FRPs such as GFRP. Two 12 mm diameter BFRP rods were inserted into two circular grooves routed the whole length of the bottom tensile laminate and centered 30 mm each edge as shown in Fig. 2.

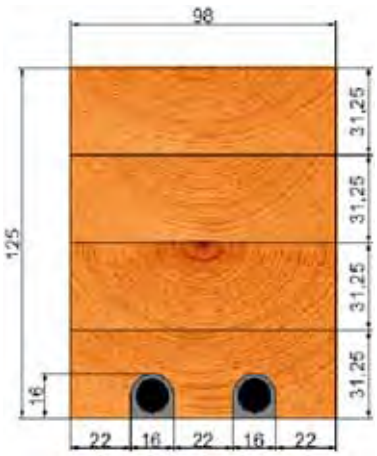

Fig. 2: Reinforcement detail

Circular grooves were chosen due to the reduced stress concentrations and improved mechanical performance [2]. This configuration accumulates to a percentage reinforcement of 1.85%. To guarantee a secure bond, each routed groove was cleaned using compressed air to ensure a dust/impurity free surface. A two-part thixotropic epoxy adhesive was used to bond the reinforcement to the timber as it is specially formulated for the bonding of FRP to timber [7]. The groove was filled to approximately two-thirds of the routed depth using an injection gun. The BFRP rod was then inserted into the groove forcing excess adhesive around the rod ensuring complete coverage on the bottom and sides. Additional adhesive was applied on top to complete the 2 mm glue line. Small rubber rings were placed at 300 mm centers to ensure that a uniform 2 mm bond line was achieved. These beams were then placed in a conditioning chamber for a period of 3 weeks to cure at a temperature of 20 ± 2°C and at a relative humidity of 65 ± 5%.

3. Experimental procedure

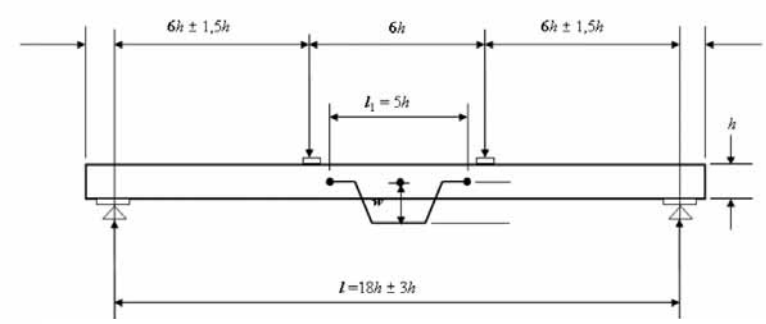

Fig. 3: Beam bending set-up (EN 408, [2])

The bending test set-up was in accordance with EN 408 [8] as seen in Fig. 3. The beams were loaded at a constant cross head rate of 0.15 mm/s (< 0.003 x h limit) to a maximum stroke of 15 mm to ensure the deflection does not exceed the elastic limit. The deflection at mid-span was measured using a linear variable displacements transducer (LVDT) fixed centrally on the top surface of the beam in order to determine the global bending stiffness. A local deflection measurement was acquired from a LVDT located centrally on a hanger. The hanger was fixed between the two loading heads with a span of 5 x h, where h is equal to the total beam height. In order to avoid indentation and inaccurate deflection measurement, steel plates were placed under each support and each load head. Polytetrafluoroethylene (PTFE) strips and packing were used as a precaution to support the beam and avoid lateral torsional buckling. The recorded local and global deflection measurements were plotted against the applied load to determine the stiffness of each beam. Eq. (1) and Eq. (2) were used to obtain the values for local and global stiffness's, respectively.

$$(EI)_{m,local} = \frac{a l_1^{\,2}\left(F_2 - F_1\right)}{16\left(w_2 - w_1\right)} \tag{1}$$

$$\left(EI\right)_{m,global} = \frac{l^3\left(F_2 - F_1\right)}{12\left(w_2 - w_1\right)}\left[\left(\frac{3a}{4l}\right) - \left(\frac{a}{l}\right)^3\right] \tag{2}$$

In Eq. (1) and Eq. (2), $\boldsymbol{a}$ is the distance between the load head and the nearest support, $\boldsymbol{l_1}$ is equal to the gauge length (5 x h) of the local modulus hanger and $\boldsymbol{l}$ is the span between the supports. $\boldsymbol{F_1}$ and $\boldsymbol{F_2}$ are the loads corresponding to 10% and 40% of the ultimate load $\boldsymbol{F_{max}}$, respectively. Similarly $\boldsymbol{w_1}$ and $\boldsymbol{w_2}$ are the deflections corresponding to 10% and 40% of the ultimate load $\boldsymbol{F_{max}}$, respectively. This test was performed on thirty six unreinforced glued laminated beams. Twenty of these glued laminated beams were subsequently reinforced and retested in the same apparatus.

4. Results

Each beam was subjected to four-point bending in its unreinforced state to determine the bending stiffness and elastic modulus. From these results, six matched groups of five beams were created. Four of these matched groups were subsequently reinforced with two near surface mounted BFRP rods as seen in Fig. 2. The percentage increase in bending stiffness was compared between beams in their unreinforced and reinforced state. The average increase in bending stiffness of each reinforced group can be seen in Tab. 1 and Fig. 4. The average increase in local bending stiffness is 16.30% with a standard deviation of 1.65%. There is an average increase in global bending stiffness of 8.80% with a standard deviation of 3.65%. The elastic modulus is measured locally and globally.

Tab. 1: Increase in Bending Stiffness

GROUP	Average Local EI Increase (%)	Average Global EI Increase (%)
1	15.30%	6.54%
2	17.86%	14.14%
3	14.51%	8.15%
4	17.54%	6.36%
Average	16.30%	8.80%
Standard Dev.	1.65%	3.65%
Median	16.42%	7.34%

Once reinforced, the local elastic modulus of all beams had a mean value of 10727 N/mm^2 and global elastic modulus had a mean value of 9307 N/mm^2. As seen in Tab. 1, the increase in global bending stiffness of group 2 is significantly larger than that realized in other groups. This may be due to the lower initial global stiffness of group 2 in its unreinforced state. The lower the initial stiffness, the greater the effect of FRP reinforcement. The addition of reinforcement has resulted in reduced variability within each group as seen in Fig. 4.

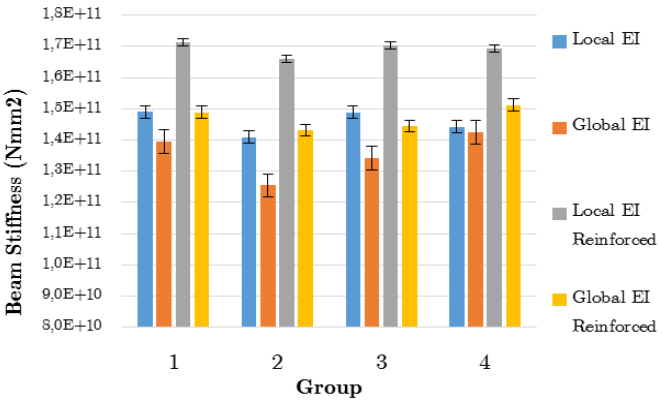

Fig. 4: Reinforced group beam stiffness

5. Conclusion

The short term bending tests on unreinforced and BFRP reinforced glued laminated beams are presented. This has enabled the formation of six matched groups for

comparative studies in future work to establish the long-term behavior of these beams. The results of the non-destructive four-point bending tests revealed that significant increases in stiffness can be achieved when reinforcing low-grade Sitka spruce. The modest percentage reinforcement of 1.85% resulted in a local bending stiffness increase of 16.30%. A reduction in the variability of properties was observed after reinforcement.

6. Acknowledgement

This work has been carried out as part of the project entitled 'Innovation in Irish timber Usage' (project ref. 11/C/207) funded by the Department of Agriculture, Food and the Marine of the Republic of Ireland under the FIRM/RSF/COFORD scheme. The authors would also like to thank ECC Ltd. (Earrai Coillte Chonnacht Teoranta) for supplying the timber used in this project.

References

[1] Raftery, G.M. and A.M. Harte, *Low-grade glued laminated timber reinforced with FRP plate.* Composites Part B: Engineering, 2011. 42(4): p. 724-735.

[2] Raftery, G., C. Whelan, and A. Harte, *Bonded in GFRP rods For the repair of Glued Laminated Timber*, in World Conference of Timber Engineering, Auckland 2012, 16-19 July. 2012: Auckland, New Zealand.

[3] Kelly, F., *Basalt FRP rods for strengthening and repair of glued laminated timber*, in Civil Engineering, College of Engineering and Informatics,. 2012, National University of Ireland, Glaway.

[4] Raftery, G., A. Harte, and P. Rodd, *Qualification of wood adhesives for structural softwood glulam with large juvenile wood content.* Journal of the Institute of Wood Science, 2008. 18(1): p. 24-34.

[5] NSAI, I.S. EN 14080 in Timber Structures - Glued laminated timber and glued solid timber - Requirements. 2013.

[6] Lopresto, V., C. Leone, and I. De Iorio, *Mechanical characterisation of basalt fibre reinforced plastic.* Composites Part B: Engineering, 2011. 42(4): p. 717-723.

[7] Rotafix, *Material Data Sheet*, Rotafix House, Editor.: Abercraf, Swansea, SA9 1UR, U.K.

[8] NSAI, I.S. EN 408 in Timber Structures - Structural Timber and Glued laminated timber - Determination of some physical and mechanical properties. 2010+A1-2012.

Enhancement of timber beams with D-shape local reinforcement

Izabela Burawska[1], Marcin Zbiec[2], Piotr Beer[3]

Summary

Local reinforcement of timber beams is material and cost effective way of upgrading wood strength parameters. It can be used in case of presence of natural wood defects, especially knots. Tests deal with strength analysis of the D-shape local reinforcement made of CFRP strip located centrally at the simulated defect and inserted into the cross section of strengthened beam. Application of reinforcement significantly changed the load-displacement dependence and increased bending strength of tested samples.

1. Introduction

Knots are natural and one of the most significant wood defects. In most cases it is not possible to avoid knots in timber, especially in lower grades, but depending on the sawing method they may have different shape and position [1]. The most adverse position of knots in bended beams, negatively affecting its strength parameters is in the tension zone of maximum moment area. Such position results in high values of stress concentration factor, leading to crack initiation under extensive load. Increase in life loads may results from changes in function of construction, what often happens in case of historical structures designed for lower load capacity values [2].

It is possible to locally reinforce critical areas of bended timber beam in aim to increase load capacity and avoid crack propagation. Designed reinforcement technique should be easy in implementation, cheap and effective.

[1] PhD student, Warsaw University of Life Sciences - SGGW, Poland

[2] Warsaw University of Life Sciences - SGGW, Poland

[3] Warsaw University of Life Sciences - SGGW, Poland

2. Materials and methods

Reinforcement technique was developed for pine wood as a species the most commonly used in construction works in Poland. Pilot tests using samples with dimensions 25mmx50mmx800mm were performed in aim to develop some assumptions of the new reinforcement technology and determine the parameters of testing procedures for further research. Because of small dimensions of samples in pilot tests, less variation of strength parameters was provided, in comparison to full-scale structural lumber.

Used samples were free of natural defects; therefore determination of reinforcement influence on wood strength parameters was possible. To ensure similarity between tested samples and cracking of the material at a specific location, openings simulating the knots were drilled. Center of the opening was located at the middle of the span. Below the opening a thin layer of wood (1,5 mm) was secured. Such position of the opening was the most unfavorable location achievable in laboratory tests [3].

Samples with average density of 560 kg/m^3 were divided into 3 series – non weakened, weakened with a bore of 12,5 mm diameter (25% of the cross-section height), strengthened with D-shape reinforcement. D-shaped reinforcement was made of CFRP tape, formed in the shape of D letter (Fig. 1). Such shape resulted from the technologically easiest shaping of the slot that could be made using circular saw. Reinforcement was placed centrally at simulated defect. It was placed inside the cross section in previously made grooves (Fig. 2). Bond between pine wood and FRP reinforcement was made with Havel Composites G60 epoxy resin.

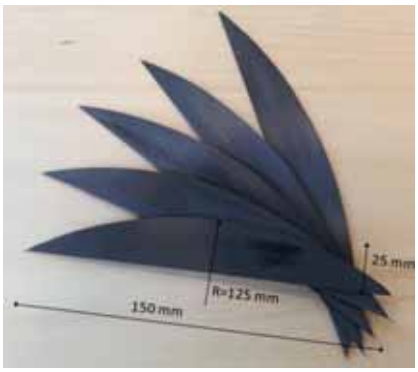

Fig. 1 The D-shape reinforcement

Fig. 2 Preparation of material

The length of reinforcement values resulted from the Saint Venant theory and numerical analysis [4]. This theory states that disturbances in uniform stress field around the openings have only local character. At the distance of few openings diameter, deviances are negligible. Reinforcement procedure assumes strengthening the whole tensioned area. Thus, height of the D-shape reinforcement was set at 25 mm. The length of strengthening resulted from diameter of saw used (250 mm).

3. Results and discussion

Samples were tested in three point bending in accordance to EN-408:2012.Three series of samples were analyzed during testing: non weakened (A-series), weakened with a bore (B-series), reinforced (C-series). On the basis of static bending tests, ultimate load, MOR, MOE and the difference of deflections in elastic range of element were determined.

Fig. 3 shows ultimate load values obtained for tested samples. Weakening by opening of 12.5 mm caused reduction in ultimate load by 39% in comparison to samples of A-series. Effect of strengthening was statistically significant. D-shape local reinforcement application caused gain in ultimate load by 35% in comparison to weakened samples.

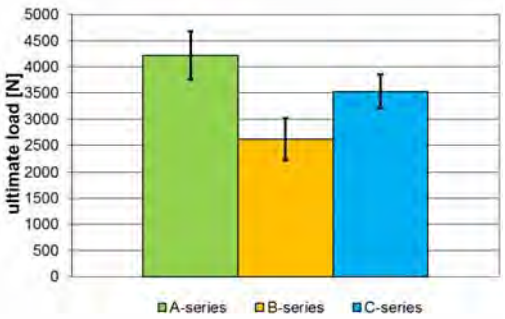

Fig. 3 Ultimate load values

Fig. 4 presents MOR values obtained during testing for A, B and C-series of samples. Samples weakened with an opening showed 38% reduction in MOR in comparison to sound samples of A-series. Testing showed significant gain in MOR values (36%) in comparison to samples of B-series.

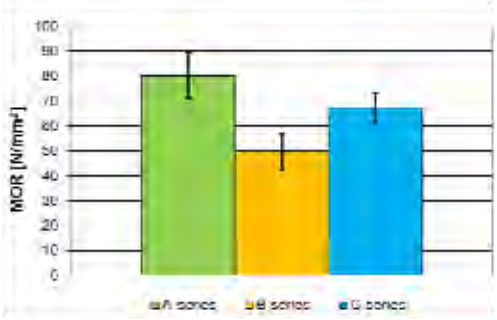

Fig. 4 MOR values

On Fig. 5 values of MOE obtained during testing are presented. Testing showed that weakening of wooden member with a hole of 25% of its height caused reduction of MOE by 12% in comparison to sound wood. Application of reinforcement caused an increase of MOE values by 10%, compare to samples of B-series. Limited length of reinforcement, even in case of material having high values of Young's modulus, did not significantly increased MOE of strengthened material.

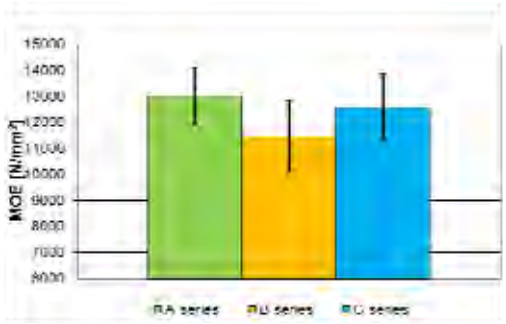

Fig. 5 MOE values

Fig. 6 shows changes in deflection values obtained at elastic range for tested samples (10-40% of destructive force). Samples of B-series showed lesser gain value within the elastic range of wooden element in comparison to samples of A-series (30%). Reinforcement caused increase of changes in deflection values by 24%.

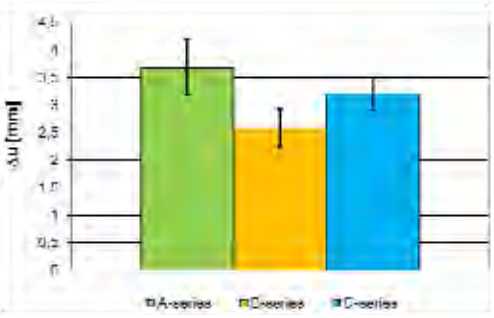

Fig. 6 Deflection gain values at elastic range

Fig. 7 shows typical character of destruction for samples of B and C-series. In case of samples weakened with an opening, crack initiation occurred below the bore, as a result of delamination of thin tensile layer. Then crack passed through the hole and along the grain. In case of C-series of samples, failure occurred due to reinforcement sliding out from the cross section as a result of very high shear stresses. After failure of reinforcement bond, crack below the hole appeared and then it was propagated through the hole and along the grain. Reinforcement significantly changed the load-displacement dependence in strengthened samples. Indirect cracks, not until failure can be noticed for samples of C-series.

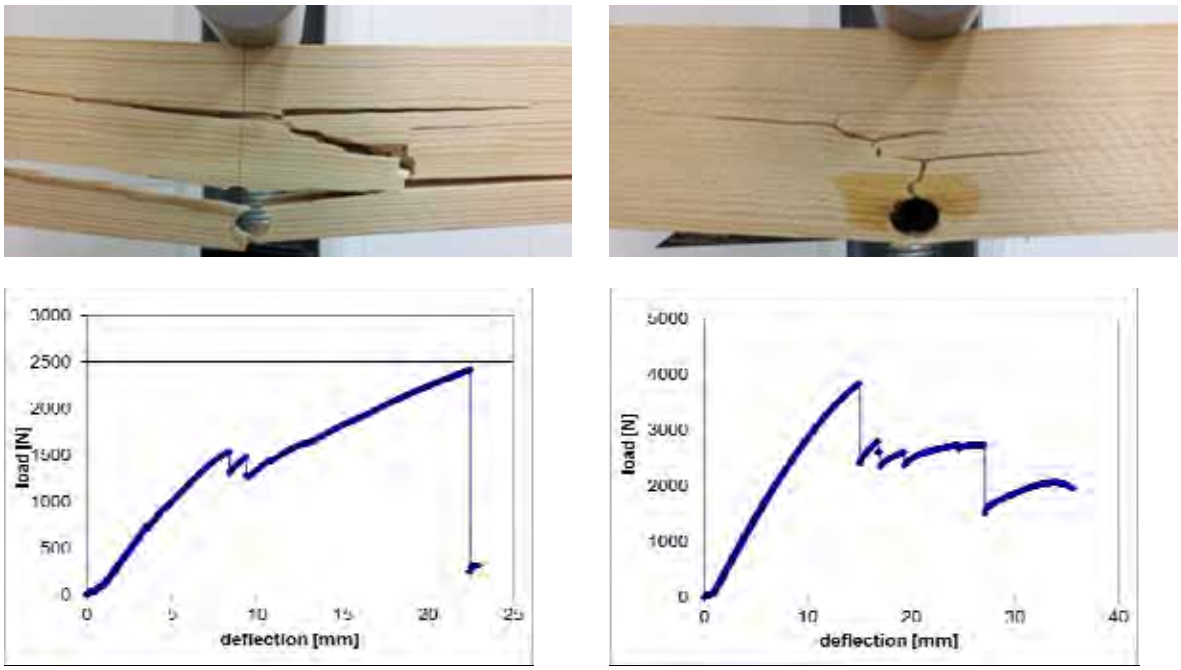

Fig. 7. Fracture type and load-deflection dependence for weakened (left) and reinforced sample (right)

4. Conclusions and challenges

Based on the studies, it was confirmed that local CFRP D-shape reinforcement is purposeful in structural timber. Because of the lower cost of reinforcing materials and minimum intervention into original structure of element, such local reinforcement may become serious alternative for full-length strengthening. It could be used especially in historical structures, where the issues of the introduction of reinforcement into the cross section and aesthetic concerns are extremely important.

There is still a need to optimize the developed reinforcement technique, both using numerical analysis and further laboratory tests of samples weakened with natural defects.

References

[1] Johansson C. J., Grading of timber with respect to mechanical properties, *Timber engineering*, Wiley, Chichester, 2003, 23-43

[2] Carolin A., Carbon Fibres Reinforced Polymers for Strengthening of Structural Elements, Luleå University of Technology, Doctoral Thesis, 2003

[3] Burawska I., Tomusiak A., Turski M., Beer P., Local concentration of stresses as a result of the notch in different positions to the bottom surface of bending solid timber beam based on numerical analysis in Solidworks Simulation environment, *Annals of Warsaw University of Life Sciences-SGGW, Forestry and Wood Technology* 73, 2011: 192-198

[4] Burawska I., Tomusiak A., Beer P.,) Influence of the length of CFRP tape reinforcement adhered to the bottom part of the bent element on the distribution of normal stresses and on the elastic curve, *Annals of Warsaw University of Life Sciences-SGGW, Forestry and Wood Technology* 73, 2011: 186-191

Reinforcement of timber floors using lightweight concrete - Mechanical behavior of the connections

Carlos Martins[1], Alfredo M.P.G. Dias[2], R. Costa[2]

Summary

This paper reports the study developed on the mechanical behavior of timber-concrete connections. This study is a part of a more wide research on the development of timber-concrete composite (TCC) panel, which had the sustainable construction as major issue. This purpose was achieved with the use of two abundant Portuguese natural resources subproducts: (i) small diameter Maritime pine logs and (ii) cork granules wastes. For the mechanical characterization three different types of connections were studied: (i) dowels, (ii) inclined cross screws and (iii) glued-in-bars. These three types of connections are cheap, easy and fast to mount and fulfill the requirements of TCC panels for residential use. Twenty connection specimens of each type were built and tested to characterize their behavior. The main mechanical properties analyzed were: (i) slip modulus, (ii) load carrying capacity and (iii) ultimate deformation. The results revealed the glued-in-bar connection as the stiffest one and the strongest one.

1. Introduction

This paper describes the research on timber-concrete connections mechanical behavior as a part of a more wide research project, which focuses on the development of TCC panels with lightweight concrete.

The development of TCC panels requires knowledge in four main areas: (i) concrete, (ii) timber elements, (iii) timber-concrete connections and (iv) the optimization of the timber-concrete composite panels.

[1] MSc, PhD candidate, Department of Civil Engineering, University of Coimbra

[2] PhD, Assistant Professor, Department of Civil Engineering, University of Coimbra

This paper is focused on the connections a key issue in the TCC panels design. Only an effective connection will assure an efficient composite behavior of the element [1]. Three types of connections were selected, tested and analyzed in the scope of this research program: (i) dowels, (ii) inclined cross screws and (iii) glued-in-bars. The dowel connectors were considered because, they were believed to be adequate to achieve the design requirements of TCC panels but also because of their reduced cost and its quick and easy installation procedure. This type of connection has been widely used for timber-concrete such as for example by Dias [2], that used three different timber species (Chestnut, Maritime pine and Spruce) and also three different classes of concrete (lightweight, normal and high strength).

Many other types of connections have been developed in the last decades [3-6] but are complex to implement in a solution that is pretended to be practical and cheaper to mount. Inclined cross screws and glued-in bar connections were also studied in this project looking forward to stiffer and stronger connection systems despite their higher complexity and cost, particularly for the glued-in-bar connections [7]. Previous researches were undertaken to study these two types of connections. A characterization of the influence of concrete and the presence of an interlayer in composite connections with inclined screws was realized by Jorge [8]. The use of glued-in-bars connections has been developed [9-11]. Martins [12] has studied inclined glued-in-bars for timber-concrete connections for building and bridge constructions.

2. Experimental campaign

The development of composite connections involved the study of a lightweight cork concrete (CC) in the first phase of the research project. The cork granules were introduced by replacing partially the sand and coarse aggregates of the reference concrete composition. The cork concrete composition used is shown in the Tab. 1.

Tab. 1: Composition of the lightweight cork concrete.

Material	Quantity (kg/m^3)
Washed Sand	465.6
Coarse (D_{max} = 12.5mm)	831.2
Cement 42,5 R type I	300.0
Water	192.2
Cork 0-3mm	16.2
Cork 3-10mm	12.4
Superplasticizer Viscocrete 20 HE	2.4

This composition yielded a uniaxial compressive strength of 20.66 MPa, a modulus of elasticity of 18.1 GPa and a density of 1964.1 kg/m^3. These cork granules are a product resulting from cork industry and it has no commercial value. According to Branco [13] the CC exhibits better insulation, thermal and shrinkage properties than others lightweight and normal concretes.

The timber-concrete connection specimens were build using two lateral timber members connected to a central concrete member. This configuration was adopted due to the simplicity of the test set up and there are no significant differences between the others test set-ups usually used in composite connections [12].

The timber members considered for the preparation of the connection specimens had round shape. This material is abundant in Portugal because they are subproducts resulting from forest management. Their structural application without processing (except debarking) is particularly interesting because this way high mechanical properties are kept intact as related by previous research works [14, 15]. The timber logs were conditioned at a climatic room with 20±2°C of temperature and 65±5% of air relative humidity. The diameters of timber logs were between 119 mm and 174 mm with a mean value of 137 mm. The densities were between 409.5 kg/m^3 and 699.0 kg/m^3 with a mean value of 537.0 kg/m^3. For dowel connections the steel fasteners were made from 8 mm nominal diameter S500 grade hot rolled ribbed deformed rebars. To ensure a tight fitting of the dowel fastener, the timber logs were predrilled with a 7 mm diameter drill and the fasteners were inserted in 10 times its diameter by hammering. The length of the dowel in the concrete element was 40 mm.

Fig. 1 shows a dowel connection in the mould ready to be cast. The inclined cross screws were produced of mild steel, 100 mm length and a head with 12 mm of diameter. The threaded part of the screws had an external diameter of 6 mm and 61 mm length. The shank part of the screws had a diameter of 4 mm and 33 mm length. The screws were mounted 45° relatively to the timber logs axis direction in a crossed layout.

Fig. 1 Dowel connection ready to be cast (top view).

Fig. 2 shows a scheme of the inclined cross screws connection. To make easier the insertion of the screws a predrilling with 2 mm was used. The connectors for glued-in-bar connections were cut from the same rebars used for dowel connections. Each connector was cut with 200 mm long and bent in 45° at 130 mm (Fig. 3). The timber logs were predrilled with 80 mm using a 10 mm diameter drill at 45° in relation to the log axis. The connectors were glued to the timber with an epoxide resin Sika®Icosit K-101 TW [16].

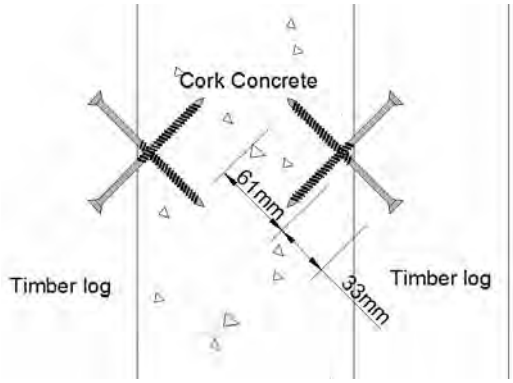

Fig. 2: Inclined cross screws dimensions and configuration (side view).

Fig. 3: Dowel connection specimen configuration before cast.

2.1 Test set-up

Twenty connection specimens of each type were tested. A push out configuration test was used. The tests were carried out 28 days after cast and the load history was based on the procedure defined in EN 26891 [17] to timber-to-timber connections. The tests aimed the determination of the (i) load carrying capacity, F_{max},, (ii) slip modulus, k_s, and (iii) ultimate slip, δ_{ult}.

The tests were monitored with a logger system TDS-602, with the measurement recorded once per second. The measurements monitored and recorded were the loads and relative displacements (slip) between the timber and lightweight cork concrete. The load was monitored through a load cell with 10tf of maximum capacity placed between a hydraulic actuator and a steel plate placed above the central plain concrete element. The relative displacements were monitored with four LVDT's with 25mm range – two LVDT's were used per shear plane. The configuration was established in order to account with any rotation of the specimen during the test or a differential behavior of connection in the two shear plane. Fig. 4 shows a schematic representation of the instrumentation (top view) and Fig. 5 shows a timber-concrete connection ready to be tested.

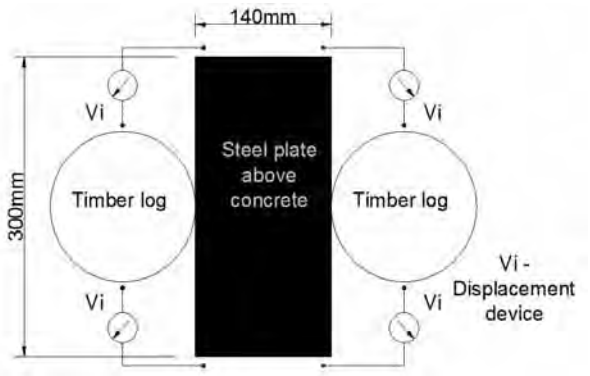

Fig. 4: Test configuration (plan view scheme)

Fig. 5: Connection specimen instrumentation

3. Experimental results and discussion

The mechanical properties of the connections were computed according EN 26891 [17]. The ultimate slip was considered as the slip measured immediately before the connection collapse or 15mm if the failure did not occur up the 15 mm defined in the standard. Tab. 2 shows the results from the three different connection configurations. The values presented are mean values (min/max values presented between brackets) and are related to one test specimen, therefore for two connections – one per shear plane. As expected, and according to what has been reported by other studies with normal and lightweight concrete [2, 4], all the connections tested shown ductile failure modes.

Tab. 2: Connection test results

	Dowel	*Inclined cross screws*	*Glued-in-bar*
F_{max} *(kN)*	24.0 [18.5 – 30.3]	21.6 [14.3 – 30.0]	46.8 [30.8 – 65.8]
K_s *(kN/mm)*	14.7 [5.9 – 37.9]	22.9 [5.2 – 88.0]	75.1 [34.3 – 178.6]
δ_{ult} *(mm)*	14.9 [14.0 – 15.0]	8.90 [5.8 – 15.0]	12.9 [4.7 – 15.0]

Typically the fastener in dowel connection specimens exhibit two plastic hinges, one in the timber side and another in the concrete side (Fig. 6.a). This failure mode is similar to the ones reported by other authors with normal strength concrete.

The inclined cross screws revealed a failure mode governed by tension/shear failure of one or more screws, Fig. 6(b) with a consequent drop of load and increase of slip. The glued-in-bar connection is governed by axial forces on the steel fastener. In spite of that a significant plastic deformation, due to bending on the steel fastener, could be observed after the tests Fig. 6(c).

(a) (b) (c)

Fig. 6: Typical failure modes: (a) dowel, (b) inclined cross screws, and (c) glued-in-bar connections.

The results show that glued-in-bar connections are the stiffest and dowel connections the ones with lower slip modulus. The inclined cross screws shows slip modulus between the former ones, although more closer to dowel connection. The relatively lower slip modulus of inclined cross screws connection is probably due the small diameter of screws. If the screws had a larger diameter (e.g. close to 8 mm of dowel and glued-in-bar rebars) and this connection type would probably have significantly higher stiffness has reported by other studies [4].

The load carrying capacity of the three types of connection is closer than their slip modulus. The glued-in-bar connections are the strongest ones and the inclined cross screws are the weakest ones. All the connections types have shown a relatively high ultimate deformation and, as expected, the higher values were obtained with dowel connections. However all the connection types have shown ultimate deformation values high enough to ensure a ductile behavior of the TCC floors in most of the situations [18].

4. Conclusions

As expected the three different configurations of connections showed different load carrying capacities and stiffness being the glued-in-bar the stiffer (75.1 kN/mm) and with maximum load (46.8 kN). Dowel connections presented the lower values with 14.7 kN/mm for stiffness and 24 kN for maximum load. Inclined cross screws showed values closer to dowel connection. The results are in line with the ones obtained in similar connectors tested in other research works. In spite of that the results seem to indicate that the use of the cork concrete tend to decrease the mechanical behavior of the connections. Nevertheless, the use of the same connectors with larger diameters could improve these results.

5. Acknowledgement

The authors wish to thank the Portuguese Foundation for Science and Technology (FCT) and the Science and Innovation Operational Program co-financed by the European Union Fund FEDER, for the support provided through the Research Project No. PTDC/ECM/099833/2008. The authors wish to thank also to Sika Portugal, Amorim Group and Cimpor for the support provided through the epoxide resin, the cork granules and the cement, respectively.

References

[1] Ceccotti, A. (1995). Timber-concrete composite structures. Timber Engineering – Step 2. H. Blass, Editor. Centrum Hout. The Netherlands.

[2] Dias, A. M. P. G. (2005). Mechanical behaviour of timber – concrete joints. PhD Thesis. Delft University of Technology.

[3] Bathon, L., and Clouston, P. (2004) Experimental and numerical results on semi prestressed wood-concrete composite floor systems for long span applications. Proceddings of the 8th World Conference on Timber Engineering. Lahti, Finland. 339-344.

[4] Ballerini, M. and Piazza, M. (2002). Connectori di calcestruzzo per strutture composte legno-clacestruzzo. Indagine sperimentale. 5th Holzbau Workshop on Composite Structures. Salerno, Italy.

[5] Van der Linden, M. (1999). Timber-concrete composite floor. PhD Thesis. TuDelft. Netherlands.

[6] Monteiro, S. R. S., Dias, A. M. P. G. and Negrão, J. H. J. O. (2013). Assessment of Timber-Concrete Connections Made with Glued Notches: Test Set-Up and Numerical Modeling. Experimental Techniques. 37: 50-65.

[7] Yeoh, D. et al. (2011). State of the Art on Timber-Concrete Composite Structures : Literature Review. Journal of Structural Engineering. 1085-1095.

[8] Jorge, L. F. C., (2005). Timber-concrete Composite Structures using LWAC. (in Portuguese). PhD Thesis. University of Coimbra, Coimbra.

[9] Brunner, M., Romer, M., and Schnüriger, M. (2007). Timber-concrete-composite with an adhesive connector (wet on wet process). Mater. Struct. 40 (1): 119-126.

[10] Miotto, J. and Dias, A. (2008). Glulam-concrete composite structures: Experimental investigations into the connection system. Proceddings of the 10th World Conference on Timber Engineering. Miyazaki, Japan.

[11] Kuhlmann, U. and Aldi, P. (2009). Prediction of the fatigue resistance of timber-concrete composite connections. Proceddings of 42nd Meeting of Working Commission W18 – Timber Structures, International Council for Research and Innovation in Building and Construction (CIB). Rotterdam. Netherlands. 10.

[12] Martins, H. (2008). Timber-concrete connections systems with mechanical fasteners associated to epoxid resin (in Portuguese). Master Thesis. University of Coimbra, Coimbra.

[13] Branco, F. G.., A. Tadeu, et al. (2007). Can Cork be used as a concrete aggregate? International Journal of Housing Science and its Applications. 31 (1): 12.

[14] Morgado, T. F. M., J. Rodrigues et. al. (2009). Bending and compression strength of Portuguese Maritime pine small-diameter poles. Forest Products journal. 59 (4):23-28.

[15] Morgado, T. F. M. (2013). Classification and structural applications of Maritime Pine round wood. (in Portuguese). PhD Thesis. University of Coimbra, Coimbra.

[16] Sika website. Sika Icosit K 101 TW. Retrieved Mar. 20. 2012 from http://prt.sika.com

[17] European Committee for Standardization CEN, EN 26891 – Timber structures – Joints made with mechanical fasteners - General principles for the determination of strength and deformation characteristics, 1991, CEN, Bruxelles, Belgium.

[18] Dias, A. M. P. G. and Jorge L. F. C. (2011). The effect of ductile connectors on the behaviour of timber-concrete composite beams. Engineering Structures. 33 (11): 10.

Experimental assessment of dynamic performance of timber-concrete composite floors

Pedro Santos[1], Alfredo M.P.G. Dias[2], L. Godinho[3]

Summary

In this paper the dynamic performance of timber-concrete floors is assessed though experimental tests. The tests were performed in a complete floor (before and after the cast) as well as in isolated timber-concrete beams for a two side support situation. Prior to the dynamic tests, the materials used in the construction of the floor were full characterized, in order to obtain the relevant mechanical properties. The isolated beams were later loaded with a static protocol in order to assess the static stiffness of each one and obtain the connector's stiffness. The results obtained are presented and discussed in this paper.

1. Introduction

Timber-concrete composites (TCC) are nowadays a versatile solution in sustainable construction, combining the timber tensile capacity with the compression performance of concrete. One of the weakest points in traditional timber floors is the vibrational behavior due to the relationship between mass and stiffness. In some cases, vibrations in timber floors tend to become annoying to users of the structure, as they receive the floor vibration through their body, by visual impression and/or by sound. Usually this issue is addressed by ensuring that the fundamental frequency is above the typical limit of 8-10Hz, above which annoying vibrations are assumed not to occur (Ljunggren et al, 2007). In case of a fundamental frequency under eight Hz EC5 (CEN, 2004a) requires a special study for residential floors.

[1] MSc, PhD candidate, Departamento de Engenharia Civil, Faculdade de Ciências e Tecnologia, Universidade de Coimbra

[2] PhD, Assistant Professor, CICC – Centro de Investigação em Ciências da Construção, Departamento de Engenharia Civil, Faculdade de Ciências e Tecnologia, Universidade de Coimbra.

[3] PhD, Assistant Professor, CICC – Centro de Investigação em Ciências da Construção, Departamento de Engenharia Civil, Faculdade de Ciências e Tecnologia, Universidade de Coimbra.

When reinforcing a timber floor with a concrete top, a series of aspects are taken into account such as: the thickness, elasticity and density of the concrete layer as well the configuration/stiffness of the connectors. From all these parameters, the connectors' stiffness seems to be the one that affects the fundamental frequency of the floor to a larger extend (Skinner et *al* (2012) and Mertens et *al* (2007)), as it allows to change the ratio of the composite action, increasing stiffness and, as a consequence, the fundamental frequency.

There are already some published works about the dynamic behavior of TCC beams, mainly experimental, such as Abd.Ghafar et al (2008) however, no published work is to be found about a typical TCC floor.

2. Experimental procedure

2.1 Material and floor description

Fig. 1 Timber floor assembling.

The timber floor to test (Figure 1), with overall dimensions of 3,5 m x 3,4 m, comprised five beams of glulam made of spruce (Abies alba) with rectangular cross section (0,2 m x 0,1 m) and a floor deck (0,02 m height) made of boards of maritime pine (Pinus pinaster) attached to the beams by means of 2 mm width steel square nails. The glulam beams were previously statically tested in order to determine the global modulus of elasticity obtained in accordance to EN408 (CEN, 2003). The floor boards, were not tested and their mechanical properties were obtained based on visual grading, in accordance with the Portuguese grading standard NP4305. The TCC floor (Figure 2) was obtained by the following steps: preparation of timber members, application of the fasteners and casting. Ribbed steel bars with 8mm of diameter, S500 class, were inserted into the beams, previously pre-drilled with 7mm, spaced at 100mm; the floor surface was covered with a plastic film, to prevent moisture transitions between concrete

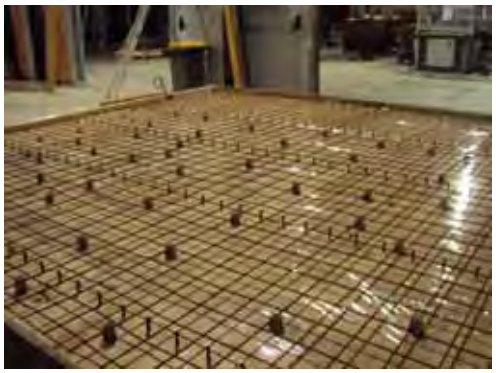

Fig. 2: TCC floor assembling.

and timber; an electro welded mesh was placed, with the aim to prevent cracking; and finally the floor was cast. The concrete used was supplied by a ready mix concrete company corresponding to a C20/25 class, for which a Young's modulus of 30 MPa can be considered.

The stiffness of the connectors was obtained from static tests to the individual TCC beams, cut off from the TCC floor following the dynamic tests. The relevant properties of the elements composing the floors are summarized in Tab. 1.

Tab. 1: Timber ant TCC floor properties.

Element	Properties		
	E_{mean} (kN/mm^2)	ρ_{mean} (kN/m^3)	K_{mean} (kN/m)
Beams	13,1	4,14	-
Boards	14	6	-
Concrete	30	24	-
Connectors	-	-	1172

2.2 Experimental tests

In the dynamic tests, the floor was supported in two sides, at a distance of 3,3 m, with the beams placed over a glulam beam of spruce at each top. The floor was excited by striking the surface with a timber beam at its center, producing a free vibration response that was measured by an accelerometer connected to an acquisition data system. The accelerometer was successively positioned along a series of positions (all of them over the middle and top of the beams positions), in a total of 15 readings (Fig. 3).

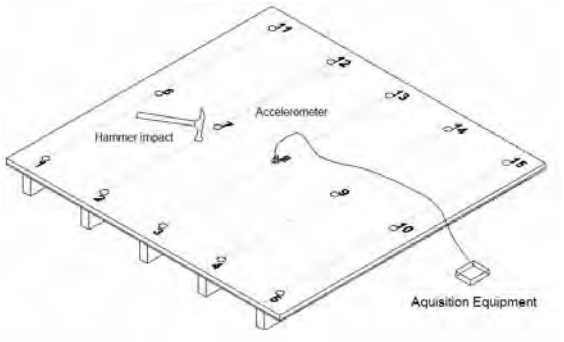

Fig. 3: Dynamic test setup for the floor.

It was observed that the modal frequencies were not significantly affected by the point of measure of the accelerometer; however, the readings taken from the points over the mid-span of each beam provided clearer frequency responses, whose peaks were easier to identify peaks, with the corresponding to the modal frequencies. This behavior can be justified by the fact that some of the modal shapes exhibit maximum deflection values at this point.

Later the floor was cut into five TCC beams (see widths in Table 2), which were statically tested to obtain its static stiffness.

Tab. 2: Width of the TCC beams.

TCC beam	1	2	3	4	5
Width (mm)	490	735	750	480	750

The connectors' stiffness was obtained by a numerical calculation using the gamma method in EC5 (CEN, 2004a). In the dynamic tests to the beams, the supports were 3,2m apart, with the beam placed over timber boards of spruce, the accelerometer was placed in the middle of the span, over the concrete, and the impact load was produced by cutting off a wire that connected a mass to the center of the beam (Figure 4).

Fig. 4: Dynamic test setup for the beam.

3. Results and discussion

The fundamental frequencies obtained for the timber floor and TCC floor and beams are presented in Table 3.

Tab. 3: Fundamental frequency for the Timber ant TCC floor and beams..

Fundamental frequency (Hz)						
Floor		TCC beam				
Timber	TCC	1	2	3	4	5
31,0	17,4	20,4	17,9	17,0	20,1	17,0

The analysis of the results shows that the frequency changes in the floor after the reinforcement, it is seen that the fundamental frequency decreases from 31,0Hz to 17,4Hz, which corresponds to a reduction of 44%. It is important to note that both values obtained for the floors are still clearly above the limits recommend by (Ljunggren et al, 2007) and the limit of 8Hz for which the EC5 (CEN, 2004) demands a special study for residential floors.

In the TCC beams, the fundamental frequency varied between 17,0 Hz and 20,4 Hz, values that do not differ significantly from those obtained for the floor, 17,4 Hz. This clearly indicates that, when supported on two sides, the fundamental frequency of a TCC floor is not affected by the transverse stiffness.

4. Acknowledgement

The authors wish to thank the Portuguese Foundation for Science and Technology (FCT) and the Science and Innovation Operational Program co-financed by the European Union Fund FEDER, for the support provided through the Research Project No. PTDC/ECM/099833/2008.

References

[1] Skinner, J., Harris, R., Paine, K., Walker, P., Bregulla, J. (2012), "The characterization of connectors for the upgrade of timber floors with thin structural toppings" WCTE 2012

[2] Mertens, C., Martin, Y., & Dobbels, F. (2007). Investigation of the vibration behaviour of timber-concrete composite floors as part of a performance evaluation for the belgian building industry. Building Acoustics, 14(1), 25– 36

[3] Abd.Ghafar, N. H., Deam, B., Fragiacomo, M., Buchanan, A. (2008), "Vibration Performance of LVL- Concrete Composite Floor Systems" WCTE 2008

[4] Ljunggren, F., Wang, J., Agren, A., (2007) "Human vibration perception from single- and dual-frequency components" Journal of Sound and Vibration 300 (2007) 13–24

[5] LNEC (1995) "NP 4305 - Structural maritime pine sawn timber – Visual Grading" Laboratório Nacional de Engenharia Civil, Portugal

[6] CEN (2003). "EN 408: Timber Structures – Structural timber and glued laminated timber – Determination of some physical and mechanical properties" European Committee for Standardization. CEN, Brussels, Belgium.

[7] CEN (2004a). "EN 1995 1-1: Eurocode 5: Design of timber structures – Part 1-1: General – Common rules and rules for buildings" European Committee for Standardization. CEN, Brussels, Belgium, 2004

The effect of mixing method on bonding performance of PVA nanocomposites

Timucin Bardak[1], Deniz Aydemir[2], Nurgul Tankut[3], Eser Sözen[4], Ali Naci Tankut[5], Serkan Peltek[6]

Summary

The aim of study is to investigate the effect of mixing methods used in preparation of the polyvinyl acetate (PVA) nanocomposites on bonding performance. In this study, PVA was selected as matrix and nanoclay as reinforcing material were used at 0.5% and 3% of filler ratio. Initially, nanoclay was mixed with mechanical stirrer, and then ultrasonic mixing was used to provide a homogenous solution with nanoclay. The obtained solution was used to prepare the nanocomposites. In preparation of the nanocomposites, three different mixing methods were used as only mechanical stirring for 20 min, mechanical stirring/ultrasonic mixing for 20 min and only ultrasonic mixing for 20 min. Dispersion quality of the nanocomposites was characterized with transmission electron microscopy (TEM). Bonding performance of the nanocomposites was determined with block shear test ASTM 905-08.

1. Introduction

Adhesives are widely used in the in the wood based composites to provide different properties under parts that joining techniques cannot do. The cost of adhesive is an important topic in the production of wood-based products [1]. Wood based material industry try to bring down the cost of production in order to increase profits with alternative methods. The one of the methods is to low-cost adhesive in the preparation or fabrication of products. Polyvinyl acetate (PVA) which has low-cost is

[1] Research Assistance, Bartin University

[2] Assistance Professor, Bartin University

[3] Professor, Bartin University

[4] Research Assistance, Bartin University

[5] Professor, Bartin University

[6] Research Assistance, Bartin University

one of examples and it has been traditionally used in many wood products, especially in furniture joining [1,2]. PVAs have many important advantages such as low-volatile compounds (VOCs) emissions, friendly environmentally, non-toxic to environment, easy to use etc. Besides the important advantages, PVAs have weak performance in locations under high humidity and high temperature (50° to up). PVAs exhibits low mechanical strength and creep performances in application areas [2].

Nanotechnology offers an important opportunity to build up alternations of adhesives with properties that cannot be provided by traditional methods. Nanoparticles incorporation into the adhesive is an economical and simple method to improve the physical and mechanical properties of adhesives. Nanoparticles has good properties such as increased aspect ratio and mechanical properties [3,4].

Many studies have provided great improve for obtaining much high performance with adding of nanoparticles into polyvinyl acetate. Nano fillers exhibit many important advantages as compare with macro/micro fillers for adhesive reinforcing. Nano fillers provide thin bond lines on surface of material and thus they can increase the bonding strength [5]. One of nano fillers which are widely used is nano clays. Nano clay has a unique structure and properties and a very high elastic modulus as compared to many biodegradable fillers. The higher elastic modulus enables nano clay to improve mechanical properties of polymers by carrying a significant portion of the applied stress [6,7]. Bonding performance can be increase many properties of polyvinyl acetate by adding to nanoclays little percentage to adhesive [8].

In this paper, it was investigated dispersion of nano clays in polyvinyl acetate with different mixing methods such as only ultrasonic mixing, both mechanical and ultrasonic mixing, and only mechanical mixing. The dispersion of nano clays in polyvinyl acetate was examined with transmission electron microscopy, and the bonding performance of the obtained adhesive was investigated with block shear test.

2. Materials and Methods

Polyvinyl acetate having a 1200 polymerization degree and a 90% hydrolysis level was purchased from Hafele Furniture and used to prepare the nanocomposites. Nano clay (NC) was purchased from Nanocor, Canada. The nano clay, which was supplied as micro fine powders under the “I” series designation, was ready for use directly into the resin system. Maple wood was used to determine the block shear strength. They

cut to 45 x 50 x 20 mm according to ASTM905 and, before bonding, samples were put into the condition chamber at 20°C with relative humidity of 60% for a week. The effect of three different mixing methods on dispersion of nano clays was studied in this study. The methods were only mechanical mixing, both mechanical and ultrasonic mixing, and only ultrasonic mixing (Tab. 1).

Tab. 1: Different mixing methods applied during the preparation of the nanocomposites

Mixing Methods		
Method 1	Method 2	Method 3
(1) Mechanical Mixing at 20 min, 1500 rpm	(1) Ultrasonic Mixing at 20 min, 60 Force (W) 60 frequencies (%)	(1) Mechanical Mixing at 20 min, 1500 rpm (2) Ultrasonic Mixing at 20 min, 60 Force (W) 60 frequencies (%)

Nano clays were to PVA as 0.5% and 3% loadings. Water-nano clays solutions were firstly prepared. For this, 0.5% nano clays were added to 10 grams of water, and then the solution was firstly mixed mechanical blender at 1500 rpm for 20 min. The solution obtained was ultrasonicated at 60 kH and 0.6 amplitute for 20 min. the same procedure was applied for 3% nano clays. The each solution was added to PVA, respectively. The temperature of the nanocomposites was kept below 50◦ C to provide decomposition of PVA by doing all works under ethylene glycol bath inside a cooler. Percentage of nanoclay in PVA (ranging from 0.5% to 3%) was based on solid mass of PVA. PVA with nanoclay were mixed with only mechanical stirrer for 20 min, both mechanical stirrer and ultrasonic mixer for 20 min, and only ultrasonic mixer (at 60 kH and 0.6 amplitute) for 20 min. For transmission electron microscopy (TEM), samples of nanocomposites were prepared by casting the PVA/nanoclay composites on Teflon sheets. Prior to further analyses, the sheets of nanocomposites were allowed to dry at room temperature for one month.

Transmission electron microscopy (TEM) allows a qualitative understanding of the internal structure, spatial distribution and dispersion of the nanoparticles within the polymer matrix, and views of the defect structure through direct visualization. Analyses were performed on a JEOL JEM 2100F HRTEM, transmission electron microscope at 80 kV. TEM specimens, having 50–70 nm thickness, were prepared by ultra microtoming the nanocomposite samples encapsulated in a polyvinyl acetate matrix.

3. Results and Discussion

Bloc shear test was applied on maple wood after they bonded with the nanocomposites. One-way ANOVA test was occurred to determine the difference of groups of the nanocomposites prepared with different mixing methods. Table 2/3 and Figure 1 show the one-way ANOVA/Duncan test and the average and standard deviation (±) of block shear strength of the wood samples.

Tab. 2: One-way ANOVA test of block shear strength of joints prepared by nanocomposites.

	Sum of Squares	d*f*	Mean Square	*F*	Sig.
Between Groups	65,5	6	10,9	21,7	0,00*
Within Groups	31,8	63	0,5		
Total	97,3	69			*P<0.05

Tab. 3: Duncan Analysis of block shear strength of joints prepared by nanocomposites.

	Samples Amount	A	B	C
3% U/M	10	10,8		
Control	10	10,4		
3% M	10		11,7	
0.5% M	10		11,8	
0.5% U/M	10		11,8	
0.5% U	10			12,7
3%U	10			13,2

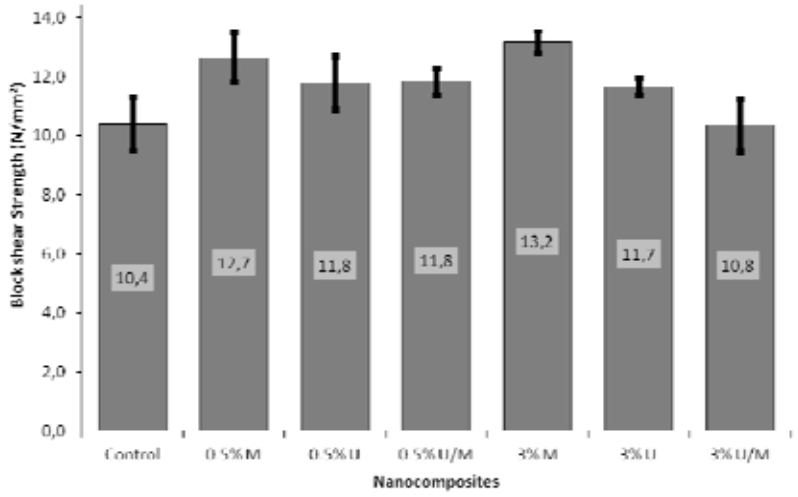

Fig. 1: Block shear strength of the wood samples.

According to Fig. 1, all formulations were found to be high as compare with control samples. The largest and lowest improving of bonding performance was determined as 13.2 for 3% NC with only mechanical mixing and 10.8 for 3% NC with ultrasonic and mechanical mixing. To evaluation, TEM images for PVA nanocomposites with NC at various loadings (0.5% and 3%) were given in Fig. 2. A good dispersion was obtained with ultrasonic/mechanical mixing (Fig 2d and Fig 3d). When the content of nano-clay increased in the polymer from 0.5% to 3%, the dispersion of nano clays changed. In only mechanical and only ultrasonic mixing, nano particles of clays was clumped together (black areas) in one parts and in other locations, the distance between nano clays increased. Nano-clay layers are present both in random and regular arrangements at both 0.5% and 3% nano-clay loading.

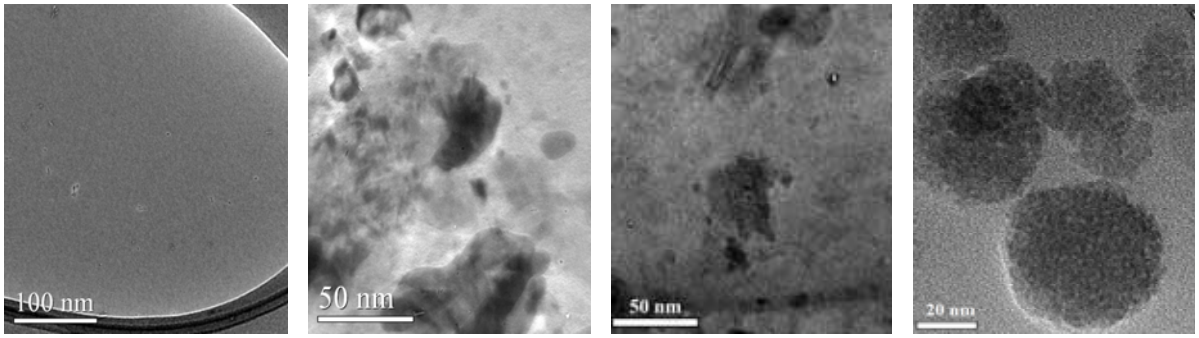

Fig. 2: Dispersion of Nano clays on the PVA Films Prepared with Different Mixing Methods for 0.5% Filler Loading ((a): pure PVA, (b): mechanical blending, (c): Ultrasonic blending, and (a): mechanical/ultrasonic blending).

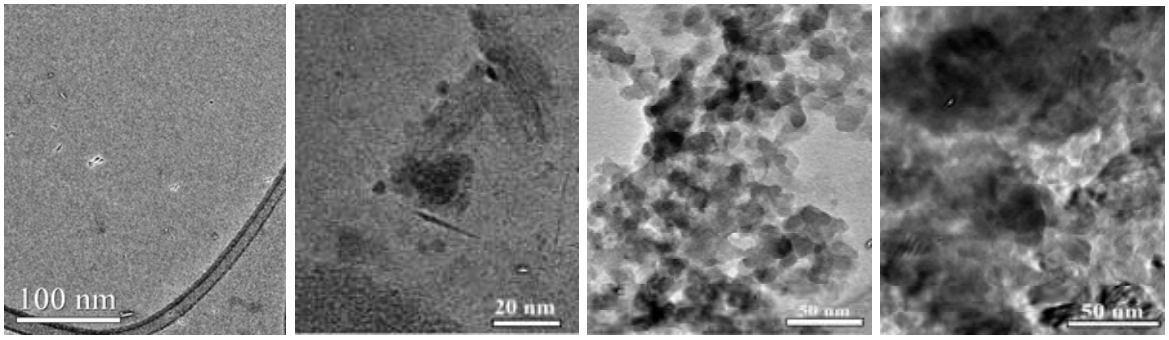

Fig. 3: Dispersion of Nano clays on the PVA Films Prepared with Different Mixing Methods for 3% Filler Loading ((a): pure PVA, (b): mechanical blending, (c): Ultrasonic blending, and (a): mechanical/ultrasonic blending).

Kaboorani and Riedl [9] evaluated that the quality of dispersion is a function of nano-clay type and loading and there is a direct link between the quality of dispersion and properties of nano-composites with TEM. At low loadings, nano-clay was found to be dispersed well in the matrix and the exfoliated structure was

obtained. When a good dispersion of nano-clay in the matrix was achieved, properties of PVA improved. Past research has shown that there is a direct link between the quality of nano-clay dispersion and the properties of nanocomposites. Exfoliated structures were reported to provide the materials with superior properties [10,11].

4. Conclusions

The dispersion of nano clays in polyvinyl acetate (PVA) was investigated on the samples prepared with different mixing methods. To determine effect of nanoclay and mixing methods on bonding performance of wood samples, block shear test was done. The results showed that block shear strength were found to be the highest for 3% mechanical mixing, also the lowest value of block shear was determined to 3% ultrasonic mixing. According TEM pictures, a good dispersion was generally found to ultrasonic/mechanical mixing. However, whereas the best dispersion was found to ultrasonic and mechanical mixing, the worst values of block shear strength were obtained to the mixing formulation. This phenomenon can be explained that the PVA with NCs solution was tried to keep at 50°C under ethylene glycol bath while blending the ultrasonic mixer. During mixing of PVA with NCs, it can be said that temperature may cause plasticizing or degradation of PVA and the block shear strength of wood samples decreased due to the phenomenon. While the loadings of nano clays increased in the PVA from 0.5% to 3%, it was found that the dispersion of nano clays changed as seen as TEM pictures.

5. Acknowledgment

The support by the Scientific and Technological Research Council of Turkey (TUBITAK COST Project No: 112R042) is gratefully acknowledged.

References

[1] Cho J, Joshi MS, Sun CT (2006). Effect of inclusion size on mechanical properties of polymeric composites with micro and nano particles. Composites Science and Technology, 66 (13): 1941–1952.

[2] Kaboorani A, Riedl B, Blanchet P (2013). Ultrasonication Technique: A Method for Dispersing Nanoclay in Wood Adhesives. Journal of Nanomaterials, Article ID 341897, 9 pages.

[3] Lopez-Suevos F, Frazier CE (2006). Fracture cleavage analysis of PVAc latex adhesives: influence of phenolic additives. Holzforschung, 60(3): 313–317.

[4] Kim S and Kim H (2006). Thermal stability and viscoelastic properties of MF/PVAc hybrid resins on the adhesion for engineered flooring in under heating system; ONDOL. Thermochimica Acta, 444(2): 134–140.

[5] Jacobs O, Xu W, Schadel B, Wu W (2006). Wear behaviour of carbon nanotube reinforced epoxy resin composites. Tribology Letters, 23(1): 65–75.

[6] Fornes, T.D., Paul, D.R., 2003. Modeling properties of nylon 6/clay nanocomposites using composite theories. Polymer 44: 4993–5013.

[7] Zeng, Q.H., Yu, A.B., Lu, G.Q., Paul, D.R., 2005. Clay-based polymer nanocomposites: research and commercial development. J Nanosci Nanotechno 5: 1574–1592.

[8] Zhai LL, Ling GP, Wang YW (2007). Effect of nano-Al_2O_3 on adhesion strength of epoxy adhesive and steel. International Journal of Adhesion & Adhesives, 28: 23–28.

[9] Kaboorani A, Riedl B (2011). Effects of adding nano-clay on performance of polyvinyl acetate (PVA) as a wood adhesive. Composites: Part A, 42: 1031–1039.

[10] Macia-Agullo TG, Fernindez-Garcia JC, Torro-Palau A, Orgiles-Barcelo AC, Martin-Martinez JMJ (1992). Addition of silica to polyurethane adhesives. J of Adhesion, 38 (1–2): 31–53.

[11] Metcalfe Porter E, Thomas MJK (2000). Nanocomposite fire retardants—a review. Fire Mater; 24: 45–52.

Ambient vibration testing to identify lateral stiffness and damping in modern multi-storey timber buildings

Thomas Reynolds[1], Wen-Shao Chang, Richard Harris[2]

Summary

The use of dimensionally-stable engineered wood products, along with enhanced connection and perpendicular-to-grain strengthening details have been a key part of the growth of multi-storey timber construction over the last ten years, resulting the construction of a number of timber buildings of seven stories and above. This study uses in-situ dynamic testing to measure the performance of the lateral-load resisting systems of these buildings, and their damping under wind-induced vibration. Both of these parameters are vital to the design of taller timber buildings in the future.

1. Introduction

Over the past ten years, multi-storey timber construction in Europe has advanced from a situation in which most European countries restricted timber construction to four stories or fewer [1], to a stage at which buildings exceeding six storey with timber as a main structural material around Europe [2-4], while a fourteen-storey building will shortly begin construction in Norway [5] and architects and engineers have conducted studies and proposed preliminary designs for far taller buildings [6, 7]. This change has been enabled by advances in fire engineering, the use of dimensionally-stable engineered wood products, and the development of systems to mitigate the

Fig. 1: Dynamic properties of the 8-storey Stadthaus building were estimated as part of this project

[1] Research Associate, University of Bath, UK

[2] University of Bath, UK

limitations of low strength and stiffness perpendicular to grain. The height and aspect ratio of the buildings completed so far is such that their lateral deflection has not been a critical design parameter, but for the buildings proposed in the future, it is expected to be an important concern [5]. The stiffness of lateral-load resisting systems in timber under static and dynamic wind loads is currently little understood, and so the development of systems to enhance that stiffness is hindered. This study seeks to develop a method by which to measure the performance of multi-storey timber structures in-situ, and compare the real performance of a range of multi-storey timber buildings.

There is currently no reliable theoretical method to predict damping in building structures, since the energy dissipation which leads to damping occurs in such a diverse range of processes and materials, some of which are part of the structural system, and some of which are not [10]. Damping must therefore be estimated based on measurements of similar structures previously completed, and this study begins to provide such measurements.

The buildings have been assessed by an ambient vibration measurement, or operational modal analysis, technique. This has the potential to be an extremely unobtrusive form of test, since no force needs to be artificially applied to the structure. Instead, the movement of the building under ambient conditions is measured by a series of accelerometers placed around the structure, and the resulting time-history is analysed to assess the natural frequencies, damping ratios and mode shapes of the structure.

2. Measurement technique

Operational modal analysis encompasses a family of methods used to identify the modal properties of a system based only on its output (its displacement, velocity or acceleration), with no quantitative information about the input (the forces applied to it). Qualitative information about the input is required in that it must be known to be stochastic with zero mean, and that it must be multi-input [8]. A stochastic load is non-harmonic, so does not produce a cyclic response which may be confused with a mode of vibration, and a multi-input load excites many parts of the structure, which ensures that the modes of vibration of interest are excited. The dynamic component of wind load satisfies these requirements, and forms a large part of the ambient forces on the structures tested in this study.

The operational modal analysis technique used here is based on the random decrement technique, which is an averaging process to used to extract an estimate of the free-decay response of the structure from the response to the multi-input, stochastic force.

Fig. 2: The test system measuring a single point, from top: accelerometers, data acquisition system, laptop and power supply

3. In-situ measurement and analysis

The movement of each structure was measured using three Integral Electronic Piezoelectric (IEPE) accelerometers capable of measuring movement at frequencies of 0.1Hz and above. Fig. 2 shows the test setup for measurements at a single point. The tests were generally carried out for 30 minutes at a time, which was found to allow for sufficient data for the averaging process, while allowing for any segments of the test with excessive noise or excessive excitation at a particular frequency to be removed. The random decrement technique gives an estimate of the autocorrelation function, two examples of which are shown in Fig. 3.

This can be analysed for modal properties of the system in a similar way to the free-decay response of a system to an impulse [9]. Measurements at a series of points can therefore be used to estimate mode shapes.

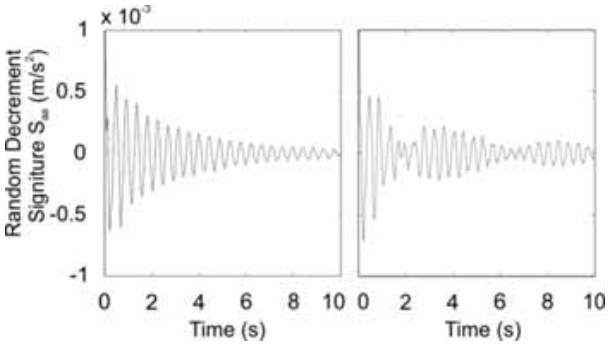

Fig. 3: Random decrement signatures at points on buildings with one dominant mode (left) and at a point with two closely-spaced modes (right)

Measurements have so far been carried out for four buildings: the 7-storey Limnologen buildings in Växjö, Sweden, 7-storey UEA student residence in in Norwich, UK, the 8-storey Stadthaus in London, and another multi-storey CLT building in London.

4. Outputs

This study begins to provide in-situ damping measurements for completed multi-storey timber buildings, whilst also providing an opportunity to compare theoretical and modeled predictions of natural frequency with those measured in-situ.

The unobtrusive nature of the test method means that it is suitable for a broad study of multi-storey buildings completed in cross-laminated timber. The project will continue by conducting laboratory tests on connections and CLT shear-wall systems, to develop predictive methods for the stiffness of such systems under in-service vibration.

References

[1] Östman, B. & Källsner, B. National building regulations in relation to multi-storey wooden buildings in Europe. *SP Trätek and Växjö University, Sweden*, 2011

[2] Unger, M., Hein, C. & Göckel, T., "LifeCycle Tower". *Fire Risk Management*, July 2010.

[3] Serrano, E.: Limnologen–Experiences from an 8-storey timber building. In: *Internationales Holzbau-Forum*, Garmisch. 2009.

[4] Thompson, H.: A Process Revealed / Auf dem Howlzweg: Stadthaus. FUEL 2009.

[5] Utne, I. 2013. *Numerical Models for Dynamic Properties of a 14 Storey Timber Building.* Master of Engineering, Norwegian University of Science and Technology.

[6] mgb Architecture and Design 2012. The Case for Tall Wood Buildings.

[7] Skidmore, Owings & Merrill LLP 2013. Timber Tower Research Project.

[8] Brincker, R., Ventura, C. & Andersen, P.: Why output-only modal testing is a desirable tool for a wide range of practical applications. In: *Proceedings of the International Modal Analysis Conference (IMAC) XXI.* Year.

[9] Magalhães, F., Cunha, Á., Caetano, E. & Brincker, R. Damping estimation using free decays and ambient vibration tests. *Mechanical Systems and Signal Processing,* 24(5): 1274-1290, 2010, DOI: 10.1016/j.ymssp.2009.02.011.

[10] Smith, R., Merello, R. & Willford, M. Intrinsic and supplementary damping in tall buildings. *Proceedings of the ICE - Structures and Buildings,* 163(2): 111-118, 2010

Increase of semi-rigidity for timber truss beam structure

Rostand Moutou Pitti[1,2,3], Eric Fournely[1,2], Serge Ekomy Ango[3]

Summary

The possibilities to take into account OSB panels and their link with low size timber truss beam as an effective mechanical connection is investigated. The load carrying capacity of the trusses in the DOREAN house structure is so studded. On the one hand, by experimental tests carried out on double shear specimens, and on the other hand by modeling a T-beam including the stiffness of the assembly between the panel and the truss beam. The connection between the OSB panel and the upper chord of the lattice beam is realized by staples. Shear tests are performed varying the number of fasteners with three thicknesses of panel and three different orientations of the staples. The T-beam obtained by the connection between the OSB panels and the DOREAN lattice beam is modeled using beam elements. The semi-rigid behavior is taken into account for all the connections between the lattice beam elements and the OSB panels.

1. Introduction

Due to the fact that the energy costs represent a significant part of household expenses, it appears necessary to improve the composition and the assembly of structural elements in timber building [1]. According to its assembly and building mode, the DOREAN's beam can contribute to solving a part of this problem. This beam is generally built from low-size timber members, assembled by nails, by plates with metal teeth or by adhesives. The efficiency of this assembly is obtained by the control of the manufacture process and the knowledge of the joints behavior [2, 3]. These beams can be used in the frame systems or slabs in combination with OSB panels.

[1] Assistance Professor, Clermont Université, UBP, Institut Pascal, Clermont-Ferrand, France

[2] Researcher, CNRS, Institut Pascal, Aubière, France

[3] Researcher, CENAREST, Institut de Recherche Technologique, Libreville, Gabon

The present work is focused on the semi-rigid behavior of the nailed and glued connection between the lattice beam members and the OSB panels. In the literature, few authors have discussed the influence of these connections in the global behavior of timber structures [4]. The experimental tests performed on push-out specimens provide the load-displacement curves of the connections between the wood members and the OSB panels. Thus, various configurations of connections are tested changing the thickness of the panels and the connection type (number and orientation of staples, glue, and panel thickness). The experimental results are used as input data in a numerical finite element model. The comparison of experimental test and simulation are presented and discussed.

2. Experimental setup

2.1 Specimens dimension

The push-out specimens are tested in universal press under compression loading to obtain the shear load on the connection. The static loading history (Fig. 1) includes a preloading phase, a partial unloading and finally a re-loading phase until failure. The first plateau after preloading is 1200 N and 600 N for the specimens loaded in the directions parallel or perpendicular to grain. The second plateau, after unloading phase is 200 N in both cases.

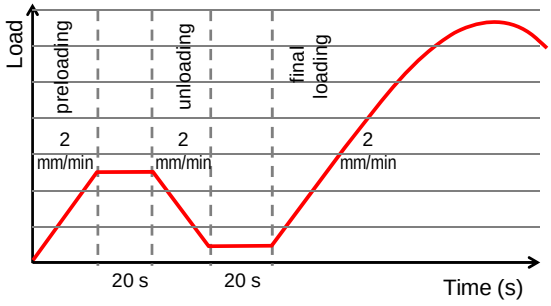

Fig. 1. Loading history during test program

The dimensions of the two types of specimens loaded in the directions parallel and perpendicular to grain with the measurement devices of load and displacements are shown in Fig 2. The relative displacements between the OSB panels and the wood member are measured on four points around the wood member using LVDT sensors. Thus, for each test, the mean value of displacement measured by the two transducers for each interface between OSB panel and wood member is considered to represent the behavior of the connection.

The orientation of the staple is defined as the angle between the longitudinal axis of the staple and the longitudinal axis of the timber element. For all the specimens the staples are positioned on one line parallel to the wood member. The spacing between

the staples is equal to 150 mm for all the specimens except for the configurations “2” and “6-3” respectively with 7 or 3 staples and a half spacing. Timber elements are made of spruce of C18 class resistance with density of 435 kg/m³ [5]. The staples are made from steel with ultimate stress f_u of 540 MPa. The shear strength of such staple using the Eurocode 5 [3] requirements is about 0.5 kN for the 3 thicknesses of panels. This strength is given for one staple and one shear plan between the wood member and the wood OSB panel. The glue is polyurethane characterized by shear strength of 1.2 MPa.

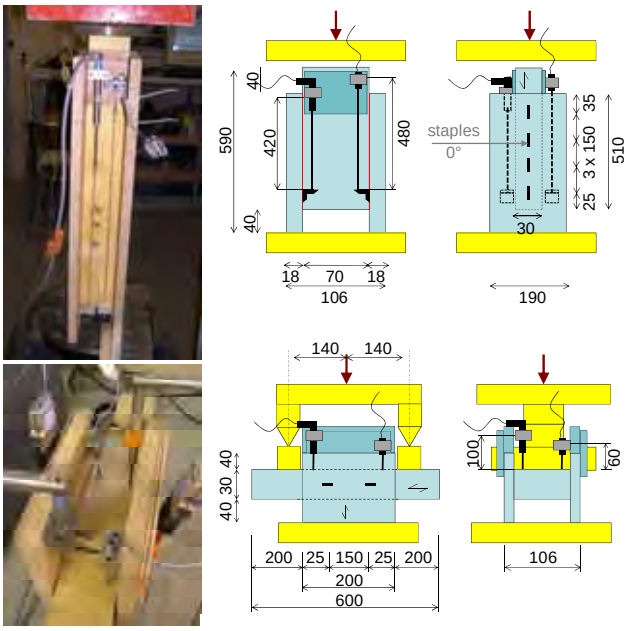

Fig. 2. Dimensions of specimens with measurement devices of load and displacement

2.2 Experimental results

The load-displacement relationships are plotted on Fig 3. The displacement for each indexes a, b and c is the mean value of the four LVDTs around the wood member. The indexes a, b and c represent three specimens tested for each configuration. Fig. 3 allows comparing the mechanical behavior between the 45° and 90° orientation of staples.

Tab. 2 gives a synthetic overview of experimental results on the whole set of specimen. F_{max} is the maximum load, F_y and dep_y are the intersection between the lines tangent to the initial and final phases (1/6 of initial tangent) of the load-displacement curves, F_u is the ultimate value of the force and dep_u is the lowest value between the displacement for F_u and the displacement corresponding to a decreasing of 20% of the load compared to F_{max}, the ductility is the ratio dep_u/dep_y.

For shear in the direction parallel to the main axis of timber element: the strength of mechanically connected joints (without glue) is between 6.8 and 8.5 kN for 4 staples. The higher values of strength are obtained for OSB 18 and the lower values for OSB 10. The best orientation of staple is an angle of 90° (staples perpendicular to the grain direction of timber element). Doubling the number of staples with half spacing induces an increasing of strength of about 75%. With the same number and

orientation of staples, the presence of glue allows reaching strength between 17.3 and 19 kN, but the static ductility is slightly reduced in comparison with the staples. For this case of joints in shear, the values of rigidity are between 5.3 and 13.9 kN/mm.

For shear in the direction perpendicular to the main axis of timber element: the strength obtained with 2 staples is around 4 kN and that of 3 staples is about 6 kN. With the same number and orientation of staples, the glue increases the strength to reach more than 10 kN with a significant decrease of the static ductility. For these configurations of joints, the values of rigidity are between 2.6 and 4.8 kN/mm.

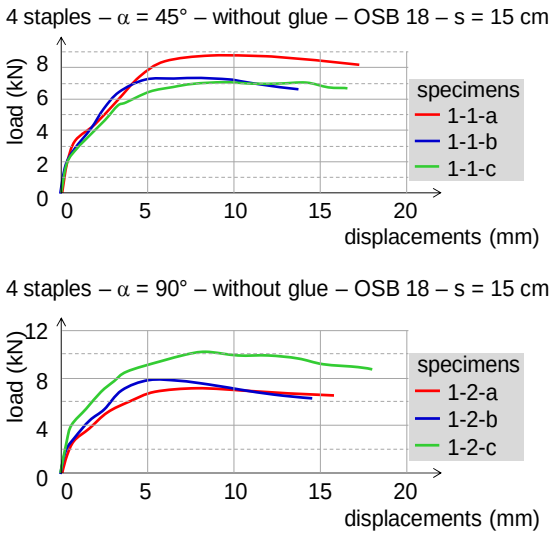

Fig. 3: Push-out test in parallel and perpendicular configuration

Tab. 1: Selection of approaches for the design of notched beams

	specimen orientation	staples	number of staples	glue	staple orientation	OSB thickness	F_{max} (kN)	F_y (kN)	F_u (kN)	dep_y (mm)	dep_u (mm)	rigidity (kN/mm)	ductility
1-1	//	yes	4	no	45	18	7.7	3.2	6.9	0.6	>18	5.3	>30
1-2	//	yes	4	no	90	18	8.5	4.1	6.8	0.7	>18	5.9	>26
1-3	//	yes	4	no	0	18	7.3	3.7	5.9	0.6	>18	6.2	>30
2	//	yes	7	no	0	18	12.8	7.3	10.2	0.8	>18	9.1	>23
3	//	no	0	yes	0	18	19	15.9	15.2	1.4	5.8	11.4	4
4-1	//	yes	4	no	0	15	7.8	2.5	6.3	0.3	>18	8.3	>60
4-2	//	yes	4	no	0	10	6.8	3.7	5.5	0.9	8.8	4.1	10
5	//	yes	4	yes	0	18	17.3	12.5	13.1	0.9	6.8	13.9	8
6-1	⊥	yes	2	no	0	18	3.8	1.8	3.1	0.7	10.3	2.6	15
6-2	⊥	yes	2	yes	0	18	10.7	5.8	8.5	1.2	7.2	4.8	6
6-3	⊥	yes	3	no	0	18	6	2.8	4.8	0.6	10.2	4.7	17

3. Finite element methods and Outlook

In order to take into account the composite behavior of a T-beam realized with a Dorean lattice beam and OSB panels connected by staples or glue, a finite element model is realized using beam elements. The mechanical properties of the Dorean beam, obtained in a previous study [1], are used in the numerical simulation of the present study. Truss elements with semi-rigid behavior at the end of the members and between the wood member and the OSB panel are considered.

To represent the composite effect between the upper chord of the truss beam and the OSB panel, short beam element is used to represent the semi-rigid behavior between the panel and the wood member (Fig. 8). The initial stiffness of the connection is obtained from the tests on shear specimens.

The OSB panel is represented by equivalent beam element (Fig. 4).The simple finite element model is performed to analyze the influence of the axial semi-rigid behavior at the end of the members and the shear semi-rigid behavior at the interface between the OSB panels and the upper chord of the lattice beam.

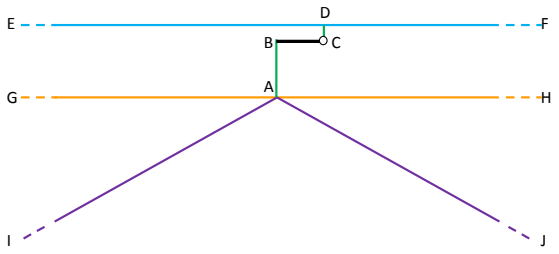

Fig. 4: Experimental tests on notched beams compared to the range of practical relevancy

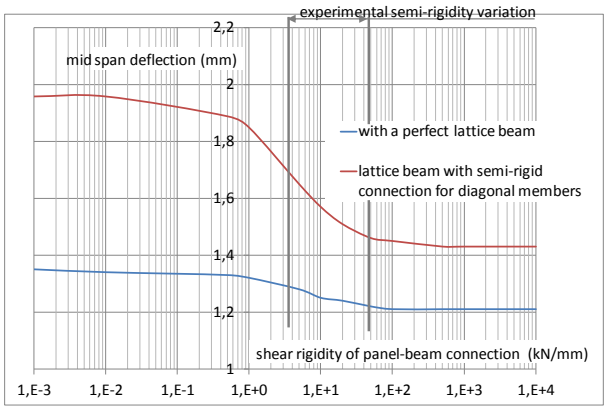

Fig. 5: Experimental tests on notched beams compared to the range of practical relevancy

Fig. 5 shows the influence of the shear semi-rigidity at the interface on the global deflection, at linear phase, of a T-beam combining lattice beam and OSB panel. The axial connections at the end of the truss members are considered rigid or semi-rigid. The comparison shows that the lattice beam with axial semi-rigidity at the end of the members is more sensitive to the evolution of the shear semi-rigidity at the interface between the panel and the upper chord. Besides, the increase of the shear rigidity increases the global stiffness of the T-beam. Here, for a span of 3.36 m, this increase is equal to 12 and 37% respectively for the perfect lattice beam and for the truss beam with semi rigid shear connection between the panel and the upper chord. This increase reaches 41% for a span of 4.45 obtained adding 2 diagonals. The results of the simple simulations illustrate the effects of shear semi-rigidity on the global behavior of the T-beam combining lattice beam and OSB panels. This preliminary study will be extended to analyze different ratios of stiffness between the truss beam and the panels. The stiffness at the interface will be analyzed considering real non-linear behavior of materials and connections.

References

[1] Fournely E., Moutou Pitti R., Bouchair A. Behaviour of timber lattice beam with semi-rigid joints: analytical and experimental study, *PRO* LIGNO, 2012, 8(3): 19-41

[2] AFNOR, NF EN 408. Structures en bois, Bois de structure et bois lamellé collé, détermination de certaines propriétés physiques et mécaniques. Mars 2004, p. 32.

[3] AFNOR, Eurocode 5 : Conception et clacul des structures en bois – généralités, règles communes et règles pour les bâtiments, NF EN 1995-1.1, 2005

[4] Zhu E.C, Z.W. Guan Z.W, Rodd P.D, Pope D.J. Finite element modelling of OSB webbed timber I-beams with interactions between openings, *Advances in Engineering Software*, 2005, 36: 797–805

[5] AFNOR, NF EN 300, Panneaux de lamelles minces, longues et orientées – OSB définitions, classification et exigences, 2006.

Experimental evaluation of timber network arch bridge

Anna W. Ostrycharczyk[1], Kjell A. Malo[2]

Summary

The network arch bridge was invented by Professor Per Tveit in the early sixties and originally based on steel arches, concrete decks and tension ties [1]. The most important feature, which makes this type of bridges distinguish from other arch bridges, is the use of inclined and crossing hangers which cross each other typically twice or more. The use of inclined hangers dramatically lowers the moment in the arch as well as it makes the bridges much stiffer [1]. The paper describes current work on evaluation of a laboratory model of a timber network arch bridge and experimental results for a dynamic behavior of the bridge. In the laboratory model of the bridge, timber was used as structural material for both arches and deck.

1. Introduction

A basic idea of network arch research is to analyze static and dynamic behavior of a bridge with design assumption like; length of the bridge more than 100m; timber as structural material for the arches and the deck, and reduced or lack of a wind bracing between arches. In addition, a new concept of hangers location is introduced. So far all hangers have been situated in one plane in network bridges. Consequently the out-of-plane stability of an arch is the same for arbitrary configurations of hangers. However, by introduction of pair of hangers where the fastening points at the 'deck level' are displaced in transversal direction, we get double inclination of hangers like in the spoked wheel of a bicycle; see Fig. 1, [2].

[1] Ph.D. Candidate, Norwegian University of Science and Technology, NTNU Trondheim, Norway

[2] Professor, Norwegian University of Science and Technology, NTNU Trondheim, Norway

This configuration, called 'spoked configuration', stiffen the arch in out-of-plane direction, and make reduction or omission of wind bracing possible. The result of a preliminary design process was the numerical and the laboratory model shown in Fig. 2 and 3.

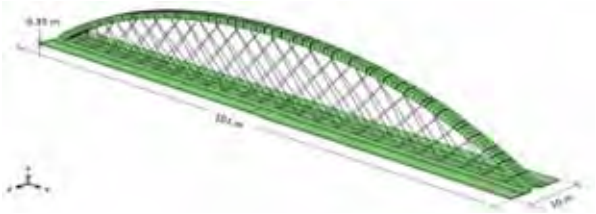

Fig. 1: Network arch with spoked configuration of hangers

The numerical model was built with beam, shell and solid elements. The laboratory model was build in scale 1:10 due to design assumptions of 100m length of the bridge, and circular arches with rise of 14 m.

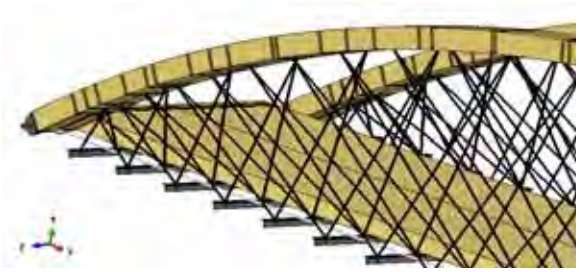

Fig. 2: Numerical model of the bridge

Fig. 3: Laboratory model of the bridge

Initial modal analysis was performed on both the numerical and the laboratory model in two phases. First only the deck was tested, and in sequence, the whole structure.

2. Evaluation of network bridge model

2.1 Evaluation of laboratory and numerical models

The effect of an increase of stiffness of the laboratory model has been studied. To achieve higher stiffness of the deck, it was clamped at the ends (Fig. 4). This procedure influenced positively on dynamic test's results. Another stiffness improvement was to pre-stress the hangers, which have shown a tendency of immediate relaxation during testing. The pre-stressing procedure was performed in steps to the point when relaxation/slip did not appear during tests. A side effect of the hangers pre-stressing procedure was the appearance of camber on the deck (Fig. 5).

Fig. 4: Clamped deck at the support

Fig. 5: Bridge with cambered deck

During this evaluation, the numerical model was improved and only beam and shell elements were used.

2.2 Tests methods

Modal analysis with modal hammer is a technique used to obtain natural frequencies and corresponding mode shapes of a structure. By impacting the structure with a modal hammer [3], a wide frequency range is excited, and the motions of the structure are recorded with an accelerometer located on the structure. The force-time history of the impact is also recorded. A basic test result is a frequency response function (FRF), which combine input force and movement of the structure caused by the impact. Evaluation of the FRF leads to recognition of natural frequencies and corresponding mode shapes. For bridge response, low frequency excitation at high input force level is usually required. To achieve that, a soft tip of the hammer was used during the tests [3]. Measurements were performed on transversal and vertical directions both on the arch and the deck, with accelerometer positioned close to support ('on side' position) and close to the middle ('center' position). The chosen accelerometer position allowed pick-up of all of the lower mode shapes (Figs. 6, 7). Commercial software from National Instruments was used to visualize mode shapes and to compute fundamental frequencies and corresponding damping ratios.

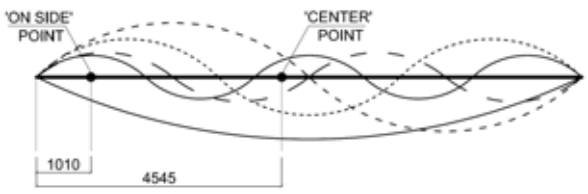

Fig. 6: Mode shapes of the deck

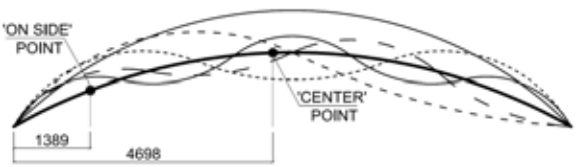

Fig. 7: Mode shapes of the arch

The laboratory tests were conducted during all steps of the pre-stressing process. Simultaneously, linear modal analysis was performed on numerical model for the structure under self weight.

3. Results

A few selected results are gathered in the Table 1. It presents natural frequencies obtained in a laboratory compared to those obtained by the numerical model for chosen mode shapes. Table 1 gives natural frequencies for transversal and vertical mode shapes (separately) for the deck, and transversal mode shapes for the arches. Results from vertical mode shapes of the arches were not measureable. Tab. 1 shows results from the start and the end of evaluation process of the bridge, for two positions of the accelerometer and the values of measured damping ratios.

Tab. 1: Comparison of natural frequencies of the bridge, obtained in a laboratory and by numerical tests; (NF-natural frequency, DR-damping ratio, n.a.-not applicable)

		First tests on the laboratory model				Last tests on the lab. model				
		Acceleration on side		Acceleration in center		Acceleration on side		Acceleration in center		Numerical results
Element /trend ▼	Mode nr. ▼	NF [Hz]	DR [%]	NF [Hz]	DR [%]	NF [Hz]	DR [%]	NF [Hz]	DR [%]	NF [Hz]
DECK trans-versal	1	n.a.	n.a.	n.a.	n.a.	16.977	2.133	17.016	2.531	24.901
	2	n.a.	n.a.	n.a.	n.a.	55.527	1.934	54.741	2.890	58.470
	3	94.878	0.101	n.a.	n.a.	107.43	1.006	107.52	1.335	96.461
DECK vertical	4	n.a.	n.a.	n.a.	n.a.	38.282	1.116	37.482	1.060	47.626
	5	n.a.	n.a.	n.a.	n.a.	51.996	0.938	53.144	1.187	61.524
	6	81.191	1.236	80.629	1.452	71.392	0.656	68.293	1.633	71.818
ARCH trans-versal	3	30.818	2.944	30.200	2.295	31.233	2.454	31.615	2.143	40.786
	4	53.270	1.912	52.995	2.096	53.357	1.968	54.321	2.365	65.010
	5	80.501	1.740	79.060	2.223	81.432	0.677	81.358	1.802	84.383

It can be noticed that the evaluation procedure of the bridge model (clamping the deck, pre-stressing hangers) allowed recording the lower mode values for tests performed on the deck, which were not measurable in the first tests. Moreover, high values of damping ratio were recorded for the corresponding lower mode values. The last obtained results approached the numerically obtained values of the natural frequencies, both for the arches and the deck.

4. Conclusion and future work

The presented results show the influence of the stiffening effect of the spoked hangers and the deck of the bridge with respect to the dynamic properties. The work presented herein is in its initial phase, and more findings related to arches with spoked hangers are expected in the near future. Further studies will be focused on derivations of mathematical models of the spoked arch. Strategies for hanger configuration will be also analyzed, as well as issues related to splicing of arches which is needed for long spans.

5. Acknowledgement

The support by The Research Council of Norway (208052) and The Association of Norwegian Glulam Producers, Skogtiltaksfondet and Norwegian Public Road Authorities is gratefully acknowledged.

References

[1] Tveit P., Information on the Network Arch, http://home.uia.no/pert/index.php/Home. [Online]

[2] Malo K. A., Ostrycharczyk A., Barli R. and Hakvåk I., On development of network arch bridges in timber, *Proceedings of International Conference on Timber Bridges*, 2013, Las Vegas, USA.

[3] Labonote N, Modal hammer for dummies, Trondheim, 2012

Structural behavior of timber frame closed panels for specification in the United Kingdom

Jesus M. Menendez[1], Kenneth Leitch[2], Robert Hairstans[3]

Summary

A series of closed timber frame wall panels were tested for racking capacity in accordance with the standard BS EN594:2011 [1]. The test program was designed to investigate the wall diaphragm performance of conventional and evolved (dual-frame) panels and for various design specifications. The resulting data was used to determine the feasibility of using locally resourced and graded timber for the manufacture of the frame and the impact of different sheathing materials on the overall structural behavior.

Through the undertaking of these tests, the effect of variables such as sheathing material, wall length and the inclusion of openings on shear walls were measured. The study concludes that low-graded timber is suitable for the manufacture of wall panels and also provides guidance for efficient structural design.

1. Introduction

Structural load bearing walls transfer dead and live loads to the foundation by the timber frame while, for these gravity loads, any contribution from the sheathing to the wall strength and stiffness is generally ignored. Furthermore, shear or racking walls also transmit lateral loads to the foundation by lateral bracing or, more frequently in off-site timber frame construction, by sheathing materials securely fixed to the frame. The sheathing must also be a wood-based panel product in accordance with BS EN 13986 [2]. However, design shear capacities per unit length are given for plasterboard-clad-only timber frame walls on the UK Non-Contradictory

[1] Doctoral researcher, Edinburgh Napier University, United Kingdom

[2] Senior researcher and lecturer, COCIS, United Kingdom

[3] Head of Centre and reader, COCIS, United Kingdom

Complimentary Information (NCCI) to Eurocode 5 document PD 6693-1 [3]. The racking or in-plane lateral resistance is determined by the length and geometry of the wall panel, the lateral shear capacity of the fasteners, the spacing of the fastener, the presence of openings, the vertical load applied and the sole plate fixing and overturning restraint.

2. Determination of the racking performance

2.1 Design of the experimental approach

During the course of this research, over 10 shear wall types of various specifications were tested at the Building Performance Assessment Centre (BPAC). At that time, BPAC held the accreditation of being a United Kingdom Accreditation Service (UKAS) test facility.

The test methodology employed was the British and European standard method BS EN 594 [1] published on July 2011. A modified horizontal version of the EN 594 test apparatus was used (Fig. 1). The timber utilized in the fabrication of the frame was graded as C16 with a cross section of 45×89 mm. Nevertheless, the characteristic density of the timber used in the frame, physical property which influences the structural performance [4], corresponded to grade C24. This panel configuration represented the structural external frame layer of a closed panel dual-system frame.

Fig. 1: Racking test apparatus as in EN 594

The shear wall test schedule was designed to investigate the effects of different variables involved in the specification of structural shear walls. However, the number of samples was insufficient to do any statistical inference. In all cases, the width of the sheathing boards was 1200 mm and the sheathing fastener specification was Timberfix360 screw 3.2×60 mm. Vertical loads of 5 kN were applied to the head binder at the stud positions. The configuration of the test schedule is shown in Tab. 1.

Tab. 1: configuration of test specimens

Ref.	Dimensions [m]	Sheathing	Thickness [mm]	Fastener spacing [mm]	Opening ([1]) [mm]
P1	2.4x1.2	OSB/3	9	75/150	No
P2	2.4x1.2	OSB/3	9	75/150	No
P3	2.4x1.2	Fibreboard MBH.HLS1	9.2	75/150	No
P4	2.4x1.2	Fibreboard MBH.HLS1	9.2	75/150	No
P5	2.4x1.2	Plasterboard	12.5	75/150	No
P6	2.4x1.2	Plasterboard	12.5	75/150	No
P7	2.4x3.6	OSB/3	9	75/150	1060x2070
P8	2.4x3.6	OSB/3	9	75/150	1060x2070
P9	2.4x4.8	OSB/3	9	75/150	1060x2070
P10	2.4x4.8	OSB/3	9	75/150	1060x2070
([1]) Openings were located at 670 mm from the left hand side stud.					

The loading protocol establishes only one stage under a constant load until failure is reached. The loading duration for the test must ensure that 90% of the F_{max} is reached within (300±120) s. The wall panel stiffness is then determined as per Equation 1.

$$R = \left[\frac{F_4 - F_2}{v_4 - v_2} \right] \qquad \text{(Eq. 1)}$$

2.2 Design approach based on analytical Eurocode theory

The recent Published Document 6693-1 [3] provides a simplified analysis of wall diaphragms. This unified method, an adaptation of the Simplified Plastic method by Kallsner, Girhammar [5], is dependent of the wall length *(L)* and geometry *($K_{i,w}$)*, the shear capacity and spacing of the sheathing fasteners *($f_{p,d,t}$)*, the existence of openings *($K_{opening}$)* and the sole plate fixing detail *($K_{i,w}$ and $f_{i,sp,d}$)*. Eq. 2 shows the expression used to calculate the racking resistance of a shear wall, *i*:

$$F_{v,Rd,i} = K_{opening} K_{i,w} f_{p.d.t} L \qquad \text{(Eq. 2)}$$

This design racking strength is valid providing that the condition shown in Eq. 3 is met, where a sheathing combination factor may apply *(K_{comb})*. This condition defines a maximum limit for racking deflection.

$$K_{i,w} \ f_{p.d.t} \leq 8\left(1 + K_{comb}\right)\frac{L}{H} \qquad \text{(Eq. 3)}$$

3. Results

The racking tests undertaken provide UKAS accredited strength and stiffness values for the closed panel system, which can be used directly for the purpose of specification. Additionally, they also provide information on the failure mechanism of the wall at the Ultimate Limit State (ULS). Wall panels were found to exhibit a brittle failure mechanism as a result of the sheathing material and fastener specification used. It was found that failure was in no way dependent on the specification of the timber. The strength and stiffness results derived from the racking tests undertaken are summarized in where applicable strength values are shown alongside those calculated using the PD6693.

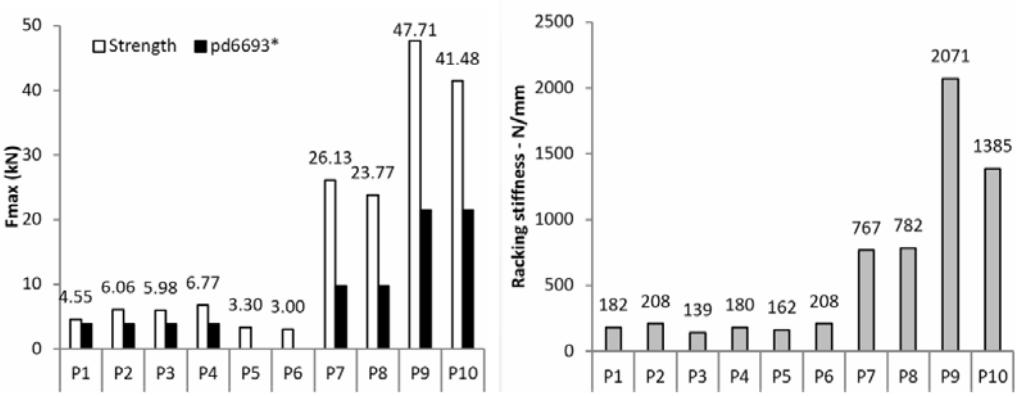

Fig. 2: Racking performance of specimens. Strength (left) and Stiffness (right)

Neither the PD6693 document nor EC5 provide guidance for the determination of the stiffness behavior shear walls subjected to racking actions. For this reason, the data provided from the racking tests is of additional relevance.

4. Discussion and conclusions

Findings from the laboratory racking test on the wall types have been summarized:

- in the case of imperforate wall panels sheathed with OSB material, as a result of the sheathing fasteners acting to resist overturning forces, ultimate failure of the wall occurred as a result of a localized brittle failure of the bottom rail;
- panels sheathed with fiberboard and plasterboard, consistent brittle failure of the sheathing material was observed;
- in the case of wall panels containing openings, failure occurred as a result of excessive displacement under racking load.

In addition, where panel was sheathed with OSB, the clear failure of the bottom rail was a consequence of insufficient edge distance, not as a result of the timber properties.

The comparison demonstrates that in all cases, even in spite of the brittle failure observed during test, the test racking strength of each wall type exceeded that which was predicted by PD 6693. In line with existent racking theory [6-8] the strength and stiffness of the wall has been found to increase in line with wall length and decrease as a result of the presence of openings.

5. Acknowledgment

The authors would like to appreciate the European Regional Development Fund funded project named Wood Products Innovation Gateway for the financial contribution to this research work.

References

[1] BSI, BS EN 594:2011, in Timber structures — Test methods — Racking strength and stiffness of timber frame wall panels. 2011, BSI.

[2] BSI, BS EN 13986, in Wood-based panels for use in construction. Characteristics, evaluation of conformity and marking. 2004, BSI: London.

[3] BSI, PD6693-1, in Complementary Information to Eurocode 5. Design of timber structures Part 1. General. Common rules and rules for buildings. 2012, British Standard Institution: London. p. 66.

[4] Leitch, K., The development of a hybrid racking panel, in School of Engineering and Built Environment. 2013, Edinburgh Napier University: Edinburgh. p. 274.

[5] Kallsner, B., U.A. Girhammar, and L. Wu. A simplified plastic model for design of partially anchored wood-framed shear walls. in CIB/W18. 2001. Venice: International Council for Research and Innivation in Building Construction.

[6] Pattonmallory, M., et al., Light-Frame Shear Wall Length and Opening Effects. Journal of Structural Engineering-Asce, 1985. **111**(10): p. 2227-2239.

[7] Dolan, J.D. and R.O. Foschi, Structural Analysis Model for Static Loads on Timber Shear Walls. Journal of Structural Engineering ASCE, 1991. **117**(3): p. 851-861.

[8] Salenikovich, A., The Racking Performance of Light-Frame Shear Walls. 2000, Virginia Polytechnic Institute and State University: Blacksburg.

Study of spreading under a compressive stress in glued laminated timber

Damien Lathuilliere[1], Jean-François Bocquet[2], Laurent Bleron[3], Frédéric Dubois[4]

Summary

This paper presents by an experimental approach, the study of the spreading of transverse compressive stress under localized supports. This study is extended to the compression load oriented at an angle to the grain. The phenomenon of the compressive stress spreading is determined according to the compressive and longitudinal shear strength. A model is proposed. Uniform compression tests of given angle were performed experimentally to identify failure modes depending on the angle between the load and the grain. These tests allowed us to identify the most relevant design code between DIN and EC5 which have slightly different approaches.

1. Introduction

1.1 Background

Today for the construction of a timber structure, whether industrial or housing, the glued laminated timber became the indispensable material for large-span structures. The construction of such structures leads to the transverse localized compressive stress. This concentration severely penalizes structures because of the weakness of the transverse compressive stress of softwood. However, a spreading effect reduces this property impact on the other mechanical properties.

In order to calculate these structures and take into account the spreading load effect, it subsists a design code predicting the support bearing capacity solicited in transverse compression. It is extracted from EN 1995-1-1 A1[1]. In the current design code, this phenomenon is established using the calculation code of effective length in

[1] PhD student – ENSTIB/LERMAB - Lorraine University, France

[2] Associate professor - ENSTIB/LERMAB - Lorraine University, France

[3] Professor - ENSTIB/LERMAB - Lorraine University, France

[4] Professor - FST/GEMH - Limoges University, France

order to simplify this code [2],[3],[4],[5],[6]. It integrates also the factor taking into account the load configuration increasing the design compressive strength perpendicular to the grain.

However, today's architecture evolves. For this reason, the structures become increasingly complex and varied. By means of these structures, the compression stress at an angle to the grain under concentrated load has to be understood, as well as the associated spreading phenomenon.

Today, it exists two standards allowing the calculation of the compression stress at an angle to the grain. The first is governed by the German standard DIN 1052 [8]. α represents the angle between the force orientation and the grain orientation. It calculates according to Eq. 1:

$$f_{c,\alpha,d} = \frac{f_{c,0,d}}{\sqrt{\left(\frac{f_{c,0,d}}{f_{c,90,d}} \cdot \sin^2\alpha\right)^2 + \left(\frac{f_{c,0,d}}{1.5 \cdot f_{v,d}} \cdot \cos\alpha \cdot \sin\alpha\right)^2 + \cos^4\alpha}} \quad (1)$$

The second standard is the European standard EN 1995-1-1 [9]. This formula is slightly modified compared to that European standard. It does not integrate the factor taking into account the load configuration ($k_{c,90}$). It is in the form of the Hankinson proposition. It calculates according to the expression:

$$f_{c,\alpha,d} = \frac{f_{c,0,d}}{\frac{f_{c,0,d}}{f_{c,90,d}} \cdot \sin^2\alpha + \cos^2\alpha} \quad (2)$$

$$\sigma_{c,\alpha,d} \leq \frac{f_{c,0,d}}{k_{c,90} \cdot \frac{f_{c,0,d}}{f_{c,90,d}} \cdot \sin^2\alpha + \cos^2\alpha} \quad (3)$$

About the spreading of the compression at an angle to the grain, the two standards do not include the spreading in the same way. The EC5 includes the phenomenon of spreading directly in the calculation Eq. 3 of the support bearing capacity solicited in compression at an angle to the grain using only the factor ($k_{c,90}$).

The DIN uses the two factors of the spreading effect integrating the variation of the angle. The calculation criterion is based according to Eq. 4.

$$\sigma_{c,\alpha,d} = \frac{F_{c,\alpha,d}}{t \cdot \ell_{ef}} \leq k_{c,\alpha} \cdot f_{c,\alpha,d} \tag{4}$$

with

$$k_{c,\alpha} = 1 + \left(k_{c,90} - 1\right) \cdot \sin\alpha$$

$$\ell_{ef} = \ell + 30 \cdot \cos\left(90 - \alpha\right) + \min\begin{cases} 30 \cdot \cos\left(90 - \alpha\right) \\ \ell_1 \end{cases}$$

ℓ_1 represents the distance between the support edge and the sample edge.

In addition, neither of these two standards does not allow the spreading of longitudinal compressive stress with a discrete support.

1.2 Objectives

The objectives of this study are to determine the spreading effect for the transverse compressive stress.

Furthermore, the confrontation between two current design codes for predicting the support bearing capacity solicited in compression at an angle to the grain and the experimental test is made, in order to determine the best code.

To finish, an analytic model is proposed predicting the support bearing capacity solicited in transverse and in compression at an angle to the grain taking into account the spreading effect.

2. Materials and methods

The experimental tests were carried out with the homogeneous glued laminated timber with a strength class GL24H are composed of Spruce (Picea abies) lamella, with a thickness of 45 mm. The load point displacement was controlled at a constant speed in order to respect the time of (300 ± 120)s. All specimens were conditioned at 12% humidity without cracking on the specimen. The mean density of all specimens is 450 kg/m^3.

2.1 Uniform compression tests

The angle of uniform compression tests (Fig. 1) varies between 0° and 90°. All specimen dimensions are listed in Tab. 2.

Fig. 1: Uniform compression test

Tab. 2: Uniform compression tests geometries

Designation	Height (mm)	Thickness (mm)	Support length (mm)	Angle (°)	Number of samples
COMP0	174	100	50	0	8
COMP10	174	100	100	10	5
COMP20	174	100	174	20	5
COMP30	174	100	174	30	5
COMP45	174	100	174	45	5
COMP60	174	100	174	60	5
COMP90	200	90/160	280/160	90	35

2.2 Compression tests

In order to study the spreading effect under the compressive stress, the experimental tests were carried out with the discrete support combined with measures of digital images. The angle of compression test (Fig. 2) takes the values 0°, 45° and 90°. The dimensions are summarized in Tab. 3.

Fig. 2: Compression test with the spreading

Tab. 3: Compression tests geometries

Designation	Height (mm)	Thickness (mm)	Support length (mm)	Angle (°)	Number of samples
COMP0-DIF	174	100	50	0	5
COMP45-DIF	174	100	50	45	5
COMP90-DIF	100	160	50	90	8

3. Results and discussion

3.1 Spreading effect in transverse compression

Further to the experimental transverse compressive tests combined with measures of digital images, the experimental results show that a spreading effect can be regarded as the phenomenon of shear of support edges associated with scale effect.

The spreading phenomenon may be calculated with Eq. 5 with three scale factor. The first factor is the height effect (k_h) representing the plasticized height. The second is the support condition effect (k_{sc}) depending if the support is continuous or discrete. The last is the thickness effect (k_t).

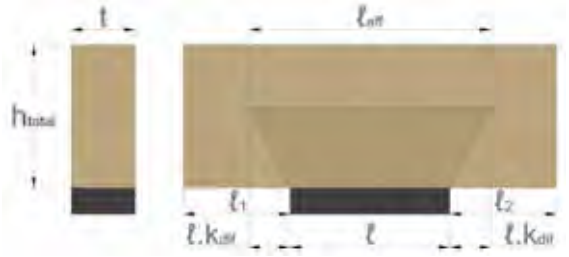

Fig. 3: Spreading effect

Applying this formula by different experimental tests on transverse compression of glulam, a difference of 9% is observed between the analytical formula and the experimental stresses of the transverse compressive at 1% plastic strain.

$$\frac{F_{c,90,mean}}{t \cdot \ell_{eff}} = f_{c,90,mean} \tag{5}$$

with

$$\ell_{ef} = \ell + \min\begin{Bmatrix} \ell + \ell \cdot k_{dif} \\ \ell_1 \end{Bmatrix} + \min\begin{Bmatrix} \ell \cdot k_{dif} \\ \ell_2 \end{Bmatrix}$$

$$k_{dif} = \left(\frac{h_{total}}{\ell} \cdot \frac{2}{3} \cdot \frac{f_{v,mean}}{f_{c,90,mean}} \cdot k_h \cdot k_t \cdot k_{sc} \right)$$

$$k_h = \begin{cases} \frac{1}{3} \text{ cases in bending} \\ \frac{1}{2} \text{ the others cases} \end{cases}$$

$$k_{sc} = \begin{cases} 1.51 \text{ discrets supports} \\ 1.85 \text{ continuous supports} \end{cases}$$

$$k_t = t^{-0.325}$$

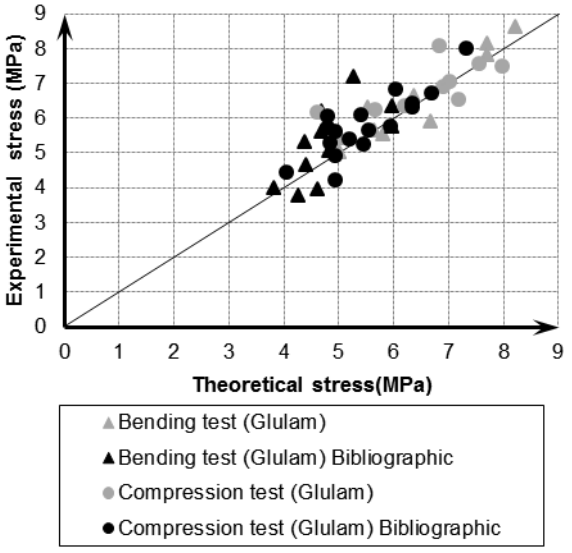

Fig. 4: A review of all mean model predictions vs. mean tests results

3.2 Uniform compression results

Firstly, the two current codes of calculations are quite similar to the glulam class GL24H (Fig. 5). However in view of the different failure modes (Tab. 4), some samples were brittle fracture (ELU). Concerning the results (ELS) corresponding to the ductile failure mode, they are calculated at 1% plastic strain.

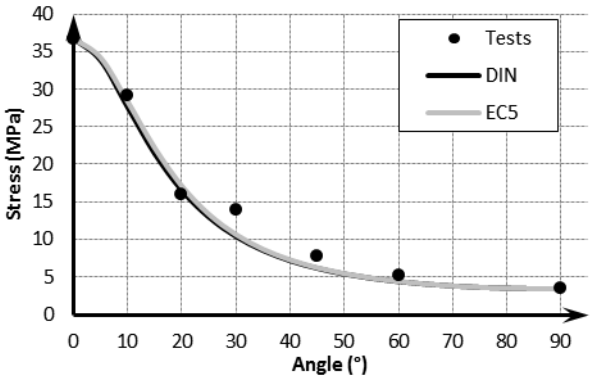

Fig. 5: Evolution of the stress according to the angle

This is possible with the DIN integrating the shear stress in the calculation of the support bearing capacity solicited in compression at an angle to the grain.

Tab. 4: Uniform compression tests results

Designation	Density (kg/m^3)	Stress (MPa)	Standard deviation (%)	Failure mode
COMP0	419	36.79	10	ELU
COMP10	469	29.15	10	ELU
COMP20	440	16.25	7	ELU
COMP30	451	13.49	9	ELU
COMP45	513	7.92	4	ELS/ELU
COMP60	460	5.26	11	ELS
COMP90	449	3.39	15	ELS

3.3 Spreading effect in compression at an angle to the grain

From Eq. 5 replacing the mean strength of uniform transverse compression $f_{c,90,mean}$ by the mean strength of uniform compression at an angle to the grain $f_{c,\alpha,mean}$ estimated by the DIN, the compression stresses at an angle to the grain will be deducted and thus be compared to the results of Tab. 5. However in view of the strain fields ε_{rr}, the plasticized height on the longitudinal compression test is not a third or a half, but the total height for the test in question. From these calculations, the model in Eq. 6 predicts $\pm$ 9% the bearing capacity of compression whether longitudinal, at an angle to the grain or transverse.

$$\frac{F_{c,\alpha,mean}}{t \cdot \ell_{eff}} = f_{c,\alpha,mean} \tag{6}$$

with

$$\ell_{ef} = \ell + \min\begin{Bmatrix} \ell + \ell \cdot k_{dif} \\ \ell_1 \end{Bmatrix} + \min\begin{Bmatrix} \ell \cdot k_{dif} \\ \ell_2 \end{Bmatrix}$$

$$k_{dif} = \left(\frac{h_{total}}{\ell} \cdot \frac{2}{3} \cdot \frac{f_{v,mean}}{f_{c,\alpha,mean}} \cdot k_h \cdot k_t \cdot k_{sc} \right)$$

3.4 Spreading effect in compression at an angle to the grain

Based on the comparison of the first two rows of Tab. 4 and Tab. 5, a difference is observed showing the identification of a spreading effect for the longitudinal compression test. In addition, according to the calculations in Tab. 5, the two codes overestimate the bearing capacity in transverse compression of 80%. On the bearing capacity in compression at an angle 45° to the grain, EC5 underestimated by 20% while the DIN overestimated by 40%. In conclusion, the analytical model needs to take into account the spreading effect in longitudinal compression. Today, the two standards do not allow it.

Tab. 5: Compression tests results

Designation	Stress (MPa)	Standard deviation (%)	Stress (DIN) (MPa)	Stress (EC5) (MPa)	Stress (4) (MPa)
COMP0-DIF	46.95	6	36.79	36.79	46.20
COMP45-DIF	11.00	7	15.36	8.98	10.87
COMP90-DIF	6.22	11	11.19	11.19	5.72

4. Conclusions

To conclude of this project, an analytical model was identify to determine the support bearing capacity solicited in longitudinal, compression at an angle to the grain and transverse compression integrating the spreading phenomenon. However, the case studies do not reflect the reality seen the longitudinal and compression at an angle to the grain tests. To do this, we should consider the real case of a column loaded in longitudinal compression with the spreading and a beam fish belly for the compression at an angle to the grain to refine the different scale factors.

In addition, the analytical model does not take into account the cracking of wood

that could affect the spreading phenomenon. Thereafter, a finite element model will be developed to refine the different scale factors and thus understand their importance on this phenomenon.

5. Acknowledgement

Our gratefulness goes to the attention of technician of ENSTIB of University of Lorraine (France) for their collaboration in the realization of tests. We also thank the CODIFAB to funding of tests. Finally, this project has received encouragement from the Laboratory of Excellence “ARBRE”.

Non-destructive examination of timber elements by radiometry

Jan Pošta[1], Jakub Dolejš[1], Lubomír Vítek[2]

Summary

This paper deals with the determination of density of wood samples by using radiometry. The possibility of using this method for inbuilt elements was investigated. Experiments were carried out on a lot of samples prepared from different wood species. The equation to calculate the density was found based on the captured radiation, width and height of the sample. The influence of the moisture content has not been demonstrated.

1. Introduction

The density is a good indicator of the mechanical properties of wood elements. It is also needed during assessment of inbuilt wood elements by using acoustic methods. However, density determination of inbuilt element is very difficult. Penetration methods are used, but they are very inaccurate and they have only local character [1]. Radiometry is a non-destructive method. Therefore, it appears as a suitable solution.

2. Radiometry

Radiometry of density is based on the passage and attenuation of gamma rays or on the dispersion of gamma rays in the measured material. To be able to determine the density based on the attenuation of gamma radiation, it is necessary to know the mass attenuation coefficient, which is dependent on the intensity of the radiation source and on the chemical composition on the sample. Wood contains around 99% carbon, hydrogen, oxygen and nitrogen. The difference in chemical composition among the kinds of wood is not too high and therefore the difference in the mass

[1] Czech Technical University in Prague, University Centre for Energy Efficient Buildings, Faculty of Civil Engineering, Czech Republic

[2] Brno University of Technology, Faculty of Civil Engineering, Czech Republic

attenuation coefficient among species is negligible [2, 3]. The question is what influence the moisture content of the sample has on the measurement results. If the source of radiation is chosen appropriately, the value of the mass attenuation coefficient of wood and water is very similar. Often, the difference is less than 10%. Therefore, if the moisture content of sample does not exceed common values for the inbuilt timber elements, the effect of moisture content is insignificant [4].

3. Experiments

The gamma rays scattering method was chosen for these experiments. The radiometric surface set, which is easily portable, was used for the measurements. The set is simply applied on the surface of sample, which is an advantage for the measurement in-situ. The emitter is on the one side of set and the detector is on the other side. The radiator is shielded by depleted ^{238}U (Fig. 1). The detector records the rays, which are scattered predominantly in the material by a Compton effect [5]. The most sensitive available emitter ^{137}Cs was used. Measurements were carried out at the Institute of Building Testing at the Technical University in Brno. The frequency of electrical pulses was observed. This frequency corresponds to the amount of detected rays for one minute and is related to the density of the material.

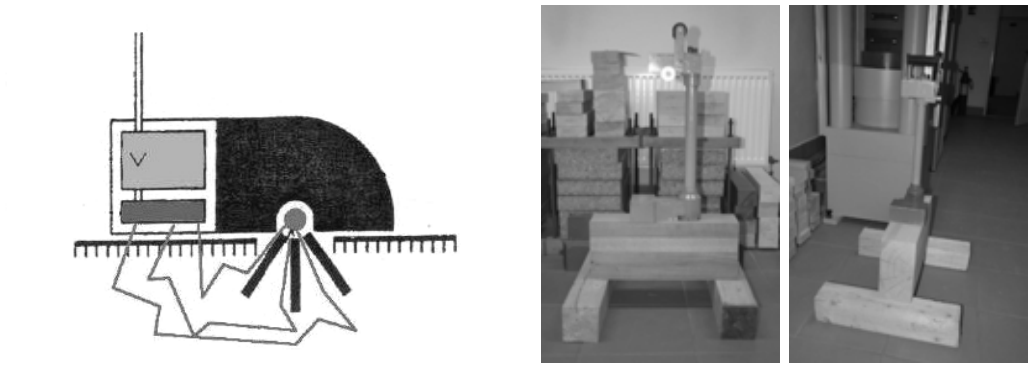

Fig. 1: Measuring of a density of timber elements by a radiometric surface set

The first set of experiments was carried out on samples from linden, larch, maple, oak, ash and locust wood. The cross sections of the samples were 120/45 mm, 120/90 mm, 120/135 mm and 120/180 mm. Based on these tests it is clear that the number of pulses captured by radiometric surface set depends on the density of the sample and on its width and height. New samples were prepared to derive the equation for calculating density by using radiometry in the next step. The spruce was chosen, as it is the most used wood in timber structures in the Czech Republic, along with species

with similar density (pine, larch). For comparison, an oak was also chosen. Samples dimensions of cross sections were 120/120, 120/140, 120/160, 120/180, 120/200, 120/220 and 120/240 mm. The frequency of captured pulses was measured for one minute by radiometric surface set. Each sample was measured five times from both top and side surface. The sample was supported at each end by two spruce beams, so that the samples were not in contact with the floor. For all thirteen different cross sections, dependence equations for pulse frequencies and density were derived (linear regression). The coefficient of determination R^2 reaches values from 0.951 to 1.000 (Tab. 1).

Tab. 1: Results of tests

	Measured from top surface						
Cross section [mm/mm]	120/120	120/140	120/160	120/180	120/200	120/220	120/240
Coefficient of correlation R	0,998	0,999	0,999	0,975	0,993	0,984	0,967
Coefficient of determination R^2	0,995	0,998	0,998	0,951	0,986	0,968	0,936
	Measured from side surface						
Cross section [mm/mm]	120/120	140/120	160/120	180/120	200/120	220/120	240/120
Coefficient of correlation R	0,998	1,000	0,995	0,992	0,993	0,993	0,981
Coefficient of determination R^2	0,995	1,000	0,991	0,983	0,986	0,987	0,963

The influence of the height and width of the samples on the frequency of pulses was investigated for each wood species separately. The correlation of the frequency of captured pulses on the height of the sample (linear regression) is very high for spruce ($R = 0.96$), pine ($R = 0.98$), and larch ($R = 0.99$). The correlation for oak was not found ($R = 0.36$). The correlation of the frequency of pulses on the width (polynomial regression) is also very high for all four wood species. The coefficient of determination R^2 is 0.97 for spruce, 0.98 for pine, 0.99 for larch and 0.99 for oak. Similar correlations were also found in the measurements mentioned above. The aim of all these experiments was to derive an equation for the calculation of density using radiometry. This equation was derived using linear regression with multiple variables. The explanatory variables represent the frequency of captured pulses, width of the sample, the square of the width and the sample height:

$$\rho_i = 7397{,}5 - 1{,}426\ n_i - 7{,}781\ b_i + 0{,}01458\ b_i^2 + 0{,}536\ h_i + e_i. \quad (1)$$

where: ρ_i = density [kg/m^3]
n_i = frequency of pulses [-]
b_i = width of sample [mm]
h_i = height of sample [mm]
e_i = random error [kg/m^3]

The coefficient of determination R^2 reaches a high value 0.974. It means that this equation is suitable for estimation of density. The maximal random error e_{max} for 95% interval of reliability equals ±73.9 kg/m^3.

4. Conclusion

The authors dealt with measuring of a density of timber elements by using radiometry. Achieved results of these experiments on the samples of identical size are very good. The coefficient of correlation R is around 0.98. A change of the sample cross section has significant influence on the results. On basis of measurements of samples with different dimensions, correlations between number of impulses and height or width were found. Subsequently, the equation for the density determination was derived based on the frequency of captured pulses, height of the sample and width of the sample. This equation was used to determine the density of a set of spruce samples. For all samples, the value of density obtained gravimetrically was in the 95% interval of reliability for derived equation of density.

5. Acknowledgement

This work has been supported by the European Union, OP RDI project No. CZ.1.05/2.1.00/03.0091 – University Centre for Energy Efficient Buildings, and project MEYS No. LD14062 – Methods for NDT evaluation of structural timber properties.

References

[1] M. Kloiber, *Nedestruktivní zjištování vlastností dreva*, PhD thesis, Mendel University in Brno, Faculty of Forestry and Wood Technology, 2007.

[2] T.L. Laufenberg, *Using gamma radiation to measure density gradients in reconstituted wood products*, in: Forest Products Journal, Vol. 36, No. 2, pp. 59-62, (1986)

[3] D. Mannes, E. Lehmann, P. Cherubini, P. Niemz, *Neutron imaging versus standard X-ray densitometry as method to measure tree-ring wood density*, in: Trees, Vol. 21, pp. 605-612, (2007)

[4] Z. Cai, *A new method of determining moisture gradient in wood*, in: Forest Products Journal, Vol. 58, No. 7/8, pp. 41-45, (2008)

[5] L. Hobst, *Zkušebnictví a technologie - Radiacní defektoskopie*, Textbooks University of Technology in Brno, 2009

Time-of-flight of transversal ultrasonic scan of wood: modeling versus measurement

Natalia Yaitskova[1]

Summary

Time-of-flight is a time for an ultrasonic pulse to cross a sample. It contains valuable information about the mechanical properties of a material. For the ultrasonic pulse propagating in wood perpendicular to the grain the relation between the time-of-flight and the elastic constants is rather complex due to the strong anisotropy of wood. With the help of some assumptions this relation can be established from the elastic theory. The analytical calculation results in a function, which represents a change of time-of-flight when the direction of propagation shifts from the radial to the tangential directions while scanning a board crosswise. The profile of time-of-flight has a V-like shape, and depends on the elastic coefficients, density and position of pith. The function takes into account the location of the pith and the geometry of the growth rings. The measurement performed on a sample of European spruce confirms the theoretical prediction.

1. Introduction

There are three main methods of ultrasonic non-destructive testing applied for wood assessment: (a) high-resolution imaging, or B-scans [1], (b) tomography [2] and (c) longitudinal pitch-catch system [3]. The high-resolution ultrasonic imaging and tomography are barely suitable for the industrial machine grading, which requires processing of 50-150 pieces per minute. Ultrasound longitudinal grading alone proved not to be very sufficient in increasing the yield in higher strength classes of wood. It is usually combined either with visual grading or with x-rays scanning [4].

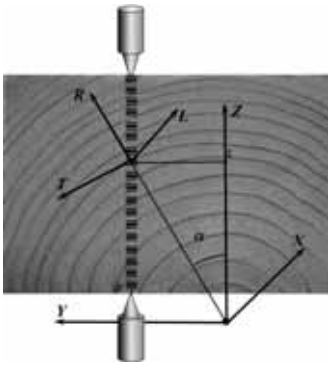

Fig. 1: Principle scheme of transversal ultrarasonic scan. Sender and receiver are placed at opposite sides of the board in a pitch-catch config.

[1] Research associate, HFM Technische Universität München, Germany

Transversal ultrasonic scan [5] is both, imaging of the defects and a direct measurement of modulus of elasticity. An ultrasonic pulse propagates in the transversal direction of wood in a so-called pitch-catch configuration (Fig. 1) and the board is scanned in x and y-directions. The raw data is a two-dimensional "ultrasonic image" of the board, where each pixel is a time-of-flight registered for each position (Fig. 2). Afterwards the image must be processed in order to obtain an indicating property – a value, relating the raw data to the wood strength class. Such image processing is a multistage task. To solve it correctly one shall be able to relate the features on the image to the properties of wood, which requires understanding of the physical principle of such imaging.

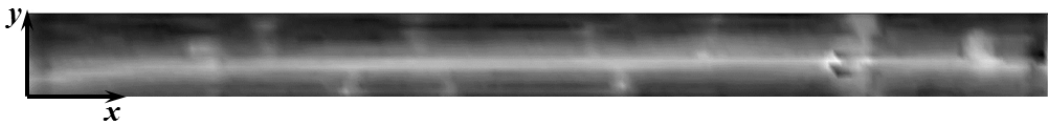

Fig. 2: "Ultrasonic image" of a spruce board. Dimensions of the scan are 1 m by 0.1 m, thickness (path length) is 0.06 m.

2. Theory

2.1 Stiffness tensor

To calculate the time-of-flight it is helpful to introduce two systems of coordinates (Fig. 1): the global one (XYZ), related to the shape of the board with the center of coordinates in pith, and the local one (LTR), related to the wood structure. The LTR system of coordinates is transformed into XYZ system of coordinates by a rotation matrix. For the ideal board its' long side is parallel to the grain and the rotation matrix includes only one angle α.

In LTR system a stiffness tensor $\hat{C}$, which describes all linear mechanical properties of the material, is symmetric and sparse. Its elements are related to the elastic constants: moduli of elasticity, shear moduli and Poisson ratios. In the following the elements of the stiffness tensor are notated as C_{ij}. The object of interest is propagation time along the direction making angle α with the radial direction, so one must rotate the stiffness tensor using Bond transformation.

The model of clean, ideal board assumes the following: the fibers are aligned strictly parallel to the long side of the cut, the annual rings have a perfect circular geometry, no knots are present, nor are cracks or any other type of defects. For a given stiffness tensor and density this ideal board possesses the maximal mechanical properties (for

example, a bending strength). Any deviation from the ideal shape: grain not parallel to the long side (fiber deviation), local change of the density (reaction wood), knots, cracks etc., will influence the mechanical properties.

2.2 Velocity of sound

A bulk wave, propagating out of principal directions (L, T or R) can be decomposed in three components: quasilongitudinal, quasitrasnverse and transvers. The transversal scan is done with the longitudinal transducers, so only one component, quasilongitudinal, is considered here. The theory of wave propagation in orthotropic medium [6] yields in following expression for the speed of sound (ν) when the propagation vector lays in RT-plane:

$$2\rho\nu^2 = \Gamma_{33} + \Gamma_{22} + \sqrt{\left(\Gamma_{33} - \Gamma_{22}\right)^2 + 4\Gamma_{23}^2}\,, \tag{1}$$

where ρ is density and Γ_{33}, Γ_{22} and Γ_{23} are algebraic expressions, containing the elements of the stiffness tensor $\hat{C}$ and the rotation angle α. As the stiffness matrix is considered to be known, free parameter here is angle α. Normalizing ν to the speed of sound in tangential direction, $\nu_T = \sqrt{C_{22}/\rho}$, one can present eq. (1) with respect to the angle α for the normalized speed:

$$\left(\frac{v}{v_T}\right)^2 = \kappa_0 + \kappa_1 \cos^2\left(\alpha\right) + \sqrt{\left(1-\kappa_0\right)^2 - \kappa_2 \cos^2\left(\alpha\right) + \kappa_3 \cos^4\left(\alpha\right)}\,, \tag{2}$$

where $\kappa_0 \ldots \kappa_3$ are coefficients, calculated from the stiffness matrix:

$$\begin{aligned}
\kappa_0 &= \frac{C_{22} + C_{44}}{2C_{22}}\,, \\
\kappa_1 &= \frac{C_{33} - C_{22}}{2C_{22}}, \\
\kappa_2 &= \kappa_1 + 1 - \frac{1}{2C_{22}^2}\left(C_{33}C_{44} + 3C_{22}C_{44} + 2C_{23}^2 + 4C_{23}C_{44}\right), \\
\kappa_3 &= \frac{1}{4C_{22}^2}\left(C_{22} + 2C_{23} + C_{33}\right)\left(C_{22} + C_{33} - 4C_{44} - 2C_{23}\right).
\end{aligned} \tag{3}$$

When $\alpha = 0$ direction of propagation coincides with the radial direction and $\left(v/v_T\right)^2 = C_{33}/C_{22}$. In the opposite case, when $\alpha = \pi/2$ direction of the propagation coincides with the tangential direction and $\left(v/v_T\right)^2 = 1$.

2.3 Time-of-flight

Angle α changes along the direction of propagation according to the law:

$$\cos(\alpha) = \left[1 + \left(y/z\right)^2\right]^{-1/2}.$$

Representing the speed as $\nu = dz/dt$ and integrating from z_1 and z_2 (positions of the transmitter and receiver with respect to the pith), for the time-of-flight we obtain:

$$t(y) = \nu_T^{-1}\left[z_2 g\left(\frac{y}{z_2}\right) - z_1 g\left(\frac{y}{z_1}\right)\right],$$

$$g(\gamma) = \gamma \int_0^{\gamma^{-1}} \left\{ \kappa_0 + \kappa_1\left(1+u^{-2}\right)^{-1} + \left[\left(1-\kappa_0\right)^2 - \kappa_2\left(1+u^{-2}\right)^{-1} + \kappa_3\left(1+u^{-2}\right)^{-2}\right]^{1/2} \right\}^{-1/2} du. \quad (4)$$

This integral can be calculated either numerically or with the help of any symbolic calculation software, for example *Mathematica* or *Maple*. It is more practical to use a much simpler expression. The function $g(\gamma)$ can be substituted by a polynomial ratio

$$g_{fit}(\gamma) = \frac{g_0 + a_1|\gamma| + a_2|\gamma|^3}{1 + b_1|\gamma| + a_2|\gamma|^3}, \quad (1)$$

where $g_0 = \sqrt{C_{22}/C_{33}}$ and a_1, a_2 and b_1 are the fitting coefficients. To calculate function $g(\gamma)$ one must choose some values for parameters $\kappa_0 \ldots \kappa_3$, which are related to the elastic constants. Of course, the values of these parameters vary between and within the species; they also depend on the growth region, the wood moisture content, density and ctr. The following calculations are done for the European Spruce with the density in a range of 390-500 kg/m^3, moisture content 8-10%. The values for elastic constants can be found in a number of publications, including the classical reference [7]. Table 1 contains the values required for the calculation of the time-of-flight for four types of spruce. The values of elastic constants are not presented here.

Tab. 1: Parameters for calculation of time-of-flight profile for four different types of spruce. Units: kg/m^3, GPa, km/sec. Kappa- and fitting coefficients are unitless.

Type	ρ	C_{22}	C_{33}	C_{44}	C_{23}	κ_0	κ_1	κ_2	κ_3	ν_T	g_0	a_1	a_2	b_1
A	390	0.53	0.87	0.046	0.28	0.54	0.32	0.74	1.14	1.16	0.780	1.38	2.28	1.10
B	430	0.59	1.1	0.064	0.35	0.55	0.43	0.7	1.27	1.17	0.733	1.43	2.20	1.20
C	440	0.45	0.80	0.072	0.21	0.58	0.39	0.61	1.09	1.01	0.749	1.44	2.27	1.21
D	500	0.82	1.01	0.074	0.36	0.54	0.11	0.65	0.76	1.28	0.903	1.48	2.68	1.16

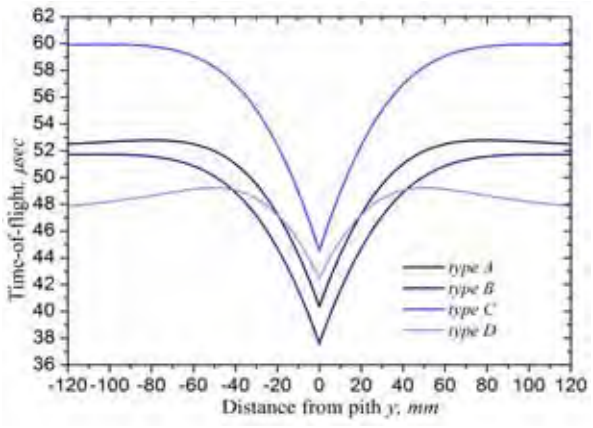

Fig. 3: Time-of-flight profiles for four different types of spruce.

Fig. 3 plots the corresponding curves for time-of-flight for the particular case when pith is located at the border of the board ($z_1 = 0$) and the thickness of the board (coinciding with z_2) equals 0.06m. On the plot the initial and fitted curves are undistinguishable. The profiles have a V-like shape with the minimal at $y = 0$, which corresponds to the radial direction of propagation. This profile is clearly distinguishable on the measured scan (Fig. 2) as a broad white line going from one end of the board to another. It follows the pith, i.e. the centre of the tree.

3. Measurements

The theoretical prediction of time-of-flight is verified by the measurement of a sample of European spruce. The average density of the sample is 405 kg/m^3, moisture content 9%, thickness of the board 0.062 m, width 0.103 m. The time-of-flight was measured using PUNDIT Mark V ultrasonic device with Exponential Probe receiving and transmitting transducers. The central frequency is 54 kHz. The diameter of the probes' tip is 6 mm.

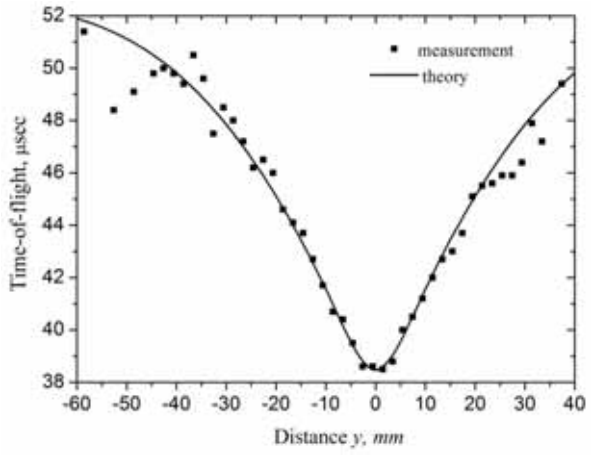

Fig. 4: Time-of-flight across a board as a function of a distance from pith: results of the measurement and the theoretical curve

Fig. 1 shows a photo of the cut of the board along the line of measurement. Pith is not included in the wood, but is located 8 mm below the cut. Fig. 4 shows the results of the scan: time-of-flight with 2 mm sampling. The 25 microsec calibration time was subtracted from each measurement. The theoretical curve (eq. 5) is fitted to the data. The fitted parameters are $g_0 = 0.75$, $a_1 = 1.47$, $a_2 = 2.20$, $b_1 = 1.15$, $\nu_T = 1.17$ km/c.

Because pith is outside of the board, the shape of the profile is somehow rounded. The sharpest profile corresponds to the case when the pith is located in the center of

the board. While the cut is changing so that the pith is shifted further from the board the curvature of the annular rings decreases, the direction of propagation approaches the radial direction and the time-of-flight curve eventually becomes a horizontal line.

On Fig. 4 there are two areas in which the measurements fall away from the theoretical curve: from -60 mm to -40 mm and from 20 mm to 30 mm. These areas correspond to the defects, which can be seen on the photo (Fig. 1) as deviation of the growth-ring structure from the circular geometry. The first zone is compressed wood and the second is knot. If one subtracts the fitted curve from the measurement, the result will contain the information about the size and location of the defects and it can be used afterwards for an automatic recognition and classification of the defects.

4. Acknowledgement

The presented study is accomplished in the FP 7, project WoodSonics, Grant 315351.

References

[1] A. Hasenstab, C. Rieck, B. Hillemeier, M. Krause, "Use of low frequency Ultrasound Echo Technique to Determine Cavities in Wooden Constructions," *Proc. International Symposium Non-Destructive Testing in Civil Engineering*, 2003, Berlin, Germany.

[2] L. Brancheriau, P. Lasaygues, E. Debieu, J.-P. Lefebvre, "Ultrasonic tomography of green wood using a non-parametric imaging algorithm with reflected waves," *Annals of Forest Science 65*, 2008, p. 712.

[3] G. Ravenshorst and J. W. van de Kuilen, "An innovative species independent strength grading model" In *WCTE: 9th world conference on timber engineering,* p. 1, 2006, Corvallis, OR, USA.

[4] J. Skog and J. Oja, "Improved log sorting combining X-ray and 3D scanning," *COST E 53 Conference - Quality Control for Wood and Wood Products*, p. 133, 2007, Warsaw, Poland

[5] M. Kabir, D. Schmoldt and M. Schafer, "Time domain ultrasonic signal characterization for defects in thin unsurfaced hardwood lumber," Wood and Fiber Science 34, pp. 165-182, 2002

[6] V. Bucur, "Acoustics of wood," Boca Raton: CRC Press, 1995.

[7] R. Hearmon, "The elasticity of wood and plywood," *Forest Production Research special report no. 7.*, 1948, H.M. Stationery Office, London.

Determination of shear properties of timber joists by torsion test method

Aamir Khokhar[1], Hexin Zhang[2]

Summary

This paper presents an experimental investigation into the evaluation of the shear modulus and shear strength of timber using torsion tests. Failure mechanism, variation in shear modulus and correlation of shear modulus and modulus of elasticity were studied. A considerable variation was noticed in shear modulus along the length of the joists but no relationship was found between shear modulus and modulus of elasticity. The test joists fractured mostly at the middle with cracks propagated towards either supports or edges. However, premature failure was also seen at the supports. The results show that torsion test method is an appropriate method and may be adopted for determination of shear properties of timber.

1. Introduction

The shear modulus and shear strength are important properties in structural timber design, specifically, for lateral-torsional stability of joists [1] and designing serviceability of wood-joist floors [2]. Testing standards [3, 4] have recommended the use of torsion to determine the shear modulus. Research investigations from Gupta et al. [5] and Harrison [6] found that torsion is better approach to obtain the shear properties than shear block and flexural test methods. However, not much research has been conducted to address a more proper use of torsion test. This research was conducted to explore and elucidate more of applicability of torsion to obtain the shear properties of timber.

[1] Lecturer, Edinburgh Napier University, UK

[2] Lecturer, Edinburgh Napier University, UK

2. Material and methods

Sitka spruce (*Picea sitchensis*) and Norway spruce (*Picea abies*) joists of nominal cross section of 45 × 100 mm were used, further detail is given in Table 1. A 1 kN-m torsion testing machine was used to test the timber joists under torsion. To measure the twisting displacement of the timber, multiple inclinometers with a range of ± 30° were attached to the upper edge of each sample.

The inclinometers were spaced at 600mm centre distance with at least 200 mm from the clamps to avoid possible end effects (Fig. 1). All test specimens were tested at 4°/min [3] until they fractured.

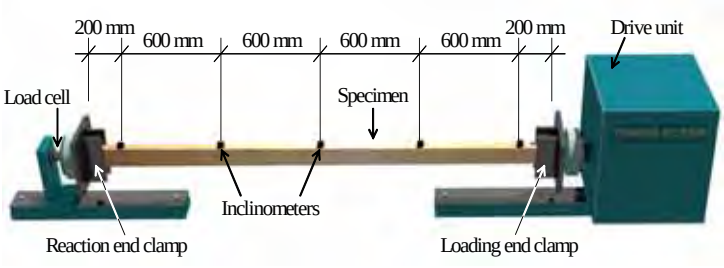

Fig. 1: Diagram for test setup of 2.8m specimen

The Saint-Venant torsion theory for rectangular sections was applied and the shear strengths were calculated on the basis of the maximum applied torque. The shear modulus was obtained by conducting linear regression analysis between 5% and 25% of the maximum applied torque and the relative twist per length.

3. Results and discussions

3.1 Determination of shear modulus and the shear strength

The results show (Table 1) that shear modulus from torsion for C16 (combined SP and NS) and C24 is slightly higher than published values for C16 (500MPa) and C24 (690 MPa) in EN338 [7].

Tab. 1: The mean shear strength and shear modulus values of tested joists

Group	Strength Grade	Length (m)	No. of Joists	Max. applied Torque (N-m)	Mean Shear Strength (MPa)	Shear modulus G (MPa)		
						Mean	Max	Min
SP	C16	1.0	15	485	7.8	490	750	300
	C16	2.0	10	460	6.7	500	560	430
	C16	2.8	12	550	7.7	530	630	410
	C16	3.6	25	475	6.7	560	715	430
	C16	Overall average		490	7.2	520	750	300
NS	C16	2.4	14	390	8.5	610	760	515
	C24	2.4	12	410	9.3	760	1100	600

Much higher shear strength values of 7.8 MPa (140% higher) of C16 (combined SP and NS) and 9.3 MPa (130% higher) of C24 were achieved when joists were tested under torque than 3.2 MPa and 4.0 MPa of EN338 [7].

3.2 Variation of shear modulus within and between samples

The variation of shear modulus was examined and was seen that shear modulus varied substantially (Fig. 2) across all the segments from each of the specimens tested. A variance component analysis was revealed that 66% of the variation in G was due to differences between specimens, while the remaining 33% was due to differences between the segments within a specimen.

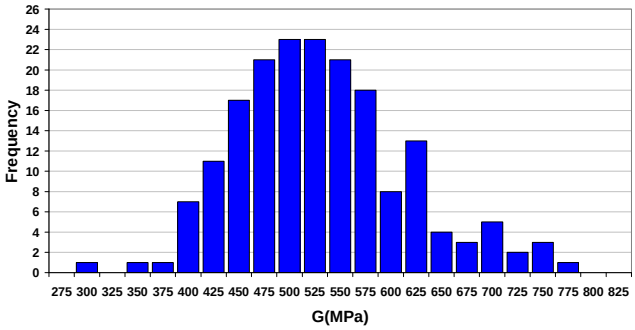

Fig. 2: Variation of shear modulus of the segments of tested samples

3.3 Failure mechanism under torsional loading

All test specimens were fractured when tested under torsion. Four different types of failure modes; crushing, shear, combined tension shear failure and horizontal shear failure were observed. The crushing failure occurred at the supports triggered mainly by clamps crushing the wood material.

The combined shear-tension and the shear failure modes mainly occurred in Sitka spruce joists. In the combined shear-tension failure mode, shear crack initiated from the middle of the long side and due to tension propagated towards, and was ended at the short side, as shown in Fig. 3. In the shear failure mode, cracks were usually started at short side, travelled as a diagonal crack along the long side to rupture specimen in shear at the other edge. The horizontal failure mode was only observed in Norway spruce specimens and that shear cracks were usually initiated from clear wood within long side and travelled parallel to the longitudinal direction towards end supports.

Fig. 3: A typical combined shear tension failure occurred in SP 2.8m joist.

3.4 Correlation of shear modulus and modulus of elasticity

A relationship of G and E was developed for 600 mm (Fig. 4), 1800 mm segments and for span. However, no correlation was found within segements and span. The mean G values in EN 338 [7] were determined from E:G ratio of 16:1. Therefore, it becomes more important to obtain G values using the torsion test method as recomenneded in EN408 [4].

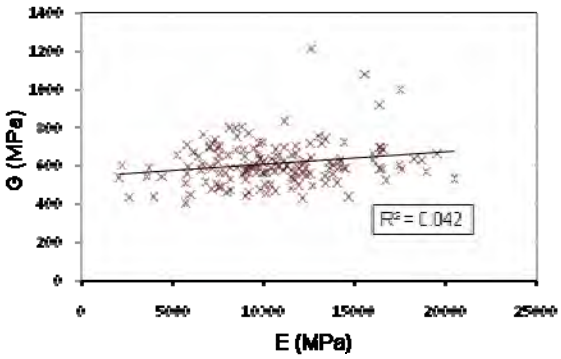

Fig. 4: Relationship between G and the E of 600 mm sections

4. Conclusions

This study has detailed the proper use of torsion test to obtain the shear modulus and shear strength of timber. It was found that samples fractured within the long side where shear stresses are presumed to be maximum and that torsion test permits measurement of variation of shear modulus within a single joist. Testing standards [3, 4] recommend torsion test to obtain shear modulus of timber. This study proposed that torsion test can be included to evaluate shear strength of timber.

References

[1] American forest and Paper Association, *National Design Specification (NDS) for Wood Construction* 2001, American forest and Paper Association, Washington D.C. USA.

[2] Foschi, R.O., Structural analysis of wood floor system, *ASCE Journal of Structural Engineering*, 1982, 108(7): 1557-1574.

[3] American Society for Testing and Materials ASTM D 198-94: Standard Methods of Static Test of Lumber in Structural Size, Volume 04.10 Wood, 1996, West Conshohocken, PA. USA.

[4] European Committee for Standardization CEN, EN 408:2009: Timber structures-structural timber and glued laminated timber- determination of some physical and mechanical properties perpendicular to the grain. 2009, CEN, Brussels, Belgium.

[5] Gupta, R., L.R. Heck, and T.H. Miller, Experimental evaluation of the torsion test for determining shear strength of structural lumber, *Journal of Testing and Evaluation*, 2002, 30(4): 283-290.

[6] Harrison, S.K., *Comparison of shear modulus test methods*, MSc. Thesis, 2006. Virginia Polytechnic and State University, VA, USA.

[7] European Committee for Standardization, CEN, EN338:2009: Timber Structures - Strength Classes, European Committee for Standardization, 2009, Brussels, Belgium.

Industrialization of physical system identification

John C. Hermanson[1], John G. Michopoulos[2], Athanasios Iliopoulos[3]

Summary

Our research seeks to industrialize material and structural system characterization or, generically, Physical System Identification (PSI) processes by creating and utilizing an automated, multi-axis, data-driven experimental and algorithmic system to identify material constitutive or system parameters. The rationale for our research is motivated by our desire to increase the efficacy and lower the cost of materials and structural systems development and certification methodologies as compared to current approaches, which rely on antiquated approaches that have not kept pace with the developments of the 21st century.

1. Introduction

Computational modeling in conjunction with mechatronic technologies, have evolved sufficiently to facilitate the data-driven constitutive characterization of materials. The need and ability to test and analyze complex materials and structural systems, especially wood and wood-based hybrid composite systems, are simultaneously being pushed by technology needs and being pulled by science requirements. The contemporary demands for cost and time reduction, multi-mission design requirements, and increased systemic complexity (such as new strengthening or stiffening methods or both for wood-based hybrid composite products) constitute the technology-push motivators. In particular, the inherent complexity of wood combined with the need for realistic predictive simulation, often requires computationally intensive mathematical models. On the other hand, the desire for engineering elegance using simple generalized theories and the need for efficient solutions that solve problems on a societal scale and the evolution of computational and data

[1] Research Scientists, Forest Products Laboratory, USA

[2] Research Scientist, Naval Research Laboratory, USA

[3] Research Assistant Professor, George Mason University, USA

acquisition technologies are the primary science pull motivators. The need to be able to predict the behavior of continuous systems under complex generalized loading conditions is primarily driven by the need to design and utilize such systems in various areas of human technological endeavors. The means of addressing this need through the ages has been generally encapsulated by an approach that seeks the development of continuous system modeling within the context of continuum mechanics. Successful models have been traditionally considered to be those that can faithfully and accurately reproduce the actual (usually experimentally established) behavior of existing systems.

Conceptually, little has changed since Leonardo da Vinci conducted the first recorded material test "testing wire at various lengths" 0 500 years ago, Fig. 1. Engineers have replaced da Vinci's sand and weigh scale with 21st century equivalents but we still cling to the single input – single output monotonic material characterization concept. Typically,

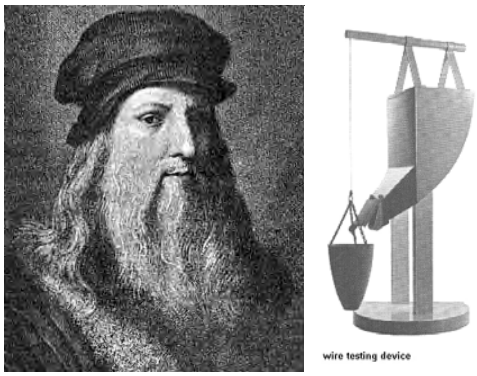

Fig. 1: Leonardo da Vinci and his first material test system

material characterization databases are built by combining information from assorted single axis tests those miss key interactive behaviors present under the multiaxial nature of realistic loadings. For example, ASTM D07 (wood) has jurisdiction over 116 standards for testing. In the synthetic composites area, the Composite Materials Handbook [2], specifies a "building blocks approach" which entails 12393 total tests that historically have required 10 to 17 years to navigate from inspiration to final product, Fig. 2.

In this vein, the Forest Products Laboratory and Naval Research Laboratory have been working in collaboration to develop an "industrialized," data-driven, constitutive characterization of materials subjected to complex loads by developing a six degree of freedom, automated, mechatronic, testing machines in conjunction with the use of energy-based inverse characterization methodologies [3].

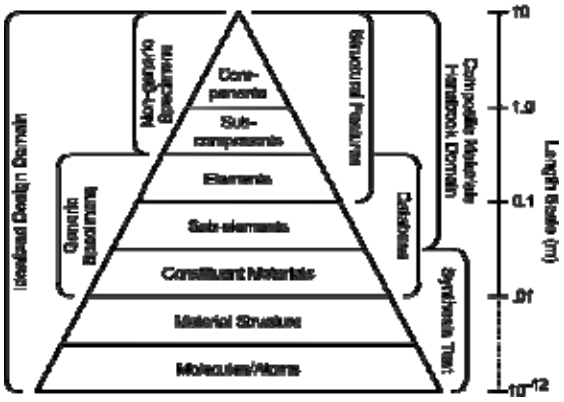

Fig. 2 Building blocks approach pyramid of tests

2. 6-DoF robotic systems for material characterization

Fig. 3: FPL66 6-6p parallel robotic mechanism

This endeavor has resulted in the design and construction of two operational mechatronically automated 6-6 hexapod material characterization systems. One system, "FPL66" Fig. 3, is designed for characterizing wood and wood-hybrid composite systems while the other "NRL66.3" is for synthetic carbon based composites. The hexapod configuration enables three translations and three rotations in any combination within the motion envelope to induce complex deformation states that realistically interrogate the physical system parameter space.

Incorporated into the 6-6p parallel robotic mechanism is a recursive hexapod set of force and displacement sensors to determine the work input into the physical system through the actuators and the resultant forces and moments through the physical system. Digital cameras record the output displacements on the surfaces. The combined measurements are used for identification of recoverable and irrecoverable strain energy density (SED) model parameters, via the solution of an appropriately formed inverse problem. The SED parameters identification is accomplished by estimating the instantaneous tangent constants for every set of measurements. The estimation is achieved by equating the variation of the external work, derived from the boundary displacement and force measurements, with that of the induced strain energy, calculated from the measured full-field 3D surface displacements [4]. An automated specimen feeder significantly reduces human involvement and increases the specimen throughput.

3. Specimen geometry and loading space

Both the specimen geometry and loading space are chosen to maximize the constitutive behavior space using the least material and loading paths possible. Unlike historic test procedures, data-driven material characterization seeks nonhomogeneous strain states. Geometric irregularities in the form of rounded notches are introduced into the specimen geometry to disturb the strain field and to ensure that some areas of the specimen (not necessarily near the notch roots but far from the grips) will experience non-linear constitutive response due to the

corresponding nonhomogeneous strain fields. A typical specimen is shown in Fig. 4. With the capability of 6 degrees of freedom (DoF) loading, the combination of different loading paths will also create unique and varied strain states within the specimen. For the sake of efficiency, the objective is to choose the least number of loading paths that encapsulate the material constitutive behavior.

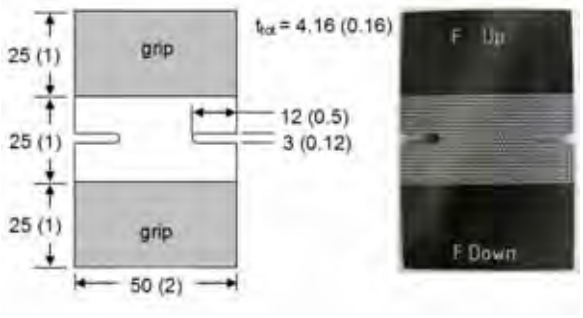

Fig. 4: A typical specimen schematic (left) and photographic view of a prepared specimen (right)

We define a path to be radially proportional from the origin of the 6 axes DoF space. The term proportional path, $\mathbf{p}_i^j$, here means that every path i when represented as a vector starting at the origin and ending at point j, can be resolved to its basis components in the 6-DoF frame $(\mathbf{u}_x, \mathbf{u}_y, \mathbf{u}_z, \mathbf{r}_x, \mathbf{r}_y, \mathbf{r}_z)$ according to $\mathbf{p}_i^j = p_{i1}^j \mathbf{u}_x + p_{i2}^j \mathbf{u}_y + p_{i3}^j \mathbf{u}_z + p_{i4}^j \mathbf{r}_x + p_{i5}^j \mathbf{r}_y + p_{i6}^j \mathbf{r}_z$ where $p_{i1}^j, p_{i2}^j, p_{i3}^j, p_{i4}^j, p_{i5}^j, p_{i6}^j$.

Based on the fact that the rotation components generate motion on the plane they are normal to, only four out of the six components can be linearly independent. Therefore, the 6-D space of motion can be reduced to one of the fifteen 4-D subspaces that can be used for defining the loading paths. The best subspace of the fifteen is chosen by numerical experiments conducted via FEA computations utilizing a priori established linear constitutive properties and a specimen geometry as described above. The best candidate is determined by the ratio of the volume of each Strain State Cloud (SSC) [5] relative to the union of the volumes of all SSCs created by all possible loading paths within all fifteen subspaces. Fig. 5 gives an example of the SSC

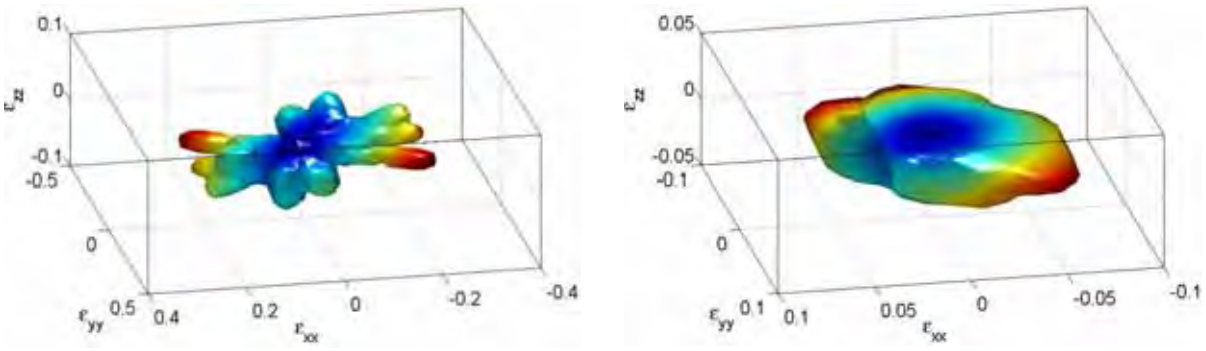

Loading case (u_y, r_x, r_y, r_z) Loading case (u_x, u_y, u_z, r_x)

Fig. 5 Comparison of the Strain State Cloud for normal strain

for two loading cases (u_y, r_x, r_y, r_z) and (u_x, u_y, u_z, r_x). Comparing the SCCs from Fig 5, loading case (u_y, r_x, r_y, r_z) has greater strain state volume than load case (u_x, u_y, u_z, r_x) thus loading case (u_y, r_x, r_y, r_z) is a better candidate. Our experience shows that the subspaces involving all three rotations and one of the two in-plane translations generate the richest strain state sets, (u_x, r_x, r_y, r_z) and (u_y, r_x, r_y, r_z).

4. Material constitutive parameters

In order to determine the material parameters the inverse problem at hand is solved through a design optimization approach that is described by the logic depicted in Fig. 6. The implementation of this logic involves a computational infrastructure that is controlled by a Matlab [6] program, where the foreword solution of the instantaneous finite element analysis (FEA) is accomplished using the ANSYS FEA application environment [7]. Details if the FEA model used for the specimens constructed and tested are not presented here due to the space limitations but they can be found in [9].

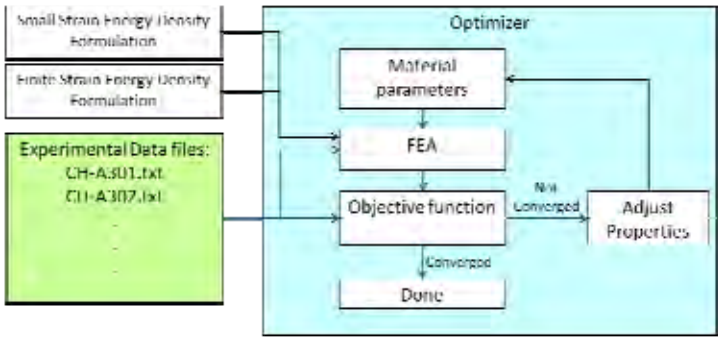

Fig. 6 A Flow diagram depicting the Physical System Identification process.

Two objective functions were constructed. Both utilized the fact that through the REMDIS-3D software [10], developed by our group, one can obtain full field measurements of the displacement and strain fields over any deformable body. Thus, our experimental measurements for the formation of the objective functions were chosen to be the strains at the nodal points of the FEM discretization. The first objective function chosen was based entirely on strains and is given by,

$$J^{\varepsilon} = \sum_{k=1}^{N} \left(\sum_{i=1}^{2} \sum_{j=i}^{2} \left(\left[\varepsilon_{ij}^{\exp} \right]_k - \left[\varepsilon_{ij}^{fem} \right]_k \right) \right)^2$$

the second objective function is given in terms of surface strain energy density according to,

$$J^U \approx \oint_{\partial\Omega}\left(U^{\exp} - U^{fem}\right)^2 dS$$
$$\approx \oint_{\partial\Omega}\left(\sum_{i=1}^{2}\sum_{j=i}^{2}\sum_{m=1}^{2}\sum_{n=m}^{2}\left(s_{ijmn}\varepsilon_{ij}^{\exp}\varepsilon_{mn}^{\exp} - s_{ijmn}\varepsilon_{ij}^{fem}\varepsilon_{mn}^{fem}\right)\right)^2 dS$$

where $\left[\varepsilon_{ij}^{\exp}\right]_k$ and $\left[\varepsilon_{ij}^{fem}\right]_k$ are the experimentally determined and the FEM produced components of strain at node k. The quantities $U^{\exp}$ and U^{fem} are the surface strain energy densities formulated by using the experimental strains and the FEM produced strains respectively. Both objective functions were implemented, and we utilized both the DIRECT global optimizer [9], which is available within Matlab [6] and a custom developed Monte-Carlo optimizer, also implemented in Matlab.

5. Validation

The validation simulations were performed for the typical double-notched characterization specimen described above, but for loading paths that were not used for determining the constitutive model itself. We are presenting a representative validation prediction. It is important to emphasize that the experimental data obtained from the associated tests were not used in determining the constitutive constants (material parameters) that are fixing the associated constitutive model.

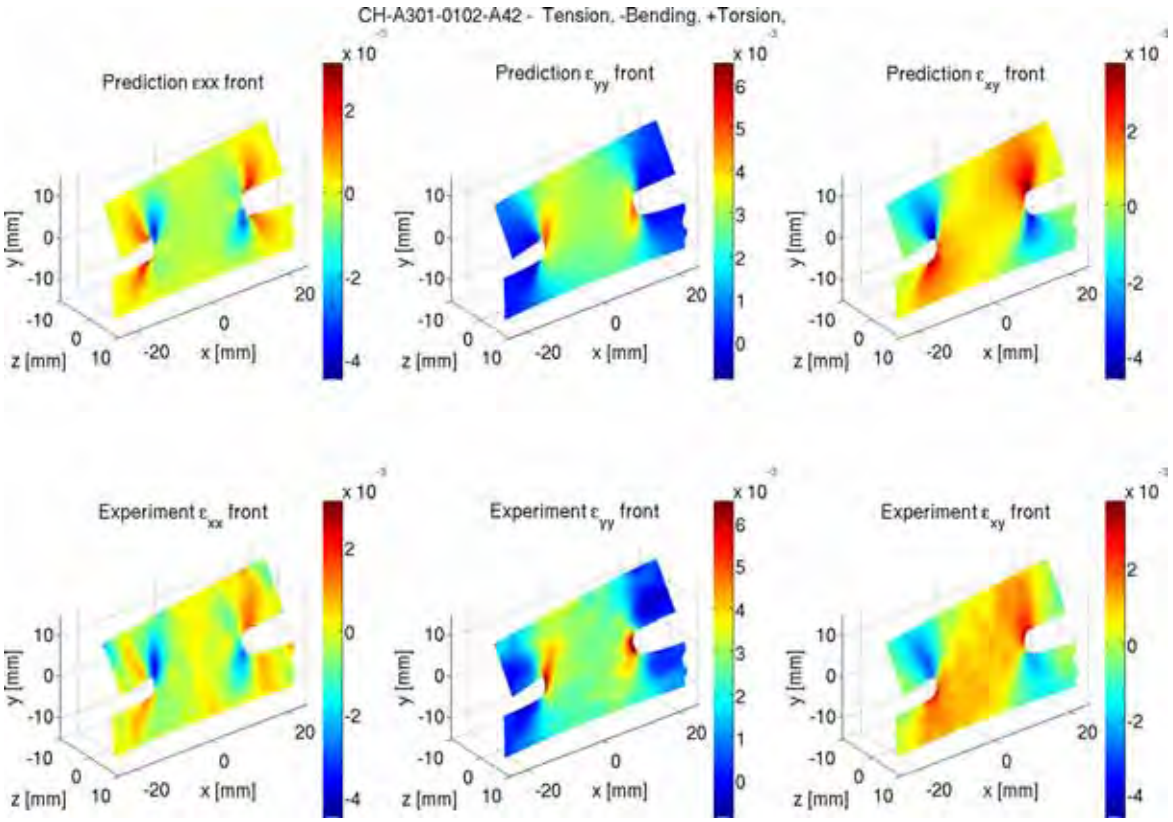

Fig. 7: Predicted (top row) vs. experimental (bottom row) strain component fields distributions for a characterization coupon under combined tension, bending and torsion loading

Fig. 7 shows three strain field distributions at the same loading step of a loading path that involves tension, out of plane bending and torsion about the longitudinal axis. All predicted strain field distributions for both of these cases, show that the predicted values are within at most 4% error of the experimental ones. This is well within the error of the RemDiS-3D experimental method [10].

6. Future work

We are currently working in extending these energy formulations to approaches that achieve two main goals. First, that those approaches do not require FEA in the loop and second, that they incorporate the stochastic nature of the material response and the acquired data in a manner that quantifies uncertainty. This quantification should utilize prior knowledge via Bayesian based stochastic formalisms, which enable incremental and recursive algorithms based on Kalman filtering and in general, information theory. We envision that the paths described above will no longer be radially proportional but continually modified based upon the knowledge acquired during testing.

7. Acknowledgement

The authors acknowledge the support by the Office of Naval Research, the National Science Foundation under Grant 0540419 and by NRL's 6.1 core-program.

References

[1] S. Timoshenko, History of Strength of Materials. McGraw-Hill, 1953, 445.

[2] Military Handbook - MIL-HDBK-17-3F: Composite Materials Handbook, Volume 3 - Polymer Matrix Composites Materials Usage, Design, and Analysis. U.S. Department of Defense, 2002.

[3] Michopoulos, J.G., J.C. Hermanson, and T. Furukawa, Towards the robotic characterization of the constitutive response of composite materials, *Composite Structures*, 2008, 86(1-3): 154-164.

[4] A.P. Iliopoulos, J.G. Michopoulos, and N.P. Andrianopoulos, Performance analysis of the mesh-free random grid method for full-field synthetic strain measurements, *Strain*, 2012, vol. 48(1): 1-15.

[5] A. P. Iliopoulos and J. G. Michopoulos, Loading subspace selection for multidimensional characterization tests via computational experiments, ASME Conference Proceedings, 2010, (44113): 101–110.

[6] The Mathworks, Matlab, http://www.mathworks.com.

[7] ANSYS, ANSYS Mechanical, http://www.ansys.com/

[8] Michopoulos, J., J.C. Hermanson, A. Iliopoulos, S. Lambrakos, and T. Furukawa, Data-driven design optimization for composite material characterization, *Journal of Computing and Information Science in Engineering*, 2011, 11(2).

[9] Michopoulos, J., J.C. Hermanson, A. Iliopoulos, S. Lambrakos, and T. Furukawa, Overview of constitutive response characterization for composite materials via data-driven design optimization, In Proceedings of the ASME 2011 International Design Engineering Technical Conferences & Computers and Information in Engineering Conference IDETC/CIE, 2011, Washington, DC, USA.

[10] Michopoulos, J. and A. Iliopoulos. A computational workbench for remote full field 3d displacement and strain measurements. In Proceedings of the ASME 2011 International Design Engineering Technical Conferences & Computers and Information in Engineering Conference IDETC/CIE, 2011, Washington, DC, USA.

[11] Jones, D.R., C.D. Perttunen, and B.E. Stuckman, Lipschitzian optimization without the Lipschitz constant, 1993, *J. Optim. Theory Appl.*, 79(1): 157–181.

In situ testing on of timber diaphragms in unreinforced masonry building

Ivan Giongo, Roberto Tomasi[1], Dimitro Dizhur, Jason Ingham[2]

Summary

Timber floors often need strengthening and stiffening as they were designed to bear moderate loads and may suffer from excessive deflections with respect to current requirements. In case of lateral seismic forces, whereas the floor is not satisfactorily connected to the adjacent walls, or the in-plane stiffness is inadequate, different collapse modes involving overturning of the walls may be observed. Masonry walls can counteract, generally, an insufficient resistance to lateral loads acting out of plane.

In order to adequately model the global behavior of a masonry skeleton, it is fundamental to characterize the in-plane stiffness of horizontal diaphragms, which plays an undeniable key-role in distributing seismic lateral loads to the resisting walls. In fact, it is expected that the more the in-plane stiffness grow, the more the collaboration between systems of piers increases. The need to increase the in-plane stiffness has induced, in the past, some strengthening solutions that recent earthquakes have demonstrated to be inadequate or, in some cases, even unfavorable. In fact, the substitution of timber floors with concrete ones, the insertion of a concrete curb "inside" the thickness of the masonry walls, could imply, respectively, a significant self-weight increase and a weakening of the existing masonry walls.

Therefore, learning from the effect of past earthquake on reinforced existing buildings, some floor refurbishment techniques have been reconsidered: the new Italian standard code on existing buildings for instance suggests new alternative strengthening techniques for the horizontal diaphragms. Some timber diaphragms, reinforced with different solutions, were investigated in an experimental campaign both in laboratory (Tomasi et. al. 2009) and *in situ* (Giongo et. al. 2013).

[1] Department of Civil, Environmental and Mechanical Engineering-University of Trento, Italy

[2] Department of Civil and Environmental Engineering-University of Auckland, New Zealand

The in situ tests were carried out on a two-story clay brick unreinforced masonry building located in Whanganui (New Zealand). In the work presented here, the outcomes of a field-testing campaign conducted on full-scale 100-year-old timber diaphragms are presented. The diaphragms consisted of 50 x 300 mm New Zealand native Rimu joists with an average spacing of 450 mm, while the flooring was made of 130 x 22 mm tongue and groove New Zealand Native Matai boards. Two specimens, measuring 5.6 and 4.7 m were subjected to both cyclic and snap back tests in the direction orthogonal to the joists.

The test setup was constructed using pulleys, wire ropes and steel tubular elements, and was designed to reproduce the parabolic load distribution suggested by FEMA 356. Such a setup is characterized as being "lightweight", "thin" and easy to relocate from one specimen to the next, without the need to move the reaction points (Fig. 1).

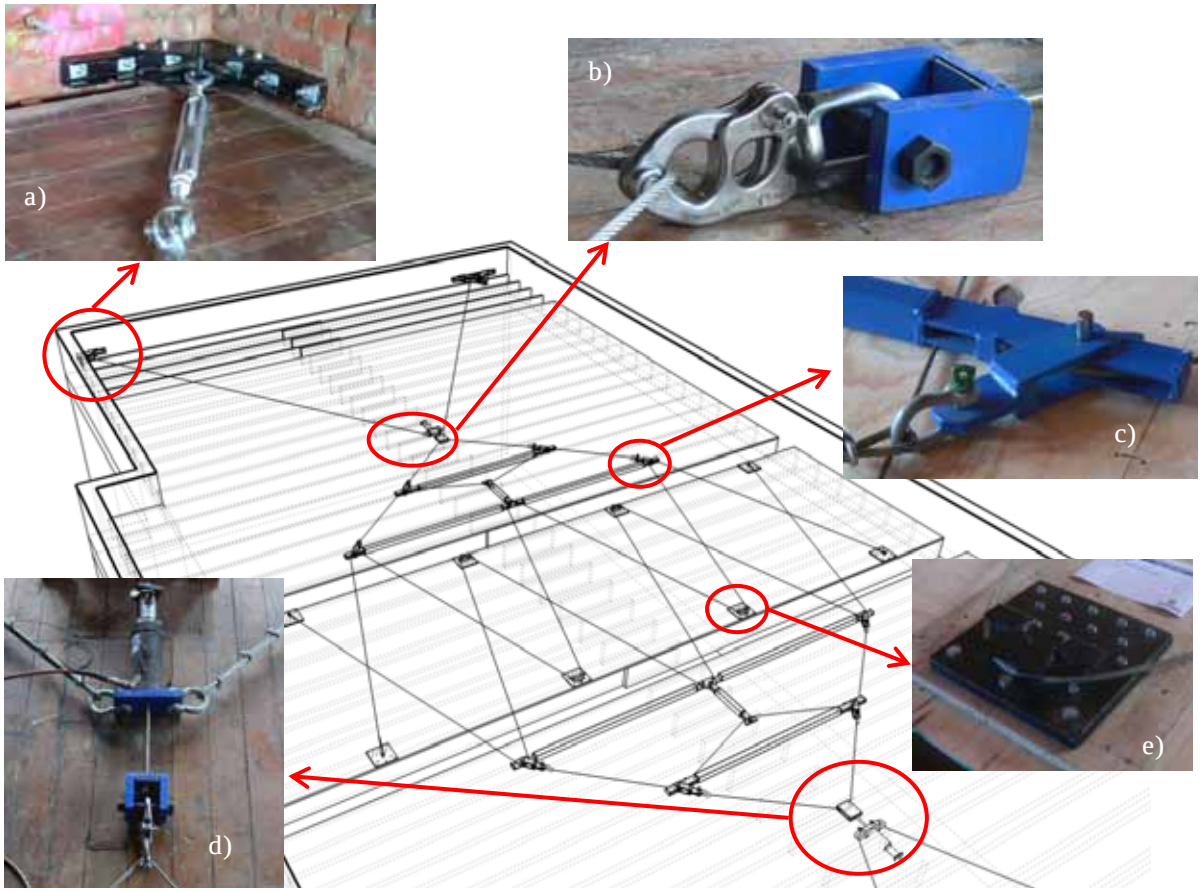

Fig. 1: Test set-up for Whanganui diaphragm test.
a) wall connection bracket;
b) snap shackle for instantaneous load-release;
c) frame pulley;
d) hydraulic actuator;
e) central loading plate

Subsequently to the testing of the diaphragms in the as-built condition, the effect of different refurbishment techniques was investigated. From the results, it seems that even "simple" and cost effective solutions such as re-nailing of the flooring and the addition of thin plywood overlays (Fig. 2a) are sufficient to achieve a significant increase in the equivalent shear stiffness. A 13 mm plasterboard ceiling lining was applied to the specimen with the re-nailed floor in order to investigate the effect on the diaphragm in-plane response produced by a 45 min fire rated system (Fig. 2b).

Fig. 2: a) Diaphragm retrofitted with a plywood panel overlay; b) fire rated ceiling lining

The dynamic properties of timber diaphragms were also studied (Fig. 3). The period of each diaphragm was determined at different target midspan displacements in order to address the nonlinearity of in-plane timber floor diaphragm response. An initial period was assessed through snap back tests conducted at a small displacement, close to what was assumed to be the nominal yield displacement, while an ultimate period was detected by imposing a snapback displacement consistent with the critical displacement causing the out-of-plane collapse of the walls. It was observed that the formula proposed by ASCE/SEI 41-06 (ASCE 2007) to estimate the diaphragm period tends to overestimate the diaphragm periods. Such overestimation can be significantly reduced by adopting an alternative formulation based on the static scheme of a shear beam under uniformly distributed load.

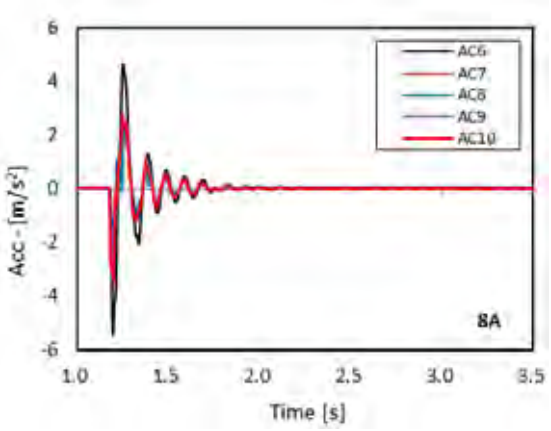

Fig. 3: Example of the accelerometer signals obtained from a snap back test

A parallel field experimental campaign was undertaken with the aim to study the effectiveness of adhesive connection anchors to transfer seismic shear action from the timber diaphragm to the resisting URM walls (Fig. 4). A total of 22 cyclic shear

tests (Fig. 4) with varying parameters were conducted. The studied parameters included: the anchor rod diameter, the embedment depth, the timber blocking thickness, the boundary conditions, the washer size and the axial pre-load of the anchor.

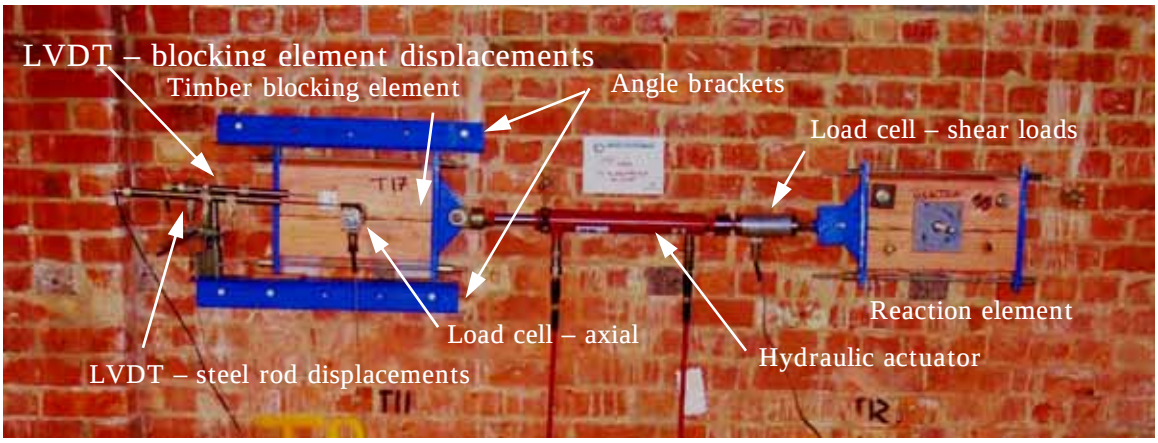

Fig. 4: Typical test setup details for in-situ testing of wall-to-diaphragm shear transferring connections in an existing clay brick URM building

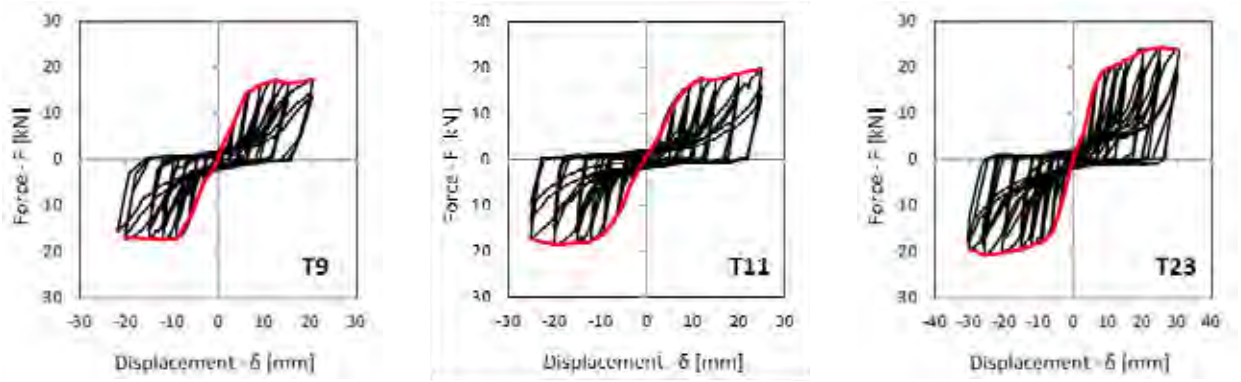

Fig. 5: Selected results of shear anchor cyclic tests (T9, T11 = 16 mm anchor diameter; T20 = 20 mm anchor diameter)

References

[1] Tomasi R., Piazza M, Baldessari C. The refurbishment of existing timber floors: characterization of the in-plane behaviour. Proceeding of the International Conference on Protection of Historical Buildings, Prohitech 09, Roma, 21-24 June 2009, CRC Press, Taylor&Francis, Vol 1.: 255-260

[2] Giongo I., Dizhur D., Tomasi R., Ingham J. In-plane assessment of existing timber diaphragms in urm buildings via quasi-static and dynamic in-situ tests. Proceeding of Shatis Conference, Trento, September 2013.

[3] ASCE. (2007). "Seismic rehabilitation of existing buildings." ASCE-SEI 41-06, Reston, VA

Characteristics of structural floor decking performance in the context of reinforced timber beam floors

Anna Rozanska[1], Ewa Sudol[2], Anna Policinska-Serwa[2]

Summary

Reinforcement of timber beam floors can take place in all or only in chosen structural layers: beams, decking and parquet. The preservation of original structural layers of the floor, together with the protection of its antique substance, is a priority in conservation activities. However, objective assessment tools are indispensable in order to evaluate the prospects of further usage of antique floors. Research shows that their state of preservation depends greatly on the presence of decking (blind floor).

The research aims at improving antique floor reinforcement methods by reinforcing the decking in a way that would ensure that the load bearing capacity is preserved and that the elastic properties are maintained as well.

The article specifies research methods that are adequate in order to evaluate the performance of a blind floor (decking) affected by static and dynamic loads, it also presents usage specifications and requirements. Different variants of structural solutions for blind floors made of boards or panels (applied in conservation practice) have been analyzed as to their susceptibility to deformations, on the basis of calculations and experimental tests of prototypes in accordance with the standards PN-EN 1195, PN-EN 12871 and PN-EN 1995-1-1.

[1] Department of Technology, Organization and Management in Wood Industry, Faculty of Wood Technology, Warsaw University of Life Sciences, Nowoursynowska 159, 02-776 Warsaw, Poland

[2] Structure and Building Elements Department, Building Research Institute, Filtrowa 1, 00-611 Warsaw, Poland

1. Research background

The floor is an important structural element that forms part of antique interiors and is protected by law, the only limit of such protection being the preservation of usage properties by the floor. The usage properties of timber floors depend on microclimate conditions, which are influenced largely by the floor structure and the species of wood that it is made of.

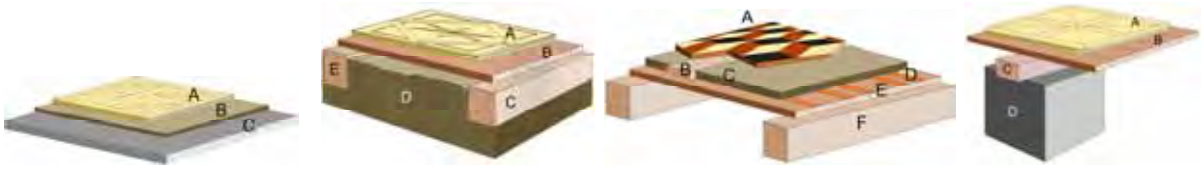

a) b) c) d)

Fig. 1: Diagram of floor structure in the Łańcut Castle:
a) panel floor in the Chapel (A panel, B sand, C concrete)
b) Ball Room (A panel, B boarding/decking, C ceiling beams, D sand)
c) plank floor in the Chinese Room (A parquet, B additional beams, C layer of sand, D boarding/decking, E strips of cloth glued to the connections, F ceiling beams)
d) Przewrotne Manor House (A panel, B boarding/decking, C ceiling beams, D bricked post)

The floor consists of one or more layers forming a plane: a subfloor and a floor covering (parquet). Wooden floors, apart from the load bearing structure and floor covering (parquet), may also optionally contain a decking (blind floor) (PN-EN 13756). The wooden floor structure in palaces and manor houses in Poland consists of various layers. It is based on joists lying in the sand or on beams suspended between bricked posts (Fig.1). In case of load bearing structures with ceiling beams, there was always a blind floor (decking) underneath the parquet. In case of load bearing structures based on joists, the parquets might have been placed on decking or supported only by joists lying in a layer of sand. The panels were fixed to the base with hand forged nails.

The parquet panels were fixed together with spline joints. Individual elements within the panels were fixed with tongue in groove joints, while the battens that form a cross within the panel filling have lap joints (Fig.2). In Versailles type parquets, the thickness of the frame was greater than the thickness of filling elements, and the bottom side of the elements was only roughly finished. In case of panels lying on decking, the surface was evened and adjusted by a layer of sand or, less frequently, wood shavings or wedges placed under central panel elements. In case of panels lying directly on joists, only the frame elements had a support, while the middle elements were suspended above an empty space.

a) b) c)

Fig. 2: Panel structure: Room 5 (a) and Room 4 (b) of the Tarnowiec Manor House and the Crow Room of the Manor House in Niwiska

A common practice to protect antique wooden parquets consists in using shoe covers or designating traffic paths and covering them with carpets. In both cases, the sand that gets between the parquet and the fabric causes parquet abrasion, and bigger particles produce scratches and indentations. Moreover, the use of carpets results in color differences between the covered and not covered parts of the parquet. Therefore, efficient ways of isolating parquets from pedestrian traffic are being searched for. One method, used in Potsdam castles among others, is a transparent platform mounted on a steel structure above stone floors. However, having little distance between the flooring and the glass pane results in water condensation, which causes excessive humidity and affects the parquet's color. Another problem consists in the weight of the metal structure, which does not permit this kind of solution to be used with beam ceilings. Optionally, the entire room can be covered with glass panes resting on punctual points of support, in order to reduce the structure's weight and to distribute it evenly on a larger surface. Unfortunately, all the proposed measures interfere significantly with the historical substance of the floor and especially its aesthetic perception, limiting some of its usage-related values as well.

What is more, antique wooden floors often require reinforcement. Reinforcement of timber beam floors can take place in all or only in chosen structural layers: beams, subfloor and parquet. The preservation of original structural layers of the floor, together with the protection of its antique substance, is a priority in conservation activities. However, objective assessment tools are indispensable in order to evaluate the prospects of further usage of antique floors. Research shows that their state of preservation depends greatly on the presence of a blind floor [1]. Additionally, in case of antique floors, there is a potential possibility of an invisible reinforcement of the decking, while preserving all the original structural layers. Therefore, the development of research in the area of subfloor reinforcement methods is extremely important for conservation.

2. Aim and scope of research

Traditional requirements for beam floors were related to their stiffness and their usage-related properties, as well as their aesthetic characteristics, and the contemporary reinforcement methods should keep the same groups of properties. If research focuses only on increasing the floor's stiffness and preserving its aesthetic value, then we lose the specific usage-related properties. This is why in our research we not only explore the reinforcement methods, but also strive to preserve the elastic properties, which are indispensable for instance in ball rooms.

The research of decking reinforcement conducted up to date omits the aspect of usage properties, which are important in view of the preservation of floor's original functions. Decking has been analyzed only as to its stiffness and deformations under static loads (PN-EN 1195 and PN-EN 12871 in accordance to PN-EN 1533), omitting the reaction to dynamic loads that antique floors might be exposed to during their usage (for instance produced by walking or dancing), so their elasticity characteristics become very important in rooms that might be affected by frequent dynamic loads. Judging by the approaches that have been applied up to date to the issues of wooden beam floor decking reinforcement, one might think that stiffness is a desired characteristic and is a selection criterion for the reinforcement method.

The research aims at improving antique floor reinforcement methods by reinforcing the decking in a way that would ensure that the load bearing capacity is preserved and that the elastic properties are maintained as well.

The article specifies research methods that are adequate in order to evaluate the performance of a blind floor (decking) affected by static and dynamic loads, it also presents usage specifications and requirements. Different variants of structural solutions for reinforced blind floors made of boards or panels (applied in conservation practice) have been analyzed as to their reaction to static and dynamic loads, on the basis of calculations and experimental tests of prototypes in accordance with the harmonized standards PN-EN 14342+A1 and PN-EN 1533, PN-EN 1195, PN-EN 12871 and PN-EN 1995-1-1.

3. Proposed research methods

In order to determine the structural role of decking, we tested different variants of structural solutions for beam floors, comparing elasticity (transfer of dynamic loads through shock absorption in accordance to the PN-EN 14808 standard) of parquets placed on decking or directly on joists, both in case of floors with continuous support (joists laying on a mineral base and joists placed on a layer of sand), as well as floors with punctual support. Afterwards, the decking was reinforced using several typical solutions proposed by other research teams [2]. Shock absorption analysis in accordance with PN-EN 14808 and analysis of deformations under dynamic loads in accordance with PN-EN 14809 were conducted for:

– original solutions,

– traditional decking reinforcements (made of boards in various layouts),

- reinforcements made of panels (OSB 3 or 4, particle boards P2 and MDF, plywood and LVL, in accordance with PN-EN 13986:2006).

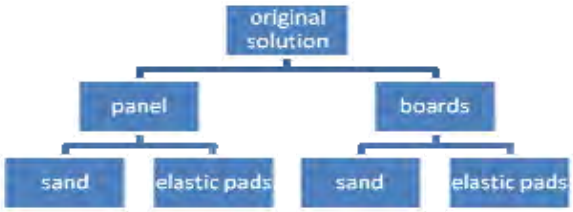

Fig.3: Variants of decking reinforcement solutions under research

The results of shock absorption tests performed on antique floor structures were compared with the results of the same structures after adding board or panel reinforcement. In order to provide the reinforced floors with elasticity characteristics similar to those of the original solution, the tested structures received a shock-absorbing layer. In the original constructions, the shock-absorbing layer was provided by sand, while during research we added various contemporary variants of shock-absorbing mats (made of rebound polyurethane foam or SBR regranulate) (Fig. 3).

In accordance with the standard PN-EN 14904, shock absorption and vertical deformation measurements are one of the basic characteristics of the floors used nowadays in buildings of sports and events facilities that are exposed to dynamic loads. The test consists in applying a dynamic load to the floor model, and simultaneously recording the value of the force absorbed by the floor, of the force rebound and the deformation. Research concerning reinforced antique floors has to include their reaction to dynamic loads, considering that the structure of antique floors is similar to the standard structural solutions of contemporary sports floors. They are often installed on a wooden framework with elastic pads and their surface is

made of wood or engineered wood materials [3]. In antique floors, the function of elastic pads (which consists in leveling, stabilizing and providing elasticity) was fulfilled by a layer of sand. Both the antique floors and the sports floor solution mentioned above can be classified as area elastic systems in accordance with the PN-EN 14904 standard. In this kind of floor systems, after applying a concentrated force, an area of vertical deformation, with a radius of about 500 mm, is created around the contact point. They are characterized by a hard surface and inert reactions.

Due to the destructive character of the tests, we used copies of antique structural solutions. They consisted of pine beams, 160 mm high, 100 mm wide, and 2400 mm long, with distance between axes of 580 mm. This non-standard distance between the beams (smaller than the one suggested by PN-EN1995-1-1) was chosen because of the necessity to compare floors with different structures, including the variant in which the parquet was placed directly on beams, with no decking. The decking was made of 25 mm thick boards.

We prepared 1:1 scale copies of nine antique oak panels from the Tarnowiec Manor House, from the beginning of the 19th century, with dimensions 580 x 580 mm. They were Versailles type panels with a pattern known from the Soubise castle, consisting of four elements of a thicker frame, 35 mm thick; and filling elements, 33 mm thick (Fig. 2b). The central motif of this panel's pattern consists of two battens forming a cross enclosed within a diagonally placed square (made of four battens). The pattern is completed by squares that fill the fields between the central battens, and four triangles that fill the corners between the battens that form the two squares. The elements in the form of triangles and squares have a tongue on each side. The battens forming the central cross motif have recesses in the middle of their length (on the bottom side of one of the elements and on the top side of the second one) which allow forming a lap joint. Similarly to the trapezoid elements around the central square motif, the battens have grooves on their longer sides, and on the shorter sides they are ended with dowel pins.

The pattern is enclosed within a frame made of four battens that have grooves on three sides, and the fourth one is ended with a dowel pin. The depth of groove is 10 mm and the tongue has 9 mm. The height of tongues and grooves is 8 mm. The thickness of the wear layer is 12 mm. The connections between panels were made with non-continuous spline joints, with 8 mm thick wood strips, with final width of about 100 mm. The fiber direction of the strips of wood forming the spline joint was

perpendicular to the fiber direction in the panel frame elements, in accordance with the original. The strips of wood used in spline joints between adjacent panels were made of 3 wood strip fragments each. The panels were fixed to the beams or to the blind floor with contemporary galvanized nails that were 1.8 mm in diameter and were 35 mm long.

Shock absorption tests are performed with the help of a device consisting of a tripod, a specialized spring and a 25 kg weight that falls onto a metal pad that is connected to a force sensor (Fig. 4a). During the test, the sensor sends the data to the computer, where they are recorded.

Vertical deformation tests consist in recording floor deformation under a dynamic load. This is done using a device called "artificial athlete" that consists of a steel base plane, a force sensor, a spring and an upper plane (at least 20 mm thick at the plate's centre), guided in a guiding tube (Fig. 4b). Deformation measurements are carried out 125 mm and 500 mm away from the contact point to which the load is applied, with the use of two electronic pick-up sensors, with measuring range of $\pm$10 mm and uncertainty not greater than 0,05 mm. The sensors are placed symmetrically around the device. The force applied to the surface and the deformation caused as a result of the impact are recorded every 5s. The procedure is repeated twice at 1 min intervals, to reach three impacts in total. Then the mean value of the deformation caused by the second and third impact is checked. Each test has to be performed at a new point (at least 100 mm from another testing point used before).

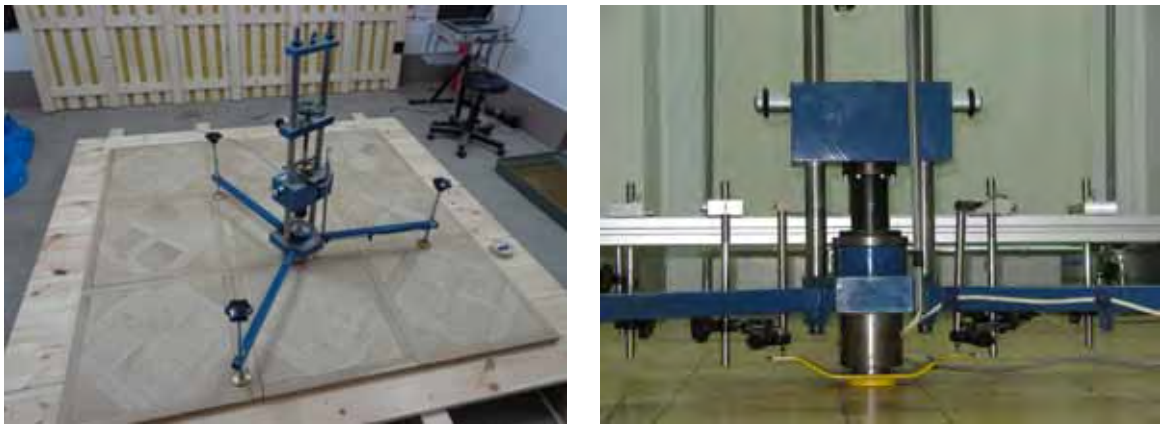

Fig.4: Shock absorption (left) and vertical deformation (right) tests on copies of parquets from room no. 4 of the Tarnowiec Manor House with the use of an "artificial athlete"

4. Conclusion

The results of tests of antique wooden floor copies with beam structure and with panel parquets are the basis for recommendation of specific structural solutions for the decking and indicate that the proposed methods are verifiable, which means that they can be used with a guarantee of success, as part of a conservation offer.

References

[1] Rozanska A., Sudol E., Wierzbicki J., Mazurek A., Beer P., Antique Wooden Floor Construction Solutions and the Possibilities of Using them in Reconstructions, *Proc. 2nd International Conference on Structural Health Assessment of Timber Structures (SHATIS'13)*, 4-6 September 2013, Trento, Italy; also in: Periodical of Advanced Materials Research Vol. 778 (2013) with the title *Structural Health Assessment of Timber Structures.*

[2] M.R. Valluzzi, E.Garbin, M. Dalla Benetta, C. Modena, Experimental Characterization of Timber Floors Strengthened by In-Plane improvement Techniques. *Proc. 2nd International Conference on Structural Health Assessment of Timber Structures (SHATIS'13)*, 4-6 September 2013, Trento, Italy; also in: Periodical of Advanced Materials Research Vol. 778 (2013) with the title *Structural Health Assessment of Timber Structures.*

[3] E. Sudol, A. Policinska-Serwa, Test of shock absorption and vertical deformation in sports floors on wooden structure, Ann. WULS-SGGW, Forestry and Wood Technology 76 (2011) 64-69.

Experimental assessment of the bending performance of old timber beams before and after retrofitting

Tiago Ilharco[1], João Miranda Guedes[2], Gabriele Romagnoli[3], Florian Kobryn[4]

Summary

Sometimes old timber structures are so badly deteriorated that partial or total replacement of an element is the viable option. Nevertheless, and although other factors should also be considered, it is a good rehabilitation practice to replace the minimum necessary elements. As presented in the technical literature, there are different techniques to retrofit a damaged timber beam. However, some of these techniques, which allow recovering partially or totally the elements initial characteristics, namely their stiffness and strength, are difficult to implement, requiring highly qualified workers and special conditions to be installed. A research experimental work that has been developed in this domain at the Faculty of Engineering of Porto University, with the collaboration of NCREP – Consultancy on Rehabilitation of Built Heritage, Ltd., aimed testing simple procedures to retrofit old timber beams, mainly by using steel screws and nailed steel strips. In particular, a set of chestnut beams (4m length and 20 cm average diameter) retrieved from old constructions of the city of Porto, Portugal, were tested before and after implementing the retrofitting solutions.

1. Labor tests

The experimental campaign consisted on performing cyclic bending tests on a set of old timber beams, according to the standard EN 408 [1]. The campaign was split in two phases. In the first phase, 20 timber beams were tested in their original conditions, allowing the assessment of the average values of stiffness and strength and

[1] NCREP – Consultancy on Rehabilitation of Built Heritage, Ltd., Porto, Portugal.

[2] FEUP - Faculty of Engineering of Porto University, Porto, Portugal.

[3] Università degli Studi di Trento, Trento, Italy.

[4] École des Ponts Paristech, Paris, France.

the detection of the corresponding failure modes [2]. In the second phase, 8 retrofitted timber beams chosen from the previous 20 were tested again, Fig. 1 [3].

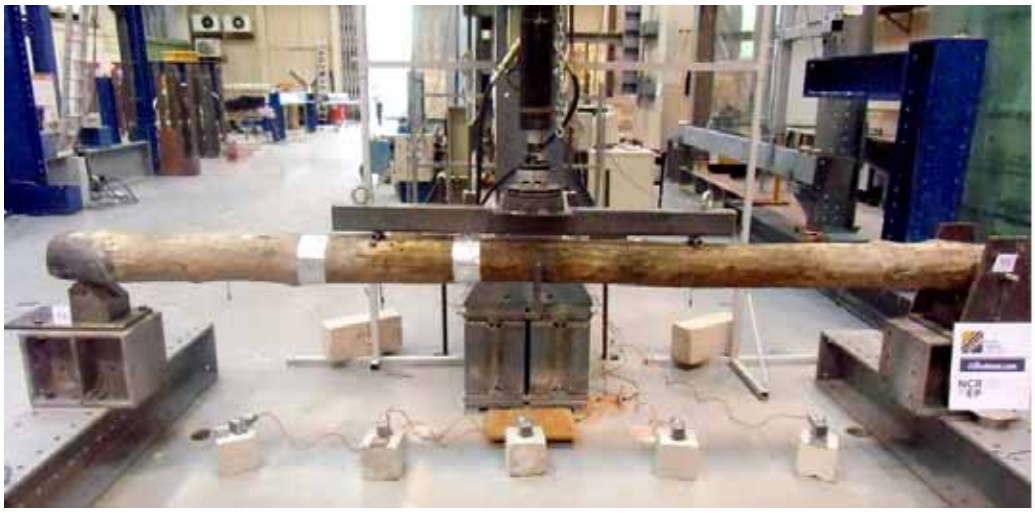

Fig. 1: Setup of bending tests.

2. Strengthening techniques

An efficient retrofitting technique should provide the beams with the stiffness and the bending strength obtained in the first phase. Moreover, and according to the purpose of this research, the applied techniques should be easy to adjust to irregular elements and, taking into consideration the recommendations on intervention on built heritage, should also be, tendentiously, reversible and low intrusive. The cost, the simplicity and speed of implementation were also important selection factors. Considering all these conditions, retrofitting techniques with screws and nailed steel strips were chosen.

The screws used were 9 mm diameter, 200 mm length VGZ Rothoblaas fully-threaded, Fig. 2. The resistance was calculated according to EC5 [4] and Johansen theory. The characteristic withdrawal capacity of the screws is 19.74 kN and the characteristic load-carrying capacity in single shear is 7.86 kN. The 2 mm thick strips used were Rothoblaas PF704025 fixed by Anker nails PF601440 (4 mm diameter and 40 mm length), Fig. 3. The resistance of these elements is given by the combination of the tensile strength of the strip and the behavior of the connectors. According to EC3 [5] and to EC5 respectively, the design value of the tension strength of the strip is 41.58 kN and the characteristic load-carrying capacity of the nails in single shear is 1.82 kN.

Fig. 2: Application of screws

Fig. 3: Application of steel strips

The design of the retrofitting elements and the prediction of the level of stress near the defects were made through a 3-dimensional finite element model in SAP2000, according to the wood properties obtained in the first phase of the tests. The stresses obtained were a good estimation for the design of the elements, even if through an elastic analysis it is difficult to have a reliable model of an anisotropic material such as wood.

The application of screws and strips was a crucial phase of the process. Their position was carefully studied according to the existent defects and to the points of maximum tensile stresses. In particular cases, a combination of the two retrofitting systems, screws and strips, was used. In order to avoid splitting of timber, especially due to the high density of chestnut wood, Ø5mm holes were done previously to the introduction of the screws. Simultaneously, to improve the axial behavior of the steel strips, a pre-tension was applied, sewing the cracks and giving ductility to the wood.

3. Tests results

The results of the two phases of some of the tests are resumed in Tab. 1. The retrofitted beams did not reach the bending strength and stiffness of the undamaged beams. From this point of view, this retrofitting solution did not perform as other more sophisticated techniques. Nevertheless, most of the beams have reported an increase in stiffness (10%) and bending strength (20%) when compared to the last loading cycle before retrofitting. Even though, in a small number of cases, the retrofitted beams showed low bending strength and brittle failure.

Tab. 1: Results of the two phases of tests of some timber beams

BEAM ID	V1		V2		V4		V6		V9		V11	
Test	1st	2nd	1st	2nd	1st	2nd	1st	2nd	1st	2nd	1st	2nd
Max load [kN]	34	37	63	61	30	25	56	42	57	55	55	47
Max displ. [mm]	80	97	89	94	50	89	86	87	85	90	54	86
$E_{m,g}$ [GPa] (1st cycle)	7,3	5,6	7,6	6,3	7,5	4,1	7,7	6,1	11,4	9,7	10,2	5,9
f_m [MPa] (max load)	27	30	39	38	21	17	42	31	46	45	45	38

Most of the retrofitted beams have shown a more ductile behavior, due to the plastic behavior of the steel connectors. This mechanic characteristic avoids sudden rupture of the beam, allows a better energy dissipation and stress distribution under dynamic loads, making failure to occur for larger deformations. Fig. 4 shows the difference of behavior between the beams during the first (red) and the second (blue) phases.

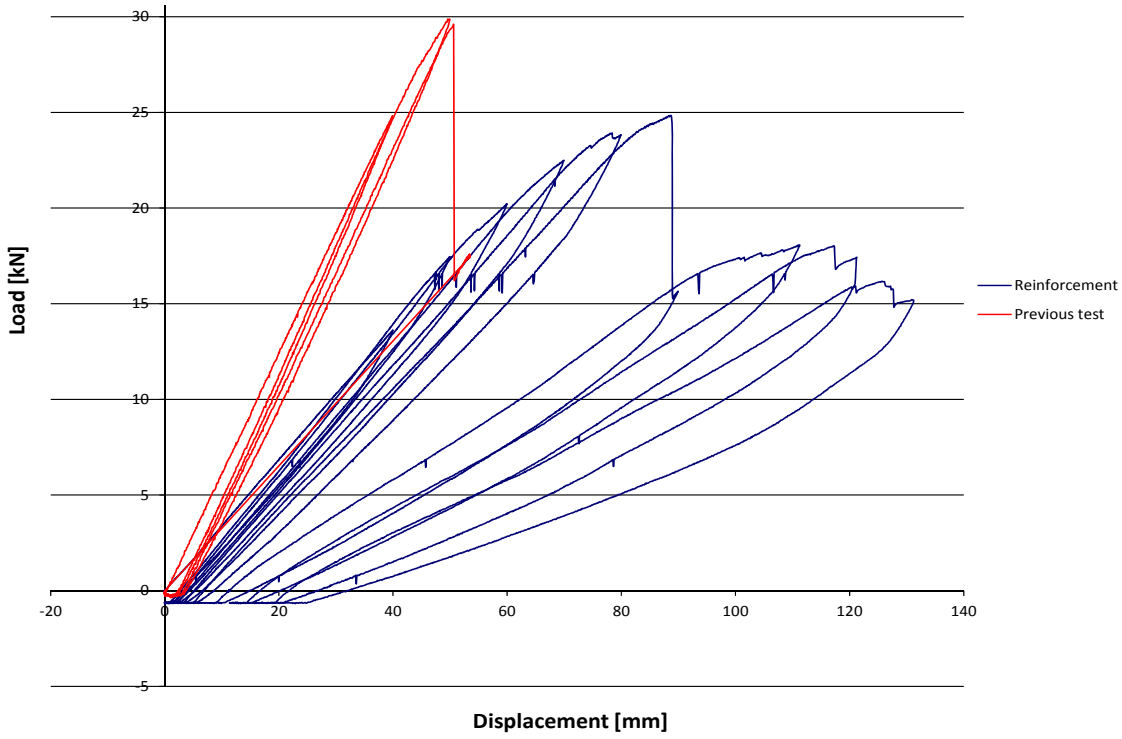

Fig. 4: Load-displacement diagram of one of the tested beams

4. Conclusions

The retrofitting of old timber beams with screws and nailed steel strips, as implemented in this experimental campaign, was not able to bring back their original strength and stiffness. It is also evident that with these simple techniques it is impossible to reach the performances offered by more sophisticated techniques. However, if all the requirements regarding the installation of the screws and steel strips are met, they are able to introduce ductility and to increase the strength and (or) stiffness of the beams comparing to the last cycle of the tests before being retrofitted. Based on these conclusions, further studies are needed to improve the efficiency of these techniques, in order to allow their use in the retrofitting of existent timber structures.

5. Acknowledgement

The authors thank Rotho Blaas and STAP for the support in the experimental tests.

References

[1] European Committee for Standardization CEN, EN 408: Timber structures – Structural timber and glued laminated timber – Determination of physical and mechanical properties, 2003, CEN, Belgium.

[2] T. Ilharco, Pavimentos de madeira em edifícios antigos. Diagnóstico e intervenção estrutural. Master Thesis, University of Porto. 2008

[3] G. Romagnoli, Strentghening and experimental assessment of old wooden beams. Master thesis. University of Trento. 2012.

[4] European Committee for Standardization CEN, EN 1995-1-1: Eurocode 5: Design of timber structures - Part 1-1: General - Common rules and rules for buildings, 2004, CEN, Belgium.

[5] European Committee for Standardization CEN, EN 1993-1-1: Eurocode 3: Design of steel structures - Part 1-1: General - Common rules and rules for buildings, 2005, CEN, Belgium

Numerical investigation of the residual load-carrying capacity of cracked timber elements

Noëlie Magnière[1], Steffen Franke[2], Bettina Franke[3]

Summary

The presence of cracks in timber elements is a reliable indicator of a structure's state. However, no standard currently provides methods to evaluate the impact of these cracks. Thus, this research investigates numerically the influence of one crack on the performances of a glulam beam. A finite element model is developed using the software ANSYS 14.0 ®. The results obtained showed that two situations could be distinguished: through and not through cracks. A model is proposed to calculate the reduction of the beam's stiffness; which only appears in case of through cracks. The load-carrying capacity, however, is influenced by both types of cracks. Several correlations between crack's characteristics and beam's load capacity have been found. Experiments are now conducted to validate further the numerical model and refine the calculation models.

1. Introduction

To efficiently implement the retrofitting of an existing timber structure, an in depth knowledge of its state must be obtained. Therefore, assessments are conducted to gather, amongst others, information regarding the element stiffness and residual load-carrying capacity (LCC). Cracks are often noticed during assessments, as they are clearly visible in dry conditions. Both standards and literature agree on the major relevance of these cracks. Indeed, the Swiss standard SN 505269/5 [1] insists several times on the importance of referencing cracks during assessments, while Vogel [2] and Blass and Frese [3] point out that 75% of failures of timber structures can be directly imputed to the propagation of cracks in the grain direction. However, no standard

[1] Research assistant, Bern University of Applied Sciences, Biel/Bienne, Switzerland

[2] Professor for Timber Constructions, Bern University of Applied Sciences, Biel/Bienne, Switzerland

[3] Research Associate, Bern University of Applied Sciences, Biel/Bienne, Switzerland

currently provides rules on how to effectively take into account the impact of those cracks on the residual performances of the element.

Therefore, the research presented studies the influence of one crack in a glued laminated (glulam) beam. Straight glulam beams of relatively large spans are considered here as they constitute the majority of the cases where cracks are encountered while assessing timber structures (see Franke and Magnière [4]). Thus, two questions are investigated:

1) When is a crack small enough that its influence can be neglected?
2) If a crack cannot be neglected, can one predict the residual performances of the cracked beam according to the characteristics of this crack?

The fundamental idea of this study is to compare the behavior of a glulam beam without cracks to that of the same beam with cracks.

2. Material and Methods

To compare the performances of a cracked beam with those of a non-cracked beam, a numerical model was developed using the finite element software ANSYS 14.0®.

2.1 The numerical model

The numerical model created for this study simulates the test in three-point bending of a glulam beam presenting initially an open crack, as shown in Fig. 1. The glulam beam, of constant dimensions of 12 000 x 600 x 140 mm^3, is constituted of elements with a linear elastic behavior. The wood principal directions (R, T and L) have been approximated to the axes of the model (X, Y and Z), as shown in Fig. 1. To simulate the presence of an initial crack and its further propagation, contact elements have been used on the surfaces of the crack plane. These contact elements follow a bilinear Cohesive Zone Material (C.Z.M.) law. A detailed description and validation and the material parameters used can be found in Franke and Quenneville [5].

The numerical beam obtained has one open crack which is defined using four parameters (x_c, y_c, l_c and d_c, as illustrated in Fig. 1). These parameters enable to simulate the performances of the beam for various crack locations and dimensions. Thereafter, a displacement controlled three-point bending test of the beam is simulated, until propagation of the initial crack or initiation of a new crack. This point of propagation/initiation of a crack is considered as the failure of the beam.

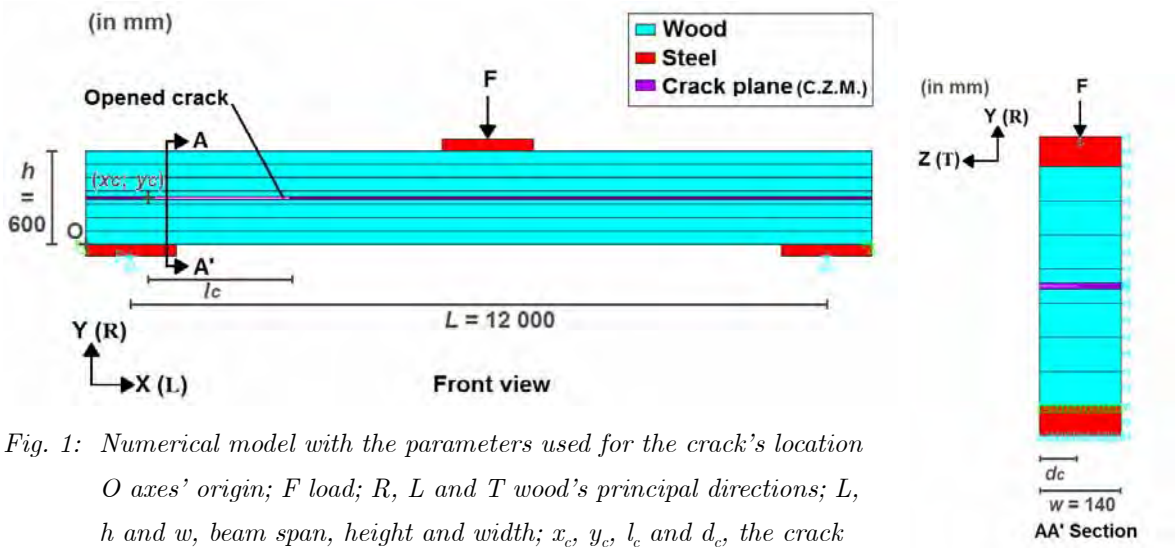

Fig. 1: Numerical model with the parameters used for the crack's location O axes' origin; F load; R, L and T wood's principal directions; L, h and w, beam span, height and width; x_c, y_c, l_c and d_c, the crack origin, height, length and depth; C.Z.M., Cohesive Zone Material

2.2 Evaluation methods and scope of testing

During the simulations, the load-displacement curves were recorded. Then, the cracked beam performances were evaluated in terms of LCC, by the crack propagation/initiation load F_{crit}, and in terms of stiffness, by the slope K in the elastic range (Fig. 2, left). A reference simulation provided the stiffness (K_{ref}) and crack initiation load (F_{ref}) of the non-cracked glulam beam. Finally, three ratios are calculated (Fig. 2, right) which quantify if, and by how much, the presence of a crack in the beam reduces its performances. The crack characteristics investigated are provided in Tab. 1.

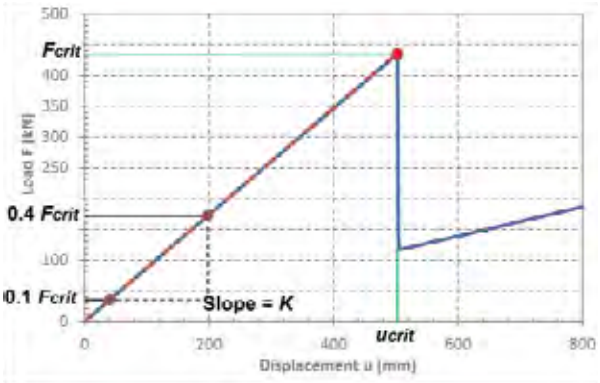

Ratios calculated based on the load-displacement curves' evaluations

Critical load ratio	F_{crit}/F_{ref}
Critical displacement ratio	u_{crit}/u_{ref}
Stiffness ratio	K/K_{ref}

Fig. 2: Evaluation of a simulation's load-displacement curve (left) and corresponding ratios (right)

Tab. 1: Range of variation of the crack characteristics

Crack origin x_c		Crack height y_c		Crack length l_c		Crack depth d_c	
x_c [mm]	x_c/L [%]	y_c [mm]	y_c/h [%]	l_c [mm]	l_c/L [%]	d_c [mm]	d_c/w [%]
0	0	30	5	600	5	10	7
1800	15	150	25	3000	25	40	29
3600	30	300	50	6000	50	70	50
6000	50	450	75	9000	75	80	57
m*	m*	570	100	12000	100	140	100

*m corresponds to a crack centered at mid-span

3. Results and discussion

3.1 Negligible cracks

The simulations showed that only through cracks produce a reduction of the stiffness of the beam (see Fig. 3, left). However, regarding the LCC, the results are less clear. Only a trend appears: the lower the crack is in the cross section, the deeper it can be without influencing the beam strength. Thus for example, as shown in Fig. 3-right, for the beam considered, a crack placed 5% higher (y_c/h) than the beam's lower face can always be neglected besides it is a through crack. Similarly, for cracks placed at a height ratio of 25%, only cracks with depth ratio (d_c/w) of 7% or less can be neglected.

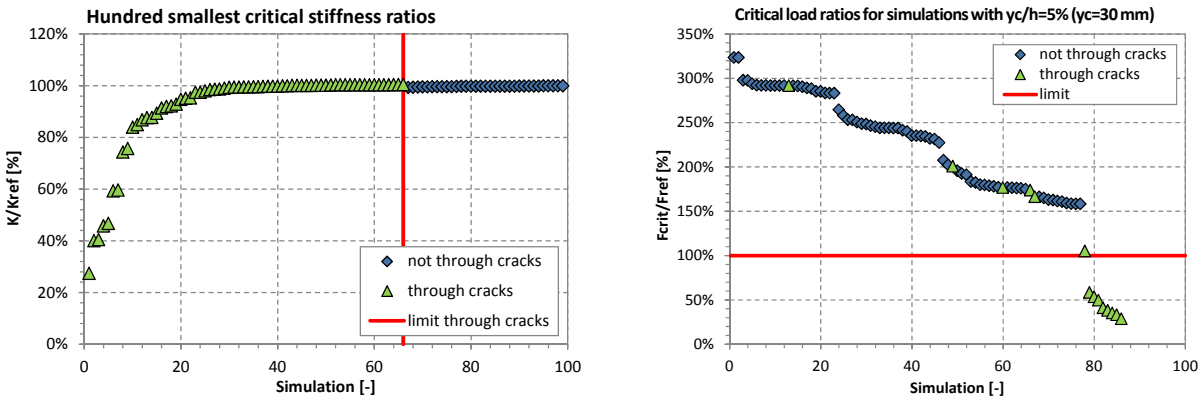

Fig. 3: Influence of through and not through cracks on the beam's stiffness (left) and critical load ratios in decreasing order for crack's height ratios of 5% (right)

3.2 Correlation between the crack's characteristic and the beam's performance

To predict the cracked beam stiffness ratio K/K_{ref}, the model provided in Fig.4 has been developed. In this model, at the crack location, the inertia of the section is reduced depending on the crack height y_c in the beam section. Then, the crack length

l_c is considered by assimilating the cracked beam, whose stiffness varies along the length, with several springs placed in series. Finally, the factor k_{ecc} accounts for the relevance of the crack with regards to stress distribution. A good correlation between the model proposed and the simulation results has been achieved as shown in Fig. 5, left.

The residual LCC of the cracked beam can also be distinguished in terms of through and not through cracks. In the case of through cracks, the critical load ratios are correlated with the crack's height in the cross section by a parabolic law (see the example in Fig. 5 right). The coefficients of this law are a power function of the crack length l_c. In the case of not through cracks, all the crack's characteristics have a direct influence on the residual LCC of the beam. However, no model combining these parameters shows a real correlation with the simulation results so far.

$$\frac{K}{K_{ref}} = \frac{L}{L + l_c\, k_{ecc}\left(\frac{h^3}{y_c^3 + (h - y_c)^3} - 1\right)} \quad \text{with} \begin{cases} k_{ecc} = 1 & \text{if End crack and } \frac{l_c}{L} > 0.25 \\ k_{ecc} = 0.3 & \text{if End crack and } \frac{l_c}{L} \leq 0.25 \\ k_{ecc} = 0.1 & \text{otherwise} \end{cases}$$

Fig. 4: Model proposed to calculate the reduction of stiffness of a beam presenting a through crack

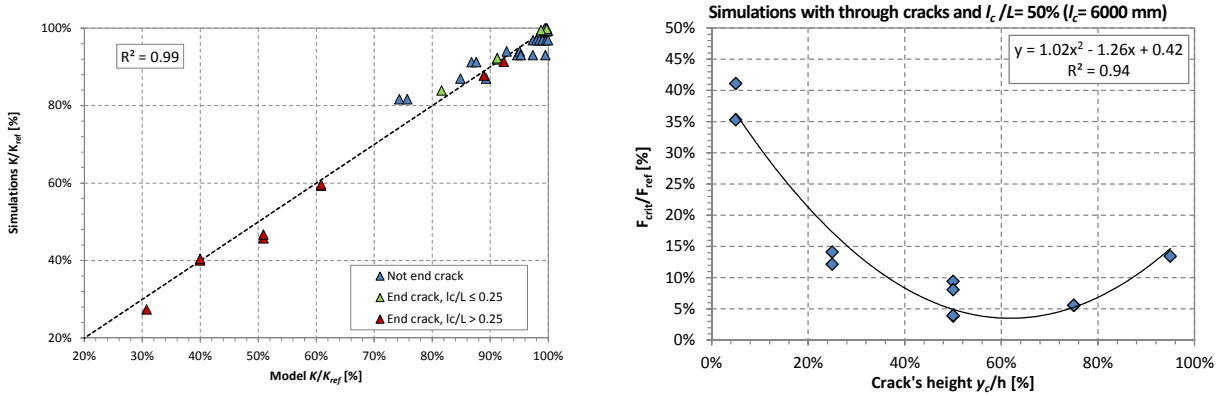

Fig. 5: Correlation between the simulation results and the stiffness ratio modeled (left) and example of load ratios depending on the crack height and corresponding parabolic black trend line (right)

4. Conclusion

The numerical simulation results reveal that the distinction between through cracks and not through cracks should be made. Indeed, both in terms of stiffness and load-carrying capacity, these two cases have a different impact on the beam performance. A calculation model is proposed to estimate the reduction of stiffness for a beam

presenting a crack. Several trends have been highlighted to correlate the residual load-carrying capacity of a cracked beam with the crack characteristics, especially in the case of through cracks.

This ongoing research project continues in collaboration with the Swiss Federal Laboratories for Materials Science and Technology. Experiments are now conducted to validate further the finite element numerical model which was developed. Moreover, numerical simulations will be calculated to focus on the correlation between load-carrying capacity and crack characteristics in the case of not through cracks.

References

[1] Swiss Society of Engineers and Architects, Standard SN 505269/5:2011 Maintenance de structures porteuses – Constructions en bois, Swiss Society of Engineers and Architects, Zurich, Switzerland.

[2] Vogel M., Überwachung von Bauwerken, *Proceedings of the Holzbautag,* Biel/Bienne, Switzerland, 2008

[3] Blass H. J. and Frese M., Schadensanalyse von Hallentragwerken aus Holz, *Band 16 der Reihe Karlsruher Berichte zum Ingenieurholzbau, KIT Scientific Publishing,* Karlsruhe, Germany, 2010

[4] Franke S. and Magnière N., Investigation on elements presenting cracks in timber structures, *submitted for publication in the Proceedings of the World Conference on Timber Engineering*, 2014

[5] Franke B. and Quenneville P., Numerical modeling of the failure behavior of dowel connections in wood. *ASCE, Journal of Engineering Mechanics* 137, 186, pp. 155-226, 2011

[6] APA The Engineered Wood Association, Technical report EWS R475E – Evaluation of check size in glued laminated timber beams, APA The Engineered Wood Association, Washington, U.S.A, 2007

Strength class of "minor" conifer species, as estimated from log acoustic measurements, small-clear data and knowledge of wood property variation

David Gil-Moreno[1], Dan Ridley-Ellis[2], J. Paul McLean[3]

Summary

It is well known that wood properties vary from species to species. Additionally, trees grow wood in response to their requirement to grow in a certain environment. Therefore, timber properties also vary by region, by forest practice, and by the changing circumstances for individual trees as they age. This paper presents results from the early stages of a PhD project that is investigating the growth and mechanical properties of timber from noble fir (*Abies procera*), western hemlock (*Tsuga heterophylla*), Norway spruce (*Picea abies*) and western red cedar (*Thuja plicata*) grown in Great Britain. While full laboratory tests on structural-size timbers and clear wood samples have not yet been realised, the use of portable acoustic tools on standing trees and logs can help to predict grade assignments of timber from each species using prior knowledge of the likely extent and sources of variation in wood properties.

1. Introduction

Sitka spruce (*Picea sitchensis*) forms the staple raw material supply for the British forest products sector. Recent outbreaks of pests and diseases, concerns about species suitability with climate change, and desire to increase biodiversity, are leading to greater planting of other species. However, little is known about the potential end use of timber from these species. There is also a desire by some architects to make use of local timber from softwood species for which there are currently no strength grading assignments.

[1] Research student, Edinburgh Napier University, United Kingdom

[2] Centre for Wood Science and Technology, Edinburgh Napier University, United Kingdom

[3] Northern Research Station, Forestry Commission, United Kingdom

Research in Sitka spruce has shown that British plantation grown timber has very different properties to that from old growth trees in the native Pacific Northwest, and plantations in other countries. Therefore, assuming timber properties for a species based on non-local published values is not valid. Assessment of properties of a species must be made on a representative sample of trees grown under similar conditions.

2. Strength classes of European timber, and limiting property

In Europe, structural timber is assigned to strength classes, most commonly to EN 338. These grades allow safe design with timber by proscribing minimum characteristic values of strength, stiffness and density at 12% moisture content. For any particular species and growth area one of these properties will be limiting. When estimating grade-outturn for a species it is necessary to know what the grade limiting property is. Overall, British Spruce (a mix of Sitka spruce and, about 10%, Norway spruce) typically attains strength class C16 limited by stiffness [1].

There are few published values for the other three species, but sufficient to estimate the grade limiting property. There are data [2] from the testing of small clear samples from the UK (Tab. 1) from which it is possible, albeit with assumption of similarity to British Sitka spruce, to estimate properties of structural-size timber.

Tab. 1: Properties of small clears for species in the UK [2] and output data from model.

At 12% moisture content	Norway spruce	Noble fir	Wester hemlock	Western red cedar	Sitka spruce
Data for small clears [2]					
Density (kg/m^3)	368	368	433	368	384
Mean stiffness (kN/mm^2)	8.5	8.1	8.0	7.0	8.1
Mean strength(kN/mm^2)	66	63	76	65	67
Estimated structural size	*(for Sitka spruce, also actual structural size data [1])*				
5th %ile strength (N/mm^2)	21.1	20.1	24.2	20.7	21.4 (19.6)
Mean stiffness (kN/mm^2)	8.1	7.7	7.6	6.65	7.7 (8.3)
5th %ile density (kg/m^3)	323	323	380	324	337 (330)

Firstly, the small clear (free of defects) values must be converted into structural size (which contains features like knots and grain deviation that reduce strength and stiffness, and are strongly influenced by environment and silviculture). Data for British Sitka spruce suggests a reduction coefficient of 0.5 for strength and 0.95 for stiffness. In order to transform density, EN 384:2010 indicates an increase factor of 1.05. Characteristic values for stiffness refer to the mean, but strength and density

refer to the lower 5th percentile. It is reasonable to assume a normal distribution, and coefficients of variation of 22% (for strength) and 10% (for density) are typical of softwoods grown in Europe.

Comparison with the strength classes in EN 338 shows the limiting property for these species is stiffness (C16: $f_{m,0,k} \geq 16$ kN/mm^2, $E_{m,0,mean} \geq 8$ kN/mm^2, $\rho_k \geq 310$ kg/m^3). Therefore, information about stiffness for a greater quantity of timber, allows a prediction of the grade outturn. Acoustic measurements on logs can help with that.

3. Non-destructive estimation of stiffness of trees and logs

The stiffness of trees and logs can be estimated using portable devices that measure stress wave (or 'acoustic') velocity. Dynamic Modulus of Elasticity (MOE_{dyn}) is calculated using the Newton-Laplace equation from measured stress wave velocity (V) and estimated, or measured, density (ρ):

$$MOE_{dyn} = \rho V^2 \tag{1}$$

Estimations of sawn timber stiffness have been achieved more successfully by applying equation (1) to logs rather than standing trees. This is primarily due to the difference in the method used to measure velocity. For logs, the resonance method can be used, which involves exciting every element of the log. For standing trees, the "time-of-flight" method must be used, which is limited by the uncertain path of the sound wave, which is not planar, and the variation in wood density, wood stiffness and moisture content within a tree which cannot be easily determined [3].

Eighteen trees from each species have been felled to produce sawlogs from which structural timber will eventually be produced for laboratory testing. The resonant velocity was measured on each of these logs using a FibreGen HM200. A disc was obtained from near to the log for assessment of bulk density and moisture content. Due to the difficulties of measuring density in the forest, the velocity on logs and assessment of the density, were taken at different times, assuming no significant changes in moisture content (during autumn-winter).

4. Estimated grade outturn of chosen species

In order to estimate the potential grade recovery of timber based on the acoustic measurements of log stiffness, the static stiffness of the sawn, dried, timber that will be produced is required. For British Sitka spruce logs (mean $MOE_{dyn.log}$, in kN/mm^2) the relationship to the static stiffness of timber (mean MOE_{Timber}, in kN/mm^2) is known [1].

$$MOE_{Timber} = -0.524 + 0.768 \times MOE_{dyn.\log} \tag{2}$$

By applying equation (2) to the mean measured log stiffness per species, and presuming a typical coefficient of variation (22%), a calculation of estimated grading yield can be made (Tab. 2).

Tab. 2: Estimated optimum grade yield for single grade/reject (from log measurements)

	C14/R	C16/R	C18/R	C20/R	C22/R	C24/R
Noble fir*	100%	73%	34%	21%	11%	2%
Western hemlock*	100%	81%	41%	26%	15%	4%
Norway spruce*	100%	96%	59%	41%	26%	8%
Western red cedar	30%	6%	1%	-	-	-

* Stiffness not significantly different at the 95% confidence level

With the data currently available, Norway spruce, noble fir and western hemlock look similarly good regarding mechanical properties (and comparable to Sitka spruce). Conversely, western red cedar is unlikely to produce large quantities of structural timber. Nevertheless, these estimations must be seen as preliminary results, and a full laboratory study is required to confirm these findings.

A laboratory study is planned and will allow validation of the estimates of strength classes from log stiffness measurements that have been presented here. Furthermore, these laboratory measurements will be structured in such a way so as to allow assessment of the within tree variation in timber properties, which is likely to be the biggest source of variation in timber properties (e.g. [1]), that is to say timber properties typically vary more within one tree than between two different trees.

5. Acknowledgements

The financial support by the Scottish Forestry Trust, Forestry Commission Scotland and Cyfoeth Naturiol Cymru (Natural Resources Wales) is gratefully acknowledged. Andrew Price (Forest Research) is thanked for help finding suitable sample sites and organizing necessary forest operations.

References

[1] Moore, J.R., Lyon, A.J., Searles, G.J., Lehneke, S.A., & Ridley-Ellis, D.J. Within- and between-stand variation in selected properties of Sitka spruce sawn timber in the UK: implications for segregation and grade recovery. *Annals of Forest Science*, 2013, 70(4): 403-414.

[2] Lavers, G.M. *The Strength Properties of Timber*, 2002, Building Research Establishment.

ISBN-10: 1-85790-183-5
ISBN-13: 978-1-85790-183-2